Fakultät für Medizin

Institut für Zellbiologie des Nervensystems

Investigation of Heterogeneity within the Oligodendrocyte Precursor Cell Population

Tobias Hoche

Vollständiger Abdruck der von der Fakultät für Medizin der Technischen Universität München zur Erlangung des akademischen Grades eines

Doctor of Philosophy (Ph.D.)

genehmigten Dissertation.

Vorsitzender: Prof. Dr. Stefan Lichtenthaler

Betreuer: Emmy-Noether Fellow Dr. Tim Czopka

Prüfer der Dissertation:

1. Prof. Dr. Mikael Simons

2. Prof. Dr. Leda Dimou

Die Dissertation wurde am 01.09.2020 bei der Fakultät für Medizin der Technischen Universität München eingereicht und durch die Fakultät für Medizin am 09.10.2020 angenommen.

ABSTRACTS

English Abstract

Myelination is absolutely critical for proper nervous system function. Myelin ensheathes axons to accelerate nerve conduction, provide trophic support and its involvement in neuronal plasticity has been described recently. Damaged myelin is a hallmark of neurological and neurodegenerative diseases like Multiple Sclerosis or leukodystrophies. In the central nervous system myelin is produced by oligodendrocytes, which requires the differentiation of oligodendrocyte precursor cells (OPCs). OPCs represent an abundant cell population in the developing and adult CNS. Additionally, OPCs have been reported to be involved in neuronal signalling. However, whether all OPCs have the same capacity to differentiate into myelinating cells is currently not well understood, as well as whether all OPCs are equally capable of communication with neurons.

Using the spinal cord as a model system, I investigated individual OPC behaviour in the living embryonic and larval zebrafish. Therefore, I established new transgenic tools, which allow for the visualization of OPCs as population and at the level of individual cells *in vivo*. By repeated imaging, different properties and fates of OPCs, i.e. regarding proliferation and differentiation, could be distinguished.

In analogy to grey and white matter in the mammalian spinal cord, the larval zebrafish spinal cord is composed of a central region containing the majority of cell somata – the 'nuclear region', and a peripheral region that is referred to as 'axodendritic region' since it contains axons, dendritic processes and myelin. While all OPCs extend their processes into the axodendritic region, the cell bodies of one OPC subgroup reside also there, whereas the cell bodies of another subgroup are located in the nuclear region. I found that these two subgroups differ significantly regarding morphology, process dynamics, and likelihood of differentiation. OPCs that exclusively reside in the axodendritic region exhibit lower process complexity and faster process remodelling. Time-lapse observation revealed that these OPCs readily differentiated into myelinating oligodendrocytes. Furthermore, I found that these differentiation-competent OPCs are generated through recent divisions of OPCs in the nuclear region, suggesting that myelination can be controlled indirectly through the regulation of cell divisions. Conversely, OPCs in the nuclear region, which exhibit a complex morphology and have not divided recently, have been never observed to differentiate directly.

In addition, in a collaborative approach I also started the molecular characterization of the observed OPC subsets. Based on differential gene expression detected by single-cell RNA-Sequencing, four OPC subclusters have been identified. One cluster comprises OPCs which are highly involved in neuronal communication, whereas another cluster represent OPCs undergoing differentiation. Using RNAScope® *in situ* hybridization for highly expressed marker genes in particular clusters, it was possible to establish a link between these two subclusters found by RNA-Sequencing and the two OPC subtypes identified by *in vivo* live imaging, respectively. The remaining two OPC subclusters most likely correspond to OPCs in the cell cycle or during the transition between OPC subtypes.

Taken together, this work reports regional, morphological, behavioural, and transcriptomic heterogeneity between OPCs with different fates *in vivo* and provides insight in the control of oligodendrocyte differentiation and axon ensheathment.

German Abstract

Myelin beschleunigt die Erregungsleitung, ermöglicht die Nährstoffversorgung von Axonen und spielt zudem eine Rolle für die neuronale Plastizität. Beschädigtes Myelin ist bei verschiedenen neurologischen und neurodegenerativen Erkrankungen, z. B. Multipler Sklerose oder Leukodystrophien, zu finden. Myelin im Zentralnervensystem wird von Oligodendrozyten in Form von axonumhüllenden Myelinscheiden produziert. Die Bildung von Oligodendrozyten und damit neuem Myelin erfordert dabei in der Regel die Differenzierung von Oligodendrozyten-Vorläuferzellen (OPCs). Darüber hinaus sind OPCs in der Lage, auch direkt mit Neuronen zu kommunizieren. Sie existieren in großer Zahl sowohl während der Entwicklung als auch noch im Erwachsenenalter. Ob alle OPCs dasselbe Potential haben, zu differenzieren und neues Myelin zu generieren, ist zurzeit noch nicht gut verstanden, ebenso ob alle OPCs in gleicher Weise mit Neuronen kommunizieren können.

Für die vorliegende Arbeit wurde das Rückenmark von embryonalen und larvalen Zebrafischen genutzt, um das Verhalten von OPCs im lebenden Tiermodell zu untersuchen. Dafür etablierte ich neue genetische Reporter zur spezifischen Markierung von OPCs als Population sowie von individuellen Zellen. Durch wiederholte Beobachtung an aufeinanderfolgenden Zeitpunkten war es möglich OPCs mit verschiedenen Eigenschaften und Proliferations- sowie Differenzierungsschicksalen zu identifizieren.

In Analogie zu grauer und weißer Substanz im Säugetier-Rückenmark besteht das Rückenmark im larvalen Zebrafisch aus einer zentralen Region, wo die Mehrheit der Zellkörper zu finden ist – der „nukleären Region“, sowie der peripheren „axodendritischen Region“, in welcher Axone, dendritische Zellfortsätze und Myelin zu finden sind. Während alle OPCs ihre Zellfortsätze in die axodendritische Region entsenden, finden sich für eine Gruppe von OPCs auch die Zellkörper in der axodendritischen Region, wohingegen die Zellkörper der anderen Gruppe von OPCs in der nukleären Region lokalisiert sind. Diese beiden OPC-Gruppen unterscheiden sich bezüglich Morphologie, Zellfortsatzdynamik und der Wahrscheinlichkeit, zu differenzieren. OPCs die ausschließlich in der axodendritische Region zu finden sind, haben eine geringere Komplexität des Zellfortsatznetzwerkes sowie eine schnellere Fortsatzdynamik. Die wiederholte Beobachtung individueller OPCs konnte zeigen, dass OPCs innerhalb der axodendritischen Region innerhalb weniger Tage zu myeliniserenden Oligodendrozyten differenzieren. Diese differenzierungskompetenten OPCs werden durch kürzlich vorangegangene Zellteilungen von „nukleären“ OPCs generiert. Dies suggeriert, dass Myelinisierung durch die Regulation von Zellteilungen kontrolliert wird. Im Gegensatz dazu wurden OPCs mit dem Soma in der nukleären Region und einer komplexen Morphologie, die sich nicht kürzlich geteilt hatten, nie dabei beobachtet, direkt zu differenzieren.

Zusätzlich wurden auch die molekularen Charakteristika der identifizieren OPC-Subgruppen im Rahmen eines Kollaborationsprojekts untersucht. Basierend auf Genexpressionsunterschieden, die per Einzelzell-RNA-Sequenzierung gefunden wurden, konnten vier distinkte OPC-Subcluster etabliert werden. Während ein Cluster OPCs enthielt, die vor allem in neuronale Kommunikation involviert waren, enthielt ein anderes Cluster OPCs kurz vor der Differenzierung. Durch RNAScope® *in situ* Hybridisierungen für Markergene, welche in bestimmten Clustern besonders exprimiert waren, gelang es, eine Verbindung zwischen diesen zwei Clustern des Sequenzierungs-Datensatzes und den zwei OPC-Subtypen, die zuvor per *in vivo* Lebendmikroskopie gefunden wurden, herzustellen. Die verbleibenden zwei Cluster repräsentieren höchstwahrscheinlich OPCs im Zellzyklus und/oder bei der Transition zwischen OPC-Subtypen.

Zusammengenommen beschreibt die vorliegende Arbeit regionale, morphologische und transkriptionelle Diversität zwischen OPCs mit verschiedenen Zellschicksalen und ermöglicht Einblicke, wie Oligodendrozyten-Differenzierung im lebenden Organismus kontrolliert wird.

ACKNOWLEDGEMENT

I am very grateful for the support I received during the time which lead finally to the writing of this PhD thesis. I would like to thank my supervisor Dr Tim Czopka for giving me the great opportunity to work about OPCs in zebrafish, enabling everything required for a successful outcome of this project, constructive feedback and joint cycling adventures back then when both of us just arrived in Munich. I am also grateful to Prof Dr Thomas Misgeld as the head of the Institute for all the administrative support and helpful scientific thoughts and comments. I would also like to thank all members of the Czopka and Misgeld labs for the pleasant and constructive working atmosphere, especially Franzi – it was an exciting time when the lab was still in the starting phase – and Stavros, who had to bear me as a roommate at several occasions, but also to Roberta whose excellent results completed the OPC heterogeneity story to a quite successful finish.

I would also like to thank the members of my thesis advisory committee Prof Dr Leda Dimou and Prof Dr Mika Simons for their time and support, and the members of their labs for fruitful discussions and joyful times at meetings. This work would not have been possible without the help of Dr Eneritz Agirre and Dr Gonçalo Castelo-Branco at the Karolinska Institute as well as the CyTUM Unit of the TUM. These were great collaborations.

The most however I must thank my wife and my children, who sometimes had a tough time when I had to spend nights and weeks end in the lab and a significant amount of my time at home in front of the computer, but they gave me every possible support and ensured always the right balance between science and “normal life”. Finally, I also want to thank my parents, who always encouraged me in following my interests.

TABLE OF CONTENT

LIST OF ABBREVATIONS

(E)GFP	enhanced green fluorescent protein
CNS	central nervous system
COP	committed oligodendrocyte precursors
dpf	days post fertilization
EYFP	enhanced yellow fluorescent proteins
FACS	fluorescence-activated cell sorting
hpf	hours post fertilization
IF	immunofluorescence (immunostaining)
IGF	insulin growth factor
IX/IJ	injection
kb	kilobase
MBP	myelin basic protein
Myrf	myelin regulatory factor
nls-Cerulean	cyan fluorescent protein targeted to the nucleus by a nuclear localization signal
nls-mApple	red fluorescent protein targeted to the nucleus by a nuclear localization signal
OL/mOL	(myelinating) oligodendrocyte
Olig1/Olig2	oligodendrocyte transcription factors
OPC	oligodendrocyte progenitor/precursor cell
PCR	polymerase chain reaction
Pre-OL	pre-oligodendrocyte (non-myelinating)
pTol2	expression vector with Tol2 transposable elements
RNA ISH	RNA *in situ* hybridization
ScRNA-Seq	single-cell RNA-Sequencing
SD	standard deviation
ST	(OPC) soma transition (from the nuclear to the axodendritic region)
tagRFP	monomeric red fluorescent protein
tSNE plot	t-distributed stochastic neighbour embedding
voxel	unit of graphic information that defines a point in three-dimensional space

1 INTRODUCTION

1.1 Myelination in the Central Nervous System: A General Introduction

Myelin in the central nervous system (CNS) is a substance which is produced by oligodendrocytes to ensheath axons of neurons. This is achieved by sheaths of lipid-rich membranes that wrap several times around the respective axons. These so called myelin sheaths can vary in length dependent on the animal species, CNS region or cell culture model from few tens up to several hundreds of micrometres (Auer et al., 2018; Bechler et al., 2015; Bunge, 1968; Hildebrand et al., 1993; Ibrahim et al., 1995). The gaps between individual myelin sheaths along a fully myelinated axon are called nodes of Ranvier and have a specific structure and composition, e.g. a high concentration of ion channels. The space between nodes of Ranvier is called internode, as there are often myelin sheaths, these terms are used quite synonymously (Nave, 2010a, b; Sherman and Brophy, 2005). This architecture enables saltatory action potential propagation in myelinated axons that is faster compared to unmyelinated axons of a similar calibre, which is considered the canonical function of myelin. CNS regions like the corpus callosum and the peripheral spinal cord which are composed primarily of myelinated axonal tracts are known as white matter, whereas regions like the cerebral cortex which comprise primarily neuronal cell bodies and only little myelin are called grey matter.

During the last years additional functional aspects emerged. Myelin sheaths seem to contribute to the general axonal survival particularly by providing trophic support predominantly by the transport of nutrients from the oligodendrocyte to the axon (Funfschilling et al., 2012; Lee et al., 2012; Saab et al., 2016). Furthermore, specialized myelination patterns can finetune action potentials in axons and hence add another level of neuronal plasticity in the CNS, which has implications on learning and memory formation. Vice versa, myelination also depends on the activity state of the axon with active axons being more prone to become fully or partly myelinated, a process described as adaptive myelination (Chang et al., 2016; de Faria et al., 2018; Fields, 2015).

The formation of myelinating OLs in the mammalian CNS starts already during embryonic development but is most prominent after birth. Oligodendrocytes develop from neural progenitor cells via intermediate stages (**Figure 1.1.1**). Neural progenitors start to give rise to neurons but switch to generate glia cells later (Kriegstein and Alvarez-Buylla, 2009). Before neural progenitor-derived cells differentiate definitely into oligodendrocytes, they enter a state when they are still able to proliferate, display a distinct ramified

morphology and express a certain set of markers (**Figure 1.4.1**). Cells at this stage are called **oligodendrocyte precursor cells** (OPCs). As the exact potential and lineage contribution of these cells is not completely resolved, some refer to them also as oligodendrocyte progenitor cells (see **section 1.3** and **Figure 1.1.1**). I decided to circumvent this issue by generally using the common abbreviation *OPCs*.

OPCs are abundantly found throughout the entire CNS during development but they also persist into adulthood still representing 2-8 % of the entire cells dependent on the region (Dawson et al., 2003). Besides being the direct source of differentiated oligodendrocytes, the second major function of OPCs as progenitor cells is to proliferate and increase the pool of cells which are then available for differentiation (see **section 1.4**). In accordance with this, OPCs are the major proliferating cell types found in the adult CNS (Geha et al., 2010; Nishiyama et al., 1999). Another interesting peculiarity is that OPCs can communicate directly with neurons via neurotransmitter signalling and that this is even conveyed by synaptic structures on OPCs (Bergles et al., 2010; Kula et al., 2019), rising speculations about the functional consequences of this signalling mechanism beyond simply regulating proliferation and differentiation of OPCs (see **section 1.6** and **Figure 1.1.1**). Furthermore, OPCs can vary regarding their morphology or cellular behaviour between different regions or even within the same region (see **section 1.7**). It is unclear if this heterogeneity reflects functionally distinct subtypes of OPCs or transitional intermediate stages occurring during the maturation process towards myelinating oligodendrocytes (**Figure 1.1.1**). To describe the entirety of these cells the term *oligodendrocyte lineage (OL-lineage) cells* is used.

One individual mature oligodendrocyte can have many myelin sheaths, which are usually established within a short time window (Czopka et al., 2013). Afterwards, most studies found the number of myelin sheaths to be static for long-term. On the other hand, few recent studies reported indirect evidence that mature myelinating oligodendrocytes in humans and primates could be capable of generating new myelin sheaths under certain conditions (Bacmeister et al., 2020; Duncan et al., 2018b; Jakel et al., 2019; Yeung et al., 2019). Consequently, there is the general view in the field that significant generation of new myelin requires the differentiation of OPCs or other immature OL-lineage cells in most situations.

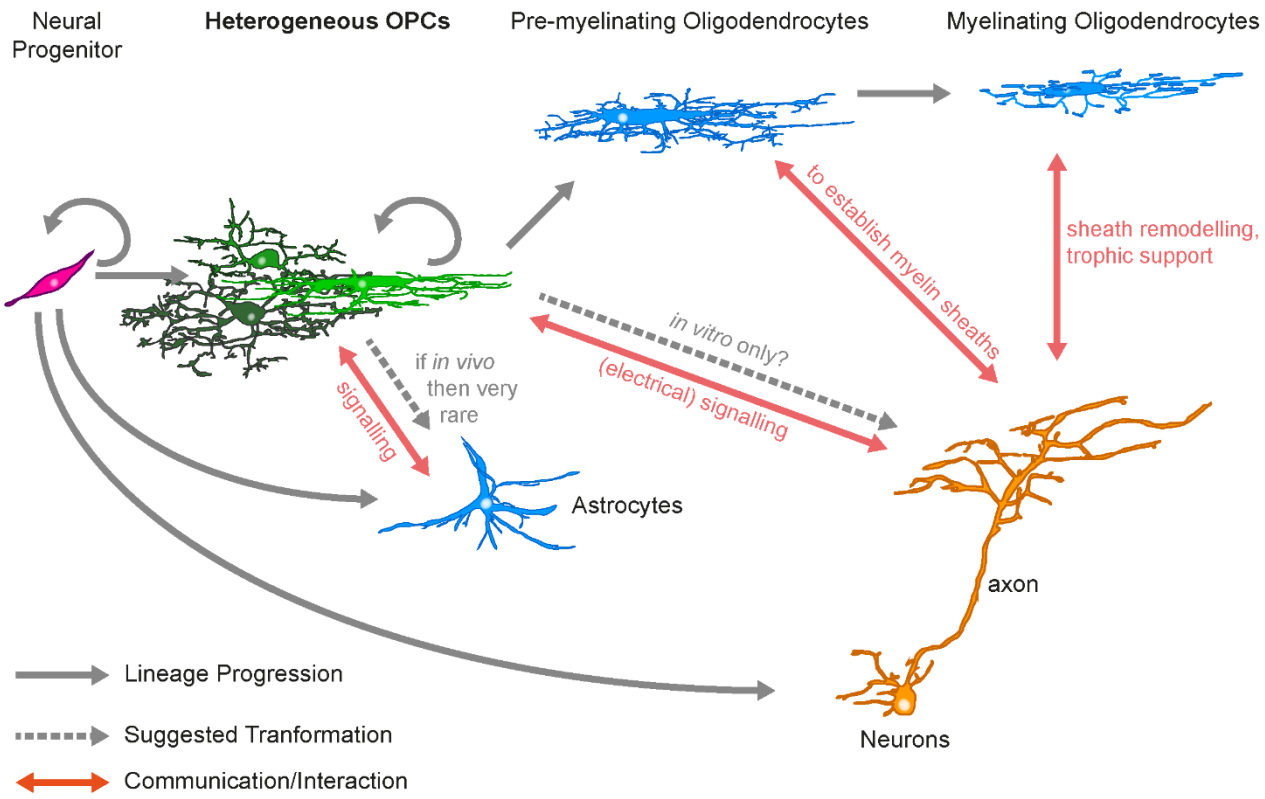

Figure 1.1.1 Cartoon showing cell types of the Central Nervous System and their relationships.

Neural progenitor cells (NPs) give rise to neurons, astrocytes (ACs) and oligodendrocyte progenitor cells (OPCs) in a temporal manner. NPs and OPCs have the potential to undergo cell division. OPCs develop via transitional stages (i.e. pre-myelinating cells) to myelinating oligodendrocytes (OLs) ensteathing axons of neurons in the CNS by myelin. Whether OPCs also have the potential to develop into neurons and astrocytes *in vivo* is highly disputed (Tognatta et al., 2017; Zhu et al., 2012). However, OL-lineage cells interact with the other cell types in the CNS. Mature OLs need to communicate with axons to establish and remodel myelin sheaths, furthermore they have been shown to provide trophic support to neurons. Also the communication between OPCs and ACs has been reported, e.g. in the context of supporting OPC cell migration. Of special interest is the interaction of OPCs and neurons as this is suggested to be mediated not only by classical signalling molecules but electrical activity via neurotransmitter receptors. OPCs are abundant in the CNS as well as regionally and temporally diverse. However, it is still quite unclear how this heterogeneity would influence their function.

1.2 Discovery of OPCs and the Initial Investigation of Their Properties

In contrast to other cell types in the CNS, particularly neurons, whose investigation started much earlier, the discovery and description of OPCs just began in the late 1970s. One of the first studies describes them as oligodendroblasts, cells that underwent proliferation in the optic nerve and were morphologically distinct from but also having morphological features of mature oligodendrocytes revealed by electron microscope autoradiograms (Skoff et al., 1976). In 1983 two different types of astroglia, protoplasmic and fibrous ones, were described. Type II preferentially was found in white matter cell cultures and expressed markers of astrocytes like GFAP as well as bound the A2B5 antibody and tetanus toxin, considered back then as evidence for an at least partly neuronal identity (Raff et al., 1983a). Subsequent studies could show that type II astrocytes have a common A2B5+ progenitor with galactocerebroside-positive (GC+) oligodendrocytes, which differentiates preferentially into one or the other cell type dependent on cell culture conditions, whereas in the more *in vivo* like situation without serum more oligodendrocytes were generated (Raff et al., 1983a; Raff et al., 1983b). Then these cells became known as O-2A progenitors (A2B5+) for the following years (Raff, 1989; Temple and Raff, 1985). Furthermore, it could be shown that rat primary glial cells from postnatal cerebellum, which have the chondoitin-sulfate proteoglycan NG2 on their surface, are also bound by A2B5 antibody; hence, NG2 glia and O-2A progenitors are overlapping populations or even identical (Levine and Stallcup, 1987). Subsequently, these cells have been detected in the adult optic nerve first and then also throughout the entire developing and mature CNS (Nishiyama et al., 1999; Nishiyama et al., 1996; Wolswijk and Noble, 1989). In summary, oligodendroglial fate seem to be the natural (intrinsic) fate of O-2A progenitors whereas astrocytic fate is most likely an induced fate (Raff, 1989). Accordingly, the terminology changed more and more from O-2A progenitors to OPCs, whereas others preferred to refer to them as NG glia (Dawson et al., 2000).

O-2A cells cultured without serum differentiated prematurely to oligodendrocytes compared to the *in vivo* situation; this effect could be reversed by adding PDGF to the culture medium (Grinspan et al., 1990b; Noble et al., 1988; Raff et al., 1988; Richardson et al., 1988), which stimulated the proliferation of O-2A cells via PDGF receptors (Grinspan et al., 1990a; Hart et al., 1989a; Hart et al., 1989b). However, the effect of PDGF does not seem to be exclusively mitogenic but also influence survival. It was shown that in normal development approximately half of the oligodendrocytes in the optic nerve and about 20 % of the premyelinating cells in the cerebral cortex undergo cell death before progressing to maturation (Barres et al., 1992a; Trapp et al., 1997). The administration of PDGF increased survival and also OL number

tremendously, arguing for the competition for survival factors by oligodendroglia cells (Barres et al., 1992b). However, it is not clear if PDGF is indeed the endogenous survival factor or just mimics the effect of an alternative *in vivo* signal.

A similar situation applies to the proliferation of oligodendrocyte precursors. A seminal study could show that proliferation is significantly decreased after reducing electrical activity in neighbouring axons either by optical nerve transection or by tetrodotoxin (TTX), whereby the latter can be rescued by PDGF treatment (Barres and Raff, 1993). Again, although activity in axons might directly regulate the release of mitogens by neurons, or stimulate other glia to produce them – the authors suggested type I astrocytes – there is also the possibility that the proliferative effect is conveyed *in vivo* by other signalling mechanisms (e.g. neurotransmitters), and that PDGF administration simply produces a similar outcome. Conversely, in other studies the treatment of O-2A cells cultures as well as slice cultures with AMPA receptor agonists, which should increase neuronal activity, results in a reduction in proliferation and also differentiation (Gallo et al., 1996; Liu and Almazan, 1995; Yuan et al., 1998). Based on this evidence, that neuronal activity influences OPCs directly, in the 1990s research focused on how oligodendroglia interact with neurons. In particular, can OPCs respond to neurotransmitter signalling and if so, do they show specific responses otherwise typical for postsynaptic neurons? Indeed, O-2A glia progenitors express a subset of ion channels, including AMPA glutamatergic receptors and GABAergic receptors, and that oligodendroglia exhibit GABA- and glutamate-activated currents in the corpus callosum as well as in the hippocampus (Barres et al., 1990; Berger et al., 1992; Patneau et al., 1994). Blocking or enhancing electrical activity in neurons did also influence myelination (Demerens et al., 1996); as only the number of myelinating OLs but not the number of cells expressing OLs markers was significantly decreased, the conclusion of this study was that electrical activity influences only OL maturation but not proliferation nor differentiation, a finding which is in contradiction with aforementioned studies (Barres and Raff, 1993). Another impulse prime the way for recent and current research in this field was the discovery of neuron-OPCs excitatory synapses in the hippocampus, based on kinetics of measured AMPAR inward currents and electron microscopic evidence (Bergles et al., 2000).

Nevertheless, many questions how OPC behaviour is regulated to generate a functional population of myelinating oligodendrocytes remained. The upcoming sections will summarize the current state of knowledge and describe the experimental approach how experimental data presented in this work can contribute to answer open questions.

1.3 Lineage Identity of OPCs

Today it is widely accepted that OPCs *in vivo* almost exclusively differentiate into oligodendrocytes (Clarke et al., 2012; Kang et al., 2010). Only a small subfraction of astrocytes in the ventral forebrain of rodents had to be shown to be most likely derived from OPCs (Zhu et al., 2008; Zhu et al., 2011). This could depend on the finetuning of locally restricted signalling and gene regulatory networks. For example, treatment with BMP4 alone was shown to be sufficient to induce GFAP+ astrocytes in OPC cultures (Petersen et al., 2017). Recent studies found no generation of neurons from OPCs and proposed that false-positive findings could arise from the Cre reporter mice used for lineage tracing (Dimou et al., 2008; Tognatta et al., 2017).

The fate specification towards the OL-lineage and maintenance of OPC identity depends on the expression of a set of transcription factors (TFs). Among the most prominent players are Olig1/2, Sox TFs like Sox8, 9, and 10, and Nkx TFs like Nkx2.2, Nkx6.1 and Nkx6.2 (Kuspert and Wegner, 2016; Lu et al., 2000; Soula et al., 2001; Weider and Wegner, 2017; Xu et al., 2000). The interdependence and redundancy of these factors in regulatory networks make it difficult to assess the role of single factors certainly (Cantone et al., 2019; Kuspert and Wegner, 2016). Olig2 and Sox10 are the most used markers for OL-lineage cells being expressed in OPCs as well as OLs (**Figure 1.4.1**).

The loss of transcription factors like Olig2 can introduce fate switch from an oligodendroglial to an astrocytic fate (Zhu et al., 2012). Furthermore, given their role as progenitor cells in the CNS and several ambiguous reports that OPCs/NG2 glia also can differentiate into neurons (Guo et al., 2010; Rivers et al., 2008), there is still the idea that transdifferentiation can be induced *in vitro* and *in vivo* to achieve neuronal regeneration in the context of injury or neurodegenerative diseases (Heinrich et al., 2014). In a recent study, at least astrocytes could be reprogrammed to neurons, which integrate in the injured brain (Mattugini et al., 2019). There is also some evidence that OPCs can differentiate into myelinating Schwann cells in response to CNS injury, , (Assinck et al., 2017; Zawadzka et al., 2010). Actually, Schwann cells are the myelinating cells of the peripheral nervous system (PNS) and are not found in the CNS. This might require special conditions like the absence of (activated) astrocytes, the modulation of the BMP and JAK-STAT signalling pathways or a specific microenvironment found in the vicinity of blood vessels and defined as vascular niche (Monteiro de Castro et al., 2015; Talbott et al., 2006; Ulanska-Poutanen et al., 2018). However, the mechanism how Schwann cell remyelination in the CNS happen is still not well understood, also its functional role remains elusive; furthermore, how long Schwann cells can survive in the CNS is not clear.

1.4 Roles of OPCs in Developmental Myelination

Around birth OPCs are evenly distributed throughout the entire CNS. But also in the adult rodent CNS OPCs represent 2-8 % of the total cells dependent on the brain region, with a higher abundance of OPCs in the white matter regions compared to grey matter (Dawson et al., 2003). With their processes they build largely non-overlapping domains by which they tile the entire vertebrate CNS (Bergles and Richardson, 2015; Hughes et al., 2013; Kirby et al., 2006). It is still not clear how it is regulated that within the same region some OPCs progress to differentiation whereas others do later or do not differentiate at all.

As already outlined above OPCs are the most proliferative cell type in the CNS and their proliferative ability depends on mitogenic signals like PDGF and insulin/IGF (see **section 1.2**). Proliferation can be seen as a way to maintain the homeostatic distribution of OPCs throughout the CNS and to increase the pool of differentiation-competent cells. Furthermore, it has been suggested that there is a direct interdependent relationship between OPC proliferation and differentiation, i.e. that the decision about differentiation could be linked to the previous last cell division. In the postnatal mouse brain the majority of OPCs differentiate within few days following cell division (Hill et al., 2014; Zhu et al., 2011). Maybe OPCs are already primed to differentiate by an intrinsic programme started with cell division, comparable to neuronal progenitor cells, within which fate deterministic molecules are distributed asymmetrically during cell division. However, based on live imaging it seems that OPCs in the postnatal mouse brain divide symmetrically and only later one or other daughter cells progress to differentiation (Zhu et al., 2011). Alternatively, OPCs could be particularly susceptible to differentiation signals during a latency period subsequent to cell division. On the other hand, long-term live imaging in the adult mouse cortex revealed that OPC cell division is either not a prerequisite for differentiation or that this happens on a significant larger time scale than during development (Hughes et al., 2013; Hughes et al., 2018). To generalize the open question which cannot be answered by the previously published studies, it is still not clear to which extent the progression from OPCs to OLs is regulated by an cell intrinsic developmental programme or extrinsic factors present in the microenvironment.

All known important cell signalling pathways have been shown to be involved in OL-linage progression (Santos et al., 2018): In general, growth factor signalling via receptor tyrosine kinases, TGFβ signalling – both act via the PI3K/Akt/mTor or Ras/MAPK pathway – as well as retinoic acid (RA), thyroidal hormons like triiodothyronine (T3), sonic hedgehoc (SHH) signalling and neurotransmitters are usually found to

facilitate OPC differentiation in OLs. Whereas Notch signalling, Wnt signalling and BMP signalling are rather inhibitory and help to maintain the progenitor state. Especially, players of the Wnt pathway were investigated intensively in this regard (Fancy et al., 2009; Fancy et al., 2011b; Lang et al., 2013). Eventually, all pathways converge downstream to specific transcription factors which change the broader transcritomic state of the cell and are involved in larger regulatory networks. The following transcription factors have been shown to influence OPC differentiation directly positively or negatively: Olig1/2 (+), Ascl1 (+), Hes1/5 (-), Sox2 (+), Tcf4 (+/-), Sox5 (-), Yy1 (+), Myrf (+) and Nkx2.2 (+) (Kuspert and Wegner, 2016). However, dependent on the context most of these factors could have additional roles in lineage specification, proliferation and maintainance within the oligodendrocyte lineage. Furthermore, different transcription factors, especially of the same class, like Sox TFs, could have overlapping functions (Weider and Wegner, 2017). In addition, these processes are also regulated on an epigenetic level by changes of the chromatin conformation and the action of a set of miRNAs (Emery and Lu, 2015; Liu et al., 2016). Ambiguous results on the roles of certain molecules in OPC regulation could also arise from different experimental settings (e.g. *in vivo* vs. *ex vivo*, white vs. grey matter, postnatal vs. adult vs. remyelination, pharmacological vs. genetic intervention) and the assessed outcomes (e.g. number of OLs, amount of myelin, number of proliferation or differentiation events).

Based on the expression patterns of different sets of markers, different stages of progression along the OL-lineage were defined. Recognized by most researches is at least the distinction into OPCs, pre-myelinating OLs (pre-OLs) and myelinating OLs, whereas pre-OLs are the cells within the OL-lineage that differentiated already and hence lost their capacity of proliferation but have not established myelin sheaths yet (**Figure 1.1.1** & **Figure 1.4.1**).

Often morphology is also considered to assess the level of OL-lineage progression. Based on cell culture and few *in vivo* observations the model was proposed that early OPCs are simple cells with only very few processes. Then process length and ramification increases with maturation (Nishiyama et al., 1999). The pre-OLs are viewed as the OL-lineage cells with the most complex morphology. This follows the rationale, that the primary function of OPC processes is thought to contact myelination-competent axons and to explore sites for future myelin sheath initiation. However, not every axoglial contact will result in the formation of an myelin sheath and only appropriate axons become myelinated – a topic of ongoing research (Almeida, 2018). Hence, the more advanced a cell is in the lineage the greater is also its process network to achive a critical number of contacts with axons and to select the right sites for myelination. Theoretically, in an alternative scenario however, OPC and pre-OL processes which undergo pruning during

myelination could also have an alternative function than site selection for myelin sheaths, a function which might be not required anymore in mature OLs. For example, they could play a role in axogliacommunication via electrical signalling (see **section 1.6**).

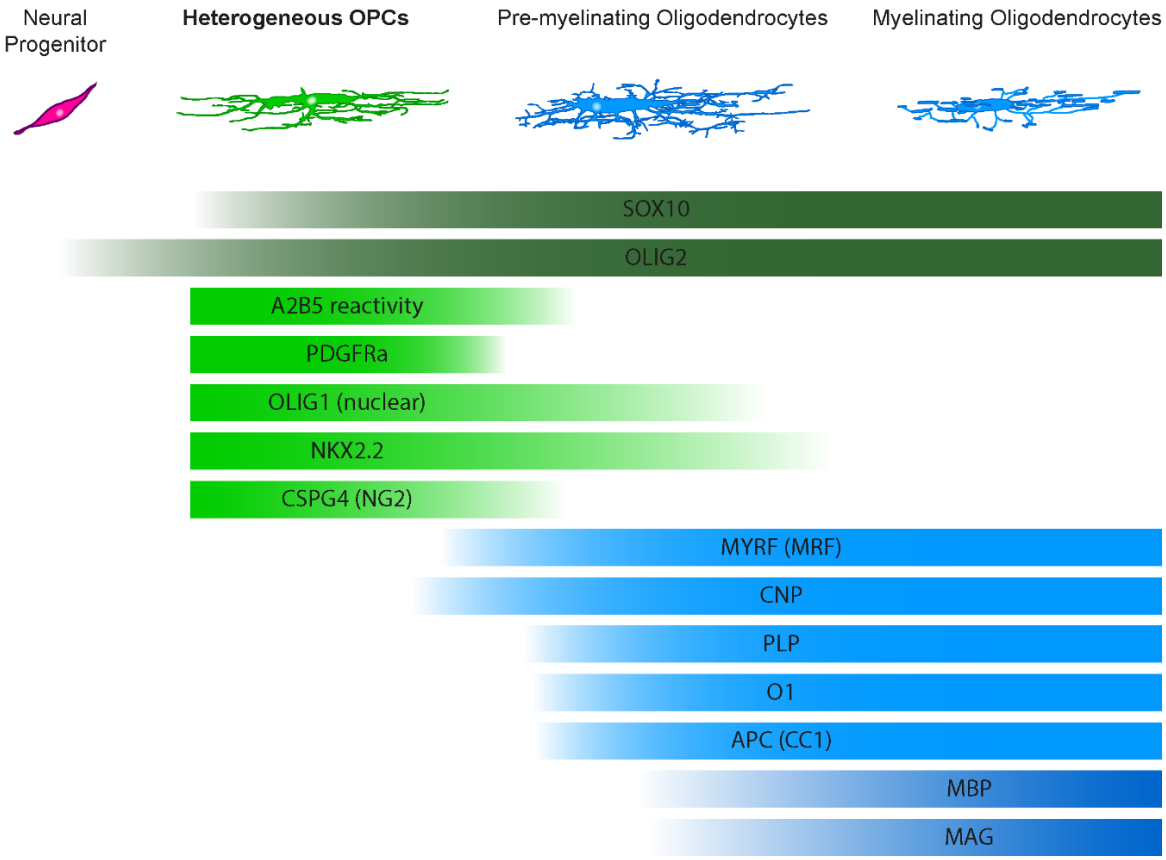

Figure 1.4.1 Marker expression in the oligodendrocyte lineage.

Overview of the most common markers used to characterize subpopulations within the OL-lineage. Some markers label all cells within the lineage (e.g. Sox10 and Olig1), whereas others label only phases in oligodendroglia development. However, as the transitional stages are not clearly distinct from each other, the same applies to the patterns of marker expression. Often a clear analysis of marker co-expression or exclusion has not been carried out; moreover, patterns of marker expression might depend on age, CNS region and experimental model (e.g. cell culture versus *in vivo* animal model). Especially species-specific expression differences, for example between human, mouse and zebrafish, are poorly understood (see section 3.3). The Figure is adapted from Fancy et al. (2011) and supplemented with data from additional publications (Fancy et al., 2011a; Lee et al., 2005; Levine and Stallcup, 1987; Raff et al., 1983b; Rowitch, 2004; Trotter and Schachner, 1989).

1.5 The Role of OPCs in Myelin Repair

Besides gaining general knowledge about nervous system function the paramount goal of research in this field is to develop therapies for conditions in which myelin is damaged or does not develop properly. For example, this can be caused by demyelinating diseases, especially Multiple Sclerosis, when myelin is attacked and destroyed by the patient's own immune system. But also in Alzheimer's Disease white matter loss is an early sign of disease (Behrendt et al., 2013; Butt et al., 2019; Svennerholm and Gottfries, 1994), which already could lead to deteriorated nerve conduction and signs of cognitive impairment. Also spinal cord injury or other types of traumatic injury to the CNS are accompanied with extensive myelin damage (Alizadeh and Karimi-Abdolrezaee, 2016; Simons et al., 2014). If ischemic stroke occurs in the white matter myelin and in consequence also the ensheathed axons are significantly affected (Aboul-Enein et al., 2003; Rosenzweig and Carmichael, 2015). In addition, inherited disorders clustered below the term leukodystrophies with an early onset often already in childhood are predominantly caused by failure of adequate myelination, for example Pelizaeus-Merzbacher disease which is associated to mutations in the PLP1 gene (Ashrafi and Tavasoli, 2017; Kevelam et al., 2016; van der Knaap and Bugiani, 2017; van der Knaap et al., 2019).

OPCs are abundantly found at sites of injury and demyelinating lesions (Hughes et al., 2013; Keirstead et al., 1998; Levine, 1994; Sim et al., 2002; Watanabe et al., 2002). This is in accordance with their role of giving rise to new OLs in response to injury and hence their importance for remyelination (Tripathi et al., 2010; Zawadzka et al., 2010). On the other hand, there are also studies showing a loss of OPCs at lesion sites especially in MS patients and presenting evidence that new myelin could be also generated by existing oligodendrocytes (Duncan et al., 2018b; Jakel et al., 2019; Yeung et al., 2019). Alternatively, a role of OPCs in wound healing independent of myelination is assumed (Hughes et al., 2013; Keirstead et al., 1998; Levine, 1994). However, it remains unclear if OPCs appear to be beneficial or detrimental in this context.

Despite new myelin is generated after demyelination, remyelination cannot be completely achieved in humans and rodent model organisms (Fancy et al., 2011a; Franklin and Ffrench-Constant, 2008; Osorio-Querejeta et al., 2017). Myelin wrapping in remyelination is usually thinner and myelination remains generally incomplete. Especially in large injuries or progressing demyelinating disease, remyelination finally fails which also results in axon damage and long lasting motoric and cognitive deficits, respectively (Franklin, 2002). Functional recovery is often not achieved or remains incomplete.

Enhancing the proliferation of OPCs or transplantation of these cells after myelin damage would be a strategy to increase the availability of myelination-competent cells in the injured tissue (Keirstead et al., 2005). Moreover, the direct stimulation of endogenous OPC differentiation and maturation appear promising to improve remyelination in this context, for example by using drugs like Clemastine and interfering with relevant signalling pathways (Deshmukh et al., 2013; Huang et al., 2011; Patel and Klein, 2011; Wang et al., 2018a). Several approaches have been tested successfully, but they still need to prove their value in the clinical setting.

Most of *in vivo* research in this field is carried out using models of adult animals as this resembles more the situation in patients. However, it is also especially important to understand the mechanism of OPC differentiation during development as it is going to be presented in this thesis to use this knowledge to facilitate the development of remyelinating therapies.

1.6 Axon-OPC Interaction via Electrical Signalling

An important aspect to understand the functionality of OPCs is to consider how they communicate with neurons. A large body of work has been published to establish that OPCs indeed respond to neuronal activity signalling and even have GABAergic and glutamatergic synapses (Bergles et al., 2010; Bergles et al., 2000; Jabs et al., 2005; Lin and Bergles, 2004a). AMPA receptors, NMDA receptors as well as voltage-gated Na^+ channels have been described in OPCs (De Biase et al., 2010; Karadottir et al., 2005). However, the functional consequence of this signalling mechanism remains still ambiguous (Kula et al., 2019). There are two prominent hypotheses how neuronal signalling would have an impact on OPCs.

The first idea considers OPCs as subunits in neuronal networks. The overall experimental evidence for this idea is sparse until now. At least, three studies described the detection of action potentials in OPCs (Chittajallu et al., 2004; Ge et al., 2009; Karadottir et al., 2008). Given the known roles of action potential-firing neurons this would suggest a function of spiking OPCs in signal conduction and long-term potentiation involved in neuronal plasticity. One study even found that neuron-OPC synapses undergo a process similar to long-term potentiation involving glial AMPA receptors (Ge et al., 2006). On the other hand, it is quite clear that OPCs do not have axons and there is also no proper evidence that OPCs can function as a pre-synapse. Moreover, action potential signalling in OPCs was disputed by other electrophysiology studies (De Biase et al., 2010).

Instead it is suggested that neuronal activity in OPCs regulate ion transport rather than leading to depolarization and axon potential transmission (De Biase et al., 2010; Lin and Bergles, 2004b). In particular, the intracellular calcium level could be affected, which is involved in many cellular signalling pathways through the activation of calcium-binding proteins. The general idea is that sensory input from the environment elicits electrical activity in axons in the CNS that are in contact with OPCs; neuronal activity regulates processes like OPC proliferation, migration, differentiation and maturation, which allows adaptive myelination in favour of these active axons and hence improves signal conduction in these axons (de Faria et al., 2018; Fields, 2015). This mechanism is of special interest as it represents a discrete additional level of neural plasticity conveyed by glial cells. Supporting this notion, glutamate vesicles can be released not only at axon terminals but also along the axon – at sites of prospective myelination – to signal to receptors on OPCs (Kukley et al., 2007; Ziskin et al., 2007). Alternatively, myelination on demand could also be a way to deal with cellular resource efficiency, as myelin is only produced where it is required.

What is the actual evidence that neuronal activity can influence the behaviour of OPCs? First, pharmacological blocking of voltage-gated sodium channels as well as nerve transection impairs the proliferation of cells which are most likely OPCs in the developing optic nerve (Barres and Raff, 1993). Other studies were molecularly more specific: the majority concentrated on the influences of glutamatergic signalling on OPCs (but also OLs) and how it is mediated by AMPA and NMDA receptors; only few studies considered the role of the neurotransmitters GABA and ATP (Hamilton et al., 2017; Wake et al., 2011; Zonouzi et al., 2015). In contrast to the first mentioned study, subsequent *in vitro* work using cell and slice cultures reported a decrease in proliferation and differentiation after pharmacological stimulation of AMPA receptors (Gallo et al., 1996; Liu and Almazan, 1995; Yuan et al., 1998). Also, more recent *in vivo* studies could not resolve these ambiguities. Electrical stimulation via an implanted electrode in the adult spinal cord increased the proliferation and differentiation of OPCs in downstream regions (Li et al., 2010), whereas monocular deprivation leading to an assumed decrease in neuronal activity increased the differentiation in the optical nerve and leaves proliferation rates unaltered (Etxeberria et al., 2016).

Blocking synaptic vesicle release either in OPC-neuron co-culture or in larval zebrafish *in vivo* resulted in reduced myelination by individual OLs and per axon (Hines et al., 2015; Mensch et al., 2015; Wake et al., 2011). However, in this context synaptic vesicles most likely regulate myelination at the level of myelin sheath establishment and do not influence OPCs directly, as their cell numbers were not altered by the manipulations in all three studies. The actual mechanism how the cells responds to vesicle-released

neurotransmitters is not clear. Even though it depends on glutamate and results in intracellular calcium rise, at least in cultured cells it does not require synaptic contact as neither PSD-95 immunoreactivity was detected nor AMPAR-mediated currents were measured (Wake et al., 2011; Wake et al., 2015). Furthermore, the same studies reported increased local MBP translation after electrical stimulation of vesicle-releasing axons (Wake et al., 2011; Wake et al., 2015). Together these studies provide evidence, that indeed electrically active axons are preferentially myelinated.

Even though a role of neuronal activity is rather undisputed, the role of AMPA glutamate receptors is quite controversial. A study carried out with slice cultures found that blocking activity or AMPA receptors increased proliferation and differentiation of OPCs, displayed by a higher abundancy of CC1+ cells among the OL-lineage cells, but conversely reduced the amount of myelination (Fannon et al., 2015). In another study, the block of AMPAR did not affect Sox10+ OL-lineage cell number or myelination in organotypic slice cultures (Hamilton et al., 2017). Which however, is at least partly in conflict with results from the same group; when they did knock out AMPARs *in vivo* (Kougioumtzidou et al., 2017), although proliferation was not changed, myelination was reduced moderately as less cells survived or matured to myelinating OLs, respectively. However, another study using genetical alteration of AMPAR found that proliferation and differentiation could be affected with opposing effects (Chen et al., 2018). Inversely, for the role of NMDA receptors in neuron-glia signalling, genetic interference by ablation of the NR1 subunit did not have a significant effect on OPC behaviour or myelination (De Biase et al., 2011; Guo et al., 2012). In line with these finding NMDAR blocking did not alter proliferation, differentiation or morphology of OPCs in cerebellar slice cultures (Fannon et al., 2015). Another paper suggests an interesting mechanism for NMDAR function in OL-lineage cells, distinguishing between a NMDAR-independent mode of myelination and a NMDAR-dependent mode which can be induced *in vitro* by neuregulin and BDNF (Lundgaard et al., 2013). However, the impaired remyelination *in vivo* observed after administration of the NMDAR blocker MK-801 to the lesion site must not be necessarily caused by an effect on OPCs. Further studies are required to figure out which hypotheses hold true and which reports were rather observations of indirect effects produced by compensational mechanisms, feedback regulation, artefacts, or redundancy.

Interestingly, synaptic input is reduced as well as the expression of ionotropic receptors and ion channels is significantly downregulated when OPCs differentiate into OLs (De Biase et al., 2010; Etxeberria et al., 2010; Kukley et al., 2010), suggesting that synaptic communication is dispensable for mature OL function. The kinetics of this downregulation are not completely clear. It is possible that pre-OLs are still capable of

using this signalling mechanism while they initiate myelin sheaths. Alternatively, if synaptic structures are already dysfunctional another mechanism must translate axonal signals into an OL response.

The picture becomes clearer if one looks on the broader picture uncoppled from the regulation of certain molecules or genetic networks. Several studies used experience-driven neuronal input to test the effect on OL-lineage cell numer and myelination. Social isolation of mice at a young age can result in abnormal behvaior but also in altered myelination in the prefrontal cortex reflected by different g-ratios and a decrease in internodes per oligodendrocyte compared to controls (Makinodan et al., 2012). Social isolation of adult mice also influences chromatine remodelling and gene expression leading to impaired adult myelinination (Liu et al., 2012). In this line, by preventing OPC differentiation and maturation by conditionally deleting myelin regulatory factor (myrf) mice were prevented from learning to master a complex wheel running task (McKenzie et al., 2014; Xiao et al., 2016). Similar results was also obtained in a spatial learning paradigm (Steadman et al., 2019).

But also successful gain-of-function experiments has been reported: Motor skill learning required to perform a skilled reaching tasks has been shown to be associated with changes in the white matter in the murine brain detected by MRI imaging and are most likely caused by learning-induced myelination increase (Sampaio-Baptista et al., 2013). Direct optogenetic stimulation of neurons in the premotor cortex results in increased proliferation, differentiation and maturation of OPCs which can be even detected in the subcortical white matter (Gibson et al., 2014). Sensory enrichment can directly lead to an increase in the formation of new mature OLs in the adult mouse somatosensory cortex (Hughes et al., 2018).

Hence, adaptive myelination is a way how environmental cues can alter neuronal circuits and thus represents an additional layer of neur(on)al plasticity implicated in learning and memory formation. Signals must be conveyed through neuronal activity to reach the OL-lineage cells in the CNS. However, how this functions exactly on a molecular and cellular level and whether there are differences regarding the kind and pattern of sensory input or the reception by target cells, respectively, needs to be further studied.

1.7 Evidence on Heterogeneity of OPCs/in the OL-Lineage

As outlines above, OL-lineage cells are abundantly found in the postnatal CNS at any age. In white matter regions they even represent the vast majority of cells. Given the described heterogeneity of neurons classified by morphology, signalling properties and neurotransmitter specificity, but also of other glial cells like astrocytes (Oberheim et al., 2012), it is highly likely that there is also a degree of heterogeneity within the OL-lineage. The peculiarity of this lineage is the high frequency of progenitor cells which can be found still in the adult CNS (Dawson et al., 2003). Hence, when examining OL-lineage cells, characterized for example by the common expression of Sox10 and Olig2, there is always a mix of OPCs and myelinating OLs and the transient states in between. Thus, heterogeneity between OL-lineage cells would not necessarily reflect functional heterogeneity but also could be developmental heterogeneity along lineage progression. However, given the occurrence of these cells in different brain regions, the spinal cord and the optic nerve, which also show differences in their myelination pattern, there is the hypothesis that OL-lineage cells also show functional heterogeneity to some extent. An interesting aspect in this regard is, if diversity would be encoded intrinsically or rather extrinsically induced by the different microenvironments in different regions. That this topic is of general interest in the field of glial cell research can be also seen by the number of review articles addressing particularly oligodendroglial heterogeneity within the last years (Dimou and Simons, 2017; Foerster et al., 2019; Hill and Nishiyama, 2014; Vigano and Dimou, 2016).

In the following, I will give a brief overview summarizing the most prominent evidence for oligodendroglia heterogeneity with a focus on OPC heterogeneity, as this will also be the focus of the experimental work presented in this thesis.

1.7.1 Heterogeneity in Gene Expression

The rise of single-cell RNA-sequencing (scRNA-Seq) technology and its application during the recent years fostered extensively the investigation of transcriptomic differences of cell populations or sub-populations through the possibility to analyse all transcribed genes at once. Many of these studies include also OL-lineage cells (van Bruggen et al., 2017). A seminal study was performed with cells sampled from 10 different regions of the juvenile and adult mouse CNS (Marques et al., 2016). Twelve different clusters comprising OL-lineage cells were found which differ regionally in abundancy but are not exclusively found in single regions. Six transcriptomically distinct types of mature myelinating OLs were found provoking the hypothesis that there could be functional differences between them. The other six clusters represent

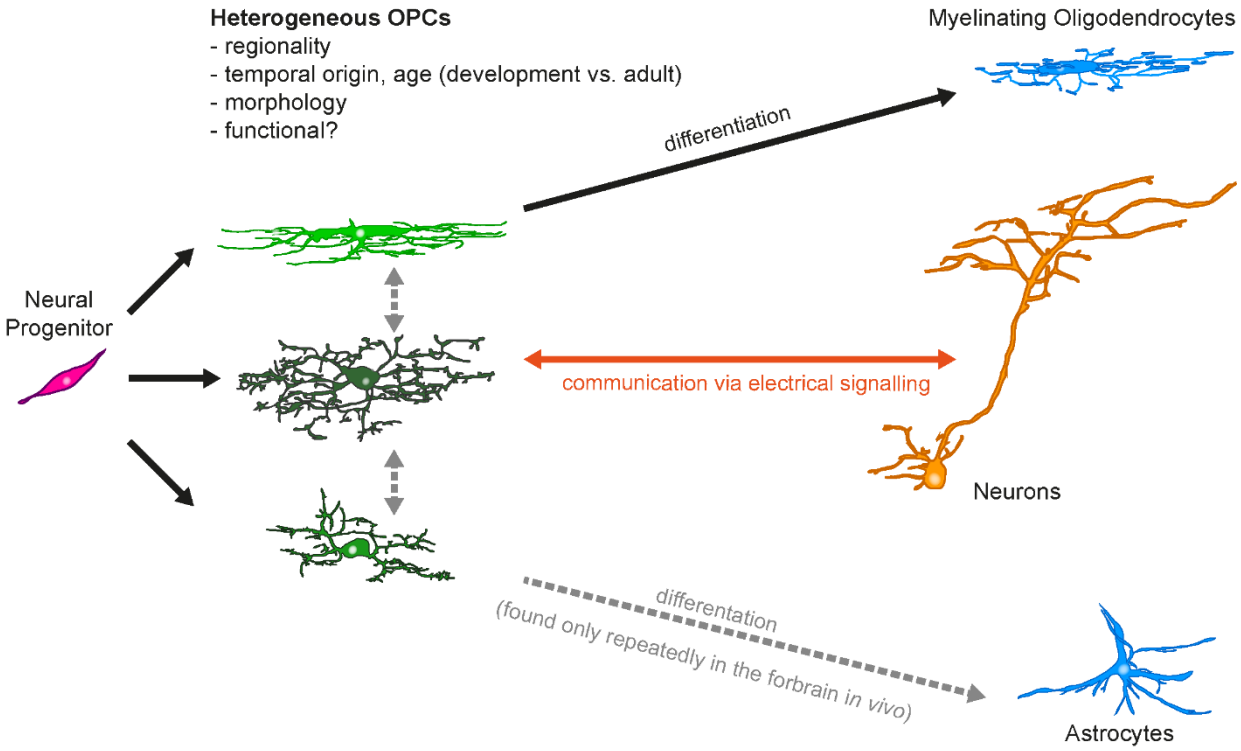

Figure 1.7.1 Cartoon showing how heterogeneous OPCs could convey different functions.

There is accumulating evidence that OPCs can have different properties dependent on their location, origin, morphology, and molecular characteristics (see below). In addition, distinct functions have been assigned to the OPC population or to parts of it. However, how heterogeneous this population is in a certain context (e.g. region) is not clear. Moreover, the contribution of individual cells has not been investigated in detail. Subtypes of OPCs could have different functions (depicted); in opposition to the idea that every OPC can fulfil every function assigned to OPCs (**Figure 1.1.1**). If subtypes exist, it would be of interest to know if they represent distinct sub-lineages or if a cell can transform from one into the other.

---

diversity along lineage progression. Only one type of OPCs was found, however an additional cluster called committed oligodendrocyte progenitors (COPs) could still be considered as OPCs. COPs still express low levels of cell cycle genes but lost typical OPC markers like *pdgfra* and *cspg4* expression and upregulated some other markers like *gpr17*. However, in accordance with their characterization as a transitional cell type COPs express only markers found also at some level in OPCs or OLs (**Table 1.7.1.1**). The same group then published a study focused particularly on OPCs including cells from the brain and the spinal cord at different ages (Marques et al., 2018). Based on their observation that the diversity of neural progenitors which give rise to OPCs as well as the diversity among OLs is much higher compared to the diversity within

OPCs, they conclude that OPCs are transcriptomically homogeneous and even represent a state of lineage convergence. Even though, based on the limited differences the authors described three subclusters of OPCs. The expression of cell cycle genes had a relatively high effect and defines one OPC subcluster. The origin at different times of development did not cause greater differences between OPCs in this study, although whether cells were obtained from P7 or juvenile adult tissue played a role to some extent. They hypothesize that one subtype might be more incorporated in the network with neurons but did not provide further proof.

In a further study a group including the same researchers also found disease specific transcriptomic profiles of OL-lineage cells, mainly oligodendrocytes, and a distorted distribution of cells between the different clusters in the mouse EAE model and human MS patients (Falcao et al., 2018; Jakel et al., 2019). Interestingly, in the EAE situation OPCs were clearly distinct from the healthy control OPCs and even constituted own clusters, whereas OPCs and COPs in the MS patients were molecularly more similar to their counterparts in the healthy individuals, however were reduced significantly in number and were only infrequently found in MS lesion and normal appearing white matter (NAWM). Another single-cell RNA-Sequencing study using a similar approach found pri-OPCs besides classical OPCs. Pri-OPCs are thought to be primitive or early OPCs characterized also by a lower expression level of classical OPCs markers *pdgfra* and *cspg4* and expression of stemness genes (Weng et al., 2019).

ScRNA-Seq has been already performed in the zebrafish CNS (Cosacak et al., 2019; Raj et al., 2018). One study combined the technique with large-scale lineage tracing by CRISPR-Cas9 barcode editing and found three OL-lineage cells clusters comprising OPCs, immature OLs and myelinating OLs (Raj et al., 2018).

As the method is quite new, it is not trivial to interpret differences reported by different studies as they could account to the cells used as input, sequencing method, used data analysis algorithms or which significance levels or thresholds were set to obtain the final results of a particular study. Taken together, gene expression patterns in OPCs seems to be relatively similar and differences restrict mainly to states along lineage progression. However, it is not clear which number of genes must be differently regulated between two subpopulations of cells or two individual cells, respectively, to result in different properties or functions. Knowing gene expression patterns can be a hint for certain cellular behaviours as these are associated with specific gene regulatory networks, but this does not replace actual phenotypic investigation of the cells of interest. So far, most of the studies using scRNA-Seq or other methods to obtain large scale gene expression data do not complement these data with methods to determine whether the identified subgroups of cells are also morphologically and functionally different.

Table 1.7.1.1 Differential gene expression in murine OPCs and COPs according to Marques et al. (2016).

	OPCs	COPs
Pdgfra	high	low
Cspg4 (NG2)	high	low
Gpr17	medium	high
Bmp4	medium	high
Fyn	medium	high
Tcf7l2	low	high
Etv6	low	high
Mpzl1	low	high

1.7.2 Functional Heterogeneity: Proliferation and Differentiation

First, even though it is acknowledged today that endogenous OPCs almost exclusively differentiate in OLs, very few cells seem to have the potential to differentiate into astrocytes, however this might be restricted to the grey matter in the ventral forebrain (Weng et al., 2019; Zhu et al., 2012). Nevertheless, likely OPCs exists that are diverse in their potency even *in vivo* (**Figure 1.7.1**).

But differences between OPCs with implication on their differentiation in OLs also have been reported. During mouse development it was shown that OPCs originate in three competing waves in the brain and at least two waves in the spinal cord (Kessaris et al., 2006). Thereby, OPCs that derived from neural progenitors of the dorsal SVZ have a greater differentiation potential compared to their ventral counterpart. In the spinal cord in particular, even as corticospinal and rubrospinal tracts were initially myelinated by ventrally derived OPCs, during postnatal development dorsally derived OPCs outcompete them and the former almost completely disappear (Tripathi et al., 2011). This indicates that even in the same environment dorsally derived OPCs must have an intrinsically encoded advantage regarding myelination. Lastly it was shown that dorsally derived OPCs in the spinal cord and corpus callosum also have a greater proliferation and differentiation potential in response to remyelination (Crawford et al., 2016). However, these studies only investigated populations of cells and did not look into how individual cells contribute to these observations.

PDGF signalling via PDGFR is a key mitogenic signalling pathway in OPCs (see **section 1.2**). However, it was shown that OPCs in the postnatal cortical white matter proliferate more frequently in response to PDGF compared to grey matter OPCs (Hill et al., 2013). This is in accordance with previous reports that OPCs in the grey matter but not in the white matter are mostly postmitotic (Dimou et al., 2008). Moreover, transplantation experiments revealed that OPCs in the cortical white matter also differentiate more

frequently regardless whether they derive from grey or white matter; however transplanted white matter OPCs are already primed intrinsically or by their tissue of origin and maintain their differentiation potential even in the grey matter microenvironment, whereas grey matter OPCs show a low differentiation rate in the grey matter as expected (Vigano et al., 2013). Furthermore, lineage-tracing revealed that OPCs that expressed GPR17 progress less frequently to become oligodendrocytes in relation to the entire OPC population; however they can rapidly differentiate in response to CNS damage (Vigano et al., 2016).

It remains an unanswered question why these functional properties are not reflected by the transcriptome of OPCs (Marques et al., 2018).

1.7.3 Functional Heterogeneity: Integrating Neuronal Activity

There is also evidence that OPCs could be different regarding their electrophysiological properties. OPCs in cortical grey matter and subcortical white matter are distinct by their potassium and natrium channel expression profiles measured by whole-cell patch-clamping (Chittajallu et al., 2004). In the aforementioned study which reported action potentials in rat white matter OPCs, these action potentials restrict only to a subset of measured OPCs (Karadottir et al., 2008).

A recent study determined the distribution and density of ion channels implicated in neuroglia communication like AMPARs, NMDARs, voltage-gated sodium (Na_V) and voltage-gated potassium channels (K_V) and could confirm the existence of regionally different channel expression profiles in four different regions (cortex, cerebellum, corpus callosum and subventricular zone) of the postnatal, juvenile and adult mouse brain. In addition, these profiles increasingly diversify with age (Spitzer et al., 2019). There might be also a relationship between ion channel expression and OPC function since Na_V channel density correlates with proliferation and NMDA receptors with differentiation rate and myelination. Expression of the latter declines also when myelination potential of OPCs declines in older mice. Interestingly, the same group reported also a difference between NMDAR-dependent and -independent myelination (Lundgaard et al., 2013), whereas other studies found no significant effects of signalling via NMDARs on OPCs in general (see **section 1.6**).

1.8 Research Question and Experimental Approach

As outlined above the general mechanisms which pathways and environmental factors influence lineage specification, proliferation and differentiation of OPCs as well as the maturation of non-myelinating pre-OL into mature myelinating OLs have been already investigated (see **section 1.4**). However, the emerging picture is not completely clear and open questions remain. For example, why do some OPCs progress to differentiation whereas others within the same region do not and remain OPCs for long-term? Does it depend on an intrinsically activated lineage progression programme or is it controlled by the microenvironment extrinsically? Can the very same OPC that have synaptic contacts with neurons can also have the potential to differentiate (Dimou and Simons, 2017)? In this regard, it is also not known if the observed heterogeneity between OPCs reflects distinct subtypes of cells within a bifurcated lineage tree or just defined states along linear lineage progression. Then, of course, it would be more likely to observe differentiation of cells that progressed the lineage already further. Are OPCs that do not differentiate for a long time just hold in an earlier developmental state or did they differentiate in another subtype likely also with another function?

What is missing so far to shed more light on these open questions are comprehensive analyses at the level of individual cells and over time. One step in this direction was done already with the application of single-cell RNA-Sequencing for OL-lineage cells (Marques et al., 2018; Marques et al., 2016). However, usually this is just a snapshot of the transcriptome, and the relationship between identified clusters is not fully clear (see **section 1.7.1**). At the moment, analysis of transcriptomic data only is not sufficient. Live imaging using suitable models could allow for the observation of individual cells over time to determine their fate and their relationship to other types and subtypes of cells. In addition, one can make advantage of additional observations generally acquired by microscopy like cell morphology and marker (co-)expression.

I present an integrative approach to investigate OPCs in the developing zebrafish *Danio rerio*, a widely used vertebrate model organism. Working with zebrafish allows an easy and fast genetic manipulation to achieve the labelling of cells of interest with fluorescent proteins (**Figure 3.1.1**). As the young zebrafish is translucent, it is the ideal model to perform high-resolution confocal imaging of labelled OPCs in an *in vivo* environment, which makes it possible to observe individual cells as well as their morphology and subcellular processes. Confocal imaging is a 3D imaging technique and hence enabled me also to determine the position of the OPCs within the tissue, in case of this work the spinal cord of the zebrafish. As the imaging itself is non-invasive, repeated imaging over longer periods of several days was possible.

Furthermore, the genetically labelled OPCs could be isolated using FACS sorting and used for single-cell RNA-Sequencing to obtain also molecular data of the imaged cells. The main interest of this work was to reveal heterogeneity within the OPC population on the single cell level regarding several cellular properties with an emphasis on fate, and to investigate how subgroups of OPCs relate to each other as well as to other cells within the OL-lineage.

To complement the obtained data also with information on how OPCs respond to neuronal activity, which might be very important to shape OPC properties and function, colleagues of mine performed calcium imaging in OPCs and used pharmacological and genetic approaches to change neuronal activity *in vivo* or to manipulated electrophysiological properties of the OPCs. These data have been published along with the data presented in this thesis (Hoche et al., 2019; Marisca et al., 2020). This allows an even more comprehensive view on OPC dynamics in the developing zebrafish as it is considered in detail in the discussion (see **section 4.2**).

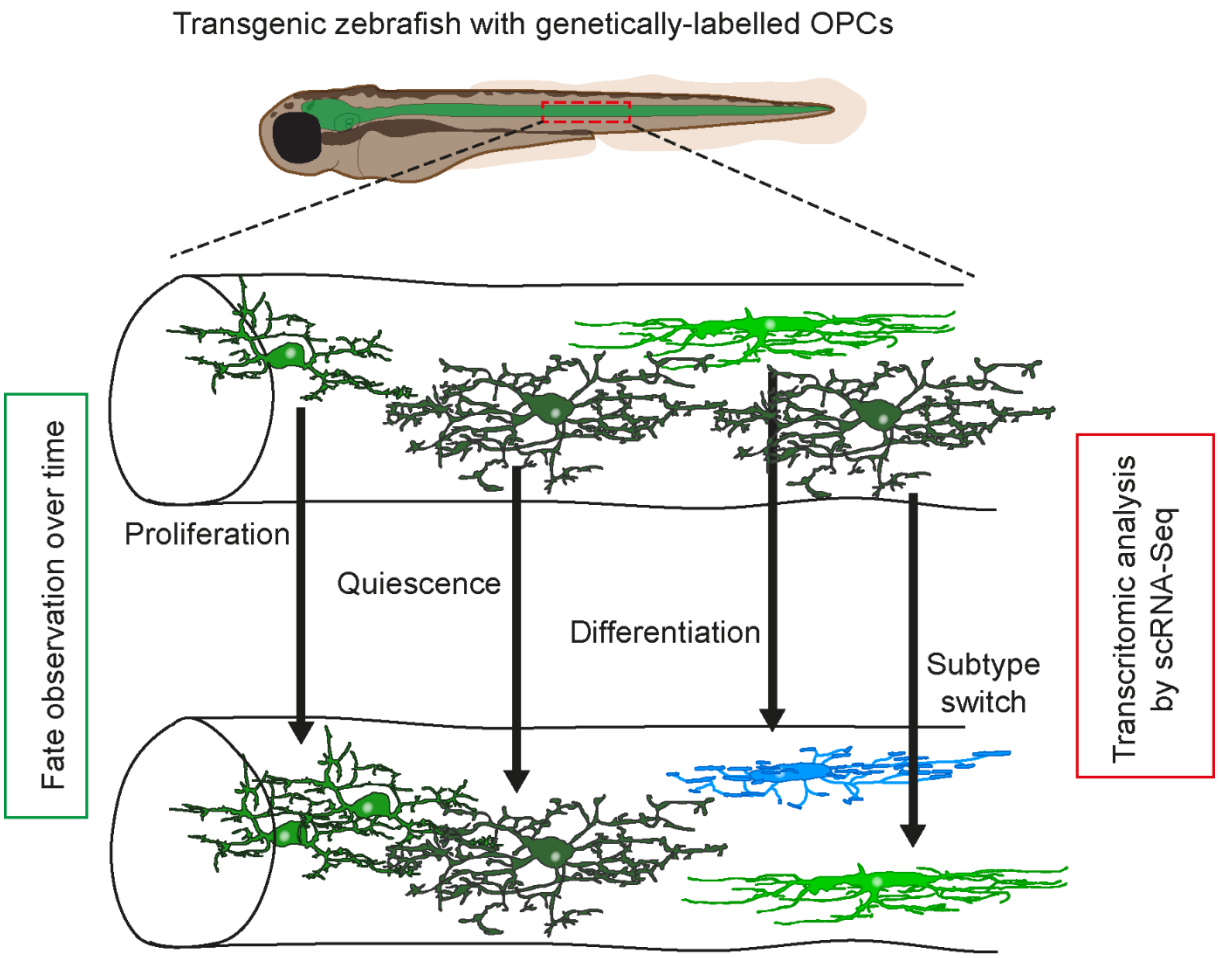

Figure 1.8.1 Cartoon showing how the observation of individual OPCs over time can be achieved.

This is in particular feasible in zebrafish due to their translucency at early age. The cells of interest express fluorescent proteins to become traceable over time through sessions of repeated imaging. This allows to assess individual cell behavior like proliferation and differentiation and how this is related to other visible properties of the cells.

2 METHODOLOGY

2.1 Experimental Methods and Materials

2.1.1 Transgenesis Constructs

The Gateway Cloning System (Invitrogen) was used in combination with regents of the Tol2kit (Kwan et al., 2007) to generate pTol2 expression constructs which drive the cell type-specific production of fluorescent proteins in zebrafish. Gateway cloning uses a modular approach allowing for the recombination of three special entry clones (p5E 5' entry clones, pME middle entry clones and p3E 3' entry clones) with an expression backbone (pDestTol2_pA) by LR clonase to obtain one expression clone (pTol2).

The entry clone **p5E_olig1(4.2)** has an incorporated genomic sequence of 4.2 kb upstream of the *olig1* gene which contains the regulatory element(s), i.e. the promotor, of the gene. This construct was generated in our laboratory and was published previously (Auer et al., 2018). The introduction of the genomic sequence in the vector was achieved by a restriction enzyme-based approach by Dr Tim Czopka. Alternatively, I amplified genomic sequences of different length from the *olig1* gene upstream region using PCR. The rationale behind was, that the likelihood to contain the complete upstream regulatory elements of the *olig1* gene increases with fragment length, however, at the same time the likelihood of genome integration decreases. Sequences for the primers used successfully are listed in **Table 2.1.1.1.** Then the PCR fragments were integrated in pDONR221 vectors using the BP clonase catalysed recombination reaction of the Gateway Cloning System. The resulting **p5E_olig1(3.2)** vector was functional to recombine in a LR reaction together with pDestTol2_pA, p3E_pA (Kwan et al., 2007) and different middle entry plasmids (pME) to generate pTol2 expression vectors driving fluorescent protein expression under the control of the genomic *olig1(3.2)* sequence. Even though there was no functional difference between the two different *olig1* p5E clones, in almost all experiments the *olig1(4.2)* fragment-driven expression constructs was used (in the following referred to as olig1 only, e.g. pTol2_olig1:memEYFP).

The pTol2 expression vectors were injected into fertilized zebrafish eggs for genomic integration and hence expression of the construct. The expression vectors pTol2_**olig1:KalTA4**, pTol2_**olig1:nls-mApple** and pTol2_**olig1:nls-Cerulean** (see also **section 3.1.1**) were also generated by a multisite LR recombination reaction using the additional entry clones pME_KalTA4 (Almeida et al., 2011), pME_nls-mApple and pME_nls-Cerulean (Tol2kit v2.0, unpublished). The expression plasmid pTol2_**olig1:memEYFP** and pTol2_**cntn1b:mCherry** were described previously (Auer et al., 2018; Czopka et al., 2013).

Table 2.1.1.1 Primers used for molecular cloning.

Primer	Sequence
attB1R_olig1_REV1	GGGGACTGCTTTTTTGTACAAACTTGctgaaaaaagatattcagagaacatgg
attB1R_olig1_REV2	GGGGACTGCTTTTTTGTACAAACTTGTTTCAGTCCGCAAACTCCAGAT (then the fragment is 360 bp shorter)
attB4_p_olig1_3.2kb_F	GGGGACAACTTTGTATAGAAAAGTTGAGCTGGGTTATTACAATCCAAATGT

2.1.2 Zebrafish Lines and Husbandry

All animals were kept at 28.5 °C with a day-night cycle (14 h of light and 10 h of darkness). Animal husbandry and experiments were according to the regulations as approved by the local authorities.

Wildtype animals used for these experiments were of the strains AB and nacre. The following used transgenic zebrafish lines were published previously: **Tg(mbp:nls-EGFP)** (Karttunen et al., 2017), **Tg(mbp:EGFP-CAAX)**^{ue2Tg} (Almeida et al., 2011), **Tg(mbp:memCerulean)** (Auer et al., 2018). The following transgenic lines were established for this work: **Tg(olig1:KalTA4)**, **Tg(olig1:memEYFP)**, **Tg(olig1:nls-Ceruelean)** and **Tg(olig1:nls-mApple)**. These lines were also recently published by us (Hoche et al., 2019).

To generate these lines, 1 nl of pTol2 expression plasmids (5-20 ng/µl DNA), Tol2 transposase mRNA (25-50 ng/µl) and 10 % Phenol red (Sigma Aldrich) were injected in zebrafish embryos at the one-cell stage (fertilized eggs, respectively). This results in genomic integration and sparse mosaic labelling of individual cells in the injected fish. For olig1-labelled OPCs the screening was usually carried out at early 3 dpf. These fish can be used already experimentally for the analysis of individual cells, i.e. to assess their morphology and dynamical behaviour over time. For the establishment of transgenic lines, the construct needs to be transmitted successfully to the germline. To test for this, labelled animals of the founder generation (F0) were raised to fertility and outcrossed to wildtype fish. The resulting offspring generation (F1) was screened again for transgene expression which is an indicator for germline transmission. Positive F1 animals could be used for further incross breeding to generate the F2 generation. Fish of the F2 generation and following generations, which had transgene expression, are considered full-transgenic animals, and could be used for population analysis of the respective cells of interest.

The advantages of embryonic and larval zebrafish as a model organism for biological experiments has been introduced above (**section 1.8** and **2.1.4**). Embryonic zebrafish usually hatch at two days after fertilization (2 dpf) from the surrounding chorion and are already motile. Until 5 dpf they feed from the nutrients stored in the yolk sack. Then they enter the larval stage and start to take up food actively and even catch prey like paramecia.

2.1.3 Zebrafish Mounting for Live Imaging

Embryonic and larval zebrafish between 2 and 28 dpf were anaesthetized with 0.2 mg/ml Tricaine mesylate (also known as MS-222; PHARMAQ) in Danieau's buffer and mounted laterally in 1 % ultrapure low melting point (LMP) agarose (Invitrogen) on a glass coverslip or in a glass bottom Petri dish suitable for imaging (Greiner CELLview™). In the first case, the coverslip was then flipped and fixed to a glass slide using high-vacuum grease. A drop of Danieau's solution (with 0.2mg/ml MS-222) was added on top of the agarose to prevent it from drying. If mounted in a Petri dish the dish was filled also with Danieau's buffer containing MS-222 (0.2mg/ml). After imaging the fish were cut out from the agarose using microsurgery scalpels and kept for following image acquisitions, or fish were sacrificed by continuing MS-222 incubation.

2.1.4 Confocal Live Imaging

The embryonic and larval zebrafish is the ideal subject for confocal live imaging due to its external development which is quite fast (compared to humans), the small size, the comparatively simple CNS despite it is still a vertebrate animal, and its optical translucency. Furthermore, a variety of genetic tools are available (Czopka and Lyons, 2011).

To image cells in zebrafish larvae in three dimensions (3D) either one of two Leica TCS SP8 confocal laser scanning microscope (CLSM) was used. As individual OPCs can cover the whole diameter of the developing zebrafish spinal cord, in laterally mounted fish usually the whole depth of spinal cord was imaged (approximately 40-50 µm). Most of the confocal images were acquired as 12-bit z-stacks images with a pixel size of 114 nm (x/y dimension) and a z-spacing of 1 µm using a 25x, 0.95NA water immersion objective. In addition, a 10x, 0.4NA air objective (voxel size 568 nm x 2µm) was used if a larger field of view was required. I used 448 nm and 458 nm wavelengths for excitation of Cerulean fluorescent protein, 488 nm for EGFP, 488 nm and 514 nm for EYFP, 552 nm and 561 nm for mApple and mCherry, and 633 nm for BODIPY (Thermo Fischer). Confocal time lapse imaging was done with an 8 kHz resonant scanner to reduce phototoxicity and to follow cell process motility. If this was not required also a conventional Galvo scanner was used. Unless stated otherwise, all *in vivo* images shown are lateral views of the zebrafish spinal cord for which anterior is oriented to the left and dorsal to the top of the image.

For repeated imaging of individually olig1:memEYFP-labelled OPCs to assess their fate over several days (e.g. **section 3.2.6**) , zebrafish embryos and larvae screened for expression were embedded every 12 or 24 hours for imaging. In older animals which are less tolerant for the anaesthesia as well as developmental

dynamics slowed down, it was necessary and sufficient to image every 48 h. After imaging the fish were removed from the agarose, kept in Danieau's buffer and re-embedded when the next image was taken.

2.1.5 Fluorescence-activated Cell Sorting (FACS)

Approximately 2000 anesthetized Tg(olig1:memEYFP) zebrafish larvae at 5 dpf were dissociated using the Papain Dissociation System (Worthington Biochemical Corporations) to generate a single-cell suspension (according to the manufacturer's instructions). Briefly, after removing the yolk by deyolking buffer (55 mM NaCl, 1.2 mM KCl, 1.25 mM NaHCO3) and extensive pipetting, the larvae were washed in Danieau's buffer twice, chemically dissociated by 30 min incubation with papain at 37 °C in a shaking incubator and subsequently mechanically dissociated by pipetting and filtering. To remove debris, cell clusters and DNA the suspension was centrifuged and filtered (30 µm Filcon syringe, BD Bioscience) several times before stored on ice in FACSmax Cell Dissociation Buffer (amsbio) with 5-10 % fetal calf serum (FCS) until cell sorting at the same day.

A MoFlo XDP cell sorter machine (Beckman Coulter) was used for fluorescence-activated cell sorting (FACS) in cooperation with the CyTUM Flow Cytometry Unit at the Technical University of Munich. Debris and cell doublets were removed additionally by using the forward and side scatter parameters. Propidium iodide staining (Thermo Fischer) was used as a dead cell marker (negative selection). In an initial sort cells that were highly EYFP-positive in comparison to cells from wildtype animals were selected. To achieve highest purity and avoid false-positive single cells the resulting cell suspension was stained with the cell viability marker Vybrant DyeCycle Ruby (Thermo Fischer, 1:500 in HBSS, Thermo Fischer, with 10% FCS) and sorted a second time for double positive cells (**Table 2.1.5.1** and **Figure 2.1.1**). During this second run, EYFP- and DyeCycle-positive single cells were sorted into 384-well plates (one cell per well) containing RNA lysis buffer (provided by the Sequencing Service of the Karolinska Institutet, Stockholm). The plate was then kept on dry ice or at -80 °C, respectively, until further processing. For subsequent single-cell RNA-Sequencing one sample plate and one validation plate (latter containing more than one cell per well in some of the wells to allow calibration of the amount of RNA) were filled and sent to our collaboration partners at the Karolinska Institute in Stockholm. Furthermore, the accuracy of single cell sorting was validated by sorting single cells in 384-well imaging plates (see **Figure 3.3.1**).

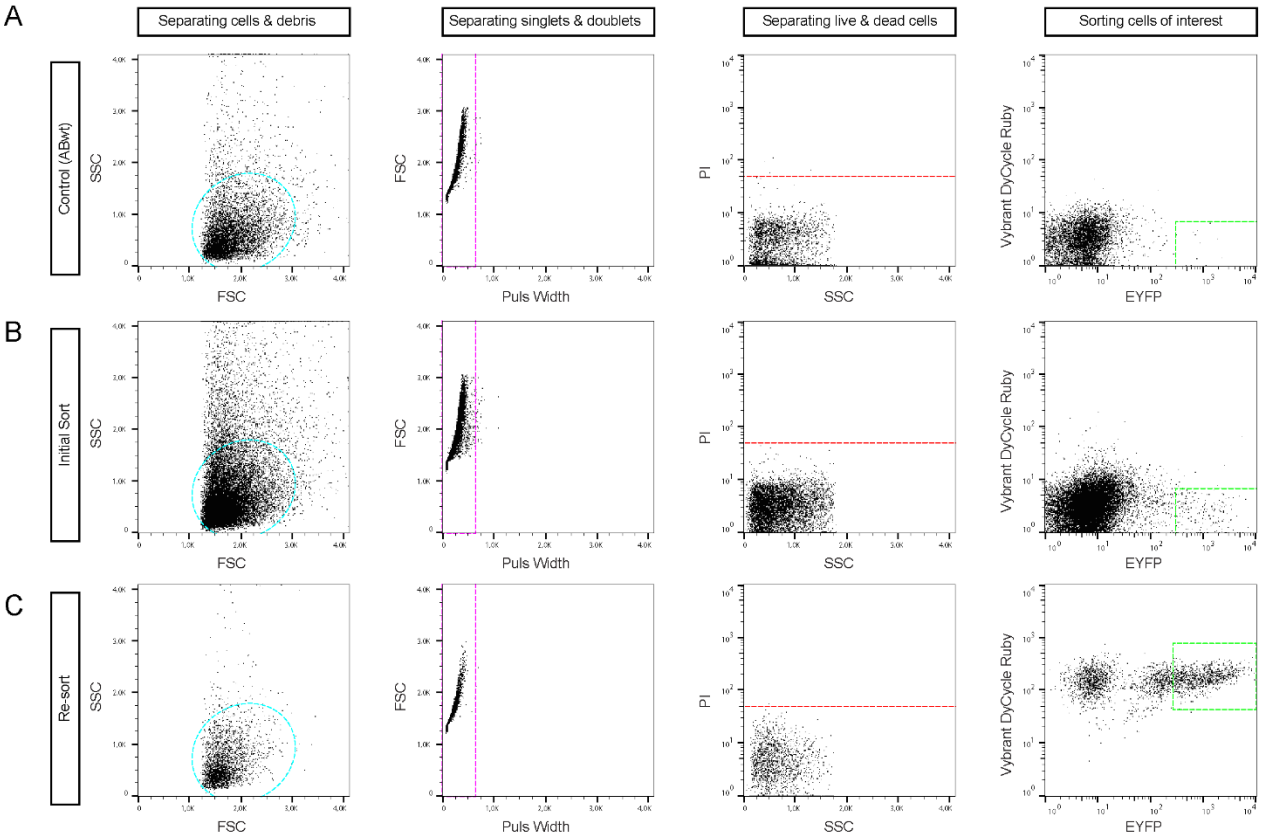

Figure 2.1.1 Cell sorting (gating strategy) for RNA-Sequencing.

Dot blot representations of the FACS sorting results. Every dot represents one event, which can be a cell or a non-cellular particle. Cells which are most likely labelled by EYFP were selected in a (virtual) four-step process. Cells within the coloured outlines were kept whereas the cells/particles outside these outlines were discarded. Axis labelling: forward scatter (FSC), side scatter (SSC), Pulse Width, Propidium Iodide (PI), EYFP, Vybrant DyeCycle Ruby.

(A) Dot blot for sorting cells from wildtype control fish. The few cells found to be fluorescent similar to EYFP-positive cells represent the false-positive rate of the sorting regime.

(B) Dot blot for sorting fluorescent cells from Tg(olig1:memEYFP) fish at 5 dpf. The graph shows only 20,000 events of the total events for better representation (see also **Table 2.1.5.1**).

(C) Dot blot for sorting fluorescent cells from the cell suspension obtained during the first sort in **B** (re-sort).

Table 2.1.5.1 Cell sorting (gating strategy) to select single EYFP-positive cells for RNA-Sequencing. Number of sorted cells in each category and percentage of the total input are given.

Gating of …	Control	1st sort	2nd sort
all events	6,860 (100 %)	5,520,000 (100 %)	2,765 (100 %)
cells	6,219 (90.7 %)	4,723,174 (85.6 %)	2,658 (96.1 %)
singlets	6,209 (90.5 %)	4,710,305 (85.3 %)	2,655 (96.0 %)
living cells	6,202 (90.4 %)	4,710,261 (85.3 %)	2,654 (96.0 %)
EYFP+ cells	12 (0.2 %)	40,993 (0.7 %)	955 (34.5 %)

2.1.6 RNA-Sequencing

The single-cell RNA-Sequencing using the SmartSeq2 technique (Picelli et al., 2013) was done by our collaboration partners at the Karolinska Institute in Stockholm, in particularly the Eukaryotic Single-Cell Genomics Facility of the Karolinska Institute. A more detailed methodical description of the single-cell RNA-Sequencing and analysis can be found in our recent publication (Marisca et al., 2020). Sequencing was performed by an Illumina HiSeq 2500 sequencer with 50 bp single reads.

2.1.7 Staining of Fixed Tissue (Immunohistochemistry and RNA *in situ* Hybridization)

2.1.7.1 Preparation of Fixed Tissue Sections

Zebrafish larvae at 7dpf were euthanized with 4 mg/ml tricaine mesylate and then fixed with 4 % paraformaldehyde (PFA) at 4 °C overnight. Subsequently larvae were dehydrated for a minimum of three days in increasing concentrations of sucrose (10 %, 20 % and 30 %) until the larvae sank to the bottom of the glass vial. Afterwards the larvae were embedded in Optimal Cutting Temperature (OCT) medium (Tissue-Tek) and froze on dry ice. The samples were stored at -80 °C until sectioning. Sectioning was performed using a Leica CM1850UV cryostat (Leica) to obtain transversal sections of the spinal cord with a thickness of 14-16 µm. Sections were stored at -80°C until RNA *in situ* hybridization or immunofluorescence staining.

2.1.7.2 RNAscope - RNA in situ hybridization

RNA *in situ* hybridization (ISH) was performed according to the manufacturer's protocol for fixed frozen samples (ACD, RNAscope® Multiplex Fluorescent Detection Reagents v2). A list of the probes that has been used for this work can be found in **Table 2.1.7.1**. For sample pre-treatment, I incubated 10 min with RNAscope® hydrogen peroxide (ACD) at room temperature and 30 min with RNAscope® Protease III (ACD) at 40 °C. The transcript-specific RNAscope® probes (ordered from ACD) were hybridized at 40°C for 2-3 h.

I did not perform multiplex ISH and did not mix probes. C2 and C3 hybridization probes were diluted in RNAscope® Probe Diluent (ACD). For signal detection TSA-conjugated Opal dyes (Perkin Elmer) were used, diluted 1:1000 in RNAscope® TSA buffer (ACD).

The fluorescence of fluorescent proteins that labelled OPCs and OLs in our transgenic fish was usually destroyed during the RNA ISH procedure. To be able to assign the ISH signal to the cells of interest, RNA ISH was followed by immunofluorescent staining against the fluorescent proteins assuming that epitopes for the antibodies are still intact.

Table 2.1.7.1 List of used RNAScope® Probes.

Gene	Catalog Number	Channel (C1-C3)	Gene Accession Number	Transcript Accession Number	Probe Pairs
dapB (neg. control)	-	1	-	-	-
myod1 (pos. control)	481231	1	ENSDARG00000030110	NM_131262.2	20
nkx2.2a	529751	1	ENSDARG00000053298	NM_001308640.1	20
cspg4	529741-C3	3	ENSDARG00000078227	XM_001923422.6	20
olig1	543511-C2	2	ENSDARG00000040948	NM_001020796.1	15
sox9b-O2	544201-C3	3	ENSDARG00000043923	ENSDART00000064500	20
kpna2	569091-C2	2	ENSDARG00000038066	NM_001002335.1	20
gpr17	504601	1	ENSDARG00000062030	XM_005165958.3	20
mki67	574951-C2	2	ENSDARG00000091150	NM_001277446.1	20
pcna	574931-C3	3	ENSDARG00000054155	NM_131404.2	20
myrf	574961-C2	2	ENSDARG00000078676	ENSDART00000157117.2	20

2.1.7.3 Immunostaining (IF)

For immunofluorescence on tissue sections, slides were washed twice with PBS and then incubated with blocking solution (0.1% Tween 20, 10% FCS, 0.1% BSA, 3% normal goat serum) for 1.5 h at room temperature. Subsequently, the primary antibody diluted in blocking solution was added overnight (4 °C). Information for antibody use can be found in **Table 2.1.7.2**. After washing thoroughly with 0.1% PBS-Tween 20, incubation with the secondary antibodies conjugated to Alexa Fluor fluorescent dyes (Invitrogen) was performed. For a list of secondary antibodies see also **Table 2.1.7.2**. Secondary antibodies were always produced from goat and used with a dilution of 1:1000. After diligent washing in PBS the slides were mounted with ProLong Diamond Antifade Mountant with DAPI (Thermo Fischer) and sealed with nail polish. Slides were stored at 4°C until imaging.

Table 2.1.7.2 List of used antibodies and dyes.

Antibody or dye	Company	Organism	Dilution
anti-DSRed **used to stain against mApple**	Takara/Clontech	rabbit (polyclonal IgG)	1:1000
anti-mCherry **used to stain against mApple**	Novus Biologicals	chicken (polyclonal IgY)	1:1000
anti-EGFP	abcam	chicken (polyclonal IgY)	1:1500
anti-Sox10	BIOZOL(GeneTex)	rabbit (polyclonal IgG)	1:2000
anti-rabbit AlexaFluor 555	Invitrogen	goat (polyclonal IgG)	1:1000
anti-chicken Alexa Fluor 488	Invitrogen	goat (polyclonal IgG)	1:1000
anti-rabbit Alexa Fluor 633	Invitrogen	goat (polyclonal IgG)	1:1000
anti-chicken Alexa Fluor 555	Invitrogen	goat (polyclonal IgG)	1:1000
Opal 650	Perkin Elmer	-	1:1000
DAPI	Thermo Fisher	-	-

2.1.7.4 Image Acquisition of Fixed Tissue

To image fixed tissue sections I used a Leica TCS SP8 confocal microscope. Different settings were used for image acquisition. In general, 12-bit Images of whole tissue sections for quantification were imaged with voxel sizes of approximately 100 nm in XY dimension and 1 µm in Z dimension using the resonant scanner for faster image acquisition. For higher-quality images of entire sections a resolution of 72 nm/0.4 µm per voxel and a higher averaging was chosen (64x line average). A 63x, 1.2NA water immersion objective was used always. Following excitation settings were used for the respective fluorescent dyes: 405 nm for DAPI (Thermo Fisher), 488 nm for Alexa Fluor 488, 561 nm for Alexa Fluor 555 and 633 nm for Alexa Fluor 633 and Opal 650.

2.1.8 Solutions and Buffers

Danieau's Buffer (amounts for preparing a 900 ml of stock solution, which was diluted 1:100 before use):

- NaCl (Roth): 91.52 g
- KCl (Roth): 1.41 g
- MgSO4 (VWR Chemicals): 2.66 g
- Ca(NO3)2 (Roth): 3.83 g
- Hepes (Roth): 32.17 g
- distilled water: 900 ml
- adjust to pH 7.6

Tricaine mesylate (4 mg/ml stock solution)

- Tricaine/MS-222 (PharmaQ, UK): 400 mg
- distilled water: 98 ml
- Tris (Alfa Aesar; adjusted to pH 9.0): 2ml
- adjust to pH 7.0

2.2 Data Analysis

2.2.1 Image Processing

Image processing was generally carried out with FIJI (Schindelin et al., 2012) or IMARIS 8.4.2 (Bitplane). If not indicated otherwise the shown images represent maximum intensity projections (MIPs) of the entire imaging depth (Z stack). If required, e.g. when the fish was occasionally twitching during live imaging, Z stacks and time lapse images were aligned using the StackReg plug-in of FIJI (by Philippe Thévenaz).

Cell counting was done either with FIJI's Cell Counter plugin on MIPs or using the Spot Tool of IMARIS. For the latter, a combination of automatic (based on intensity thresholding) and manual spot detection was applied.

2.2.2 OPC Morphology Reconstruction with IMARIS

The Filament Tracer Tool of IMARIS was used to trace the entire process tree of individual OPCs combining automatic dendrite detection (Dendrite Starting Point Diameter = 7.58 µm, Dendrite Seed Point Diameter = 0.300 µm) with semi-automatic/manual correction to maximize the accuracy of the tracing. This allows to measure summed process length and branch point number of a cell. The traced filaments were converted to a separated channel (using the Create a Filament Channel extension), which then was used to reconstruct a hull around the filaments using the Surface Tool (Surface Grain Size = 1.50 µm, Manual Threshold Value = 0.1). The volume of the hull is a representative measure of the volume occupied by one cell and its (remodelling) processes (see also **section 3.1.4**). For a better comparability between individual cells or the same cell at different times I combined summed process length (L), branch point number (N) and occupied volume (V) to one value termed *cell complexity* ((N/L)*V; see **Figure 3.1.4**). This value matches usually also with the observer's impression of morphological complexity as a cell is the more complex the more branches it has and the more volume it occupies. For example, a cell with only few processes even if these are quite long ones cannot occupy a large volume. Hence, even if the process length is high, the complexity of a cell can be low, whereas branch point number and volume do always positively correlate with complexity.

2.2.3 OPC Process Remodelling

The process remodelling was assessed by measuring the proportion of stable processes over time. In a first step, two-dimensional MIPs of the OPC at every time imaged were generated and the resulting greyscale

image was inverted so that cells appear darker than the background. If a process was remodelled, i.e. extended or retracted, compared to the start of the observation, there are dark pixels at the beginning and bright pixels at the later time at the same position when comparing the two images. Then all acquired images were projected (MIP) along the time axis from the starting of the time lapse imaging until the different times analysed (10 min, 30 min, 60 min etc.). As the brightest pixel at a position is shown in the resulting projection image for every XY position, only stable processes remain visible, whereas remodelled processes disappear (becoming part of the bright background). The stable processes were measured using the NeuronJ plug-in in FIJI (Meijering et al., 2004).

2.2.4 Analysis of Clonal OPC Trees

Individually labelled olig1:memEYFP OPCs were imaged over several consecutive days with adequate temporal resolution between 12 h and 2 d following their properties and fate long-term (see also **section 2.1.4**). A time series starts always with a single OPC with its soma in the nuclear region of the zebrafish spinal cord (compare **section 3.1.3**), the 'mother cell'. By proliferation, change of different properties over time and differentiation there are diverse outcomes for the respective daughter cells. As inclusion criterium for the finally analysed dataset, the duration of a time series of an individual OPC must be at least 96 h, that is five consecutive days (n=92), or until all daughter cells undergo differentiation, which is assessed by the formation of myelin sheaths even if this happen in a time frame shorter than 96 h (n=22). The latter examples were valid to include as the result after 96 h of observation or later could not change anymore. There is a formal difference between OPC differentiation and pre-OL myelination, which however was not relevant in this context (see **section 1.4** and **3.2.3**). The fate of individual cells was reconstructed as clonal trees (see **Figure 3.2.8A**).

For the prospective quantification, the status of cells at the end of the time series were analysed, based on the rationale that the longer the observation the more informative it was too. This was basically done to elucidate the potential of OPCs with the soma in the nuclear region. Retrospective analyses, i.e. of myelinating OLs, could give insight where these cells derive from or how proliferation and differentiation relate in individual cells. As the actual cell division or onset of myelination happens usually between two imaging sessions, the time before or after must be chosen as a reference point for time calculation. How this was done in detail for the individual analyses is described in the Results section.

2.2.5 Analysis of Single-cell RNA-Sequencing Data

Like the RNA-sequencing, also the bioinformatical analysis was done by our collaboration partners at the Karolinska Institute in Stockholm, namely by Dr Eneritz Agirre under the supervision of Dr Gonçalo Castelo-Branco. The exact methodological details are described in our common publication (Marisca et al., 2020). In brief, the reads were aligned to the current zebrafish reference genome (GRCz11) with ENSEMBL94 annotations for transcripts. Aligned sequences were used to determine gene expression levels as transcripts per million (TPM). These values were used to generate an expression matrix for every well on the 384-well sequencing plate. In average, 800,000 reads were found in each cell representing an average of approximately 5,000 genes per cell. 310 cells remain based on the inclusion criteria of a minimum of 500 detected genes per cell and a mitochondrial gene fraction below 0.05%. Cell clustering and further processing was carried out using the R package Seurat v3.0 (Butler et al., 2018; Stuart et al., 2019) based on a shared-nearest neighbour graph and a smart local moving algorithm. Individual cells in clusters were visualized as two-dimensional t-distributed stochastic neighbour embedding graph (t-SNE). Lists of differentially expressed genes between clusters were obtained by comparing gene expressions by Mann-Whitney U test (also referred to as Wilcoxon rank sum test).

2.2.6 Gene Ontology Term Analysis

Gene Ontology (GO) Term analysis of the different clusters was performed with GlueGo (Bindea et al., 2009) based on a list of differentially expressed genes in a particular group. Usually only upregulated genes were used as input, but there is the theoretically possibility to run the analysis also for downregulated genes. Importantly, it also makes a difference which groups was compared to obtain these lists of genes, for example, if one group was only compared to another group or to several distinct groups.

GO term analysis does also not consider the level of expression of the genes used as an input for the analysis (all input genes have the same priority). Hence, I chose input lists composed of the top 30 upregulated genes within each cluster identified within the single-cell RNA-Sequencing data, which are relatively short. This number was chosen quite arbitrary with the aim to obtain only meaningful GO terms as an output. But it would be equally valid to choose longer lists to increase the chance that several genes are included that together account for significant GO terms. Instead of using a defined number of genes, one can also define the included genes by the relative expression level, but also in this case one has to choose this level quite arbitrarily as it is difficult to assess how much upregulation is required to be considered also biologically meaningful.

I selected significant terms ($p<0.05$, Right-sided hypergeometric test for Enrichment, Benjamin-Hochberg p value correction) from following databases: GO/Biological Processes (updated at 10-04-2019), GO/Molecular Function (10-04-2019), and Reactome/Pathways (17-03-2019) for all GO Tree Intervals using GO Term Fusion. The associated genes must represent at least 1% of all the genes assigned to this term. The Kappa score for GO term grouping was always 0.4. To reduce the resulting GO and Reactome terms to a manageable number, the number of genes that has to be associated with a certain term, was varied between clusters as the only parameter. The requirement of a higher number of associated genes results in fewer significant GO and Reactome terms.

2.2.7 Data Analysis RNAScope

At least 100 OPCs (mApple+ EGFP-) were analysed in several fixed tissue sections of the spinal cord from different fish in at least three independent experiments per RNAscope probe. In general, only few OPCs (between 1 and 5) were found per section with a higher frequency in the nuclear region compared to the axodendritic region (see **Figure 3.1.3**).

A cell was considered as positive for a respective RNAscope probe if two or more spots could be certainly assigned to the cell body. Also, the intensity and size of the single dots was considered in addition (brighter and bigger dots could represent the signal from several detected mRNAs). By imaging a set of negative controls from different independent experiments I calculated the probability for a false-positive dot to be approximately 1:10 (not shown). This was done by counting how many false-positive signals were found within the volume of an entire average section and then calculating the number of false-positive signals which is to be expected in the volume of an OPC cell body of average size (which was approximately 0,1). Hence, the likelihood that two false-positive signals are detected in one cell and therefore the chance of including a false-positive cell in our analysis is approximately 1:100. As the total number of cells analysed for each probe is also in this range, a false-positive cell should not occur more than once. This matters only if cells had a general low expression level for respective genes with none or only one detected spot, usually an expressing cell had more individual signals clearly distinct from two.

2.2.8 Statistics

GraphPad Prism 8 and Microsoft Excel were used to obtain descriptive statistics. Statistical testing was performed with Prism 8. Prior to testing for significance, all data were tested for normal distribution using the Shapiro-Wilk test. According to the test numbers are given as mean ± standard deviation (normally distributed data) or median with 25^{th} and 75^{th} percentiles (non-normally distributed data).

For normally distributed data comparing several groups, one-way or two-way analysis of variance (ANOVA) with Tukey's multiple comparisons test was used in dependence of the experimental conditions. If data did not pass the normality test, statistical tests for non-normally distributed data were applied. For the comparison of two groups, this was Mann-Whitney U test.

For the analysis of contingency tables obtained for the comparison of the fraction of RNA ISH-positive cells between the nuclear and axodendritic region of the spinal cord, Fisher's exact test were used always for better uniformity, even though Chi-squared test would have been equally suitable in some cases. To test for correlation the Pearson's R coefficient was calculated. The used significant levels for statistical testing were $p < 0.05$ (*), $p < 0.01$ (**) and $p < 0.001$ (***).

3 RESULTS

3.1 Characterization of OPCs in the Zebrafish Spinal Cord

3.1.1 Generation of New Transgenic Tools for the Visualization of OPCs in Living Zebrafish

Several transgenic zebrafish lines were available to label OPCs *in vivo* (Czopka, 2015). However, none of these lines satisfy the requirements to study individual cells with high resolution over longer time. Often the expressed fluorescent proteins are not only specific to OPCs but also label other cell types like neurons and their axons, mature oligodendrocytes (and the myelin produced by them) as well as neural progenitor cells. For example, in the **Tg(nkx2.2a:mEGFP)** transgenic line there is a strong fluorescence expression in floor plate cells of the spinal cord whereas already at the age of 3 dpf only a subset of OPCs is labelled (**Figure 3.1.1B**). In contrast, in **Tg(olig2:DsRed)** transgenic fish many more cells than only OPCs are labelled as all cells of the pMN domain and their progeny including motor neurons (MNs) are labelled in addition (Rowitch, 2004), which impede the observation of individual OPCs (**Figure 1.1.1C**). In the **Tg(sox10:memRFP)** transgenic line all OL-lineage cells are labelled but OPCs are masked by OLs and their myelin sheaths soon after onset of myelination (not shown). In summary this makes it difficult to observe OPCs as a population or with a focus on their morphology and its change over time, respectively.

A previous study could show that EGFP driven by the *olig1* promotor is expressed in zebrafish OPCs with high specificity (Schebesta and Serluca, 2009). Hence, we decided to adopt this approach to visualize OPCs by the expression of fluorescent proteins driven by an *olig1* gene upstream sequence that comprises *olig1* upstream regulatory elements (see **section 2.1.1**). The following genetic expression constructs were generated using the *olig1(4.2 kb)* fragment by a common effort of me and the colleagues in our laboratory:

1. olig1:memEYFP
2. olig1:nls-mApple
3. olig1:nls-Cerulean
4. olig1:KalTA4

By the expression of the **olig1:memEYFP** construct a membrane bound EYFP is targeted to the cell membranes of OPCs allowing to visualize their cellular morphology, which is particularly characterized by a network of branched motile processes (**Figure 3.1.1C-F**). This enables time-course observation of individual cells, their fate, their location and their detailed morphology (**Figure 3.1.1D&E**).

Olig1 expression is downregulated in zebrafish during lineage progression towards myelinating oligodendrocytes (see **section 3.3**). However, fluorescent proteins have a certain decay time, and even if OPCs progress to myelinating OLs there is still fluorescent protein left, which can label the cells. As a myelin sheath is composed of packed membranes, membrane-targeted protein is especially concentrated in those sheaths. Therefore, by using the olig1:memYFP construct, it is possible to observe the transition from the progenitor stage to myelinating OLs through the formation of characteristic myelin sheaths, even without incorporating a second marker for mature oligodendrocytes (**Figure 3.1.1E**; see **section 3.2.3**). As the fluorescent protein is degraded afterwards and no new protein is produced in mature OLs, the fluorescence intensity declines and vanishes finally in differentiated cells. This was of advantage for my imaging experiments as OLs and their myelin cannot significantly disturb the imaging of the remaining OPCs.

In contrast, from the **olig1:nls-mApple** and **olig1:nls-Cerulean** expression constructs (together referred to as olig1:nls-XFP) red and blue fluorescent protein are produced, respectively, which are targeted to the nucleus of the OPC as the proteins contain a nuclear localization signal (NLS). In consequence, only nuclei are labelled by these constructs, which allows adequate separation of individual cells even with whole population labelling and makes it feasible to observe population dynamics over time, i.e. proliferation and migration. For this purpose, the olig1:nls-XFP constructs were advantageous compared to the olig1:memEYFP construct (**Figure 3.1.1B&G**). However, as outlined above, fluorescent protein is not degraded immediately with differentiation, which makes it possible that a nuclearly labelled cell is already an oligodendrocyte. To assess differentiation of mApple-expressing OPCs the combination with a marker for myelinating OLs such as mbp:nls-EGFP (Karttunen et al., 2017) is required. Differentiation is then displayed by a concurrent decrease in mApple fluorescent and an increase in EGFP fluorescence in the cell's nucleus (**Figure 3.1.1G** and **Figure 3.2.2A**). Using this combination, one can define OPC identity of an mApple-positive cell as there is no co-labelling with EGFP.

As described above oligodendrocyte lineage progression is viewed as a multistep process and at least pre-OLs are an important intermediate stage in addition to OPCs and myelinating OLs (De Biase et al., 2010; Trotter and Schachner, 1989). Pre-OLs are of particular importance as it is suggested that at this stage the decision is made whether an OL initiate myelination or rather undergo cell death (see **section 1.2** & **3.2.3**). Pre-OLs already left the cell cycle, and hence are per definition no longer OPCs, but do not yet possess myelin sheaths. No *bona fide* discrimination of pre-OLs is possible using our genetic models. There is no definite morphological sign to distinguish them from OPCs, but also no established markers in zebrafish

(**Figure 1.4.1**). However, when one takes together cell morphology, fate analysis and transcriptomic data, one can identify a transitional cell type in zebrafish which possibly represents pre-OLs (see **section 3.2.3**).

The **olig1:KalTA4** allows for the translation of KalTA4 protein, which is an optimized Gal4 (Distel et al., 2009), and hence is used to utilize the GAL4-UAS expression system. The combination with appropriate UAS promoter-lines driving fluorescent reporter proteins, such as Tg(UAS:memEYFP) or Tg(UAS:memRFP), results in a salt-and-pepper labelling pattern of the OPC population (**Figure 3.1.1F**). This can be of advantage if a high expression level in many cells is required but labelling all cells would make the analysis difficult.

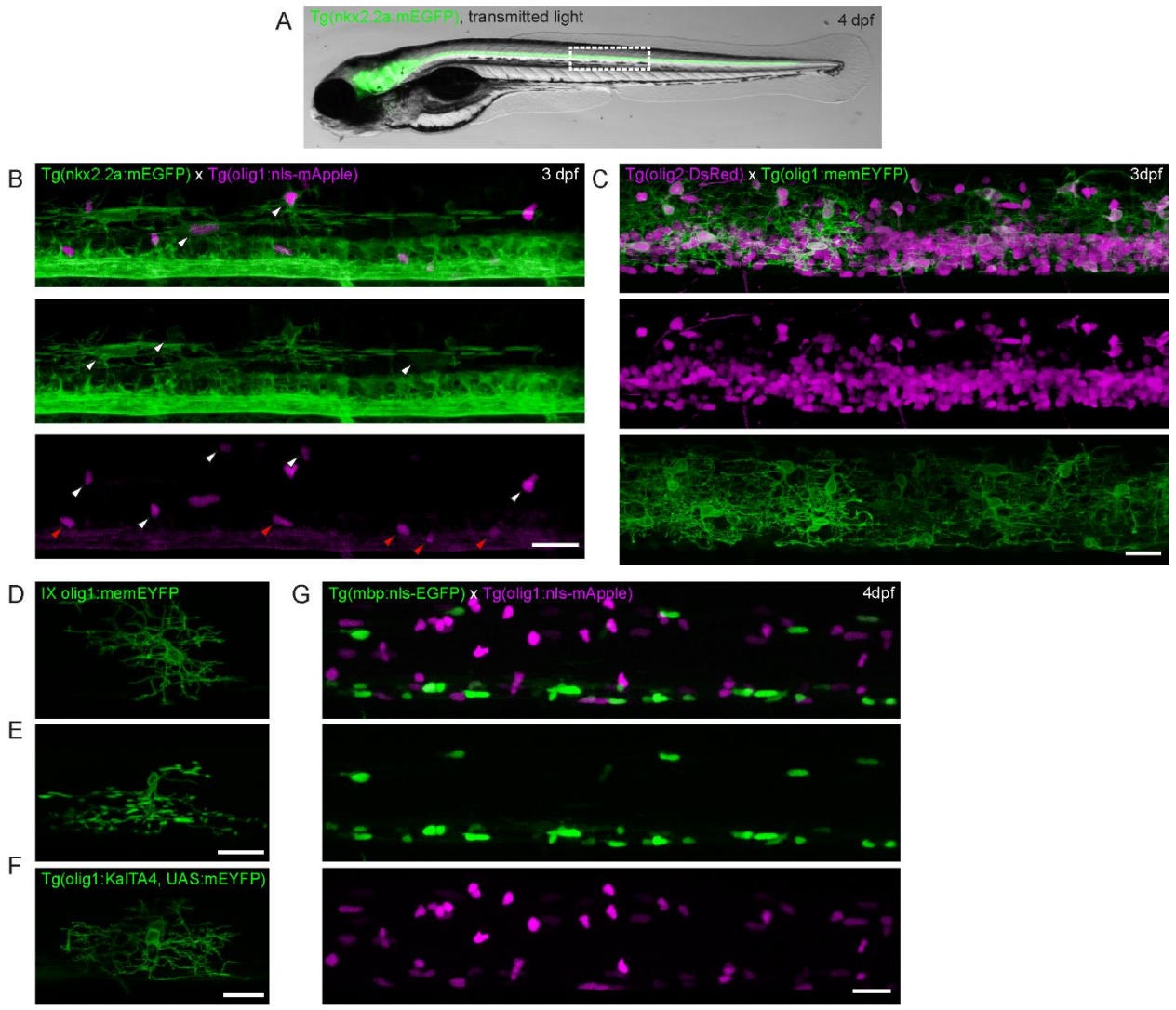

Figure 3.1.1 Visualization of OL-lineage cells in the zebrafish embryo and larvae.

(A) Whole body image of an 4dpf-old zebrafish expressing EGFP in the CNS. The dashed line indicates the region of the spinal cord where most of the imaging was performed (with somite 17 in the image centre).
(B) Confocal image of a double-transgenic Tg(nkx2.2a:mEGFP) x Tg(olig1:nls-mApple) fish (hemicord). Double positive cells (n=2) are indicated by white arrowheads in the top panel, cells that express only EGFP (n=3; n(OLs)=2) or mApple (n=5) are marked, respectively. Some cells might express EGFP (red arrowhead, n=5), however this cannot be assessed due to the bright labelling of neighbouring floor plate cells.
(C) Confocal image of a double-transgenic Tg(olig2:DsRed) x Tg(olig1:memEYFP) fish. Many more cells in the spinal cord are olig2+ compared to olig1+ cells (**C** and **B**). Olig1:memEYFP labels OPCs exclusively, whereas olig2:DsRed labels cells of the pMN domain and its progeny.
(D) Confocal image of an OPC individually labelled with olig1:memEYFP (3 dpf) showing a high degree of process branching.
(E) Confocal image of an early myelinating OL individually labelled with olig1:memEYFP (14 dpf) only few hours after myelin sheaths were initially established.
(F) Confocal image of OPCs in a Tg(olig1:KalTA4, UAS:memEYFP) fish (5 dpf). OPCs are labelled in a salt-and-pepper fashion (compare to **C**).
(G) Confocal image of a double-transgenic Tg(mbp:nls-EGFP) x Tg(olig1:nls-mApple) fish. Myelinating OLs express EGFP (shown in green), whereas OPCs exclusively express mApple fluorescent protein (shown in magenta).
Scale bar in all images: 20 μm.

3.1.2 Description of the Spinal Cord Anatomy in Larval Zebrafish based on Transgene Expression

OPCs have been described previously as being regionally diverse (see **section 1.7**). Hence, it would be important to figure out whether different regional compartments exist within our model system, the embryonic and larval zebrafish spinal cord, to compare OPCs between them and identify possible differences in OPC properties. Based on live imaging of laterally embedded Tg(olig1:memEYFP) zebrafish embryos (dorsal is up in the images, compare **Figure 1.1.1A**) the spinal cord looks homogenous without regional differences (**Figure 3.1.2A**). However, when myelin is labelled in addition, there is clearly more myelin in the peripheral dorsal and ventral parts sparing the medial part of the spinal cord (**Figure 3.1.2A**). This is not surprising, as by the sparse labelling of neurons and their axons one can see, that also axons run preferentially in dorsal and ventral tracts (**Figure 3.1.2B&C**). In the rotational view of the respective images it also becomes clear that axons and myelin are in the periphery of the spinal cord, whereas cell bodies can be found in the central region (**Figure 3.1.2C**). A hallmark of the ventral axonal tract is the big Mauthner axon, which is usually myelinated early in development and is important for the motoric escape response (**Figure 3.1.2D**). Using this approach, it is also possible to investigate the myelination of individual axons (**Figure 3.1.2D**), which can be used to investigate sheath remodelling over time (Auer et al., 2018).

The differential spatial distribution of cell somata and axons becomes even clearer by imaging transversal sections of the zebrafish spinal cord. The majority of cell nuclei are concentrated in the centre of the spinal cord; hence I termed this area **nuclear region** (**Figure 3.1.2E**). As most of the somata in this region are thought to belong to neurons, the compartment is also referred to as **neuronal region** (Marisca et al., 2020). Only few somata can be found outside of this region in the spinal cord. I did not investigate the identity of the cells lining the border of the spinal cord in detail, but these cells are assumed to be cells of meninges and endothelium and do not belong to the CNS directly. For example, in zebrafish with vessel labelling, these cells are observed to embrace the spinal cord tightly (single observation, no images acquired). Some of these cells are cspg4 (NG2)-positive (**Figure 3.3.3B**), which is known to be expressed also in pericytes (Ozerdem et al., 2001). The region where only few nuclei but many axons and most myelin can be found, is referred to as **axodendritic region**, as OPCs and neurons extend their dendritic processes to this region (**Figure 3.1.2C&E**). Due to the fact, that the axodendritic region is rich in dendrites and synaptic contacts (Marisca et al., 2020), it represents more than only white matter but also has certain properties of grey matter. Therefore, the discrimination between grey and white matter which was used previously to determine OPC heterogeneity spatially in the adult mouse brain (Hill et al., 2013; Vigano et al., 2013), does not apply identically to the zebrafish spinal cord (see also **section 4.2.2 & 4.2.4**).

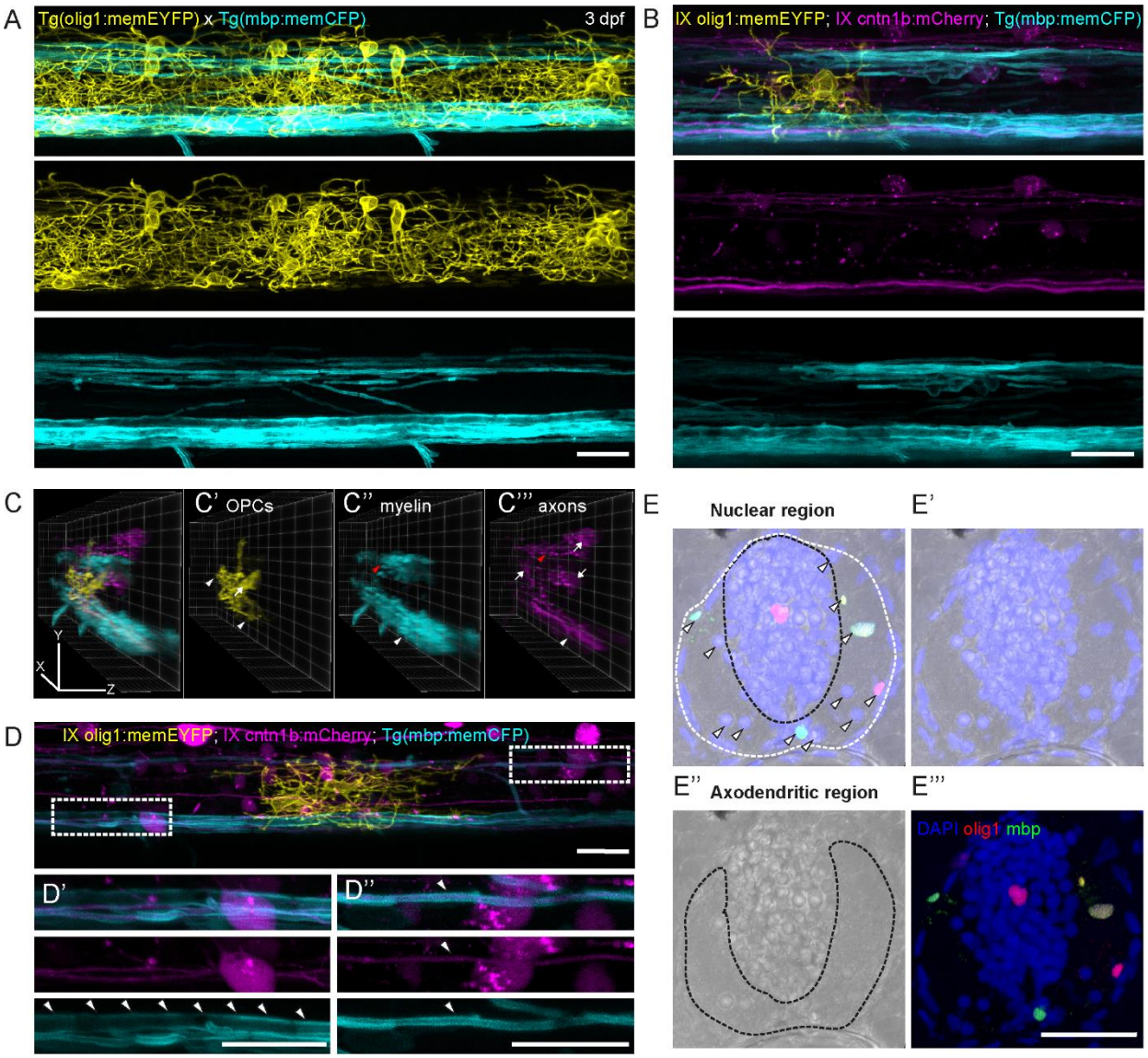

Figure 3.1.2 Spinal cord anatomy in early developing zebrafish.

(A) Confocal image of a double-transgenic Tg(olig1:memEYFP) x Tg(mbp:memCFP) fish (dorsal up).

(B) Confocal image of a Tg(mbp:memCFP) fish injected with olig1:memEYFP and cntn1b:mCherry expression constructs (resulting in sparse labelling of OPCs and axons).

(C) Rotational views of the image shown in **B** generated by the ClearVolume plug-in of FIJI. (C') The white arrow points to the soma of an OPC, the white arrowheads to its processes. (C'') The red arrowhead points to myelin of the dorsal tract and the white one to myelin of the ventral tract. (C''') The white arrows point to neuronal somata, the red arrowhead to the dorsal and the white arrowhead to the ventral axonal tract, respectively.

(D) Another example as shown in **B**. (D') Myelin ensheathment of the Mauthner axon (white arrowheads). The axon itself is not labelled. (D'') Myelin ensheathment of a cntn1b:mCherry labelled axon.

(E) Confocal image of a transverse section of the Tg(olig1:nls-mApple) x Tg(mbp:nls-EGFP) spinal cord from fixed-frozen tissue. Nuclei in blue, OPCs in red and OLs in green; transmitted light (PTM-Trans) is shown in the greyscale channel in E, E' and E''. The dashed white line in E marks the borders of the spinal cord; the dashed black line in E outlines the nuclear region, dashed line in E'' outlines the axodendritic region. Arrowheads point somata outside the nuclear region.
Scale bar in all images: 20 µm.

3.1.3 Localization of OPCs within the Embryonic and Larval Zebrafish Spinal Cord

Based on the observation that the majority of the mostly neuronal cell bodies reside in the medial spinal cord whereas the myelinated axons are found in the periphery, the next step was to focus on the localization of OL-lineage cells. Remarkably, cell bodies of OPCs and myelinating OLs can be localized in the nuclear region as well as in the axodendritic region (**Figure 3.1.2E** & **Figure 3.1.3A**). I quantified the distribution of olig1:nls-mApple-positive and mbp:nls-EGFP-negative OPC somata between nuclear and axodendritic region in fixed tissue sections of 7-day old larvae (n(sections)=606): the majority of OPCs (n=578; 60 %) is located in the nuclear region, whereas the smaller fraction (n=383, 40 %) is located in the axodendritic region (**Figure 3.1.3B**). The distribution of OLs is approximately 10 % in the nuclear region and 90 % in the axodendritic region (see **section 3.2.5**). However, one should consider that these numbers depend on proliferation and differentiation of the OPCs and that the frequency of these events do change over time, i.e. slow down with ongoing development (see **section 3.2.6**). Hence, the ratio of 'nuclear' to 'axodendritic' OPCs undergoes temporal changes.

Alternatively, there is also the possibility to quantify OL-lineage cell distribution between the two regions in confocal live images of Tg(olig1:nls-mApple) x Tg(mbp:nls-EGFP) double-transgenic fish: either by determining the position of the somata within the Z stack of the whole spinal cord or simply by the shape of the somata in the maximum projection. Cells in the nuclear region have a roundish soma, whereas cells in the axodendritic region have an oval soma (**Figure 3.1.1G** & **Figure 3.2.5**), which is most likely caused by biomechanical constraints in the respective area. For example, axonal tracts running in anterior posterior direction likely also cause forces that squeeze the cell nuclei in the axodendritic region in this dimension. These forces likely do not exist in the nuclear region (see **section 4.2.4**). Moreover, to distinguish between nuclear or axodendritic regions in a single plane of a confocal image, one can label cell membranes using lipophilic dyes like BODIPY (**Figure 3.1.3C&D**). As the axodendritic region has a high content of axons,

dendrites and myelin, which are composed basically of cell membranes, there is a uniform staining observed there. In the nuclear region, the cell bodies are spared by the staining resulting in a sieve-like appearance (**Figure 3.1.3C&D**).

When performing live imaging at several levels along the right-left axis of the fish (**Figure 3.1.3C**) as well as along the dorsoventral axis (**Figure 3.1.3D**), I could confirm the previous finding from fixed sections that the majority of cell bodies of OPCs are localized in the nuclear region and fewer OPC somata can be detected in the axodendritic region (not quantified). In contrast, almost all the OPC processes observed are in the axodendritic region (**Figure 3.1.3C&D**). The few processes found in the nuclear region only connect cell bodies in the nuclear region to the elaborated process network in the axodendritic region. The predominant localization of OPC processes in this region was independent of the position of the according cell body (**Figure 3.1.5**).

This suggests that the targets that OPCs contact with their processes are in the axodendritic region and that this is most likely relevant for their function. OPCs have been shown to interact with axons and even build synapses with them (see **section 1.1 & 1.6**).

Figure 3.1.3 Spatial distribution of OPCs in the spinal cord.

(A) Confocal images of transverse sections of the spinal cord. Fixed frozen sections from Tg(olig1:nls-mApple) x Tg(mbp:nls-EGFP) fish. Two example images are shown. Nuclei in blue, OPCs in red (only) and OLs in green (and red). The dashed white line in A' and A''' marks the borders of the spinal cord; the dashed grey line separates the nuclear region from the axodendritic region.

(B) Quantification of the distribution of OPCs in the spinal cord from 606 sections as shown in **A**.

(C) Sagittal view of the spinal cord as MIP and as single planes along the right-left axis (z-axis of imaging; C'-C''''). Tg(olig1:memYFP), Tg(mbp:memCFP) fish stained with BODIPY to label membranes. The white arrowheads point to cell bodies in the nuclear region, the red arrowhead points to a cell body in the axodendritic region.

(D) Horizontal view of the spinal cord as MIP and as single planes along the dorsoventral axis (z-axis of imaging; D'-D''). Tg(olig1:memYFP), Tg(mbp:memCFP) fish stained with BODIPY to label membranes.

Morphology of OPCs in the zebrafish spinal cord. The white arrowheads point to cell bodies in the nuclear region, the red arrowheads point to cell bodies in the axodendritic region.

Scale bar in all images: 20 µm.

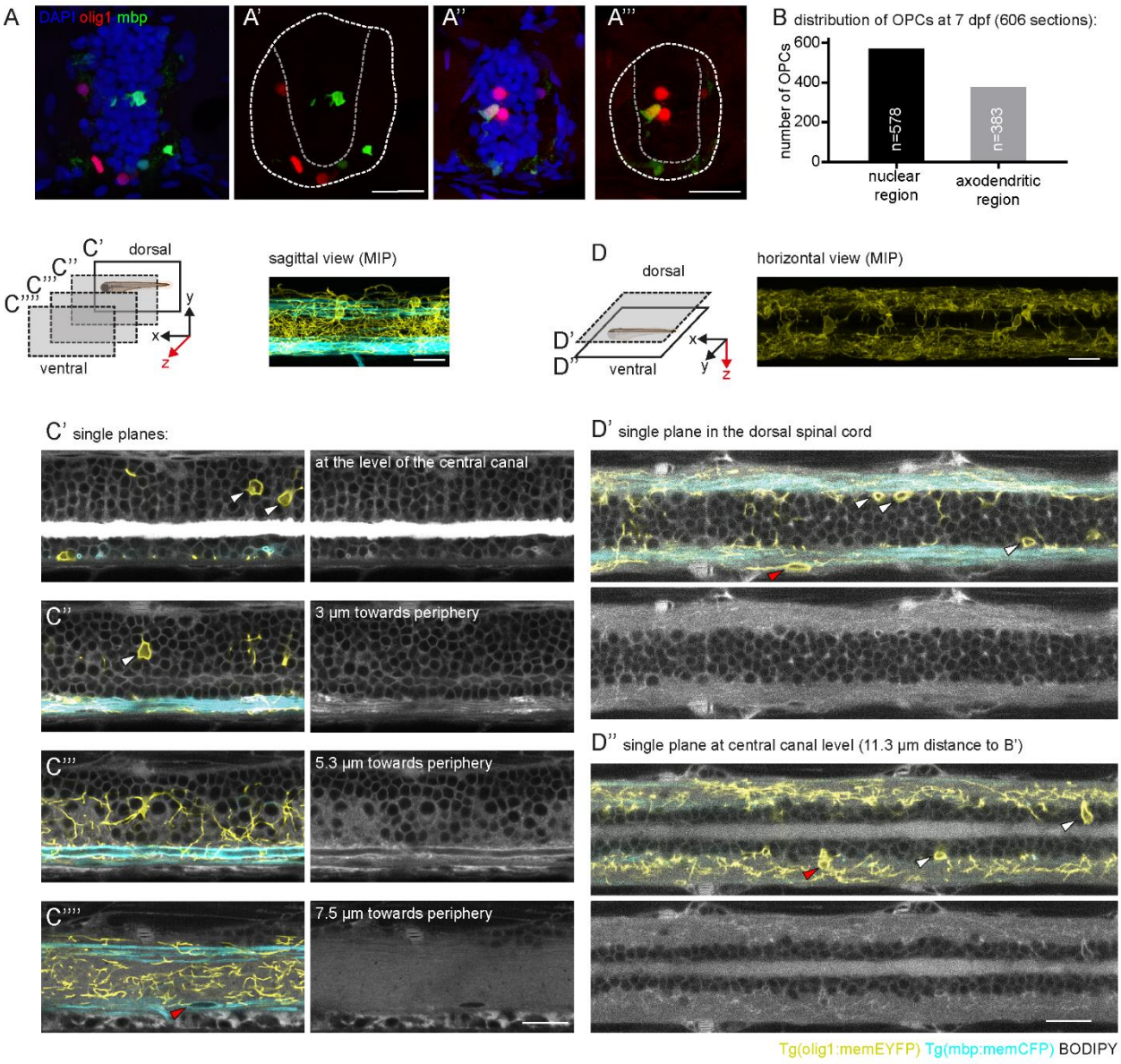
A
DAPI olig1 mbp
A'
A''
A'''
B distribution of OPCs at 7 dpf (606 sections):
number of OPCs
600
400
200
0
n=578
n=383
nuclear region
axodendritic region
C'
C''
C'''
C''''
dorsal
ventral
y
x
z
sagittal view (MIP)
D
dorsal
D'
D''
ventral
x
y
z
horizontal view (MIP)
C' single planes:
at the level of the central canal
C''
3 µm towards periphery
C'''
5.3 µm towards periphery
C''''
7.5 µm towards periphery
D' single plane in the dorsal spinal cord
D'' single plane at central canal level (11.3 µm distance to B')
Tg(olig1:memEYFP) Tg(mbp:memCFP) BODIPY

3.1.4 Morphology of OPCs in the Zebrafish Spinal Cord

Cellular morphology was another property I was interested in whether it would differ between individual OPCs and OPCs in different regions, respectively. Using olig1:memEYFP injections, it was feasible to visualize the morphology of single isolated cells in high detail, which even made it feasible to assess morphology quantitatively.

OPCs can have different morphologies ranging from very simple to highly complex and can extend processes either to only to one or both sides of the spinal cord, respectively (**Figure 3.1.4A&B**). The 90° rotations of the individual cells also show again that almost all of the process terminals are in the axodendritic region (compare **section 3.1.3**).

For the direct comparison of the morphology between individual cells, a single value termed '**cell complexity'** was established integrating three significant parameters of the process network: branch point number, summed process length and occupied volume (**Figure 3.1.4B&C**). These were obtained from a 3D reconstruction of the cell using IMARIS software (see **section 2.2.2**). The high number of rather simple OPCs (cell complexity < 1000) must not necessarily reflect the actual proportion of these cells of the entire OPC population, but accounts for the fact that it was more often feasible to measure these cells reliably (**Figure 3.1.4D**). In accordance with the wide range of observed morphologies, also the measured complexity can vary extensively: between 50 (simple) and 5500 (complex) based on the analysed example OPCs (**Figure 3.1.4D**). The graph reflects a distribution of cell complexities along a **continuum** between the two extremes instead of distinct groups. However, individual cells can be highly different regarding their morphology, which raises the question if the morphological differences do correlate also with other cellular properties or fate of OPCs. For this purpose, especially simple and complex cells were chosen for comparisons in the following experiments (see **sections 3.1.5, 3.1.6** & **3.2**).

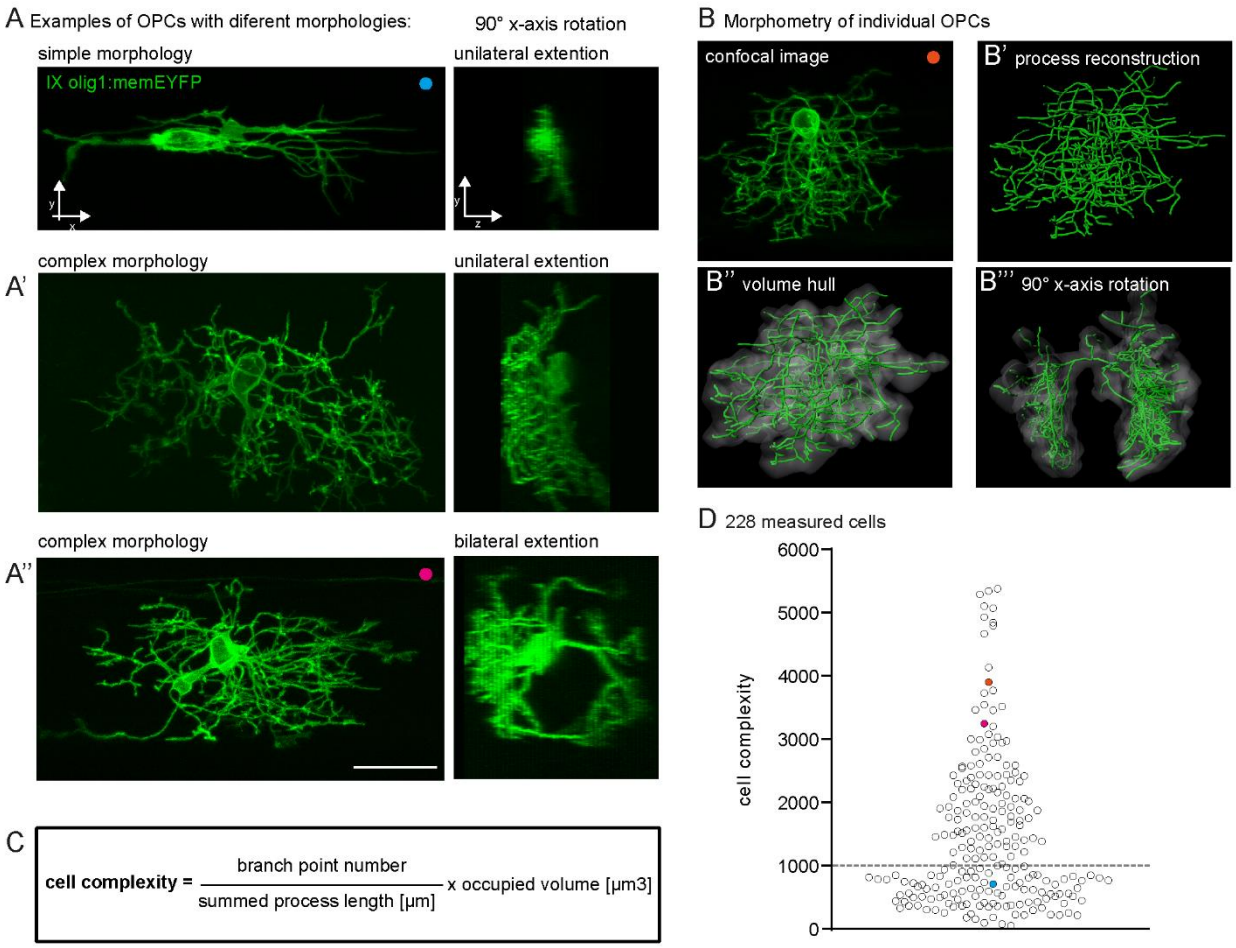

Figure 3.1.4 Morphologically diversity of OPCs.

(A) Confocal images of three individual olig1:memEYFP-labelled OPCs with different morphologies and different territorial occupancy. The cell bodies reside in the left hemicord in all examples.

(B) Morphometry of an individual OPC based on 3D reconstruction using IMARIS. (B') Process reconstruction. (B'') Reconstructed volume around the reconstructed process network. (B''') View of the reconstructed example cell after 90° rotation around the x-axis.

(C) Formula to obtain a single value for cell (process) complexity based on measured properties.

(D) Graph showing the distribution of the cell complexity values for a set of 228 OPCs from zebrafish between 3 and 16 dpf covering the entire range of morphological diversity from very simple to highly complex. The coloured dots represent the complexity values of cells shown in A, A'' and B.

Scale bar in all images: 20 µm.

3.1.5 Correlation of Cell Complexity with Soma Position

Since OPCs in the zebrafish spinal cord could have their soma either in the nuclear or axodendritic region (see **section 3.1.3**) and regarding their morphology also express a wide range of process network complexity (see **section 3.1.4**), it would be interesting to know if the OPCs in a specific region have a preference for a certain morphology. For example, are OPCs in the axodendritic region rather simpler or more complex than their counterparts in the nuclear region? If OPCs in different regions indeed have also different properties, this would help to define distinct OPC subgroups.

To this aim, I labelled individual OPCs, measured their cell complexity (**Figure 3.1.5A&B**) and determined the positions of the somata either by BODIPY labelling (**Figure 3.1.5C**) or position in the Z stack together with soma shape (as described in **section 3.1.3**). OPCs with cell complexity values corresponding to a complex morphology were found with much higher frequency in the nuclear region (median with 25^{th} and 75^{th} percentiles: 2100 [1500; 3200]), whereas most of the OPCs in the axodendritic region (600 [400; 1500]) had cell complexity values typically for cells with a simple morphology (**Figure 3.1.5D**). Occasionally, OPCs with a certain morphology are not restricted exclusively to a certain region (**Figure 3.1.5D&E**). For example, OPCs could have a complex morphology but an oval soma and reside in the axodendritic region (**Figure 3.1.5E**). On the other hand, OPCs with a simple morphology and round soma has also been observed in the nuclear region (**Figure 3.1.5E** & **Figure 3.2.6D**).

In summary the data show that there is a general correlation between cell soma position and morphology of OPCs in the spinal cord, which provokes the question if axodendritic and nuclear OPCs are also different regarding additional properties like cell behaviour over time.

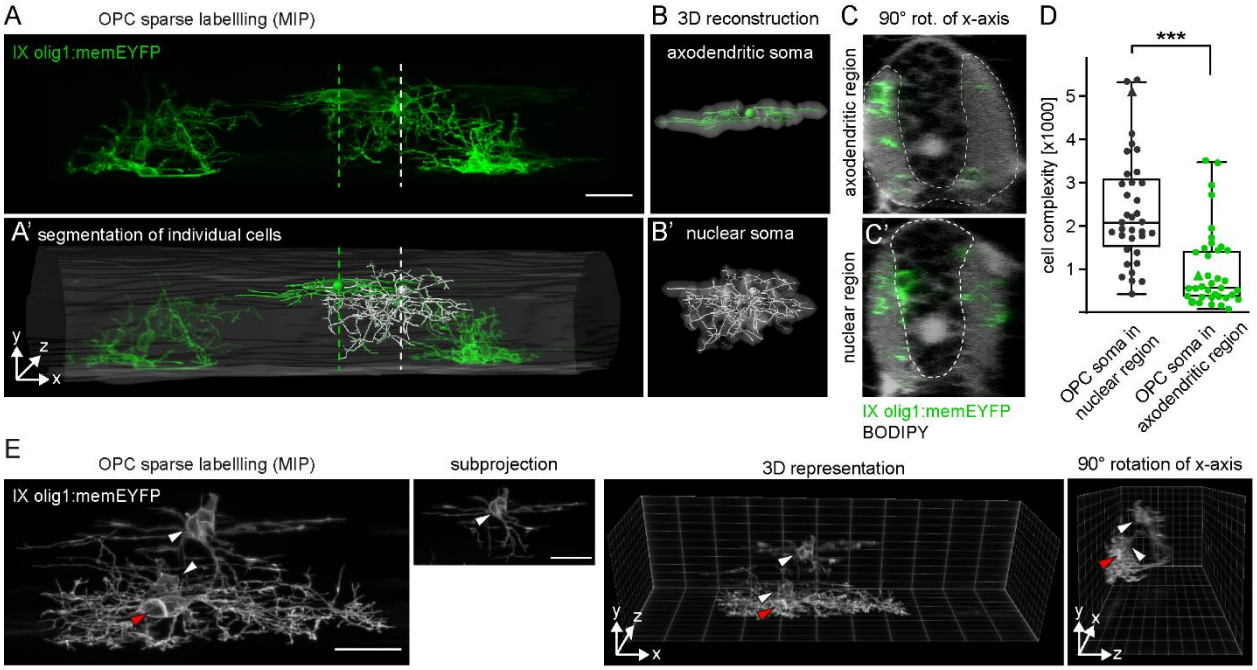

Figure 3.1.5 Cellular complexity correlates with position within the spinal cord.

(A) Confocal image of six individual olig1:memEYFP-labelled OPCs with different morphologies. (**A'**) 3D representation of the same image overlaid with process network reconstruction of two example cells in white and green and the outlines of the spinal cord. The white and green dashed lines mark the centres of the somata of the respective cells and the intersectional plane for the rotational views shown in **C**.

(B) 3D reconstructions of the white and green cell shown in **A**. The cell soma is indicated by a coloured sphere, the volume occupied by the cell is shown as a grey shade around the process network.

(C) Transversal view of the confocal image in **A** at the positions indicated by the green (**C**) and white (**C'**) dashed line (90° rotation of x-axis around the y-axis). The dashed line in **C** outlines the axodendritic region, the dashed line in **C'** outlines the nuclear region identified by BODIPY staining.

(D) Quantification of cell complexity of OPCs in the nuclear (n=36) versus the axodendritic region (n=38) in 4 dpf old fish. The triangles are the cells shown in **A-C**. Boxes indicate the median with 25th and 75th percentiles, whiskers minimum and maximum. Mann-Whitney U test (U=211): $p<0.001$. Data from 23 animals in 11 experiments.

(E) Individual olig1:memEYFP-labelled OPCs (confocal image, 3D representation and 90° rotation of x-axis around the y-axis). The red arrowhead points to a cell with a complex morphology but soma in the axodendritic region, the white arrowheads point to somata of simple OPCs in the nuclear region.

Scale bar in all images: 20 µm.

3.1.6 Remodelling Behaviour of OPCs

One advantage of live imaging is the possibility of repeated imaging, which allows to observe the change of morphology (and position) over time. Hence, I imaged individually labelled OPCs with their soma in nuclear and axodendritic positions, respectively, with high temporal resolution (5 min) over short periods of time (2.5 hours) to assess if they differ regarding their process dynamics. In the presented image series (**Figure 3.1.6A-C**) the fraction of processes that underwent extension or retraction since the start of imaging is shown in magenta, whereas the stable processes are shown in green (see **section 2.2.3**). OPC processes are motile and undergo extensive extension and retraction; hence, the longer one would observe one cell, the more of the processes would appear in magenta. Remarkably, 'nuclear' OPCs seem to remodel only terminal processes (**Figure 3.1.6A**), whereas 'axodendritic' OPCs remodel also major branches (**Figure 3.1.6B**).

Furthermore, one can measure the fraction of processes that remain stable within a certain time (see **section 2.2.3** and **Figure 3.1.6D**). Time lapse movies (n('nuclear' OPCs)=4; n('axodendritic')=4) in young zebrafish between 3 and 7 dpf were recorded of which seven were longer than 150 min. There was a significant difference in the proportion of the stable processes after 150 min of imaging between OPCs in the nuclear (mean±SD: 38.8±10.7%, n=4) and axodendritic region (8.7±4.6%, n=3), respectively (**Figure 3.1.6D**). Moreover, there is a positive correlation between cell complexity at the start of imaging and the rate of process remodelling. The more complex the morphology of an OPC, the more stable are its processes over time (**Figure 3.1.6E**).

In addition, I acquired one example with two OPCs in the nuclear region with rather complex morphologies in 14-day old larvae (**Figure 3.1.6C**). The percentages of stable processes after 60 and 150 min (74 % and 68 %) is even higher than for 'nuclear' OPCs in younger fish (**Figure 3.1.6D**) suggesting that process remodelling slows down with age.

Figure 3.1.6 Process remodelling in OPCs.

(A-C) Example images of individually labelled olig1:memEYFP OPCs at 0 min, 30 min and 60 min of a time-lapse movie. One image was recorded every 5 min. **(A'-C')** Projections of the images from start until the indicated time are shown with the processes which remain stable in green and remodelled processes in magenta. **(A)** Example of an OPC with the soma in the nuclear region and a rather complex morphology. **(B)** Example of an OPC with the soma in the axodendritic region and a rather simple morphology. **(C)** Example of two OPCs with the somata in the nuclear region in 14 dpf old fish. The cell analysed in **D** is marked by a red arrowhead.

(D) Quantification of process maintenance over the time course of observation. OPCs with the soma in the nuclear region (n=4) are shown as grey data points connected by dashed lines; OPCs with the soma in the axodendritic region (n(≤60 min)=4; n(>60 min)=3) are shown as green data points. The black (nuclear region) and dark green (axodendritic region) data points connected with solid lines represent the means of the respective groups; error bars indicate the SD. Two-way repeated ANOVA comparing 'nuclear' and 'axodendritic' OPCs imaged over 150 min: F(1, 5)=22.32; p=0.005. One cell was analysed per fish. The blue datapoints show the example from the 14-dpf old zebrafish imaged in **C**.

(E) Correlation analysis of process remodelling after 60 and 150 min and the cell complexity at the start of imaging (0 min). Colour code as in **D**. 60 min: Pearson's r=0.97 with [0.859;0.995] 95 % CI, p<0.0001; linear regression model y=0.02*x+11.48 (R^2=0,95). 150 min: Pearson's r=0.97 with [0.833;0.996] 95 % CI, p=0.0002; y=0.02*x-2,68 (R^2=0,95).

Scale bar in all images: 20 µm.

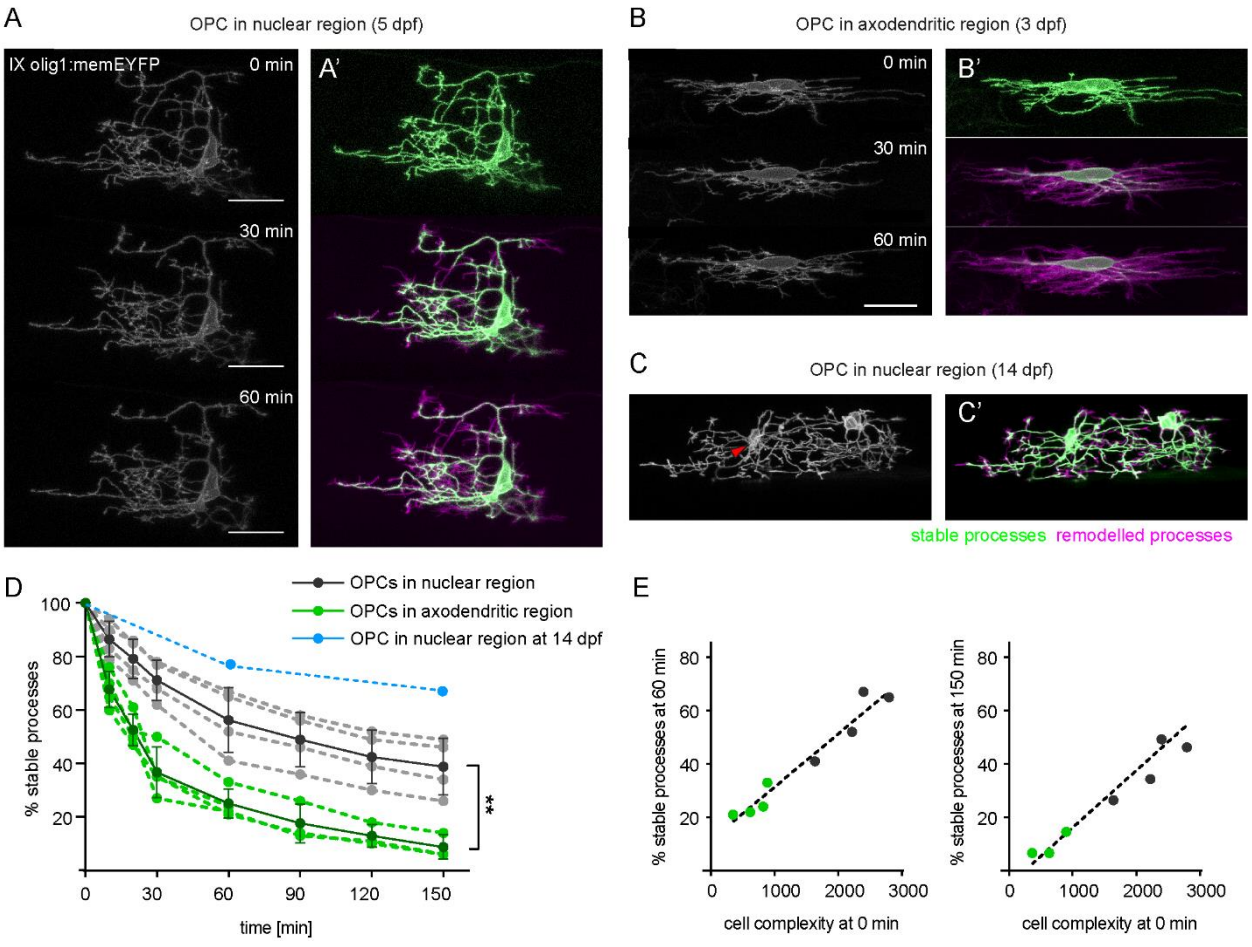

3.1.7 Summary - Properties of OPCs in the Zebrafish Spinal Cord

In the first part, OPCs in the zebrafish spinal cord were assessed regarding their localization, morphology, and process remodelling. Even though, somata of OPCs can be in the nuclear or axodendritic region, respectively, an important finding is that all cellular processes project to the axodendritic region in the vicinity of the same axons. In general, there is a positive correlation of a nuclear OPC soma position with complex cell morphology and a slow process remodelling rate, whereas OPCs with the soma in the axodendritic area mostly have a simple morphology but fast process remodelling (see **sections 3.1.5 & 3.1.6**). However, this notion does not apply exclusively to all OPCs (**Figure 3.1.5E**); thus there is still the open question if these relationships between the parameters are causal. Cell complexity and process stability are continuous variables and the analysed cells are distributed within a certain range. OPC localization to the nuclear or axodendritic region is the only binary parameter which can be used group OPCs in two comparable entities. However, it was not answered yet whether OPCs can change their position and whether this would influence their other properties (see **section 3.2.6**).

Heterogenous OPCs may also have different functional properties, which in a progenitor cell type would primarily regard aspects of proliferation and differentiation like cell cycle length, proliferation frequency or differentiation capacity. The aim of the following work was to reveal whether there are indeed functional differences between OPCs in the spinal cord and how different OPC subgroups relate to each other.

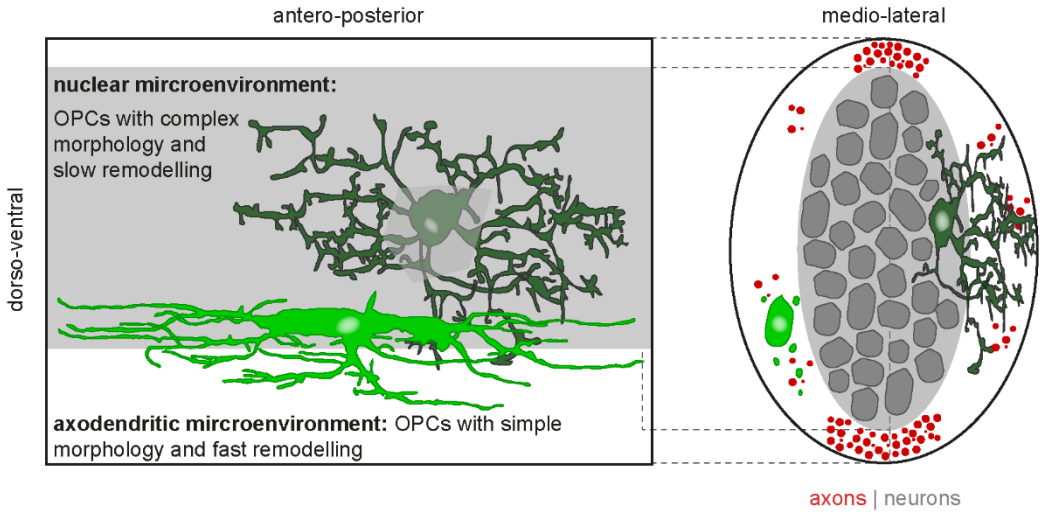

Figure 3.1.7 Cartoon summarizing the previous results regarding OPC heterogeneity.

OPCs in the spinal cord of the developing zebrafish can differ regarding soma position, morphology, and process remodelling.

3.2 Characterization of OPCs Behaviour Over Time by *in vivo* Imaging

3.2.1 OPC and OL number Over Time

To investigate whether there are not only morphological but also functional differences between OPCs in the spinal cord, i.e. regarding proliferation and differentiation, one has to observe OPCs over longer time scales of several hours or even days to assess which OPCs show which behaviour. To this aim, I started with a general assessment of the OL-lineage during early zebrafish development.

The first olig1:memEYFP-labelled OPCs emerged between 2-3 dpf (**Figure 3.2.1A**) shortly before also the first mbp:nls-EGFP-positive OLs could be observed at 3 dpf (**Figure 3.2.1B**).

Whereas the number of the OPCs was altered only moderately from 3 dpf until 28 dpf, the number of myelinating oligodendrocytes increased strongly during the same time (**Figure 3.2.1B&C** and **Table 1.7.1.1**). There were only 7.3±5.7 OLs counted per field of view at 3 dpf but the OLs (n=44.7±6.0) outnumber the OPCs (n=22.3±4.3) already at 7 dpf. The highest rates of OL generation were measured until 10 dpf (7.0 cells/day between 3-10 dpf compared 1.8 cells/day between 10 -28 dpf; calculation based on means). Concurrently the number of OPCs decreased slightly but significant (29.6±6.4 at 3 dpf versus 19.3±4.5 at 10 dpf; **Figure 3.2.1C**) probably as a consequence of differentiation. The initial OPC number is restored between 10 and 28 dpf (32.0±5.9 at 28 dpf). This could be theoretically achieved in two ways: either by proliferation of existing OPCs or by addition of new OPCs by development from neural progenitors (NPs). The experimental setup did not allow to distinguish between these two possibilities as the temporal resolution was not high enough, however time lapse imaging described below indicates that NPs are not involved (see **section 3.2.3** and **3.2.6**).

The steady addition of new OLs, even if the process slows down after 10 dpf can be probably explained by animal growth. The number of sheaths per OL is established shortly after initiation of the first myelin sheath (Czopka et al., 2013), afterwards there is only occasional sheath retraction. Individual sheaths are limited in their growth capacity (Auer et al., 2018), hence new myelin sheaths are required to cover the length of the axon in a growing organism adequately. These new myelin sheaths are generated by newly differentiated oligodendrocytes. Therefore, after a phase of logarithmic growth until approximately 10 dpf to establish the initial OL population the relationship between OL number and animal age resemble more a linear growth synchronized with body growth (**Figure 3.2.1C**). However, after the zebrafish start eating

at 5 dpf they can vary quite extensively in size dependent on their food intake, which likely caused the observed higher variability in cell numbers in older larvae.

In summary, during the first month of zebrafish development there emerged a population of OPCs that remains almost constant over time giving rise to an ever-increasing population of myelinating OLs.

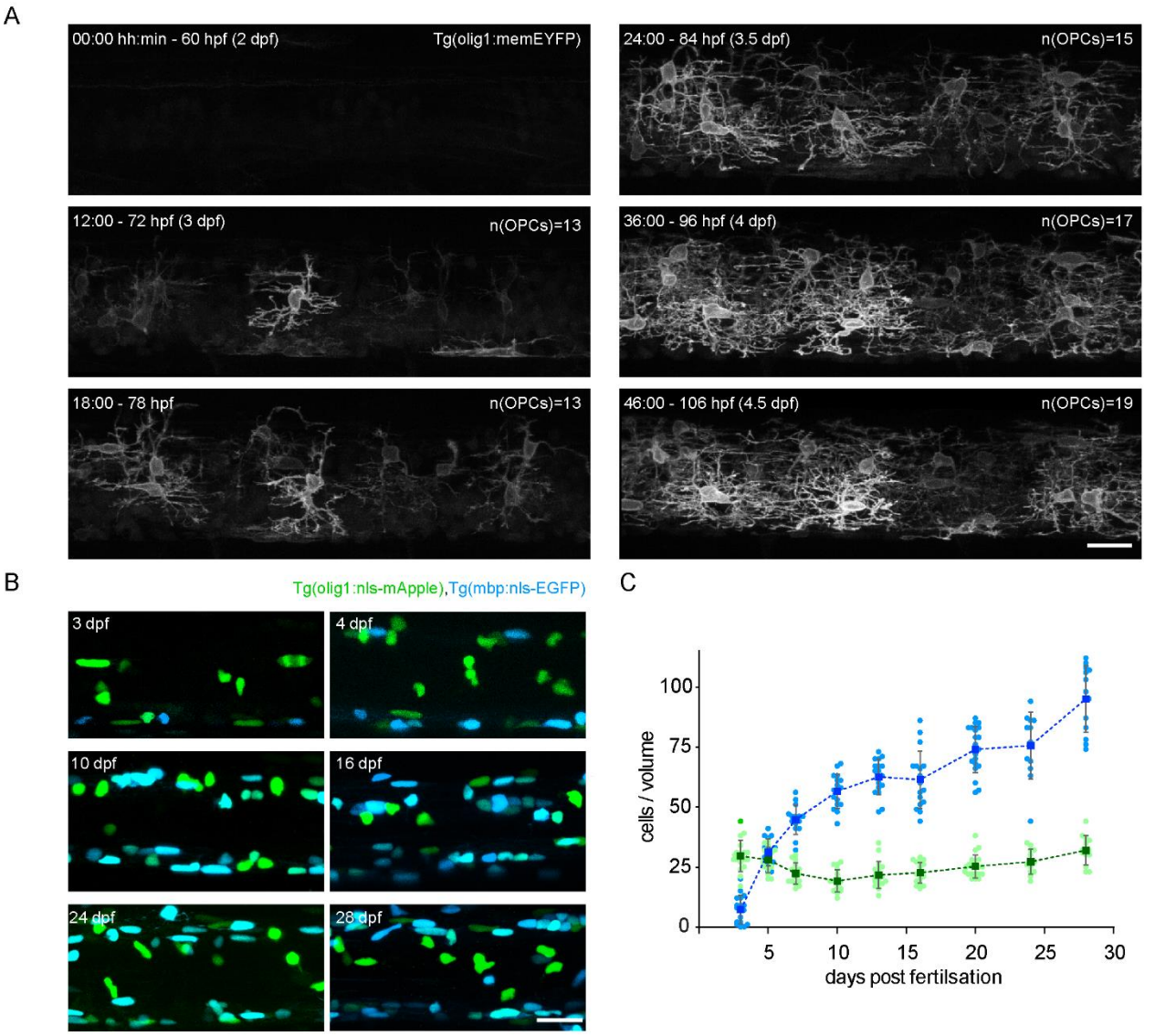

Figure 3.2.1 Numbers of OPCs and OLs in the zebrafish spinal cord.

(A) Confocal time lapse imaging of OPC appearance in the spinal cord in Tg(olig1:memEYFP) zebrafish embryos between 60 and 106 hpf. There were no labelled OPCs in the beginning whereas the population is almost established in number at 72 hpf (n=13) and until 106 hpf (n=19) new cell are generated with a much lower rate.
(B) Confocal images of the double-transgenic Tg(olig1:nls-mApple),Tg(mbp:nls-EGFP) spinal cord at different ages between 3 and 28 dpf. OPCs (mApple+, EGFP-) are shown in green, mOLs in blue (EGFP+ only) or cyan (EGFP+ and still mApple+).
(C) Graph showing the development of OPC (green) and mOL (blue) numbers between 3 and 28 dpf in a 233 µm long part of the spinal cord (somite 17 was always in the centre of the image). Mean with SD is shown (connected with a dashed line for better visualization). Averaged data from 142 fish in 9 independent experiments (2-4 experiments for each age). **OPC statistics**: one-way ANOVA (even though OPC numbers at 20 dpf are slightly divergent from normal distribution by Shapiro-Wilk test, $p=0.0179$), $F(8, 133)=9.559$, $p<0.001$. **OL statistics**: one-way ANOVA (as all groups passed normality test with $p>0.05$), $F(8, 133)=119.2$, $p<0.001$.
Scale bar in all images: 20 µm.

Table 3.2.1.1 Numbers of OPCs and OLs in the zebrafish spinal cord.

A visualization of the data is shown in **Figure 3.2.1C**.

Age (dpf)	3	5	7	10	13	16	20	24	28
Fish (n)	17	15	15	16	17	17	20	12	13
OPC number (mean ± SD)	29,6 ±6,4	28,1 ±5,2	22,3 ±4,3	19,3 ±4,5	21,7 ±5,4	22,6 ±4,2	25,3 ±4,6	27,3 ±5,1	32,0 ±5,9
OL number (mean ± SD)	7,3 ±5,7	31,1 ±5,5	44,7 ±6,0	56,6 ±6,9	62,6 ±7,2	61,5 ±11,6	74,1 ±9,4	75,7 ±13,3	95,2 ±13,4

3.2.2 OL-lineage Cell Population Analysis

Next, I was interested in the fate of individual OPCs over time. By grouping OPC fates in certain categories it should later become feasible to figure out whether OPC fate correlates with the other properties used to distinguish individual OPCs, which could lead to the identification of functionally distinct OPC subtypes. In the first instance, I focused solely on fate observation on a relatively short time scale shortly after establishment of the OPC population at 3 dpf to get an initial idea of possible OPC behaviours. This was achieved by continuous time lapse imaging in three double-transgenic Tg(olig1:nls-mApple),Tg(mbp:nls-EGFP) embryos in which all OPCs and OLs should be labelled (**Figure 3.2.2A**). To be able to follow individual cells, a temporal resolution of minimally 30 min was required as some OPCs appeared to be highly migratory. As the fish must be embedded the entire time and is constantly exposed to light and according phototoxicity, an observation of more than 48 h was not feasible without detrimental effects on the animal. To be sure to perform the experiment only with healthy fish the observation time was limited to 36 h (from 3.0 dpf to 4.5 dpf) and blood flow and tissue integrity were controlled regularly.

Whereas the number of OPCs decreases slightly (in 2 of 3 fish), there was a 4-5-fold increase in the OL number (**Figure 3.2.2B**), in accordance with the results from **section 3.2.1**. In general, some OPCs were migratory or underwent proliferation, differentiation (indicated by the onset of EGFP expression) or both, whereas others did not (**Figure 3.2.2A&C**). In consistence with the current state of knowledge, no proliferation or migration of myelinating OLs was observed. In detail, one can distinguish five possible fates for individual OPCs which occur also with different frequencies (**Figure 3.2.2C**):

1. Cells that neither divided nor differentiated: 24 % (example in **Figure 3.2.2A**)
2. Cells that differentiated directly without proliferation: 42% (example in **Figure 3.2.2A**)
3. Cells that divided one or several times but none of the daughter cells differentiated until the end of the imaging: 27% (example in **Figure 3.2.2A**)
4. Cells that divided one or several times and all the daughter cells differentiated: 6%
5. Cells that divided ($\geq$1x) and only one or several of the daughter cells differentiated: 1%

However, one has to pay attention that the observed frequencies highly depend on duration of observation as well as likely on the age of the animal assuming that OPC dynamics would change over time. OPCs could have been divided before as well as could have been divided or differentiated afterwards. Specifically, the likelihood that an OPC differentiates increases with increasing duration of observation, at the same time the frequencies of fates 1 and 3 would decrease.

More definite conclusions could be drawn if several proliferation events or a proliferation followed by differentiation occurred in the same OPC clone (included in fates 3, 4 and 5, n=57). There were 31 OPCs that underwent repeated proliferation. Thereby, the average time between two cell divisions was 16.8±5.5 h (**Figure 3.2.2D**). Of the OPCs which divided and differentiated in 83 % (10/12) of the cases both daughter cells undergo differentiation. This points in the direction of previously reported findings that OPC cell division increases the likelihood of subsequent differentiation (Hill et al., 2014). The average time difference between cell division and differentiation was 23.3±7.3 h (**Figure 3.2.2D**). This would implicate that only for cells that differentiate in the last third (24-36 h) of 36h imaging observation the previous proliferation is likely captured, which probably results in an overestimation of direct differentiations (fate 2) in the presented results of this experiment (**Figure 3.2.2C**).

In all three fish, only two new OPCs appeared, visualized by increasing mApple fluorescence, that did not clearly derive from another *olig1*-labelled OPCs. This supports the previous result that the founder population of OPCs was indeed generated between 48 and 72h of development (2-3 dpf) and new OPCs are usually not generated from neural precursors afterwards but by OPC proliferation (**Figure 3.2.2E** and **Figure 3.2.1A**).

These findings were crucial for the analysis of the following experiments observing individual OPCs over longer time which however does not allow such high temporal resolution (see **section 3.2.6**). Knowing that OPCs arose from other OPCs as well as knowing the time course of differentiation and proliferation in early zebrafish development helped to elucidate the origin of new OPCs and OLs even with time spacing of 12 h or 24 h between the single observations.

Recurring to the question if there is behavioural heterogeneity in OPCs, the results provoke the following questions: Does a fraction of OPCs really do not contribute to myelination; and how are these cells different from the OPCs that readily differentiate in mOLs?

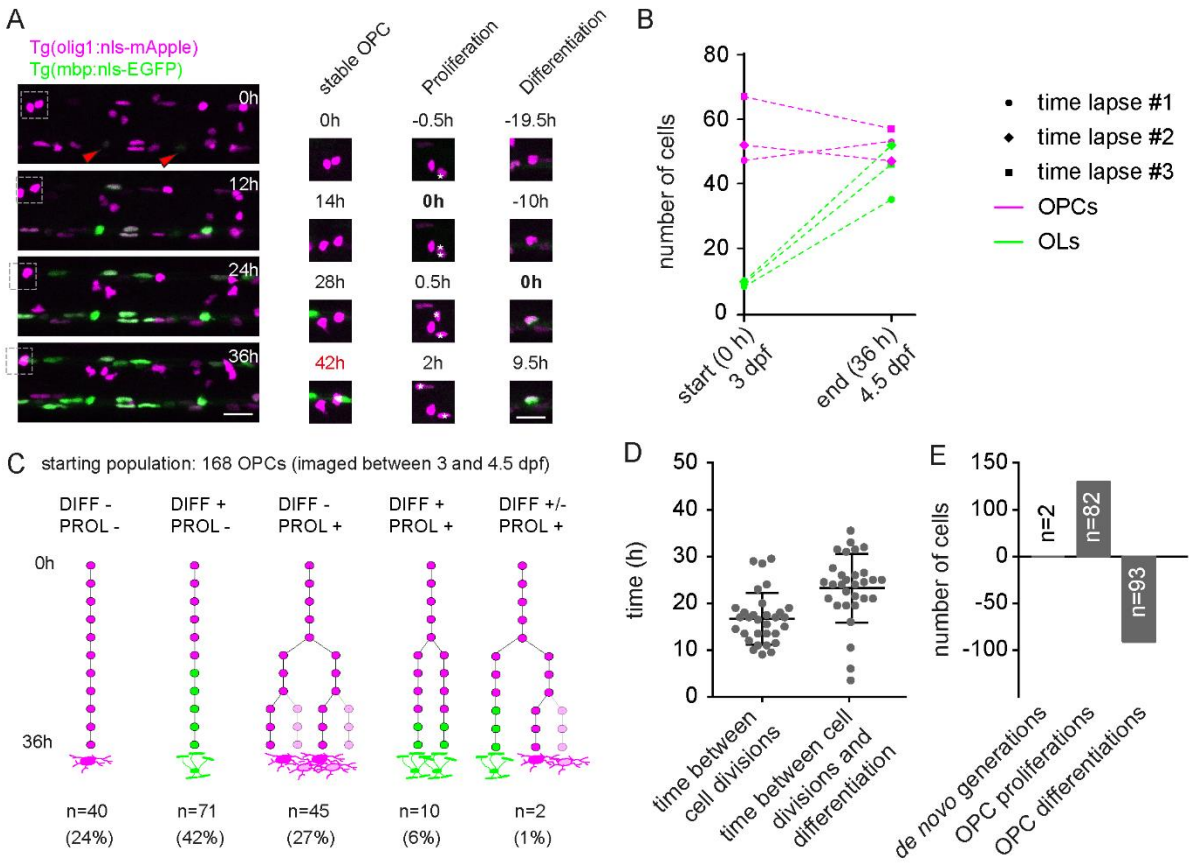

Figure 3.2.2 Time-Lapse Imaging of OPCs and OLs between 3 to 4.5 dpf.

(A) Confocal time lapse images of double-transgenic Tg(olig1:nls-mApple),Tg(mbp:nls-EGFP) embryos at different times within 36 h of imaging. Left side: MIP of a stretch of the whole spinal cord. The boxed area shows the example of stable OPCs (right). Right side: individual OPC behaviours are shown (time stamps indicate the time relative to the respective event). Scale bar in all images: 20 µm.

(B) The number of OPCs (magenta) and OLs (green) at the start and end of observation (n(fish)=3).

(C) Schematic overview showing the fates of individual OPCs during observation. All possible fates regarding proliferation and differentiation occurred but with different frequencies. The starting population (n=168 OPCs in 3 animals) also includes the two OPCs that were actually not present at the start of imaging but emerged later (compare **E**). Number of cells at the end of observation: n(OPCs)=157; n(OLs)=133.

(D) Graph showing the time between two cell divisions (n=31) or cell division followed by differentiation (n=30) of the same cell.

(E) Numbers of cells that are added to (generated from NPs or by OPC division) and lost from the OPC population (by differentiation) during 36 hours of imaging.

3.2.3 Short-term Fate analysis of individual OPCs

As OPCs could show indeed a variety of behaviours within a given time frame, the next question to answer was whether the previously described morphologically different OPCs which also have a certain regional preference also have distinct proliferation behaviours or differentiation fates, respectively.

Remarkably, the OPCs that underwent differentiation during the population time-lapse observation were primarily found in the axodendritic compartment based on the assessment of their soma shape (see **section 3.1.3**), which was rather oval than roundish (**Figure 3.2.2A**). To investigate this in more detail, I imaged 34 individually labelled OPCs at 3 to 5 dpf which either had a clear axodendritic or nuclear soma localization (**Figure 3.2.3A&B** and **Table 3.2.3.1**). The imaging was carried out continuously for at least 24 hours or until they started to form myelin sheaths. OPCs in the axodendritic region differentiated frequently (81 %). Interestingly, no cell in the nuclear region differentiated in this dataset (despite this has been observed in the context of other imaging experiments as described below, see **Figure 3.2.4** and **Figure 3.2.5**). Proliferation of OPCs occurred in the nuclear as well as in the axodendritic region (38 % and 19 %). There was only one example of an OPC that proliferated prior to differentiation, which is in line with the previous findings that there is roughly a gap of 24 hours between these two events (see **Figure 3.2.2D**), which is already the maximum length of the observation in this experiment. Only one OPC in the axodendritic region neither differentiated nor proliferated, whereas 8 of 13 cells were inactive in the nuclear region.

In addition, I measured cell complexity of the imaged OPCs at the start of observation. All the cells that underwent differentiation also had a simple morphology (**Figure 3.2.3A&B**). Interestingly, this would be in contradiction with the assumption of morphological advancement during OL-lineage progression which suggests that the most complex cells are also most likely to differentiate (see **section 1.4**). Therefore, I assessed OPC morphology prior to differentiation in more detail. Even though there were intercellular differences, there was a trend that 'axodendritic' OPCs were more complex closer myelin induction with a steep increase in complexity within the 5 hours directly before (**Figure 3.2.3A&C**). For one example OPC, I measured the complexity at 4.7 h and 0.5 h prior to the first myelin sheath formation and there was a 3.5-fold increase of the complexity value (667 to 2353) within this time (**Figure 3.2.3C**). This finding is further supported by examples from another dataset for which individual OPCs were imaged repeatedly every 12 h. Occasionally, OPCs in the axodendritic region were observed that acquired a much more complex morphology before the first myelin sheaths were formed (**Figure 3.2.3D&E**).

Consequently, there must be two subgroups of cells with morphology considered rather as complex within the OL-lineage. One group that does not participate in myelin formation or at least is less likely to do so and a second group that is highly transient and therefore is found less frequently, which occurs immediately prior to the initiation of the first myelin sheaths. According to the current state of knowledge on OL-lineage cell development, the second group is likely to correspond to cells known as pre-OLs – postmitotic oligodendrocytes prior to myelination, and thus are referred to in the following as zebrafish pre-OLs (**zf-pre-OLs**). In line with this view, these cells in zebrafish were never observed to divide in contrast to cells in the first group which divide regularly and hence are considered OPCs (**Figure 3.2.3B** and **section 3.2.6**). This is in line with the observation that OPCs proliferate rarely within the 24 hours before starting myelination (**Figure 3.2.2D**). As zf-pre-OLs represent a transitional stage between 'axodendritic' OPCs and myelinating OLs their somata were also found predominantly in the axodendritic region, in distinction to complex OPCs (**Figure 3.2.2D**). Furthermore, there are also morphological differences: The processes of 'nuclear' OPCs have an overall radial orientation (compare **Figure 3.2.3A**), whereas zf-pre-OLs processes are much more aligned with the spinal axons running in anterior-posterior direction (**Figure 3.2.2D**). Unfortunately, these differences were neither reflected in branch point density, summed process length or occupied volume of the individual cells (not shown). Despite the re-occurrence of zf-pre-OLs in different experimental settings, due to their transiency and the absence of an appropriate marker for pre-OLs in zebrafish the number of their observations was quite low and hence the results on this topic should be still considered as preliminary.

Table 3.2.3.1 Short-term fates of 'nuclear' and 'axodendritic' OPCs.

n=34	**nuclear region**	**axodendritic region**
Differentiation	0	16
Proliferation	5	3
Proliferation and Differentiation	0	1
Nothing	8	1
sum	13	21

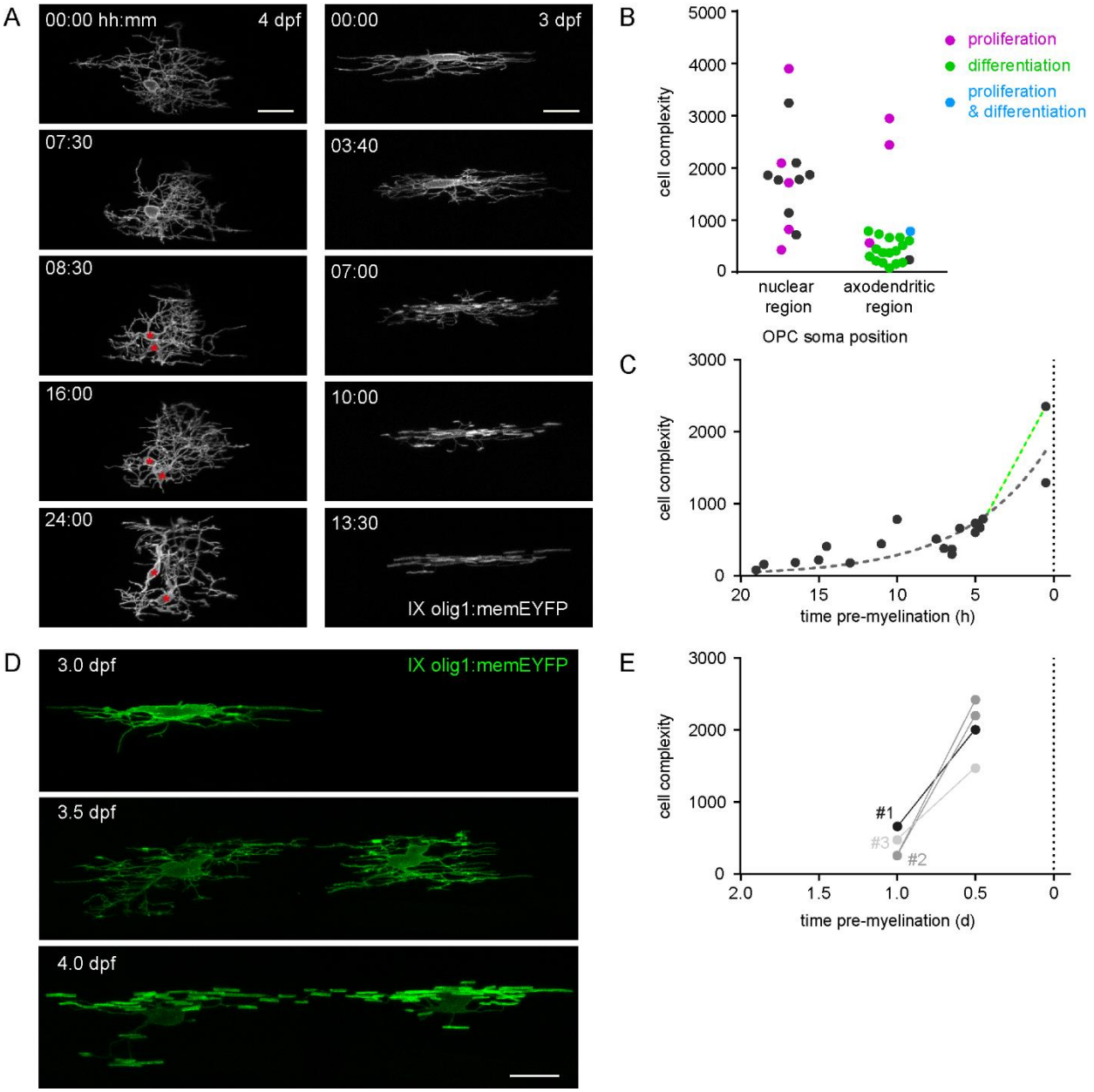

Figure 3.2.3 'Axodendritic' OPCs with simple morphology are more prone for differentiation.

(A) Confocal time lapse images of individually olig1:memEYFP-labelled OPCs. Imaging was carried out for 24 h every 10 min or until they start to form myelin sheaths (differentiation). Left: example of an OPC with complex morphology in the nuclear region undergoing proliferation. The daughter cells are marked with red asterisks. Right: example of an OPC with simple morphology in the axodendritic region undergoing differentiation within 7 h of imaging.**(B)** Quantification of data from 34 OPCs in the axodendritic (n=21) and nuclear (n=13) compartment imaged between 3 and 5 dpf (data from 11 animals in 8 independent experiments). Different fates are indicated by colour: proliferation (magenta), differentiation (green) or both (blue). In addition, their complexity value at the beginning of the imaging is indicated by the Y dimension. **Proliferation statistics**: 5/13 versus 4/21, two-tailed

Fisher's exact test, p=0.254. **Differentiation statistics**: 0/13 versus 17/21, two-tailed Fisher's exact test, p<0.001.
(C) Graph showing the complexity values of OPCs which differentiated during time lapse observation (n=18; one cell was measured twice at different times connected by the dashed blue line) in relation to the time of differentiation (x=0). The dashed green line represents an exponential growth curve fit to the data using a nonlinear regression model (Y0=1915 [1454;2400]; k=-0.189 [-0.265;-0.126];
Tau=-5.304 [-7.911;-3.772]; Doubling time=-3.676 [-5.484;-2.614]; d(f)=17; R^2=0.767).
(D) Confocal images of an individually labelled olig1:memEYFP OPCs in the axodendritic region that divided and differentiated within one day.
(E) Quantification of the complexity values of OPCs prior to differentiation. Three examples are shown, images of example #2 are shown in **D**. Complexity values (1.0 and 0.5 d pre-myelination): #1 (667; 2043), #2 (251; 2248 & 2476), #3 (424; 1438).
Scale bar in all images: 20 µm.

3.2.4 'Axodendritic' OPCs are the Source of Oligodendrocytes Irrespective of Age

The previous results from 3 to 5 dpf old zebrafish embryos showed that it is the 'axodendritic' type of OPCs with a rather simple morphology that differentiates to oligodendrocytes, whereas the 'nuclear' OPCs with complex morphology were not observed to do so. However, it is possibility that the latter only differentiate later in development. Unfortunately, developing zebrafish gradually lose their accessibility for confocal imaging with age. Nevertheless, I advanced the observation of differentiating OPCs up to almost three weeks of age to figure out whether the preferential differentiation of OPCs with axodendritic soma localization was just a transient peculiarity of very young zebrafish embryos or not. Beyond that age it becomes increasingly difficult to perform live imaging in the zebrafish, as imaging depth of single-photon confocal microscopy is limiting especially in larger animals; furthermore, the fish become less translucent, build pigments and are less tolerant to anaesthesia.

I imaged individual OPCs repeatedly over several days and focused on the observed differentiation events (**Figure 3.2.4**). Also in fish older than two weeks of age, myelinating OLs derived from OPCs in the axodendritic compartment displaying a simple morphology (**Figure 3.2.4A**, cells #1, #2 and #4). However, the process of differentiation was slower than in younger fish. In the shown examples axodendritic OPCs require 2 to 3 days to initiate myelination, which is achieved in embryonic fish usually within one day or less (compare **Figure 3.2.3Figure 3.2.3**). Due to this deceleration the previous described transitional state of zf-pre-OLs was observed more frequently in older fish as it persists presumably for more than one day at this age (**Figure 3.2.4A&B**, cell #1 and #2 at 15 dpf, and #3 and #4 at 17 dpf).

When I measured the OPC complexity within one day (12 h or 24 h) before the cell was observed to differentiate and form myelin sheaths during the first week of zebrafish development (3-7 dpf), the majority of cells were in the axodendritic (n=21/22) region and had usually low complexity values (<1000) (**Figure 3.2.4C**). In older fish the differentiation process is comparatively delayed as described above , so I considered the cell complexity rather within 48 hours before myelin sheaths were observed the first time, to reduce the confounding by zf-pre-OLs that display also a complex morphology prior to myelination (as still seen in the graph for the two cells measured at 12 dpf, **Figure 3.2.4C**). In general, also the OPCs that were observed to differentiate in older fish were predominantly found in the axodendritic region (n=18/19) and had a simple morphology.

However, taken together at a low level I observed OPCs in the nuclear region that undergo differentiation in different experimental settings (**Figure 3.2.4A** cell #3 and **Figure 3.2.4C**; OLs with a roundish soma in **Figure 3.2.2A**). Some more examples could be considered if cells for which the complexity value was not

measured were also included in the analysis (**Figure 3.2.4D**). For this, I determined the localization of all imaged newly differentiated OLs between 4 and 18 dpf before and after myelination starts (n=256). Most OLs were found again in the axodendritic region and derived from OPCs which had been there already directly prior to differentiation (n=200, 78%). In some cases OPCs transit their soma from the nuclear to the axodendritic region directly prior to differentiation (n=18, 7%; compare **section 3.2.6**). The OLs found in the nuclear region derived from OPCs with their soma also in this region (n=37, 14%). There was only one observed exception when an OL with a cell body in the nuclear region derived from an 'axodendritic' OPC between 3 and 4 dpf. Differentiation in the nuclear region did not increase significantly with age (13% during the first week versus 23% during the third week of zebrafish development), arguing against the hypotheses that 'nuclear' OPCs act as a reserve that is activated in later development, at least not during the period analysed.

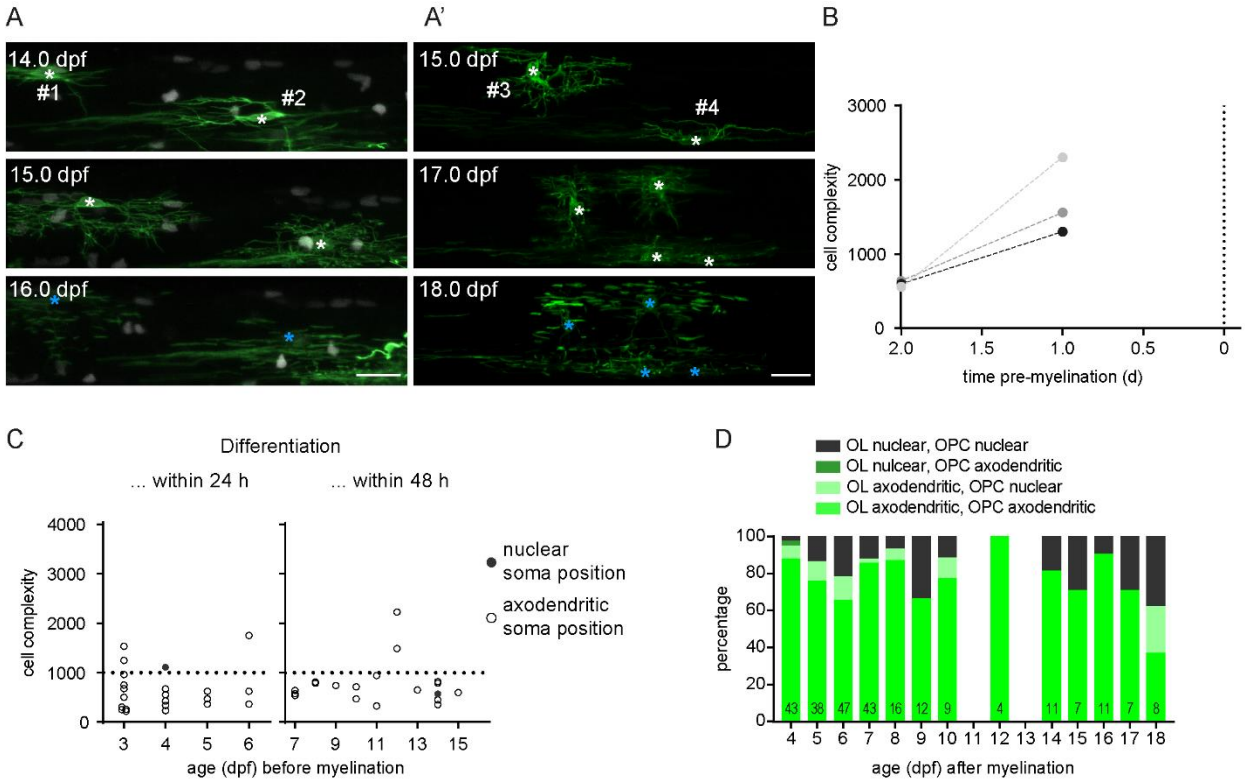

Figure 3.2.4 Differentiation occurs predominantly in the axodendritic region.

(A) Series of confocal images of individually olig1:memEYFP-labelled OPCs imaged consecutively over several days during the third week post-fertilization. **(A)** Two OPCs (#1, #2) differentiated in the axodendritic region. **(A')** One OPC divided and differentiated in the nuclear region (#3), the other OPC proliferate and differentiates in the axodendritic region (#4). Asterisk label OPCs (white) and OL somata (blue).Scale bar in all images: 20 µm.

(B) Cell complexity of OPCs prior to myelin formation during the third week post-fertilization (n=3).

(C) Quantification of the complexity and position of OPCs that are going to differentiate during the first week post-fertilization (within 24 h, n=22, left graph) or later (within 48 h, n=19, right graph).

(D) Graph showing the positions of OLs which were observed before and after differentiation over three weeks of zebrafish development. Absolute numbers are indicated in the bars. The 'after differentiation' time is defined as the time when a former OPC was observed to produced myelin sheaths. The 'before myelination' time is retrospectively defined as the last time, when the cell was still without myelin sheaths. Comparison of differentiation in the axodendritic region during the first week (3-6 dpf; 111/128; 87%) and third week (14-18 dpf; 34/44; 77%): two-tailed Fisher's exact test, p=0.153.

3.2.5 Oligodendrocyte Frequency in the Nuclear Region

Based on individually labelled cells there is always the chance that some form of unintended selection bias is introduced, especially when using relative low numbers as often done in *in vivo* imaging. Thus, it is difficult to determine absolute numbers for OPC differentiation in the nuclear region by time-lapse imaging of individual cells. Therefore, as a complementary approach I quantified the number of myelinating OLs in the nuclear region in full-transgenic Tg(mbp:nls-EGFP) fish between 3 dpf and 28 dpf based on their position in the 3D image and soma shape. As these cells are not migratory, they must be derived of OPCs that cell bodies also resided in this region prior to differentiation. At all ages analysed no more than 12.7±5.2% (16 dpf) of the OLs were in the nuclear region (**Figure 3.2.5** and **Table 3.2.5.1**).

Taken together with the previous section, it could be confirmed that the majority of differentiation events took place in the axodendritic compartment by OPCs with a simple morphology in the young zebrafish embryos as well as in the older larvae up to 28 dpf and most likely beyond.

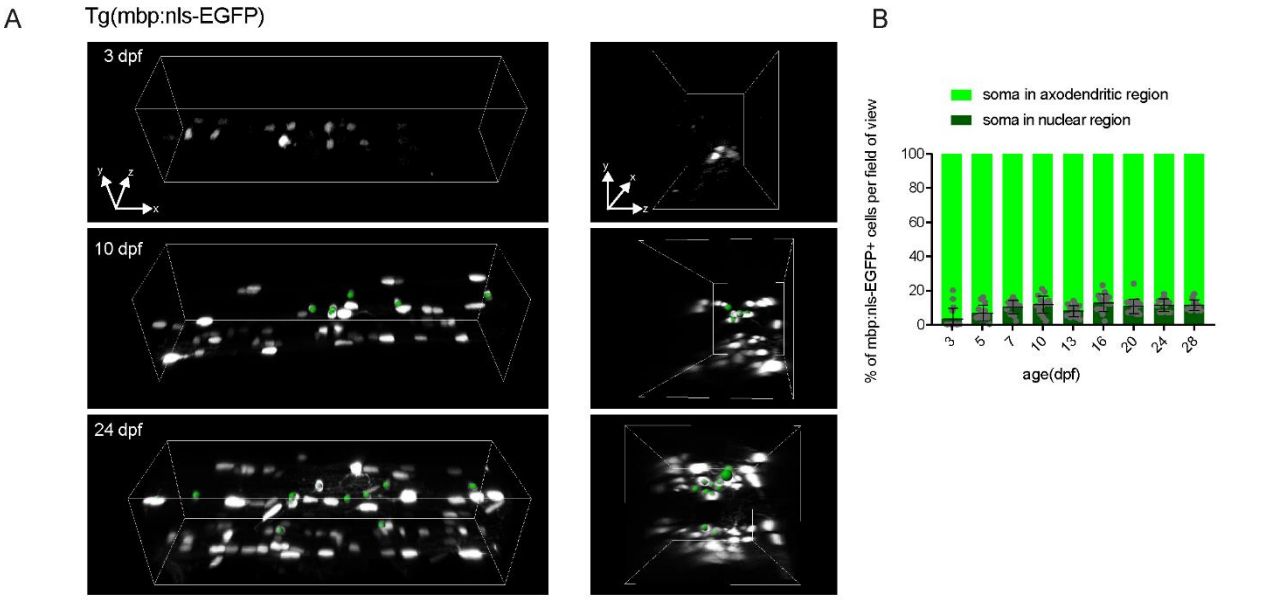

Figure 3.2.5 Oligodendrocyte somata in the nuclear region.

(A) 3D representations of the Tg(mbp:nls-EGFP) transgenic spinal cord at 3 dpf, 10 dpf and 24 dpf. Slightly tilted lateral view (left) and 90° rotation around the y-axis (right). X-axis: anterior-posterior, y-axis: dorsal-ventral, z-axis: left-right. OLs in the nuclear region are marked by green spheres (3/10/24 dpf: n=0/5/11).

(B) Graph showing the fraction of OLs in the axodendritic (light green) and nuclear region (dark green) in Tg(mbp:nls-EGFP) transgenic zebrafish between 3 and 28 dpf. See also **Table 3.2.5.1**.

Table 3.2.5.1 Number of OLs with their soma in the nuclear region.

Age (dpf)	3	5	7	10	13	16	20	24	28
'nuclear' OL number (mean ± SD)	0,5 ±0,9	2,2 ±1,7	4,7 ±1,8	6,7 ±3,0	4,9 ±2,1	8,1 ±4,2	8,0 ±3,7	8,3 ±2,1	10,7 ±2,6
'axodendritic' OL number (mean ± SD)	6,8 ±5,1	28,9 ±4,5	40,1 ±5,2	49,9 ±6,1	57,4 ±6,8	53,4 ±8,9	66,1 ±8,0	67,3 ±13,3	84,5 ±13,2
'nuclear' OL frequency (%) (mean ± SD)	3,2 ±6,1	6,7 ±4,4	10,2 ±3,7	11,7 ±4,9	7,9 ±3,1	12,7 ±5,2	10,6 ±4,1	11,4 ±3,6	11,4 ±2,9
Number of animals	17	15	15	16	16	17	20	12	13

3.2.6 Fate of Complex OPCs in the Nuclear Region

When the majority of myelinating OLs is generated from simple OPCs in the axodendritic region, what is the role of the complex OPCs that have their cell soma preferentially in the nuclear region? Furthermore, as the myelination-competent OPCs seem to differentiate with a higher frequency as they proliferate (**Figure 3.2.3**), how is it achieved that their pool is not depleted over time? To answer these questions, I extended the observation of individual olig1:memEYFP-labelled OPCs (as in **Figure 3.2.3D** and **Figure 3.2.4A**) over several days. An observational interval of 12 h or even 24 h was sufficient to trace proliferations and differentiation events of individual cells given their cycle times and differentiation frequency (**Figure 3.2.2D**). The observation was not started before 3 dpf, when the OPC population is already established; if new labelled cells appear, they are expected to derive from other labelled OPCs in the spinal cord (**Figure 3.2.2**). From the consecutive image series, it was possible to track proliferation and differentiation fate of the starting cells and to reconstruct clonal trees (**Figure 3.2.8A**). I acquired more than 100 examples of OPCs that had a complex morphology and a nuclear soma localization in the beginning followed for up to 11 days (see below **section 3.2.6.3**).

3.2.6.1 Examples of Possible OPC Fates and Behaviour During Long-Term Observation

The most significant finding was, that over time these cells could indeed give rise to myelinating OLs (**Figure 3.2.6C&D** and **Figure 3.2.7A**). Based on proliferation and differentiation, OPC fates could be grouped in five major categories (see also **Figure 3.2.2**): OPCs that did not undergo neither proliferation nor differentiation (**fate 1**); OPCs that differentiated directly without prior division (**fate 2**), OPCs that proliferated but none of the daughter cells differentiated during the time of observation (**fate 3**); OPCs that proliferated and subsequently daughter cells differentiated. For the latter fate, it was distinguished whether after proliferation(s) all daughter cells differentiated (**fate 4**) or only a part of the daughter cells did so (**fate 5**). The distribution of the clonal example trees among these categories is shown in **Figure 3.2.9A** (fate 4 and 5 is shown as a common group). Representative image series for the respective fates are shown in **Figure 3.2.6**. In the first example (fate 1), two OPCs were imaged over ten days. During this time, no proliferation or differentiation occurred (**Figure 3.2.6A**). The second example shows an OPC that proliferated (fate 3) but both daughter cells remained OPCs with their soma localized in the nuclear region and a complex morphology at least for 4 days after proliferation (**Figure 3.2.6B**). Another example (fate 5) shows an OPC that proliferated once between 4 and 5 dpf; one daughter cell remained in the nuclear region whereas the other cell, which already had a simpler morphology after the cell division, migrated its soma to the axodendritic region around 6 dpf and differentiated one day later at 7 dpf (**Figure 3.2.6C**). One

'nuclear' OPC can also give rise to several myelinating OLs undergoing several rounds of cell cycle (**Figure 3.2.6D**, image series for fate 4; **Figure 3.2.7A**, another image series for fate 5).

This exemplifies how complex OPCs with the soma in the nuclear region undergo morphological and regional transformation into simple, 'axodendritic' OPCs to produce myelinating OLs. However, in the minority of cases when OLs with the soma in the nuclear region were generated, the re-localization of the soma to the axodendritic region was not required (**Figure 3.2.6D'**, see also **Figure 3.2.4A'**).

Figure 3.2.6 Clonal analysis of individual OPCs.

Series of confocal images over several days starting with individually olig1:memEYFP-labelled OPCs in the nuclear region. For **B**, **C** and **D** the respective clonal trees are depicted next to the images. Open circles are OPCs, crosses are myelinating OLs in the nuclear (dark green) or axodendritic region (light green).

(A) Two OPCs that did not undergo neither proliferation nor differentiation (6-16 dpf).

(B) One OPC that divided but did not form myelinating OLs between (3-7 dpf).

(C) One OPC that divided and one daughter cell (indicated by arrowheads) differentiated in the axodendritic region (3-7 dpf).

(D) One OPC that underwent several rounds of proliferation (n=5) and all daughter cell (n=6) differentiated (4-9 dpf). OPC cell bodies were indicated by a white arrowhead from 5 dpf on. A blue arrowhead points to an OL cell body at the first image after differentiation. Additionally, some individual cells are labelled with an "ab" code for better traceability. In the boxed area at 6 dpf and 6.5 dpf, the intensity has been increased for better visibility of the OPC at the distal side of the spinal cord. At 7.5 dpf a sub-projection of several confocal planes with this cell is shown instead in the upper right corner (to avoid overexcitation of the OPC at the proximal side).

(D') One OPC that underwent several rounds of proliferation (n=4) and all daughter cell (n=5) differentiated (4-10 dpf). The dashed boxes at 7.5 dpf and 8 dpf indicate the position of the sub-projection shown next to the image with an additional cell at the distal side of the spinal cord. Two of the observed cells did not differentiate with the soma in the axodendritic but the nuclear region.

Scale bar in all images: 20 µm.

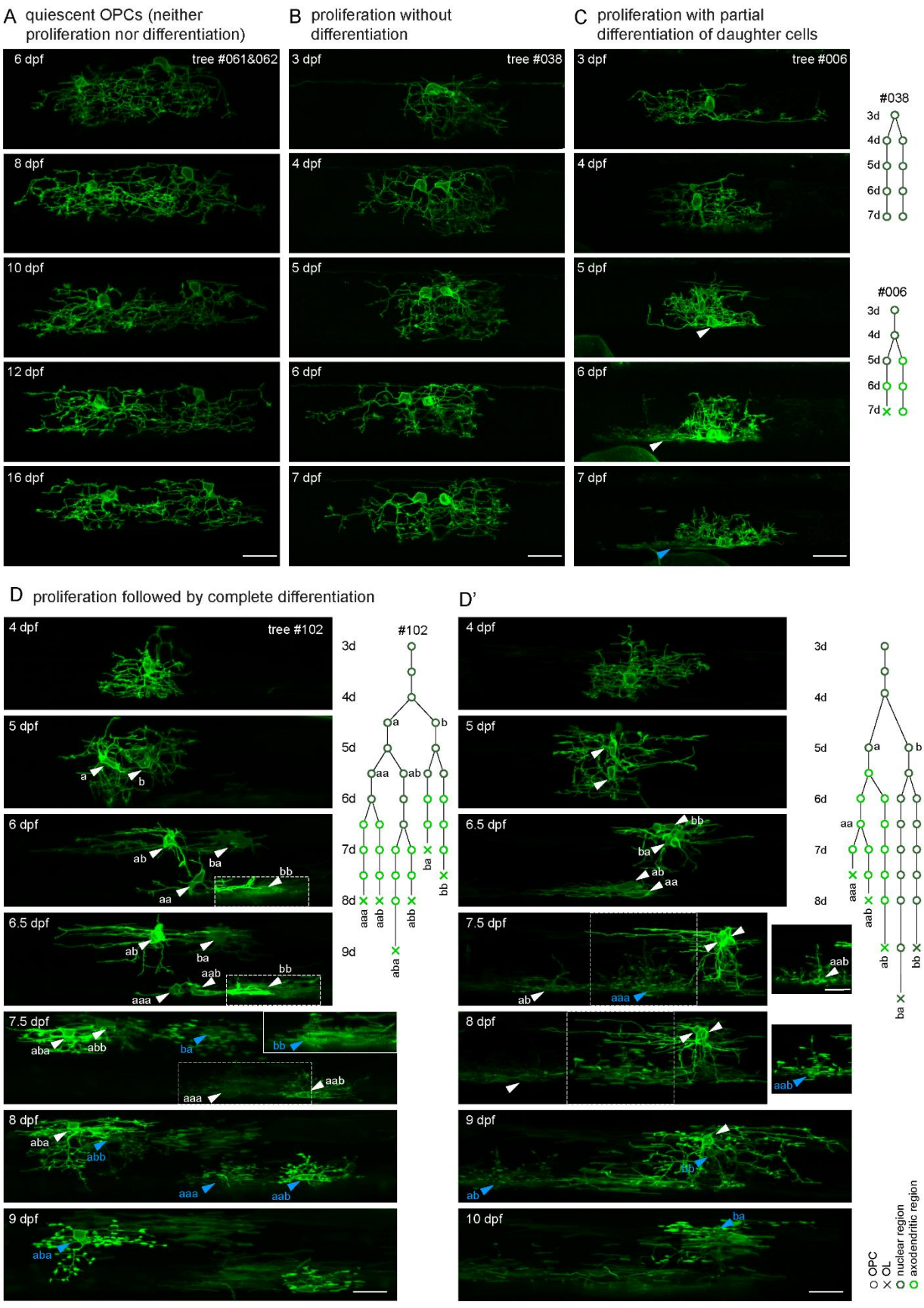
A quiescent OPCs (neither proliferation nor differentiation)
B proliferation without differentiation
C proliferation with partial differentiation of daughter cells
6 dpf
tree #061&062
8 dpf
10 dpf
12 dpf
16 dpf
3 dpf
tree #038
4 dpf
5 dpf
6 dpf
7 dpf
3 dpf
tree #006
4 dpf
5 dpf
6 dpf
7 dpf
#038
3d
4d
5d
6d
7d
#006
3d
4d
5d
6d
7d
D proliferation followed by complete differentiation
D'
4 dpf
tree #102
5 dpf
6 dpf
6.5 dpf
7.5 dpf
8 dpf
9 dpf
#102
3d
4d
5d
6d
7d
8d
9d
a
b
aa
ab
ba
bb
aaa
aab
aba
abb
4 dpf
5 dpf
6.5 dpf
7.5 dpf
8 dpf
9 dpf
10 dpf
OPC
OL
nuclear region
axodendritic region

3.2.6.2 Morphology Change and Differentiation

Regardless whether OLs derived from a complex, 'nuclear' OPC have their soma localized finally in the nuclear or axodendritic region, they always went through a transient phase in which they dramatically simplify their process network (**Figure 3.2.6C&D**).

In addition, using 3D visualization and careful reconstruction of the cell morphology (see **section 2.2.2** and **3.1.4**) could improve the traceability of individual OPCs and in addition allowed to assess their morphology quantitatively. **Figure 3.2.7A** shows an OPC with an asymmetric fate (fate 5) for which this was done. After initial proliferation between 3 and 4 dpf, there was an already simpler daughter cell (reconstructed in blue) with its soma still in the nuclear region that divided again before 5 dpf; then both daughter cells transit completely to the axodendritic region and initiate myelination. The complex daughter cell (reconstructed in green) divided also a second time after the first division, but both daughter cells stayed in the nuclear region and maintained the typical morphology of OPCs located there (**Figure 3.2.6A**).

Some measured examples how cell complexity values changes over time for different fates are shown in **Figure 3.2.72B-E.** OPCs with their soma in the nuclear region that did not divide (fate 1) increased their complexity steadily (**Figure 3.2.7B**). A cell division reduced the complexity significantly as both daughter cells inherited processes. But the complexity of daughter cells increased again approximately to the level prior to division if they did not translocate their soma to the axodendritic region (**Figure 3.2.7C&E**). For the OPC that divided symmetrically and both daughter cell somata stayed in the nuclear region (fate 3), the resulting daughter cells had a similar complexity value, indicating that the process network was split roughly in equal parts (**Figure 3.2.7C**). A symmetric division after which both daughter cells moved to the axodendritic region (fate 4) usually was accompanied with a reduction in complexity values (**Figure 3.2.7D**).

If an asymmetric division was observed when one daughter cell stayed in the nuclear region whereas the other transited to the axodendritic region (fate 5). This transition was usually undergone by the cell that inherited less of the process network of the mother cell and hence had a simpler morphology after proliferation (**Figure 3.2.7E**).

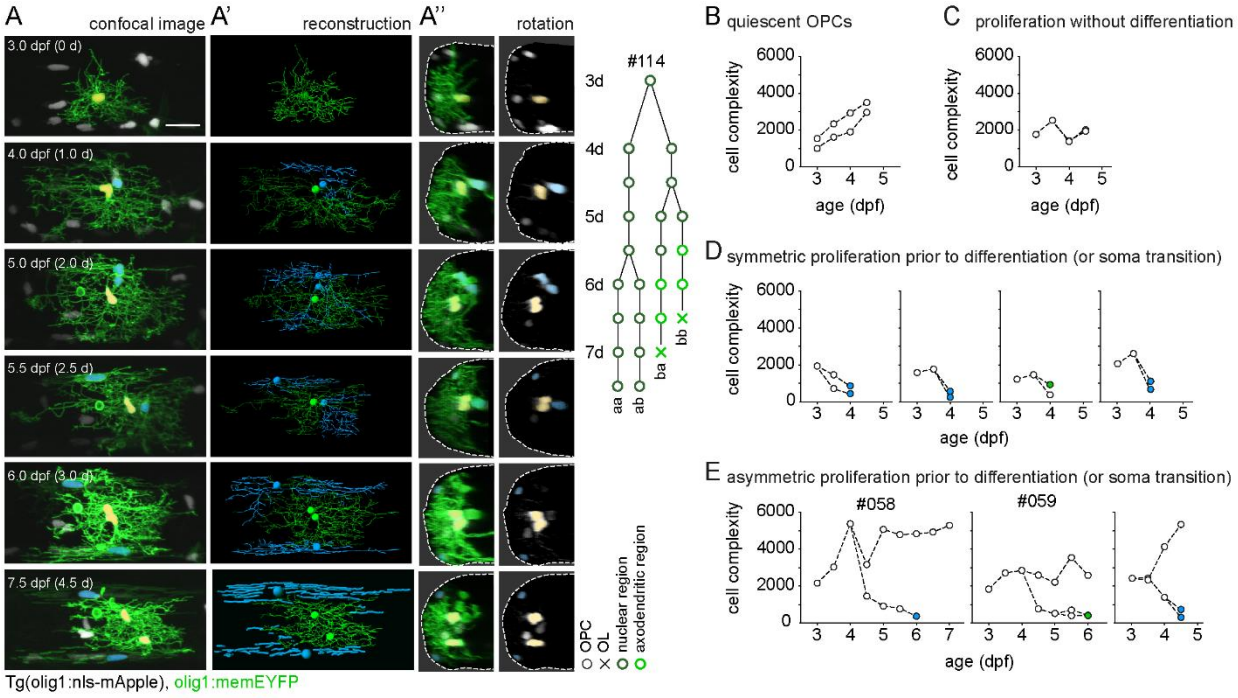

Figure 3.2.7 Morphology change over time.

(A) Series of confocal images between 3 and 7.5 dpf starting with an individually olig1:memEYFP-labelled OPC in the nuclear region in Tg(olig1:nls-mApple) transgenic fish. For better visualization only the proximal side of the spinal cord is shown as well as olig1:nls-mApple-positive nuclei of the reconstructed OPCs are false-coloured in yellow or blue. **(A')** 3D reconstruction of the cells shown in **A**. Processes of the yellow coloured cell (a) and its progeny (aa, ab) are shown in green, processes of the blue cell (b) and its progeny (ba, bb) are shown in blue. **(A'')** 90° rotational view of the proximal hemi-spinal cord. Dashed lines depict the outline of the spinal cord. The right panel shows the olig1:nls-mApple channel only with pseudo-colouring. Scale bar: 20 µm.

(B-E) Graphs showing the cell complexity within example clonal OPCs trees over time measured from the 3D reconstructions as shown in **A'**. Coloured data point indicate OPCs that were observed to transit to the axodendritic region (green) or to differentiate (blue) within 24 h after this measurement.

(B) OPCs that did not undergo neither proliferation nor differentiation (fate 1).

(C) OPCs that divided did not form myelinating OLs (fate 3).

(D) OPCs that divided, all daughter cells differentiated or translocated to the axodendritic region (fate 4).

(E) OPCs that divided and one or several daughter cells differentiated or translocated to the axodendritic region (fate 5).

3.2.6.3 Quantitative Fate Analysis

The final dataset consists of clonal trees of 114 OPCs with a complex morphology and a nuclear soma localization as a starting population (**Figure 3.2.8A**), which were included when either imaging was feasible for at least five consecutive days (≥96 hours, n=92) or when the cell or their progeny fully differentiated before (n=22). Most of the observations were carried out between 3 and 7 dpf. For 29 included OPCs an observation even longer than 96 h up to 11 days was achieved (**Figure 3.2.8B**). As shown before, OPCs with their soma in the nuclear region can give rise to axodendritic OPCs. The transformation process from one OPC subtype to the other requires however the translocation of the soma. Therefore, in addition to **differentiation** and **proliferation**, I also assessed if **soma transitions** from the nuclear to the axodendritic region occurred. The main results are already revealed by grouping the trees for the three categorizing variables and by comparing the frequencies (**Figure 3.2.8C** and **Table 3.2.6.1**). The trees could be assigned to 13 possible groups. However, within all trees analysed, only examples for 10 of these groups were observed, of which only 6 different fates occurred more than 5 times (**Figure 3.2.8C**). In addition, a retrospective analysis of individual cells (n=270) within the 114 clonal trees was carried out (**Figure 3.2.9B-D**). To reduce complexity, in the following mostly the correlation of two out of the three events (proliferation, soma transition, differentiation) was assessed in dependence of time.

Table 3.2.6.1 Frequency of possible fates in 114 clonal OPC trees.

Compare also **Figure 3.2.9C.**

Proliferation	Soma transition	Differentiation (Myelination)	Frequency (n)
NO	NO	NO	29
		YES	0
	YES	None	2
		YES	0
YES	None	None	23
		Some	0
		All	1
	Some	None	12
		Some	8
		All	10
	All	None	5
		Some	2
		All	22

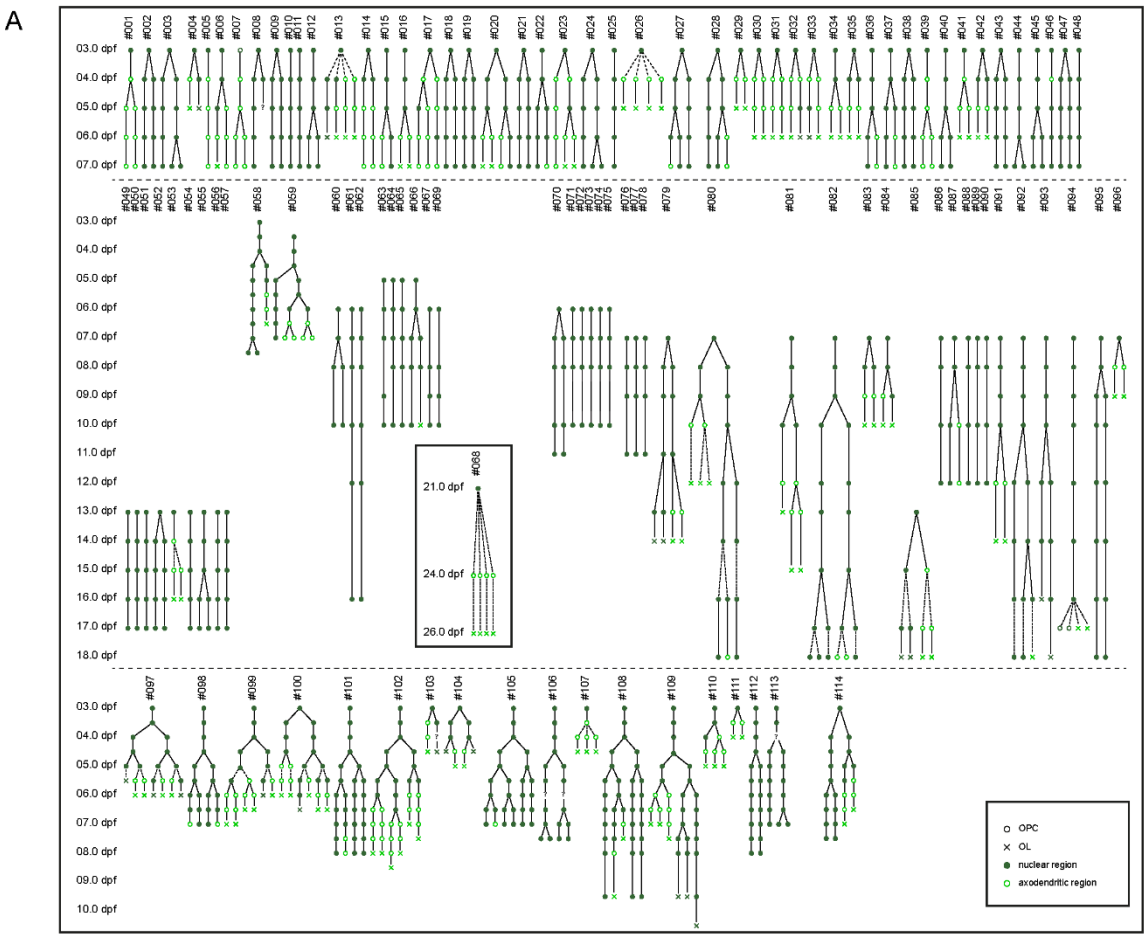
A
OPC
OL
nuclear region
axodendritic region
21.0 dpf
24.0 dpf
26.0 dpf
B
0
5
10
15
20
25
30
days post fertilization (dpf)
C
No Proliferation
Proliferation (one or more cell divisions)
No Differentiation
Differentiation
No Soma transition
Soma transition
of some daughter cells
of all daughter cells
n=29
n=23
n=1
n=8
n=12
n=10
n=2
n=5
n=2
n=22
n=114

Figure 3.2.8 Fate analysis overview.

(A) olig1:memEYFP OPCs in the nuclear region (n=114) were observed between 3 to 26 dpf for at least 5 consecutive days or until all cells of the respective clone did differentiate. Open circles are OPCs, crosses are differentiated cells in the nuclear (dark green) or axodendritic region (light green), respectively. Of the starting population 118 'nuclear' OPCs, 33 'axodendritic' OPCs, 98 'axodendritic' OLs and 21 'medial' OLs were generated during observation (sum: n=270). The data derived from 45 fish in 9 independent experiments (several clutches were pooled per experiment).
(B) Overview of the length of the individual clonal analyses sorted by start of the observation and length from top to bottom (n=114).
(C) Classification of the observed fates in 10 different groups based on the factors proliferation, soma translocation and differentiation (subclassified if all or only some daughter cells underwent soma translocation and differentiation).

3.2.6.4 Proliferation and Differentiation

Regarding only proliferation and differentiation there is a distribution of fates between quiescence (27 %, n=31), proliferation not followed by differentiation (35 %, n=40) and proliferation followed by differentiation (38 %, n=43). Proliferation without subsequent differentiation occur either to maintain OPC number or the observation stopped before OPCs did differentiate. However, if cells were observed for 96 h prior to differentiation there was always a cell division. Remarkably, without prior proliferation differentiation of complex, 'nuclear' OPCs was never observed (**Figure 3.2.8A&C** and **Figure 3.2.9A:** 0/31 cases in non-proliferating cells versus 43/83 cases of differentiation after proliferation). This indicates that a recent cell division is a prerequisite for OPC differentiation into myelinating OLs.

Interestingly, the proportions of quiescence and proliferating OPCs are shifted in young versus older larvae. Whereas there was a higher frequency of trees with proliferating OPCs (followed by differentiation or not) in the young animals (90 % versus 46 %), the largest fraction of OPCs observed in the old fish remained quiescent (54 %). However, also the generation of new OLs from OPCs was more frequent in the younger animals (**Figure 3.2.1C** and **Figure 3.2.9A,** 43 % of trees with differentiating progeny versus 30 % of trees in older animals) which required the generation of new OPCs to prevent the depletion of the OPC pool.

To investigate the timing between OPC differentiation and previous proliferation, all the 119 myelinating OLs generated within the 114 clonal trees were analysed retrospectively (**Figure 3.2.9B**). The vast majority of cells differentiated within 3 days after proliferation (92 %), few differentiated at the fourth day after proliferation (5 %) and almost no cells differentiated afterwards. As the frequency of differentiation at four days after proliferation was decreased significantly, one can be quite confident that almost no events were missed as imaging over 5 consecutive days was an inclusion criterion for this dataset. The very few examples of differentiation beyond 4 days post-proliferation were observed in the nuclear region (n=3; trees #93 and #109), suggesting that this microenvironment might be less supportive for differentiation and hence differentiation took longer. On the other hand, this observation could be also caused by slower developmental kinetics in older fish or might have technical reasons like the poor temporal coverage in these examples or the assignment of a cell's origin to the wrong proliferation event.

3.2.6.5 Proliferation and Soma Transition

As most of the OPCs differentiated in the axodendritic region (**Figure 3.2.9B**, 82 % in this dataset) but axodendritic OPCs derive from OPCs with their soma in the nuclear region (see **section 3.2.6.1**) a previous soma transition was required. However, it is not clear how cell division and soma translocation relate to each other in a timely manner. Hence, I calculated the time between a soma transition event from the nuclear to the axodendritic region and the closest proliferation event for all cells that ended up as lateral OLs (n=98) within the 114 analysed trees (**Figure 3.2.9C**). In addition, I also checked all soma transition events observed (n=174) without a necessary association with differentiation, which includes additional OPCs that were not included in the previously analysed data and calculated the time since or until the closest proliferation event, respectively (**Figure 3.2.9C**). It was apparent that there was a high coincidence of proliferation and soma transition. Most of the times both events occurred within the same day (59 % for all soma transitions). In some cases, the division occurred one day before soma transition (18 %) and only very few examples were found for which the proliferation preceded the soma transition even longer (5 %) or occurred even after soma transition (11 %). The examples in the last group most likely account for proliferative events of OPCs with a complex morphology but not a nuclear soma position without a direct link to differentiation; alternatively, an previous proliferation event of an OPC in the nuclear region prior to soma transition could be before the start of the observation (**Figure 3.2.8**A, for example #1, #7, #17, #39, #41 and #53). Conclusively, soma transitions that were associated with subsequent differentiation occur concurrently but more likely shortly after OPC proliferation.

3.2.6.6 Soma Transition and Differentiation

Based on the observation that OPC soma transition to the axodendritic region, occurs together or shortly after proliferation events that precede differentiation, a correlation of soma transition and differentiation is also expected.

In 69 % (n=42/61) of the OPC clones which had progeny that transit to the axodendritic region, these cells differentiated (**Figure 3.2.8C**). If translocation happened towards the end of the observation period, it was more likely to miss the differentiation after soma transition; hence, in the remaining 31 % trees some OPCs presumably underwent differentiation soon after imaging stopped (as soma transition was coincidental with proliferation there should be a similar timing as shown in **Figure 3.2.9B**). Only in 11 trees differentiation in the nuclear compartment was observed without previous soma transition, however in 10 of these cases sister cells transited to the axodendritic region at the same time and differentiated (**Figure 3.2.8C**).

Differentiation after proliferation and soma transition together was much more frequent (71%, n(trees)=42/59) than differentiation after proliferation without soma transition (20 %, n=11/54; **Figure 3.2.8**). Soma transition occurred without proliferation, but this was rare (n=2) and is rather associated with occasionally observed complex OPCs in the axodendritic region than with differentiation and can be reversible (**Figure 3.1.5E** and **Figure 3.2.8C**, #5 and #46). Since occasionally OPCs can also differentiate in the nuclear region however (**Figure 3.2.4A**, **Figure 3.2.6D'**, **Figure 3.2.8A&C** and **Figure 3.2.9B**), soma transition is not compulsory for differentiation in general.

I also analysed the fate of differentiated cells in the axodendritic region retrospectively and determined the position of the individual cells over a several days prior to differentiation (**Figure 3.2.9D**). In case of a cell division the mother cell was followed further. These cells only spent a limited time in the axodendritic region after entering it from the nuclear region and quickly progress to differentiation. Consequently, I inferred that 'axodendritic' OPCs are not a self-maintaining subpopulation but depend on the generation from OPCs in the nuclear region.

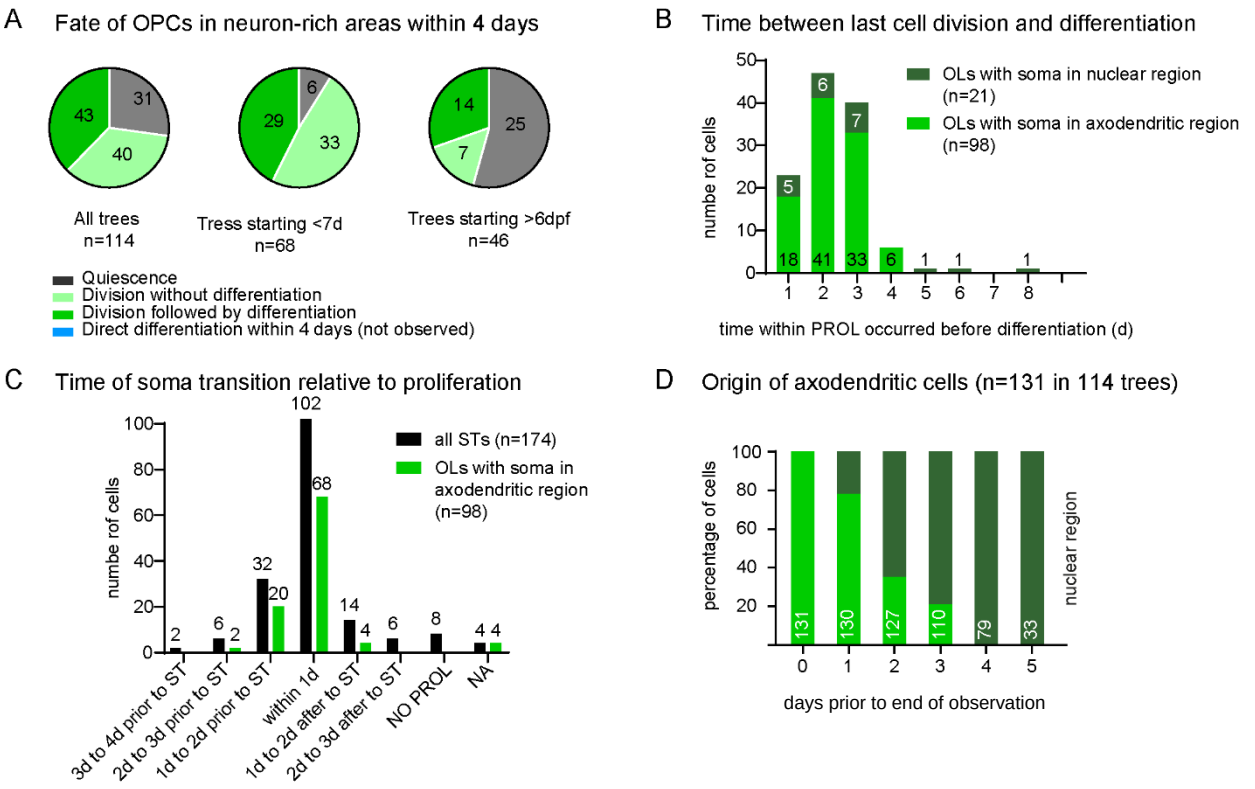

Figure 3.2.9 Analysis of the clonal OPC trees regarding proliferation, soma translocation and differentiation.

(A) Fates of the 114 analysed OPC trees grouped for the occurrence of proliferation and differentiation.

(B) Time between differentiation and previous proliferation for the OLs generated from the 114 analysed OPC fates (n=119). Numbers of cells observed at the respective times are indicated at the bars.

(C) Time of soma translocation in relation to a proliferation event for the cells that differentiated in the axodendritic region within the 114 analysed clonal OPC trees (green, n=98) and all observed cells that underwent soma translocations and proliferation (black, n=174). Numbers of cells in the respective groups are indicated at the bars. Every cell in the axodendritic region that shuttled once its soma from the nuclear region was counted as one event even when the soma transition event occurred in a common mother cell (i.e. when proliferation occurred after soma transition, n=20). For some examples, the observation time was too short to capture a previous or subsequent proliferation event (n(NO PROL)=8). For the 4 cells for which an analysis was not possible the observation interval was insufficient to draw confident conclusions (see **Figure 3.2.8A**, #68).

(D) Retrospective analysis of the position of 131 axodendritic cells from the 114 OPC trees in the axodendritic region over 5 d prior to differentiation. Numbers of cells observed are indicated at the bars.

3.2.7 Summary - Behaviour and Fate of OPCs Over Time

The founders of the olig1-positive OPC population arise between 2 and 3 dpf in the zebrafish spinal cord. Most of these cells extend their process network until the cell acquires a complex morphology. These cells can remain quiescent over days – even though this is more likely to be observed in fish older than 7 dpf after the initial peak of myelination – or undergo cell division. After division, the daughter cell can stay in the nuclear region and retain properties of the mother cell. Alternatively, one or both daughter cells can also transit their soma to the axodendritic region, which was usually observed shortly after proliferation. These OPCs, which are then completely in the axodendritic region can undergo a second or even third round of proliferation before they irrevocably proceed to differentiate into myelinating OLs. As 'axodendritic' OPCs readily differentiate within few days and proliferate less frequently, they are not a self-maintaining subpopulation, new myelination-competent OPCs must be substituted by proliferation of 'nuclear' OPCs.

In vivo live imaging over several days revealed that cell proliferation of OPCs with the soma in the nuclear region seems to be required (but not sufficient) to generate the myelination-competent OPC cell type in the axodendritic region. Furthermore, there is a dramatic reduction in process network complexity of the OPCs during the transition from the 'nuclear' type to the myelinating type in the axodendritic region. Some examples of OPCs that differentiate despite their soma resides in the nuclear region show however that soma transition to the axodendritic region might favour differentiation but is not compulsory.

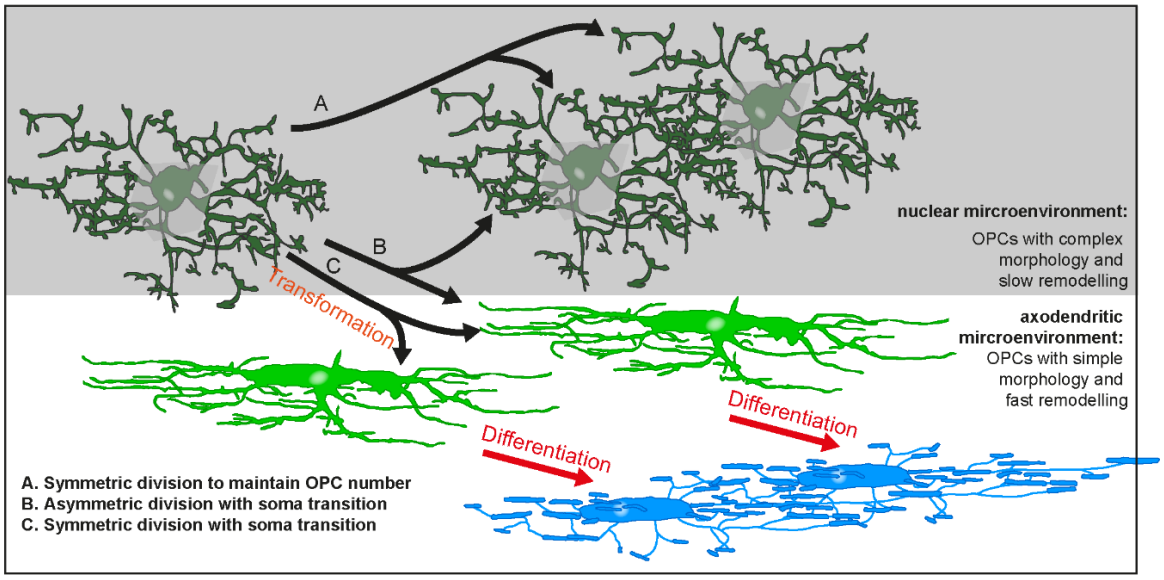

Figure 3.2.10 Cartoon showing how oligodendrogenesis is achieved by OPC subgroups in the zebrafish spinal cord.

3.3 Molecular Characterization of OL-Lineage Cell Subgroups

3.3.1 Approach: FACS Sorting, scRNASeq and RNAScope ISH

An inherent weakness of the live imaging approach is that the information on the molecular status of the imaged cell is limited. On the other side, single-cell RNA-Sequencing, which is established more and more as the method of choice for the generation of large scale transcriptomic data, yields a huge amount of molecular information but cannot discriminate whether observed differences represent different types of cells with different functions or just a sequence of successive states of the same cell type. However, RNA-Sequencing can be used to identify distinct subclusters of OPCs in the zebrafish. These subgroups are characterized by the expression levels of certain genes, which can be also evaluated for their spatial distribution through RNA *in situ* hybridization. Since OPC subgroups as identified by *in vivo* live imaging predominantly separate spatially, this can be used to assign these groups to certain clusters revealed by RNA-Sequencing. Consequently, it becomes possible to assign fates and behaviours to certain molecular characterized subtypes and to overcome the limitations of both methods (**Table 3.3.1.1**).

To achieve this, our group established a regime to obtain single cells from 5 dpf old zebrafish larvae, which could be sort for the cell type of interest namely OPCs. The sorted cells then were used for the single-cell Sequencing (**Figure 3.3.1A**). Transgenic Tg(olig1:memEYFP) larvae were used the different types of OL-lineage cells previously described are labelled: complex OPCs homing in the nuclear region of the spinal cord, simple OPCs usually found in the axodendritic region of the spinal cord and young OLs which still have not degraded the fluorescent protein entirely (**Figure 3.2.10** and **Figure 3.3.1D**). Of the prepared single-cell suspension, debris, non-separated cells and dead cells were excluded by the gating strategy and all viable cells which had a high EYFP-fluorescence signal were selected for further sequencing or control experiments (see **section 2.1.5** and **Figure 2.1.1**).

Table 3.3.1.1 Approach to connect gene expression data to the live imaging data.

	Gene expression	Regional information	Cell behaviour over time
Single-cell RNA-sequencing			
RNAScope *in situ* hybridization			
Confocal Live Imaging			

I tested the single-cell sorting accuracy by sorting single cells on 384-well imaging plates and staining of viable cells with DyeCycle Ruby and Hoechst 33342. Some examples are shown in **Figure 3.3.1B**. When 100 cells were sorted in one well, I could count 91 viable cells afterwards. When sorting 10 cells per well I could find 9 cells in average. Also, when only one cell was sorted to the well it could be identified not only by transmitted light and EYFP fluorescence but also by DyeCycle Ruby staining. Of 102 imaged wells which are expected to contain a single cell, this was confirmed in 67 wells, only one well contained more than one cell, in 34 wells no cell was found (**Figure 3.3.1C** and **Table 3.3.1.2**). Thus, sorting accuracy could be also confirmed by imaging. The slight differences observed between expected and detected cell numbers might account to the difficulties to detect single cells in wells by imaging, caused by the relatively low resolution for whole-well imaging and that cells were hidden in the shadow of the well's rim.

Table 3.3.1.2 Confirmation of single cell sorting.

sorted cells	detected cells (av)	SD	missing	number of wells
100	91,4	6,3	8,6	17
10	8,9	1,2	1,1	14
1	68 (+1)	-	34	102

The single-cell RNA-Sequencing was carried out by our collaborators at the Karolinska Institute in Stockholm using the SmartSeq2 technique. Based on the gene expression data they categorized single cells to transcriptomically distinct clusters with Seurat v3 (Butler et al., 2018; Stuart et al., 2019). Subsequently, I tested zebrafish specific RNAScope© *in situ* hybridization (ISH) probes for candidate genes that are highly expressed within certain clusters compared to other clusters and which could therefore be used as markers for these clusters. RNA *in situ* hybridization is the preferred method for the validation of RNA-Sequencing data by imaging, i.e. on fixed tissue sections. Using this strategy, it was possible to determine if the candidate genes are differently expressed in the nuclear and axodendritic region of the zebrafish spinal cord (**Figure 3.3.1D**). Eventually, the differentially localized cells were assigned to certain clusters revealed by RNA-Sequencing.

Based on the lists of differentially expressed genes between clusters, I also performed Gene Ontology (GO) term analysis to retrieve information on possible functional properties of cells within these clusters (**Figure 3.3.2**, **Figure 3.3.3, Figure 3.3.4** and **Figure 3.3.5**). The assumed functions for a certain cluster based on GO terms are expected to match with the behaviour of the according OPC subgroups identified by *in vivo* live imaging.

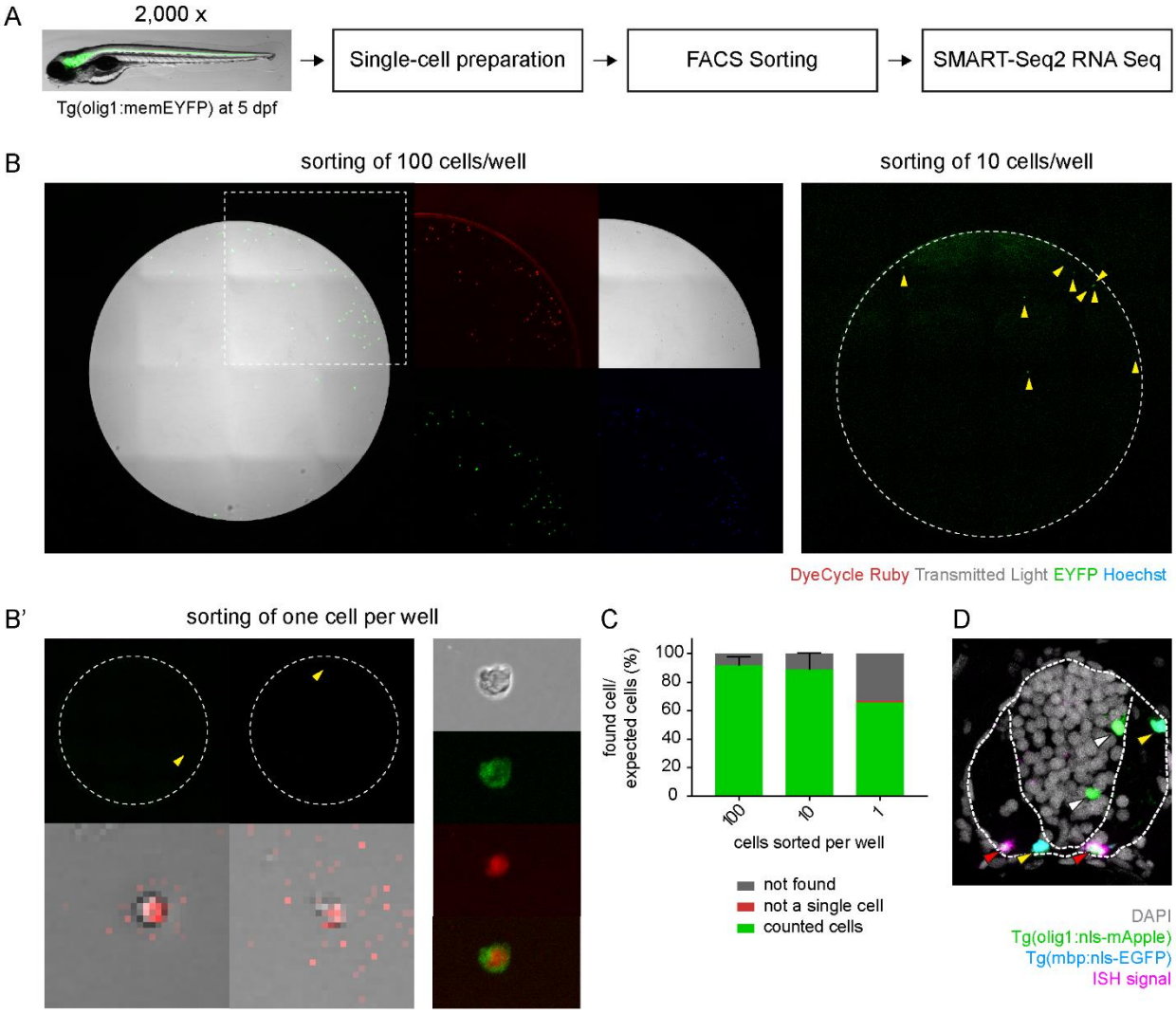

Figure 3.3.1 Single cell sorting of olig1+ cells

(A) Workflow of single-cell RNA-Sequencing. The single-cell solution was prepared from approximately 2,000 Tg(olig1:EYFP) zebrafish larvae at 5 dpf. Subsequently, single cells were sorted in single wells on 384-well plates.

(B) Example confocal images of whole wells expected to contain 100 and 10 cells per well (left and right panel) and sorted single cells (**B'**, whole well image and magnification of single cells). Identification of single cells by fluorescence expression (EYFP), morphology (transmitted light) and viable dyes DyeCycle Ruby and Hoechst 33342.

(C) Bar graph confirming the accuracy of single cell sorting.

(D) RNAScope ISH on fixed transversal spinal cord sections. The dashed white lines indicate the outlines of the spinal cord and the border between nuclear and axodendritic region, respectively. 'Nuclear' OPCs, 'axodendritic' OPCs (both green) and OLs (blue, or cyan if they express the OPC-label in addition) are indicated by arrowheads in white, red and yellow. In this example, the RNA ISH signal was specific to the OPCs in the axodendritic region.

3.3.2 Different Clusters Identified by Single-Cell RNA-Sequencing

Initially, five different clusters were identified from the single-cell sequencing data (**Figure 3.3.2A**). Three are OL-lineage cells clusters (#1-3), i.e. two OPC clusters and one cluster consisting of OLs. Two more clusters (#4 & #5) do not comprise OL-lineage cells. OL-lineage identity was confirmed by the expression of widely used OL-lineage markers like *olig2*, *sox10* and *nkx2.2a* based on the sequencing data (**Figure 3.3.2B-D**). Furthermore, the expression of *nkx2.2a* could be confirmed in almost all mApple-labelled OPCs in the spinal cord *in vivo* (135/139) by RNA ISH regardless of their position in the nuclear or axodendritic area (**Figure 3.3.2B**). The presence of Sox10 was also shown in all mApple- and EGFP-positive cells (117/117) by immunostaining against Sox10 protein (**Figure 3.3.2C**). This confirmed that the olig1-positive OPCs observed in the zebrafish spinal cord by *in vivo* live imaging are also the cells which were analysed by single-cell RNA-sequencing. However, given the volume of brain and spinal cord in the zebrafish and the respective frequency distribution of OL-lineage cells most of the analysed cells were probably derived from brain tissue.

Interestingly, *pdgfra* was not detected in the OL-lineage cells by RNA-Sequencing but in the two additional clusters #4 and #5 (**Figure 3.3.2E**), which are devoid of the other OL-lineage markers like *olig2*, *ppp1r14bb*, *nkx2.2a* and *sox10* (**Figure 3.3.2B-D**). Performing GO term analysis on the most upregulated genes in two *pdgfra*-expressing cell clusters (**Table 3.3.2.1**) does not give a definite hint on their function nor identity (therefore not shown). The potential identity of cells in cluster #4 and #5 is discussed below (see **section 4.1.7**). However, based on their expression profile these clusters most likely include cells, which does not belong to the OL-lineage and thus were not analysed in more detail.

Within the three OL-lineage clusters, cells classified as OLs express genes like *mpz*, *mbpa*, *mag* and *myrf* – markers widely used to characterize myelinating cells in the CNS (see **Figure 3.3.2L**, **Table 8.1.1.1** and **section 3.3.4**). I was most interested in the genetic and functional properties of OPCs (clusters #1 and #2). As an initial step, a GO term analysis based on a list of genes which are differentially expressed between these two clusters (**Table 3.3.2.2**) was conducted. As only two clusters were compared the genes upregulated in one cluster are downregulated in the other. GO terms for OPC cluster #1 (**Table 3.3.2.3**) are mainly related to neuronal communication based on neurotransmitters and neurotransmitter metabolism, which I summarize here as **'neuronal activity signature'**. GO terms of OPC cluster #2 are associated mainly with **proliferation and cell division** (**Table 3.3.2.4**).

Table 3.3.2.1 Upregulated genes in the non-OL-lineage clusters #4 and #5.

Normalized relative expression levels are shown as logarithmic fold change (log(FC)) [data were provided by Eneritz Agirre and Gonçalo Castelo-Branco].

Cluster #4 versus ALL		Cluster #5 versus ALL	
gene	**log(FC)**	**gene**	**log(FC)**
kalrnb	0,65	*col8a2*	1,53
dkk1b	0,64	*krt94*	1,27
pitx1	0,60	*meox1*	1,02
aifm4	0,58	*klf2a*	0,97
scinla	0,56	*anxa2a*	0,81
BX548011.4	0,55	*LO018188.1*	0,72
zic1	0,55	*scube3*	0,71
nck2b	0,54	*tbx18*	0,71
slc43a2a	0,54	*crispld1a*	0,71
ccdc3a	0,54	*crabp2b*	0,70
ADAMTSL4	0,54	*lmx1bb*	0,67
CABZ01063602.1	0,53	*angptl6*	0,67
asap1a	0,52	*angptl5*	0,66
agtr1b	0,52	*dachc*	0,66
adamts12	0,51	*shhb*	0,66

Table 3.3.2.2 Most differentially regulated genes between OPC clusters #1 and #2.

According tSNE plots for some example genes (highlighted in bold) are shown in **Figure 3.3.2** [data were provided by Eneritz Agirre and Gonçalo Castelo-Branco].

	OPC #1 versus OPC #2		OPC #2 versus OPC #1	
#	**gene**	**log(FC)**	**gene**	**log(FC)**
1.	*qdpra*	1,23	***kpna2***	3,23
2.	*hsp90b1*	1,16	*tuba8l*	3,16
3.	***calr***	1,10	*top2a*	2,96
4.	*glula*	1,07	*cenpf*	2,89
5.	*ptgdsb.2*	0,96	*aspm*	2,89
6.	*s1pr1*	0,88	***mki67***	2,74
7.	*camk2n1a*	0,88	*plk1*	2,71
8.	*ndrg3a*	0,85	*cdk1*	2,65
9.	*kcnip1b*	0,81	*ccnb1*	2,42
10.	*gria2b*	0,80	*tpx2*	2,39
11.	*gria1a*	0,80	***kif11***	2,38
12.	*ngfra*	0,79	*nusap1*	2,37
13.	*fez1*	0,79	*hmgb2a*	2,26
14.	*mdkb*	0,79	***pcna***	2,21
15.	***aplnrb***	0,78	*ccna2*	2,17
16.	*tmem145*	0,78	*hmgn2*	2,04
17.	*pygmb*	0,78	*kifc1*	2,01
18.	*scg2b*	0,77	*tacc3*	2,00
19.	*slc6a1a*	0,76	*prc1b*	1,97
20.	*hist2h2l*	0,76	*ube2c*	1,97
21	*ca6*	0,75	*lbr*	1,90
22.	*pdia3*	0,74	*cdc20*	1,83
23	*calr3a*	0,74	*cenpe*	1,82
24.	*slc6a1b*	0,74	*g2e3*	1,81
25.	*calr3b*	0,73	*slc29a2*	1,78
26.	*atcaya*	0,73	*kif2c*	1,76
27.	*snap25a*	0,72	*aurkb*	1,75
28.	*slc1a2b*	0,68	*hmga1a*	1,75
29.	*camk2d2*	0,68	*tuba8l4*	1,74
30.	*ncalda*	0,68	*mad2l1*	1,71

Table 3.3.2.3 GO terms based on upregulated genes in OPC cluster #1 compared with cluster #2.

The settings were chosen as described in **section 2.2.6**, the minimum number of associated genes was set to n=2. The *p* value was corrected used Benjamini-Hochberg correction. GO terms are sorted by the percentage of detected associated genes of all associated genes for a term. The number of associated genes and their names are also listed.

Term ID	GO term	*p* value	% of genes	# of genes	Detected genes
R-DRE:888593	Reuptake of GABA	2,31E-05	100,00	2,00	[slc6a1a, slc6a1b]
R-DRE:112313	**Neurotransmitter uptake and metabolism in glial cells**	1,38E-04	33,33	2,00	[glula, slc1a2b]
R-DRE:210455	Astrocytic Glutamate-Glutamine Uptake and Metabolism	1,38E-04	33,33	2,00	[glula, slc1a2b]
R-DRE:888590	**GABA synthesis, release, reuptake, and degradation**	1,61E-04	28,57	2,00	[slc6a1a, slc6a1b]
R-DRE:442660	Na+/Cl- dependent neurotransmitter transporters	4,32E-04	16,67	2,00	[slc6a1a, slc6a1b]
GO:0005332	gamma-aminobutyric acid: sodium symporter activity	5,20E-04	14,29	2,00	[slc6a1a, slc6a1b]
R-DRE:112310	**Neurotransmitter release cycle**	8,83E-05	9,09	3,00	[slc1a2b, slc6a1a, slc6a1b]
R-DRE:425366	Transport of bile salts and organic acids, metal ions and amine compounds	4,67E-03	3,77	2,00	[slc6a1a, slc6a1b]
GO:0004970	**ionotropic glutamate receptor activity**	4,83E-03	3,57	2,00	[gria1a, gria2b]
R-DRE:112315	**Transmission across Chemical Synapses**	5,26E-06	3,39	6,00	[glula, gria2b, ncalda, slc1a2b, slc6a1a, slc6a1b]
GO:0007626	locomotory behaviour	8,50E-04	3,26	3,00	[ca6, slc1a2b, snap25a]
R-DRE:8957275	Post-translational protein phosphorylation	8,61E-03	2,56	2,00	[hsp90b1, scg2b]
GO:0006836	neurotransmitter transport	1,74E-03	2,46	3,00	[slc6a1a, slc6a1b, snap25a]
R-DRE:381426	Regulation of Insulin-like Growth Factor (IGF) transport and uptake by Insulin-like Growth Factor Binding Proteins (IGFBPs)	1,04E-02	2,25	2,00	[hsp90b1, scg2b]
R-DRE:112316	Neuronal System	2,99E-05	2,08	6,00	[glula, gria2b, ncalda, slc1a2b, slc6a1a, slc6a1b]
GO:0015293	symporter activity	2,61E-03	2,07	3,00	[slc1a2b, slc6a1a, slc6a1b]
GO:0045765	regulation of angiogenesis	1,16E-02	2,06	2,00	[aplnrb, s1pr1]
R-DRE:425407	SLC-mediated transmembrane transport	3,11E-03	1,89	3,00	[slc1a2b, slc6a1a, slc6a1b]
R-DRE:112314	**Neurotransmitter receptors and postsynaptic signal transmission**	1,80E-02	1,59	2,00	[gria2b, ncalda]
R-DRE:449147	Signalling by Interleukins	2,05E-02	1,44	2,00	[hsp90b1, snap25a]
R-DRE:1280215	Cytokine Signalling in Immune system	3,37E-02	1,07	2,00	[hsp90b1, snap25a]

Table 3.3.2.4 List of GO terms based on upregulated genes in OPC cluster #2 compared to OPC cluster #1.

Term ID	GO term	*p* value	% of genes	# of genes	Detected genes
GO:0022402	cell cycle process	9,50E-16	3,08	15,00	[aspm, aurkb, ccna2, ccnb1, cdk1, cenpe, kif11, kifc1, mad2l1, nusap1, plk1, prc1b, tacc3, top2a, tpx2]
GO:0007049	**cell cycle**	2,70E-15	1,98	17,00	[aspm, aurkb, ccna2, ccnb1, cdk1, cenpe, kif11, kifc1, mad2l1, nusap1, plk1, prc1b, tacc3, top2a, tpx2, tuba8l, tuba8l4]
GO:1903047	**mitotic cell cycle process**	2,06E-14	4,26	12,00	[aurkb, ccna2, ccnb1, cdk1, cenpe, kif11, kifc1, mad2l1, nusap1, tacc3, top2a, tpx2]
GO:1903047	mitotic cell cycle process	2,06E-14	4,26	12,00	[aurkb, ccna2, ccnb1, cdk1, cenpe, kif11, kifc1, mad2l1, nusap1, tacc3, top2a, tpx2]
GO:0007017	microtubule-based process	5,76E-12	2,59	12,00	[aspm, aurkb, cenpe, kif11, kif2c, kifc1, nusap1, prc1b, tacc3, tpx2, tuba8l, tuba8l4]
GO:0000280	**nuclear division**	1,74E-11	4,92	9,00	[aurkb, ccna2, ccnb1, cenpe, kif11, kifc1, mad2l1, nusap1, top2a]
GO:0000226	**microtubule cytoskeleton organization**	5,05E-11	3,23	10,00	[aspm, aurkb, kif11, kifc1, nusap1, prc1b, tacc3, tpx2, tuba8l, tuba8l4]
GO:1902850	microtubule cytoskeleton organization involved in mitosis	1,24E-09	9,52	6,00	[aurkb, kif11, kifc1, nusap1, tacc3, tpx2]
GO:1902850	microtubule cytoskeleton organization involved in mitosis	1,24E-09	9,52	6,00	[aurkb, kif11, kifc1, nusap1, tacc3, tpx2]
GO:0051726	regulation of cell cycle	2,26E-09	2,12	10,00	[aurkb, ccna2, ccnb1, cdk1, kif11, mad2l1, plk1, prc1b, top2a, tpx2]
R-DRE:69618	Mitotic Spindle Checkpoint	3,58E-09	7,69	6,00	[aurkb, cdc20, cenpe, cenpf, kif2c, ube2c]
GO:0007051	spindle organization	4,29E-09	7,23	6,00	[aspm, aurkb, kif11, kifc1, tacc3, tpx2]
R-DRE:2500257	Resolution of Sister Chromatid Cohesion	4,38E-09	7,32	6,00	[aurkb, cdc20, cdk1, cenpe, cenpf, kif2c]
R-DRE:69278	Cell Cycle, Mitotic	6,59E-09	2,28	9,00	[aurkb, cdc20, cdk1, cenpe, cenpf, kif2c, pcna, tpx2, ube2c]
R-DRE:69620	**Cell Cycle Checkpoints**	8,56E-09	4,00	7,00	[aurkb, cdc20, cdk1, cenpe, cenpf, kif2c, ube2c]
R-DRE:2467813	Separation of Sister Chromatids	8,64E-09	6,12	6,00	[aurkb, cdc20, cenpe, cenpf, kif2c, ube2c]
GO:0010564	regulation of cell cycle process	8,86E-09	4,02	7,00	[aurkb, ccna2, ccnb1, mad2l1, plk1, prc1b, tpx2]
R-DRE:1640170	Cell Cycle	8,99E-09	2,12	9,00	[aurkb, cdc20, cdk1, cenpe, cenpf, kif2c, pcna, tpx2, ube2c]
R-DRE:2555396	Mitotic Metaphase and Anaphase	9,15E-09	6,00	6,00	[aurkb, cdc20, cenpe, cenpf, kif2c, ube2c]
R-DRE:68882	Mitotic Anaphase	9,15E-09	6,00	6,00	[aurkb, cdc20, cenpe, cenpf, kif2c, ube2c]
R-DRE:68877	Mitotic Prometaphase	3,77E-08	4,65	6,00	[aurkb, cdc20, cdk1, cenpe, cenpf, kif2c]
R-DRE:68886	M Phase	1,25E-07	2,59	7,00	[aurkb, cdc20, cdk1, cenpe, cenpf, kif2c, ube2c]
GO:0007346	regulation of mitotic cell cycle	1,37E-07	2,54	7,00	[aurkb, ccna2, ccnb1, cdk1, mad2l1, top2a, tpx2]
GO:0008017	microtubule binding	2,66E-07	3,26	6,00	[cenpe, kif11, kif2c, kifc1, nusap1, prc1b]

Focusing on the expression patterns of most differentially expressed genes regardless of their function, it was remarkable that many of the genes which were upregulated in OPC cluster #1 were also expressed in cells of OPC cluster #2 (**Table 8.1.1.1** and **Figure 3.3.2F&H**). However, many genes were not equally expressed in the entire cluster #2 but rather in cells which localize in the tSNE plots at high and a low tSNE2/tSNE1 ratios while sparing the cells with intermediate tSNE2/tSNE1 ratios (e.g. *aplnrb* and *glula*), whereas other genes like *calr*, *ptgdsb.2*, *s1pr1* had a higher expression in those cells within OPC #2 that are spatially more adjacent to the OPC #1 cluster in the tSNE plot (**Figure 3.3.2F**). Conversely, gene expression which was high in OPC cluster #2 was often completely absent in OPC cluster #1 (**Figure 3.3.2I&J**). Instead, for most genes within OPC cluster #2 there was a gradient of expression levels either with a peak of expression at low tSNE2/tSNE1 ratios (e.g. *pcna*, *rpa1*, *mcm2*; **Figure 3.3.2I**) or high tSNE2/tSNE1 ratios (e.g. *mki67*, *kpna2* and *kif11*; **Figure 3.3.2J**), respectively. Furthermore, the group of cells with intermediate tSNE2/tSNE1 ratios within the OPC cluster #2 is characterized by high expression of genes which were otherwise not or significantly less expressed within OPC #1 and the other OPC #2 cells, e.g. *myrf*, *gpr17* and *sox9b* (**Figure 3.3.2K**).

Due to the revealed heterogeneity within OPC cluster #2 based on individual gene expression, the unsupervised clustering was performed again with settings to achieve a higher depth. This results in the subdivision of former OPC cluster #2 into subclusters #2a, #2b and #2c, whereas the other clusters (OPC #1, mOL and the non-OL-lineage clusters #4 and #5) remain unchanged (**Figure 3.3.2G**). In the following, the individual OL-lineage clusters are analysed in detail including implications on presumptive functions of cells within these clusters. Furthermore, RNA *in situ* hybridization was used to establish a link between the distinct subclusters and the subgroups of OPCs found by *in vivo* live imaging.

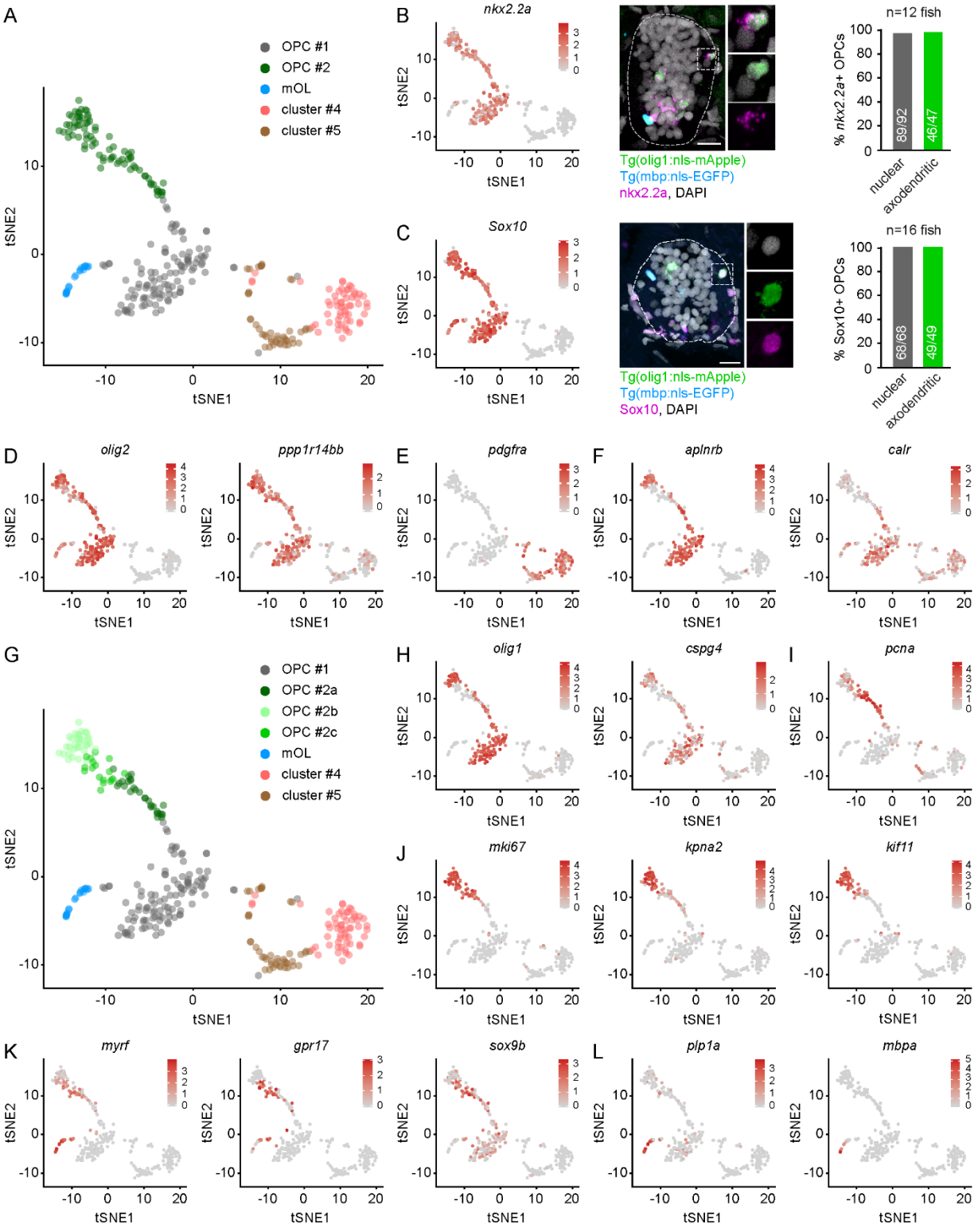
A
OPC #1
OPC #2
mOL
cluster #4
cluster #5
tSNE1
tSNE2
B
nkx2.2a
C
Sox10
Tg(olig1:nls-mApple)
Tg(mbp:nls-EGFP)
nkx2.2a, DAPI
Sox10, DAPI
n=12 fish
% nkx2.2a+ OPCs
89/92
46/47
nuclear
axodendritic
n=16 fish
% Sox10+ OPCs
68/68
49/49
D
olig2
ppp1r14bb
E
pdgfra
F
aplnrb
calr
G
OPC #2a
OPC #2b
OPC #2c
H
olig1
cspg4
I
pcna
J
mki67
kpna2
kif11
K
myrf
gpr17
sox9b
L
plp1a
mbpa

Figure 3.3.2 Cells sequenced by scRNASeq form different clusters and are the OL-lineage cells examined by *in vivo* live imaging.

(A) Visualization of the single-cell RNA-sequencing results from Tg(olig1:memEYFP) larvae at 5 dpf as tSNE plot. Five different cell clusters were identified initially. Each data point represents one cell (n=310).

(B) Confirmation of OL-lineage cell identity through co-labelling of a *nkx2.2a* RNA ISH probe with mApple+/EGFP- OPCs in fixed tissue sections of the spinal cord. The expression plot (left panel), an example image of the entire spinal cord with a magnified view of a *nkx2.2a*-positive OPC in the boxed area (middle) and the quantification from different sections across several fish (right) is shown. In addition, *nkx2.2a* is expressed by cells in the floor plate of the spinal cord. Scale bar in all images: 10 µm.

(C) Confirmation of OL-lineage cell identity through co-labelling of Sox10 immunostaining with mApple+/EGFP- OPCs. Sox10 immunoreactivity is also detected in EGFP+ OLs and other cells which do not belong to the OL-lineage.

(D) tSNE visualization of the specific marker genes *olig2* (OL-lineage) and *ppp1r14bb* (OPCs).

(E) tSNE visualization of the *pdgfra,* which was absent in OL-lineage cells in the zebrafish.

(F) tSNE visualization of the gene expression patterns of *aplnrb* and *calr*, which were upregulated in OPC #1 but also expressed in specific subgroups of OPC #2.

(G) tSNE visualization of the single-cell RNA-sequencing dataset with subclusters of OPC cluster #2: OPC #1 (n=110), OPC #2a (n=28), OPC #2b (n=33), OPC #2c (n=18), mOLs (n=19).

(H) tSNE visualization of marker genes upregulated in OPC #1.

(I) tSNE visualization of *pcna*, a marker gene specifically upregulated in OPC #2a.

(J) tSNE visualization of marker genes upregulated in OPC #2b.

(K) tSNE visualization of marker genes upregulated in OPC #2c.

(L) tSNE visualization of marker genes upregulated in the mOL cluster.

[tSNE plots were provided by Eneritz Agirre and Gonçalo Castelo-Branco]

3.3.3 OPCs that Communicate with Neurons (OPC #1)

There are two approaches to assess differential gene expression in OPC cluster #1. First, one can compare OPCs in cluster #1 to the other OPCs outside this cluster (OPC clusters #2a-c) to focus on their unique properties as an OPC subpopulation. This was basically presented in **section 3.2.2**. Alternatively, one could focus on which genes make OPC #1 distinctive compared to all the other clusters in our analyses including OPC #2, mOLs and non-OL-lineage cells in clusters #4 and #5. This would put more emphasis on genes which are important for OPC function in general. However, there is a large overlap between the list of regulated genes obtained by these two ways of comparisons (**Table 3.3.3.1** and **Table 3.3.3.2**) as well as the lists of GO terms generated based on these genes (**Table 3.3.3.2** and **Table 3.3.2.3**). As already introduced above, genes upregulated in OPC cluster #1 are mainly associated with neuronal activity and signalling. Among the reoccurring GO terms were *neurotransmitter uptake and metabolism in glial cells*, *transmission across chemical synapses*, and *ionotropic glutamate receptor activity*.

Table 3.3.3.1 Upregulated gene expression in OPC cluster #1.

Comparison between the cells within OPC cluster #1 with the entirety of cells outside this cluster, in distinction to **Table 3.3.2.2** in which OPC cluster #1 is only compared to OPC cluster #2 (the genes found in both tables are highlighted in bold) [data were provided by Eneritz Agirre & Gonçalo Castelo-Branco].

OPCs versus ALL						
#	**gene**	**log(FC)**		**#**	**gene**	**log(FC)**
1.	***glula***	1.66		17.	*tmem178b*	1.30
2.	***aplnrb***	1.58		18.	***camk2n1a***	1.30
3.	***gria1a***	1.50		19.	*olig1*	1.29
4.	***slc1a2b***	1.48		20.	*nlgn3a*	1.29
5.	***gria2b***	1.47		21	*cspg5a*	1.26
6.	***atcaya***	1.42		22.	*sema5a*	1.25
7.	*wscd1b*	1.41		23	*lrrn1*	1.22
8.	***ncalda***	1.36		24.	*fabp7a*	1.22
9.	***mdkb***	1.36		25.	***ndrg3a***	1.21
10.	*gpm6aa*	1.36		26.	*rassf2a*	1.21
11.	***scg2b***	1.35		27.	*ttyh3b*	1.20
12.	***slc6a1a***	1.33		28.	*spock3*	1.18
13.	*nrxn1a*	1.32		29.	*kiaa1549la*	1.18
14.	*pcdh2ab9*	1.31		30.	***pygmb***	1.17
15.	*ckbb*	1.31		195.	*cspg4*	0.80
16.	*grin1b*	1.31				

Table 3.3.3.2 GO term analysis of OPC cluster #1.

Based on the list of genes shown in **Table 3.3.3.1**. The settings were chosen as described in **section 2.2.6**, the minimum number of associated genes was set to n=2. The *p* value was corrected used Benjamini-Hochberg correction. The highlighted terms (bold) are already found in **Table 3.3.2.3**.

Term ID	GO term	*p* value	% of genes	# of genes	Detected genes
R-DRE:210455	**Astrocytic Glutamate-Glutamine Uptake And Metabolism**	1.51E-04	33.33	2.00	[glula, slc1a2b]
R-DRE:112313	**Neurotransmitter uptake and metabolism In glial cells**	1.51E-04	33.33	2.00	[glula, slc1a2b]
R-DRE:6794361	Neurexins and neuroligins	1.14E-03	9.09	2.00	[nlgn3a, nrxn1a]
R-DRE:112310	**Neurotransmitter release cycle**	1.94E-03	6.06	2.00	[slc1a2b, slc6a1a]
GO:0004970	**ionotropic glutamate receptor activity**	2.77E-04	5.36	3.00	[gria1a, gria2b, grin1b]
R-DRE:6794362	Protein-protein interactions at synapses	2.72E-04	5.00	3.00	[grin1b, nlgn3a, nrxn1a]
R-DRE:112315	**Transmission across Chemical Synapses**	1.48E-06	3.39	6.00	[glula, gria2b, grin1b, ncalda, slc1a2b, slc6a1a]
R-DRE:112316	**Neuronal System**	9.85E-08	2.78	8.00	[glula, gria2b, grin1b, ncalda, nlgn3a, nrxn1a, slc1a2b, slc6a1a]
R-DRE:112314	**Neurotransmitter receptors and postsynaptic signal transmission**	1.73E-03	2.38	3.00	[gria2b, grin1b, ncalda]
GO:0050804	modulation of chemical synaptic transmission	1.87E-02	1.69	2.00	[atcaya, nlgn3a]
R-DRE:71291	Metabolism of amino acids and derivatives	2.39E-02	1.42	2.00	[ckbb, glula]
R-DRE:425407	**SLC-mediated transmembrane transport**	2.74E-02	1.26	2.00	[slc1a2b, slc6a1a]
R-DRE:71387	Metabolism of carbohydrates	2.68E-02	1.22	2.00	[cspg5a, pygmb]
R-DRE:422475	Axon guidance	3.20E-02	1.06	2.00	[grin1b, sema5a]
GO:0022839	ion gated channel activity	3.57E-03	1.06	4.00	[gria1a, gria2b, grin1b, ttyh3b]

However, the individual terms were often based only on low numbers of redundant genes (n=2 for most of the terms). Additional methodical problems with GO term analysis was already described in the **section 2.2.6**. Hence, I decided to look up published functions for individual regulated genes in addition. Violin expression plots of most of the mentioned genes can be found below (**Figure 3.3.3A**).

Among the 30 most upregulated genes in OPC cluster #1 compared to OPC cluster #2 (**Table 3.3.2.2**) were neurotransmitter receptors genes like the glutamatergic AMPA receptors subunit genes *gria2b*, *gria1a*. Furthermore, a number of genes involved in neurotransmitter uptake, metabolism and release was detected. The Quinoid Dihydropteridine Reductase gene *qdpra* is important for the recycling of the enzymatic cofactor tetrahydrobiopterin which in turn is involved neurotransmitter metabolism (Thony et al., 2000). Glutamine synthetase *glula* synthesized glutamine from glutamate; glutamine can then be

transported back to neurons (Hayashi, 2018). *slc6a1a/b* is a GABA uptake transporter, whereas *slc1a2b* is a glutamate uptake transporter. *atcaya* is suggested to regulate glutaminase (Buschdorf et al., 2006). *snap25a* and *scg2b* are involved in vesicle release (Hotta et al., 2009). Another group of proteins exerting their function via calcium sensing/binding: Calreticulins *calr* and *calr3a/b* (and its interactor *pdia3*), Calcium/Calmodulin Dependent Protein Kinase *camk2d2*, calcium sensors *kcnip1b* and *ncalda* (An et al., 2000; Kool et al., 2019; Lu et al., 2015). Also, some genes promoting neurite outgrowth like *fez1* and *mdkb* were upregulated (Chen et al., 2017; Maturana et al., 2010; Winkler and Yao, 2014). Some of them like *hsp90b1*, *calr* and *calr3a/b* are also reported to act as chaperones.

When comparing OPC #1 genes to all other clusters, there were high expression levels found for several additional genes (**Table 3.3.3.1**). Both apelin receptor genes *aplnra* and *aplnrb* were upregulated. Even though there is no confirmed function in OPCs yet, these genes were already found in another recent study (Raj et al., 2018). Also, the role of NMDA receptor-mediated signalling in OPCs is not clear, the receptor subunit *grin1a and grin1b* are also highly expressed. Furthermore, semaphorin 5A (*sema5a*) was found, which is described to have an inhibitory influence on neuronal axon growth (Goldberg et al., 2004). Interestingly, cells in OPC cluster #1 express not only post-synaptic neurolignins (*nlgn3a*) but also pre-synaptic neurorexins (*nrxn1a*), provoking the question if OPCs not just receive synaptic input but are also able to elicit synaptic signals.

Furthermore, also the genes *cspg4* and *olig1* were among the upregulated candidates. Even though these two genes are usually considered as pan-OPC markers, mRNA was preferentially detected in cells of OPC #1, and also at some lower level in OPC subclusters #2a and #2b, but not in OPC #2c (as described above, see **section 3.3.2** and **Figure 3.3.2F&H**). The advantage to use these markers is their OL-lineage specificity in the CNS. Other genes like *gria1a* are assumedly not suitable as OL-lineage markers as they are also expressed in neurons, which are more abundant in the spinal cord nuclear region compared to OPCs and would mask their signal. By RNA ISH, I detected that with 82 % in the nuclear region significantly more cells expressed *cspg4* than in the axodendritic region with 34% (**Figure 3.3.3B**). Similar results were obtained for *olig1* expression: 70% *olig1*-positive cells in the nuclear region vs. 26% in the axodendritic region (**Figure 3.3.3C**). Interestingly, even though *olig1*-driven EYFP labelling was used to sort cells for scRNASeq, the *olig1* transcripts was not in all analysed cells and also was not detected in all mApple-positive cells in tissue section (discussed below, **section 3.3.4**). EGFP-positive OLs also did not express *cspg4* or *olig1* in accordance with the results from scRNASeq (**Figure 3.3.3B&C**). This allows the conclusion

that OPC clusters #1 but maybe also #2a and #2b are associated with the OPC subgroup observed by *in vivo* live imaging which was characterized by a 'nuclear' soma localization and complex morphology.

Another aspect which is discussed below in more detail (**section 3.3.4**), is the observation that within OPC cluster #1 there is a small subgroup of cells (n=4, with the lowest tSNE1 values in this cluster, close to the OL cluster) which was negative for many characteristic markers which were otherwise upregulated in OPC cluster #1 (**Figure 3.3.2F-H**).

Figure 3.3.3 Gene expression and functional association within OPC cluster #1.

(A) Violin plots showing the relative expression (log(TPM)) of marker genes upregulated in the OPC cluster #1 [violin plots were provided by Eneritz Agirre and Gonçalo Castelo-Branco].

(B) RNA ISH for *cspg4* in Tg(olig1:nls-mApple, mbp:nls-EGFP) fish at 7 dpf. *Cspg4*-positive cells compared in the nuclear and axodendritic region ($p < 0.001$, two-tailed Fisher's exact test, n = 15 animals in 4 experiments). The outline of the spinal cord is indicated by a dashed line. Boxed areas show magnified views of a *cspg4*-positive OPC in the nuclear region (') and a *cspg4*-negative OPC in the axodendritic region ('').

(C) RNA ISH for *olig1* in Tg(olig1:nls-mApple, mbp:nls-EGFP) fish at 7 dpf. *Olig1*-positive cells compared in the nuclear and axodendritic region ($p < 0.001$, two-tailed Fisher's exact test, n = 12 animals in 3 exp.). Boxed areas show magnified views of an *olig1*-positive OPC in the nuclear region (') and an *olig1*-negative OPC in the axodendritic region ('').

Scale bar in all images: 10 µm.

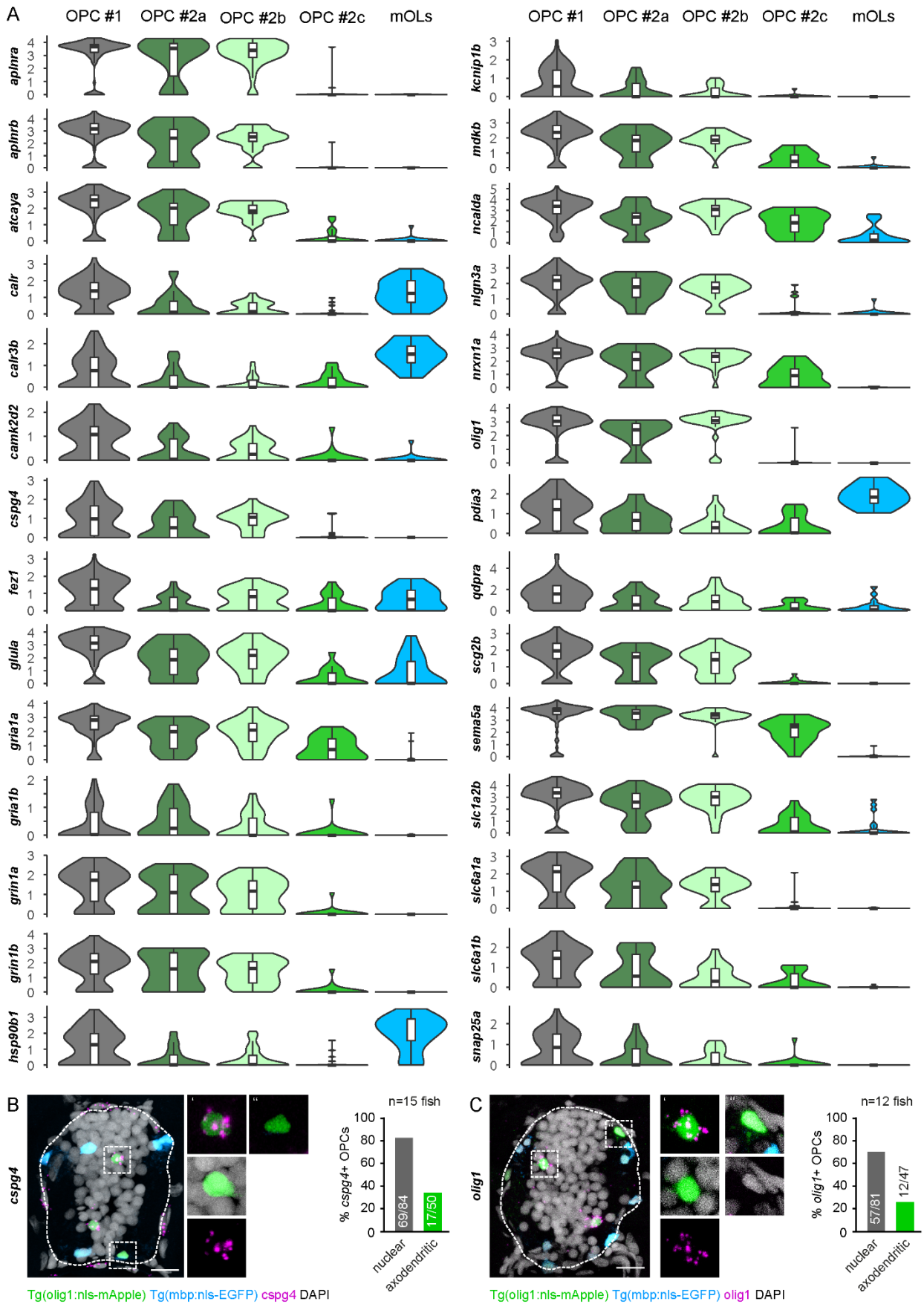
A
OPC #1
OPC #2a
OPC #2b
OPC #2c
mOLs
aplnra
aplnrb
atcaya
calr
calr3b
camk2d2
cspg4
fez1
glula
gria1a
gria1b
grin1a
grin1b
hsp90b1
kcnip1b
mdkb
ncalda
nlgn3a
nrxn1a
olig1
pdia3
qdpra
scg2b
sema5a
slc1a2b
slc6a1a
slc6a1b
snap25a
B
cspg4
n=15 fish
% cspg4+ OPCs
69/84
17/50
nuclear
axodendritic
Tg(olig1:nls-mApple) Tg(mbp:nls-EGFP) cspg4 DAPI
C
olig1
n=12 fish
% olig1+ OPCs
57/81
12/47
nuclear
axodendritic
Tg(olig1:nls-mApple) Tg(mbp:nls-EGFP) olig1 DAPI

3.3.4 OPCs that Execute Myelination (OPCs #2c)

Many genes were differently expressed between OPC clusters #1, #2a and #2b – which could be linked to OPCs with the soma in the nuclear region – compared to OPC cluster #2c (**Figure 3.3.4A** and **Figure 3.3.2H&K**). Indeed, cells from OPC cluster #2c were located preferentially in a position in the axodendritic region based on a set of RNA ISH markers (**Figure 3.3.4B-D**): e.g. *gpr17* (expressing cells in the nuclear region vs. axodendritic region: 35% versus 69%), *sox9b* (14% vs. 42%) and *myrf* (26% vs. 58%). Hence, OPC cluster #2c most likely refers to the cells mostly found in the axodendritic region with a simpler morphology and which are prone to differentiate to myelinating oligodendrocytes. That some cells expressing these genes were also found in the nuclear region is not surprising as also the live imaging data showed that a minority of these OPCs reside with their somata in this region and differentiated there (compare **section 3.2.4** and **3.2.5**). In accordance, genes which were highly expressed in OPC clusters #1, #2a, #2b but had low expression in OPC cluster #2c, like *cspg4* and *olig1* were found also less frequently expressed in cells with their soma in the axodendritic region (**Figure 3.3.3B&C**).

Interestingly, *olig1* expression seemed to be absent in cells of OPC cluster #2c, even though *olig1* promotor driven EYFP was used to FACS-sort cells for the single-cell RNA-Sequencing. As these cells express the general OL-lineage markers *sox10, olig2* and *nkx2.2a*, they most likely expressed *olig1* earlier and the fluorescent protein made during this period was not yet completely degraded at the time of FACS sorting. This is in agreement with the observation that axodendritic OPCs are dimmer during live imaging compared to complex OPCs with the soma in the nuclear region and that they derive from the latter cells (**Figure 3.2.6**).

Some of the genes upregulated in this cluster (**Table 3.3.4.1** and **Table 8.1.1.1**, e.g. *cnp*, *draxin*, *gpr17*, *mycb*, *myrf*, *prdm8*, *yy1b*) have known or assumed roles in oligodendrocyte differentiation. The most prominent candidate in this regard is probably *myrf*, which is an important transcription factor regulating the transition to myelinating oligodendrocytes (Emery et al., 2009). In contrast to most of the other genes in the list of upregulated genes, which had the highest expression within OPC cluster #2c cells, *myrf* expression is initiated in these cells but increased during the course of differentiation (**Figure 3.3.4B** and **Figure 3.3.2**). The roles of other genes like *gpr17* and *mycb* in differentiation are not fully understood. *Gpr17*-positive OPCs in the mouse was shown to be the ones which rarely differentiate (Vigano et al., 2016). *Myc* was shown to influence OPC differentiation but in a negative way (Magri et al., 2014). Other genes, like *prdm8*, *sox9b* and *sox8a* are suggested to promote OPC differentiation based on homologies with known regulators of OPC differentiation.

The GO term analysis was dominated by the high expression of genes involved in cell cycle regulation and almost exclusively found respective GO terms with the remarkable exception that *oligodendrocyte differentiation* was among the significant terms (**Table 3.3.4.2**). To eliminate the upregulated cell cycle associated genes from the input list, gene expression in OPC #2c was also compared exclusively to other proliferating cells in clusters OPC #2a and #2b (**Table 3.3.4.1**, right side). There was again a single term *glial cell differentiation* whereas all the others relate to translation and RNA processing (**Table 3.3.4.3**) indicating that these cells undergo a functional switch or maybe prepare already for the synthesis of myelin.

As introduced already in the previous section a small group of 4 cells within OPC cluster #1 had high expression levels of the same genes as OPC cluster #2c (**Figure 3.3.2H,** e.g. *myrf, gpr17* and *sox9b;* also *prdm8, myrf, egfra*). However, in contrast to all other cells of the OPC cluster #2c these four cells were lacking the gene expression signature associated with proliferation (**Figure 3.3.2I&J**, e.g. *pcna*, *mki67* and *knpn2*). I hypothesize that these cells correspond to **pre-OLs** that I have seen rarely also during live imaging; transitional cells shortly prior to myelination with the soma preferentially localized in the axodendritic region and a highly branched morphology (see **section 3.2.3**). Unfortunately, these small group did not show up as a distinct subcluster in the scRNA-Sequencing dataset as the number of cells was presumably too low to achieve statistical significance. Hence, also a list of specifically regulated genes could not be obtained. Furthermore, the distinction from OPC cluster #2c cells by RNA ISH would be difficult as they share the same territories with pre-OLs. Thus, this hypothesis could not be properly confirmed.

Cells in OPC cluster #2c are not differentiated oligodendrocytes for two reasons. First, they still have a signature of proliferation with high expression of genes like cdk1, mki67, top2a and nusap1 (**Table 8.1.1.1**); also the axodendritic OPCs in the live imaging dataset were able to divide prior to differentiation (**Figure 3.2.3B**). Second, with the exception of *myrf* they do not yet express typical markers of OLs like *mpz*, *mag* and *mbpa* (**Figure 3.3.4E** and **Table 8.1.1.1**). However, the expression of myelin genes, was not tested via RNA *in situ* hybridization to show that they are absent in OPCs.

Table 3.3.4.1 Gene expression in OPC cluster #2c.

Comparison between the cells within OPC cluster #2c with the entirety of cells outside this cluster (left side), and with cells in clusters #2a and #2b (right side) to demask the effect of cell cycle gene upregulation [data were provided by Eneritz Agirre & Gonçalo Castelo-Branco].

OPC #2c versus ALL		
#	**Gene**	**avg_logFC**
1.	*gpr17*	1,94
2.	*prdm8*	1,85
3.	*draxin*	1,82
4.	*hmgn2*	1,81
5.	*hmgb2a*	1,70
6.	*lmnb1*	1,67
7.	*cdk1*	1,60
8.	*mki67*	1,56
9.	*top2a*	1,52
10.	*plk1*	1,50
11.	*aspm*	1,50
12.	*hmga1a*	1,50
13.	*lbr*	1,47
14.	*nusap1*	1,45
15.	*ccnb1*	1,45
16.	*sox9b*	1,44
17.	*tuba8l4*	1,44
18.	*cenpe*	1,38
19.	*hmgb2b*	1,36
20.	*kpna2*	1,35
21	*zeb2a*	1,34
22.	*tnr*	1,34
23	*marcksb*	1,32
24.	*cenpf*	1,31
25.	*sox8b*	1,30
26.	*kif11*	1,30
27.	*mycb*	1,29
28.	*tuba8l*	1,27
29.	*wu:fb44b02*	1,27
30.	*tpx2*	1,27
84.	*myrf*	0,97

OPC #2c versus OPC#2		
#	**Gene**	**avg_logFC**
1.	*gpr17*	1,72
2.	*draxin*	1,52
3.	*prdm8*	1,40
4.	*myrf*	1,32
5.	*vav3b*	1,29
6.	*znf217*	1,19
7.	*mycb*	1,13
8.	*egfra*	1,10
9.	*ugt8*	1,09
10.	*sox8b*	1,09
11.	*zeb2a*	1,08
12.	*pmp22a*	1,05
13.	*tp53i11b*	1,03
14.	*shroom2a*	1,00
15.	*rpl3*	0,92
16.	*rpsa*	0,92
17.	*erbb3b*	0,91
18.	*rps9*	0,87
19.	*rps8a*	0,84
20.	*rreb1a*	0,80
21	*rps27a*	0,79
22.	*socs5b*	0,77
23	*rpl23a*	0,76
24.	*rpl7a*	0,75
25.	*srsf5a*	0,72
26.	*sdr16c5b*	0,72
27.	*rplp1*	0,72
28.	*ninj2*	0,72
29.	*fut9a*	0,69
30.	*gadd45gb.1*	0,66
31.	*sema6dl*	0,65

Table 3.3.4.2 GO term analysis of cells within OPC cluster #2c compared to all other clusters.

Based on the list of genes shown in **Table 3.3.4.1** (right side). The settings were chosen as described in **section 2.2.6**, the minimum number of associated genes was set to n=3. The *p* value was corrected used Benjamini-Hochberg correction.

Term ID	GO term	*p* value	% of genes	# of genes	Detected genes
GO:0048709	**oligodendrocyte differentiation**	9,94E-05	6,25	3,00	[prdm8, sox8b, sox9b]
GO:1902850	microtubule cytoskeleton organization involved in mitosis	1,87E-04	4,76	3,00	[kif11, nusap1, tpx2]
R-DRE:2500257	Resolution of Sister Chromatid Cohesion	3,78E-04	3,66	3,00	[cdk1, cenpe, cenpf]
GO:0007051	**spindle organization**	3,64E-04	3,61	3,00	[aspm, kif11, tpx2]
GO:0000819	sister chromatid segregation	4,46E-04	3,30	3,00	[cenpe, nusap1, top2a]
R-DRE:68877	Mitotic Prometaphase	9,75E-05	3,10	4,00	[cdk1, cenpe, cenpf, numa1]
GO:0000280	**nuclear division**	2,80E-05	2,73	5,00	[ccnb1, cenpe, kif11, nusap1, top2a]
GO:1903047	mitotic cell cycle process	1,01E-06	2,48	7,00	[ccnb1, cdk1, cenpe, kif11, nusap1, top2a, tpx2]
GO:0000278	**mitotic cell cycle**	8,44E-10	2,30	11,00	[aspm, ccnb1, cdk1, cenpe, kif11, nusap1, plk1, top2a, tpx2, tuba8l, tuba8l4]
R-DRE:68886	**M Phase**	1,01E-04	1,85	5,00	[cdk1, cenpe, cenpf, lmnb1, numa1]
GO:0022402	cell cycle process	2,36E-07	1,85	9,00	[aspm, ccnb1, cdk1, cenpe, kif11, nusap1, plk1, top2a, tpx2]
GO:0008017	microtubule binding	2,70E-03	1,63	3,00	[cenpe, kif11, nusap1]
GO:0010564	regulation of cell cycle process	2,57E-03	1,72	3,00	[ccnb1, plk1, tpx2]
R-DRE:69620	Cell Cycle Checkpoints	2,47E-03	1,71	3,00	[cdk1, cenpe, cenpf]
R-DRE:69278	Cell Cycle, Mitotic	7,22E-05	1,52	6,00	[cdk1, cenpe, cenpf, lmnb1, numa1, tpx2]
GO:0007017	microtubule-based process	2,12E-05	1,51	7,00	[aspm, cenpe, kif11, nusap1, tpx2, tuba8l, tuba8l4]
GO:0007346	regulation of mitotic cell cycle	9,01E-04	1,45	4,00	[ccnb1, cdk1, top2a, tpx2]
R-DRE:1640170	Cell Cycle	9,47E-05	1,41	6,00	[cdk1, cenpe, cenpf, lmnb1, numa1, tpx2]
GO:0051726	regulation of cell cycle	1,07E-04	1,27	6,00	[ccnb1, cdk1, kif11, plk1, top2a, tpx2]
GO:0022414	reproductive process	8,74E-03	1,05	3,00	[ccnb1, numa1, top2a]

Table 3.3.4.3 GO term analysis of cells within OPC cluster #2c compared to subclusters #2a and #2b.

Based on the list of genes shown in **Table 3.3.4.1** (left side). The settings were chosen as described in **section 2.2.6**, the minimum number of associated genes was set to n=3. The *p* value was corrected used Benjamini-Hochberg correction.

Term ID	GO term	*p* value	% of genes	# of genes	Detected genes
R-DRE:72695	Formation of the ternary complex, and subsequently, the 43S complex	0,00	9,52	4,00	[rps27a, rps8a, rps9, rpsa]
R-DRE:975956	Nonsense Mediated Decay (NMD) independent of the Exon Junction Complex (EJC)	0,00	8,82	6,00	[rpl7a, rplp1, rps27a, rps8a, rps9, rpsa]
R-DRE:1799339	SRP-dependent cotranslational protein targeting to membrane	0,00	8,70	6,00	[rpl7a, rplp1, rps27a, rps8a, rps9, rpsa]
R-DRE:72649	Translation initiation complex formation	0,00	8,33	4,00	[rps27a, rps8a, rps9, rpsa]
R-DRE:72662	Activation of the mRNA upon binding of the cap-binding complex and eIFs, and subsequent binding to 43S	0,00	8,16	4,00	[rps27a, rps8a, rps9, rpsa]
R-DRE:72702	Ribosomal scanning and start codon recognition	0,00	8,16	4,00	[rps27a, rps8a, rps9, rpsa]
R-DRE:72689	Formation of a pool of free 40S subunits	0,00	8,00	6,00	[rpl7a, rplp1, rps27a, rps8a, rps9, rpsa]
R-DRE:927802	**Nonsense-Mediated Decay (NMD)**	0,00	7,79	6,00	[rpl7a, rplp1, rps27a, rps8a, rps9, rpsa]
R-DRE:975957	Nonsense Mediated Decay (NMD) enhanced by the Exon Junction Complex (EJC)	0,00	7,79	6,00	[rpl7a, rplp1, rps27a, rps8a, rps9, rpsa]
R-DRE:156827	L13a-mediated translational silencing of Ceruloplasmin expression	0,00	7,14	6,00	[rpl7a, rplp1, rps27a, rps8a, rps9, rpsa]
R-DRE:72706	GTP hydrolysis and joining of the 60S ribosomal subunit	0,00	7,06	6,00	[rpl7a, rplp1, rps27a, rps8a, rps9, rpsa]
GO:0042255	**ribosome assembly**	0,00	6,82	3,00	[rpl23a, rpl3, rpsa]
R-DRE:72613	Eukaryotic Translation Initiation	0,00	6,67	6,00	[rpl7a, rplp1, rps27a, rps8a, rps9, rpsa]
R-DRE:72737	Cap-dependent Translation Initiation	0,00	6,67	6,00	[rpl7a, rplp1, rps27a, rps8a, rps9, rpsa]
GO:0042273	ribosomal large subunit biogenesis	0,00	5,08	3,00	[rpl23a, rpl3, rpl7a]
GO:0003735	structural constituent of ribosome	0,00	4,55	7,00	[rpl23a, rpl3, rplp1, rps27a, rps8a, rps9, rpsa]
R-DRE:72766	**Translation**	0,00	3,80	6,00	[rpl7a, rplp1, rps27a, rps8a, rps9, rpsa]
GO:0010001	**glial cell differentiation**	0,00	3,57	3,00	[erbb3b, prdm8, sox8b]
R-DRE:6791226	Major pathway of rRNA processing in the nucleolus and cytosol	0,00	3,57	3,00	[rpl7a, rplp1, rps9]
R-DRE:72312	rRNA processing	0,00	3,57	3,00	[rpl7a, rplp1, rps9]
R-DRE:8868773	rRNA processing in the nucleus and cytosol	0,00	3,57	3,00	[rpl7a, rplp1, rps9]
GO:0042254	ribosome biogenesis	0,00	2,50	5,00	[rpl23a, rpl3, rpl7a, rps8a, rpsa]
GO:0006364	**rRNA processing**	0,00	2,31	3,00	[rpl7a, rps8a, rpsa]
R-DRE:8953854	Metabolism of RNA	0,00	1,74	6,00	[rpl7a, rplp1, rps27a, rps8a, rps9, rpsa]
GO:0006412	**translation**	0,00	1,58	7,00	[rpl23a, rpl3, rplp1, rps27a, rps8a, rps9, rpsa]

A list of upregulated genes in oligodendrocytes is shown below (**Table 3.3.4.4** and **Figure 3.3.4E**). GO term analysis based on these genes resulted only in one significant term, which was *phospholipid transport* (**Table 3.3.4.5**)**.** Furthermore, the number of proper OLs in our dataset is small and does not allow elaborate conclusions, which was also not an aim of this work. Apart from this, basal functions of OLs are quite clear and have been extensively investigated.

Table 3.3.4.4 Gene expression in mOLs.

Comparison of mOLs with the entirety of cells outside of this cluster.

OLs versus ALL					
#	**Gene**	**log(FC)**	**#**	**Gene**	**log(FC)**
1.	*mpz*	3,58	17.	*tlcd2*	1,13
2.	*apoeb*	3,24	18.	*atp11a*	1,13
3.	*tlcd1*	2,17	19.	*jakmip3*	1,11
4.	*elovl7a*	2,14	20.	*cx47.1*	1,10
5.	*HEPACAM*	1,91	21	*sema4ga*	1,10
6.	*CU234171.1*	1,84	22.	*abtb2a*	1,09
7.	*plcxd1*	1,73	23	*TPPP*	1,07
8.	*cd9b*	1,50	24.	*crp1*	1,07
9.	*fabp2*	1,45	25.	*b3gat1b*	1,06
10.	*zgc:153981*	1,42	26.	*reep3a*	1,06
11.	*CABZ01114053.1*	1,42	27.	*ston2*	1,06
12.	*btbd11b*	1,32	28.	*pld1a*	1,05
13.	*rgra*	1,31	29.	*usp54a*	1,01
14.	*rgl3a*	1,21	30.	*pacs2*	1,01
15.	*cfl1l*	1,19			
16.	*htra1b*	1,16			

Table 3.3.4.5 GO term analysis of the mOL cluster.

Based on the list of genes shown in **Table 3.3.4.4**. The settings were chosen as described in **section 2.2.6**, the minimum number of associated genes was set to n=2. The *p* value was corrected used Benjamini-Hochberg correction.

Term ID	**GO term**	***p* value**	**% of genes**	**# of genes**	**Detected genes**
GO:0015914	phospholipid transport	0,01	2,17	2,00	[apoeb, atp11a]

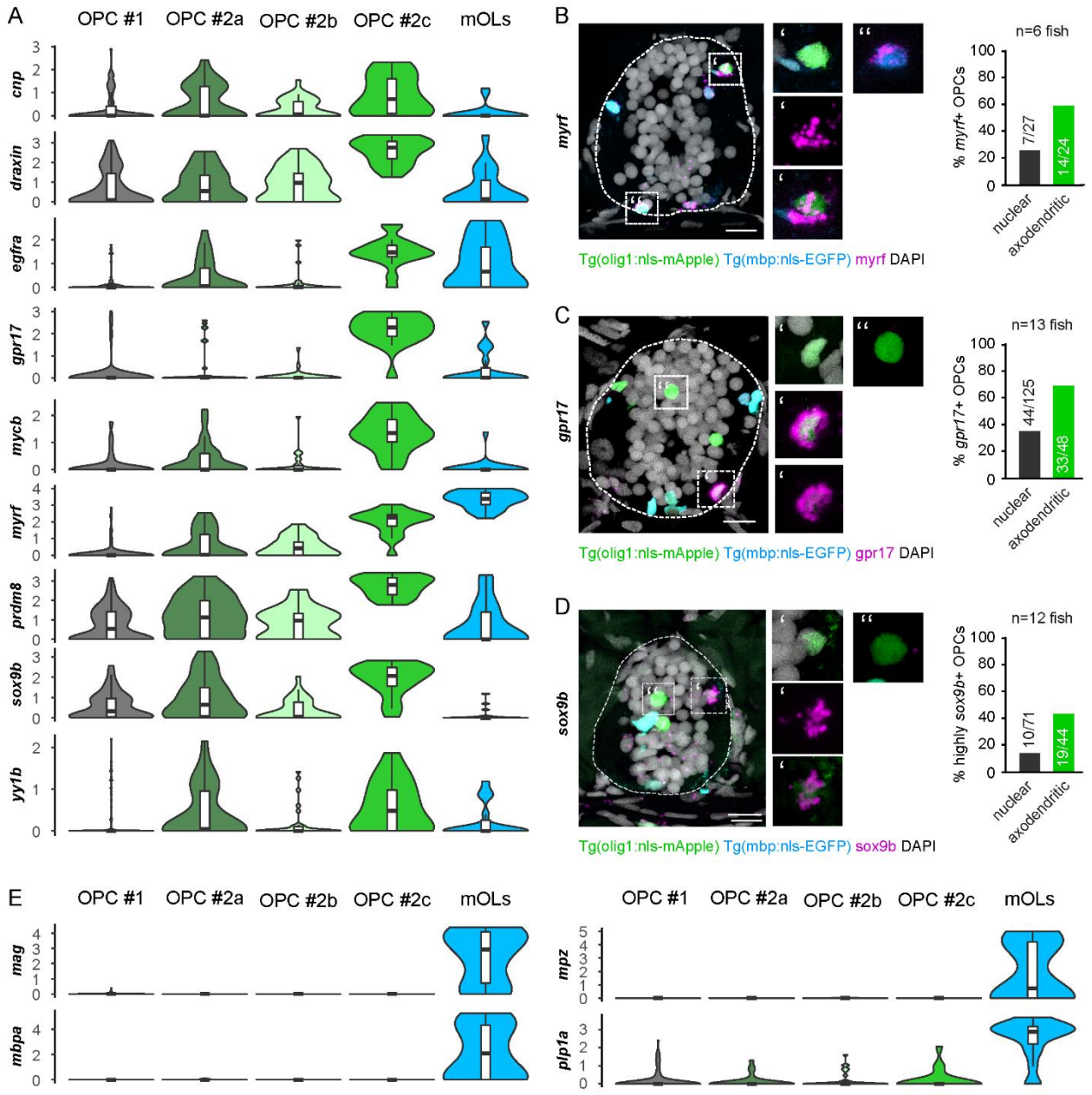

Figure 3.3.4 Gene expression and functional association within OPC cluster #2c.

(A) Violin plots showing the relative expression (log(TPM)) of marker genes upregulated in the OPC cluster #2c.

(B) RNA ISH for *myrf* in Tg(olig1:nls-mApple, mbp:nls-EGFP) fish at 7 dpf. *Myrf*-positive cells compared in the nuclear and axodendritic region (p = 0.025, two-tailed Fisher's exact test, n=6 animals in 2 experiments). The outline of the spinal cord is indicated by a dashed line. Boxed areas show magnified views of a *myrf*-positive OPC in the axodendritic region (') and a *myrf*-positive OL ('').

(C) RNA ISH for *gpr17*. *Gpr17*-positive cells compared in the nuclear and axodendritic region (p < 0.001, two-tailed Fisher's exact test, n=13 animals in 3 experiments). Boxed areas show magnified views of a *gpr17*-positive OPC in

the axodendritic region (‘) and a *gpr17*-negative OPC in the nuclear region (‘’).

(D) RNA ISH for *sox9b*. High-*Sox9b*-expressing cells (more than 10 single dots per cell) compared in the nuclear and axodendritic region ($p < 0.001$, two-tailed Fisher’s exact test, n=12 animals in 3 experiments). Boxed areas show magnified views of a *sox9b*-positive OPC in the axodendritic region (‘) and a *sox9b*-negative OPC in the nuclear region (‘’). Scale bar in all images: 10 µm.

(E) Violin plots showing the relative expression (log(TPM)) of specific marker genes upregulated in the mOL cluster. [violin plots were provided by Eneritz Agirre and Gonçalo Castelo-Branco]

3.3.5 Proliferating OPCs without a Signature of Differentiation (OPCs #2a & #2b)

The remaining OPC subclusters #2a and #2b were basically characterized by their high expression of cell cycle markers (e.g. *pcna* and *mki67*, respectively) in addition to their OL-lineage signature (**Figure 3.3.5A** and **Figure 3.3.2G-J**). Unlike OPC cluster #2c they lack gene expression associated with OPC differentiation and induction of myelination (**Figure 3.3.2K** and **Figure 3.3.4A**). Instead they expressed almost all the genes which were also upregulated in OPC cluster #1 at a slightly lower level (**Figure 3.3.3A**, e.g. *cspg4*, *olig1* and *gria2b*). However, the expression of proliferation-associated genes was such high as well as these genes were so abundant, that the regulation of other genes was less important to define these clusters. Due to the strong signature of proliferation OPC subclusters #2a, #2b and #2c were identified as a common cluster initially (**Figure 3.3.2A**).

Interestingly, most proliferation-associated genes were not equally expressed in OPC #2a and #2b but had their peak of expression either in one or the other subcluster (**Figure 3.3.5A** and **Figure 3.3.2I&J**). Genes which were upregulated in OPC subcluster #2a compared to all the other clusters in the analysis (**Table 3.3.5.1**, left side) are functionally associated with *synthesis of DNA* and *DNA replication* according to the GO term analysis (**Table 3.3.5.2**), which allows the conclusion that cells of cluster #2a are in the (G1)/S-phase of the cell cycle. In contrast, genes which were upregulated in OPC subcluster #2b (**Table 3.3.5.1**, right side) are functionally associated with mitosis and microtubule organization (**Table 3.3.5.3**). Hence, cells in this subcluster were basically in the G2/M-phase. The comparisons of cells in subclusters OPC #2a and #2b only to the other proliferating cells (OPC #2a to #2b+c, and OPC #2b to #2a+c) resulted in very similar lists of genes as the comparison with all other cells and hence also the associated GO terms were

similar (hence not shown particularly). In summary, the proliferating OPCs which were not committed to differentiation yet were subdivided by cell cycle phase in OPC clusters #2a and #2b.

I tested several genes associated with either OPC #2a or OPC #2b with RNA ISH. However, this was not successful: For example, the *kpna2* ISH probe did not label OPCs but OLs, cells which do not undergo proliferation anymore, indicating that there could have been a problem with the *in-situ* hybridization probe (**Figure 3.3.5B**). The *tuba8l* probe was not specific to OL-lineage cells nor any other individual cells (**Figure 3.3.5D**), which could mean that sample preparation procedure for this probe would be required to be different from the other probes or it binds also to other tubulin genes. The widely used cell cycle marker *mki67* could be detected by RNA ISH but only occasionally (**Figure 3.3.5C**). It remains elusive why none of the tested cell cycle markers lead to the expected results (see **section 4.2.2**). Despite it was not possible to detect proliferation markers in OPCs by RNA ISH, the *in vivo* live imaging data showed clearly that OPCs in the nuclear and axodendritic region proliferate frequently (**section 3.2.2 to 3.2.6**). Furthermore, work by colleagues in our laboratory could further confirm by EdU incorporation that OPCs in the nuclear and axodendritic region proliferate to a comparable extent (Marisca et al., 2020).

As OPC subclusters #2a and #2b share common gene expression profiles with non-myelinating OPCs of cluster #1, which were involved in neuronal signalling, as well as OPC #2c, which proliferate and are prone to differentiate, I hypothesize that these subclusters represent intermediate stages during the transformation process between the two subgroups of OPCs found by *in vivo* live imaging and single-cell RNA-Sequencing. This is also in accordance with the observation that proliferation, which had a strong signature in OPC #2a and #2b, precedes differentiation of OPCs into myelinating OLs (see **section 3.2.6**).

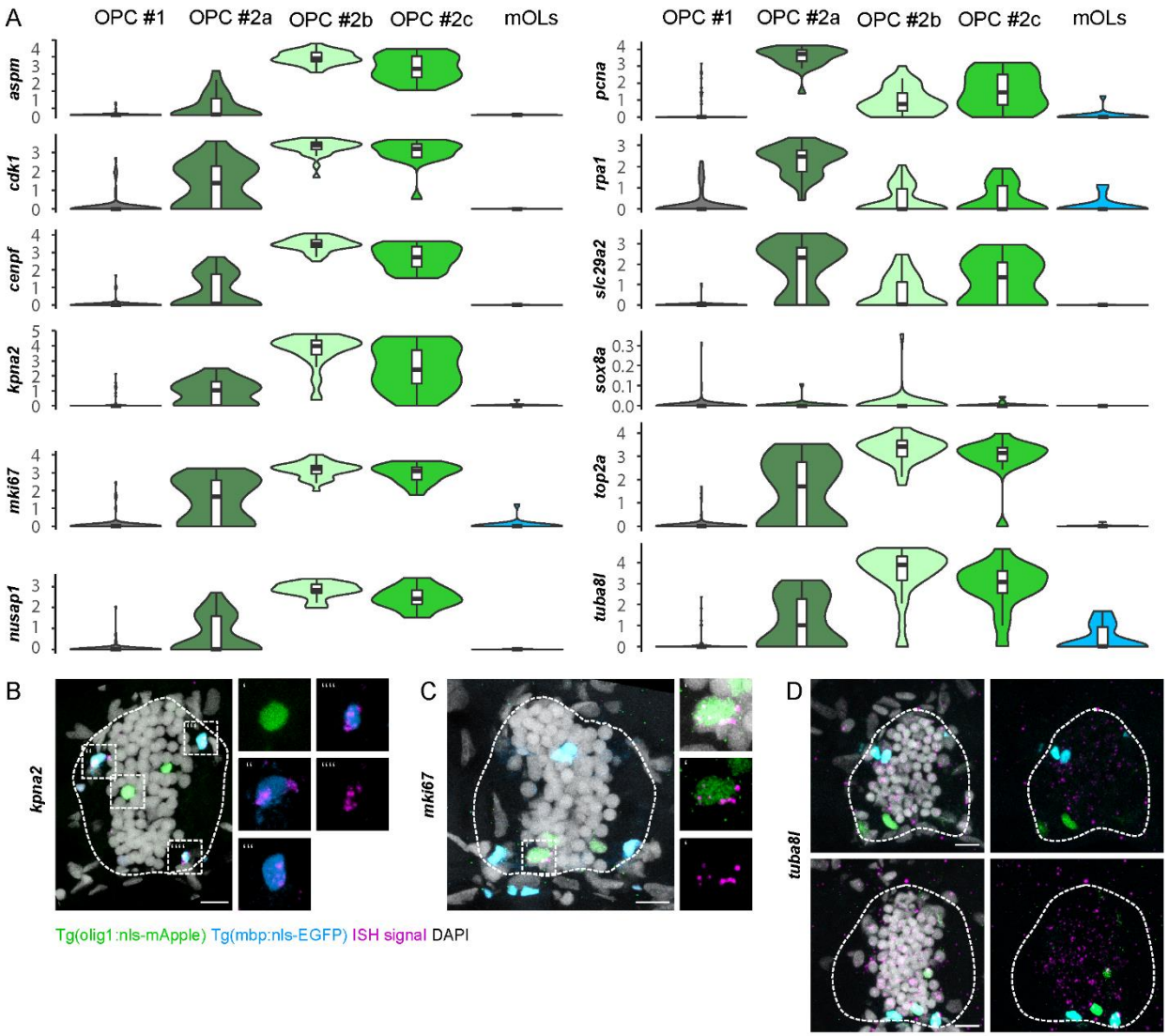

Figure 3.3.5 Gene expression and functional association within OPC cluster #2a and #2b.

(A) Violin plots showing the relative expression (log(TPM)) of specific marker genes upregulated in the OPC cluster #2, especially in subgroups #2a and #2b [violin plots were provided by Eneritz Agirre and Gonçalo Castelo-Branco].

(B) RNA ISH for *kpna2* in Tg(olig1:nls-mApple, mbp:nls-EGFP) fish at 7 dpf. Cells labelled with the *kpna2* ISH probe in the zebrafish spinal cord were mbp:nls-EGFP-labelled OLs and not OPCs as expected from the scRNASeq data. The outline of the spinal cord is indicated by a dashed line. Boxed areas show magnified views of a *kpna2*-negative OPC (') and of *kpna2*-positive OLs. Scale bar in all images: 10 µm.

(C) RNA ISH for *mki67*. Only one *mki67*-positive cell (shown) was found among approximately 140 imaged OPCs from spinal cord and brain (no detailed quantification was conducted), which is again in contradiction with the expected frequency of *mki67*-positive OPCs based on the scRNASeq data.

(D) RNA ISH for *tuba8l*, which was not specific to OL-lineage cells and therefore not suitable for quantification.

Table 3.3.5.1 Gene expression in OPC cluster #2a and #2b.

Compared are the cells within one subcluster with the entirety of cells outside this cluster.

	OPC #2a versus ALL		OPC #2b versus ALL	
#	**Gene**	**avg_logFC**	**Gene**	**avg_logFC**
1.	*pcna*	2,72	*kpna2*	2,86
2.	*rpa1*	1,99	*cenpf*	2,62
3.	*slc29a2*	1,96	*aspm*	2,55
4.	*fen1*	1,84	*tuba8l*	2,48
5.	*rrm2*	1,83	*kif11*	2,45
6.	*dnmt1*	1,78	*plk1*	2,36
7.	*zgc:110540*	1,72	*ccnb1*	2,23
8.	*stmn1a*	1,63	*tpx2*	2,21
9.	*mcm5*	1,60	*top2a*	2,17
10.	*dnajc9*	1,60	*cdk1*	2,16
11.	*rrm1*	1,58	*nusap1*	2,15
12.	*rbbp4*	1,53	*ube2c*	2,10
13.	*slbp*	1,52	*mki67*	2,10
14.	*lig1*	1,50	*tacc3*	2,08
15.	*rrm2*	1,47	*cdc20*	2,06
16.	*rpa2*	1,44	*cdc14b*	2,03
17.	*mcm2*	1,44	*prc1b*	1,94
18.	*chaf1a*	1,41	*kifc1*	1,92
19.	*nasp*	1,41	*prc1a*	1,92
20.	*atad2*	1,40	*g2e3*	1,91
21	*mcm3*	1,40	*ccna2*	1,86
22.	*mibp*	1,33	*cenpe*	1,77
23	*rfc5*	1,32	*cdca8*	1,75
24.	*mcm4*	1,30	*ccnf*	1,74
25.	*sumo3b*	1,29	*anln*	1,73
26.	*tubb2b*	1,28	*mastl*	1,73
27.	*asf1ba*	1,21	*mad2l1*	1,71
28.	*dck*	1,20	*ccnb3*	1,71
29.	*atad5a*	1,20	*rtkn2a*	1,70
30.	*cdca7a*	1,20	*kif2c*	1,70

Table 3.3.5.2 GO term analysis of cells within OPC cluster #2a.

Based on the list of genes shown in **Table 3.3.5.1** (left side). The settings were chosen as described in **section 2.2.6**, the minimum number of associated genes was set to n=6. The *p* value was corrected used Benjamini-Hochberg correction.

Term ID	GO term	*p* value	% of genes	# of genes	Detected genes
R-DRE:69186	Lagging Strand Synthesis	2,79E-14	50,00	6,00	[fen1, lig1, pcna, rfc5, rpa1, rpa2]
R-DRE:69190	**DNA strand elongation**	4,14E-14	46,15	6,00	[fen1, lig1, pcna, rfc5, rpa1, rpa2]
R-DRE:5651801	PCNA-Dependent Long Patch Base Excision Repair	4,14E-14	46,15	6,00	[fen1, lig1, pcna, rfc5, rpa1, rpa2]
R-DRE:110373	Resolution of AP sites via the multiple-nucleotide patch replacement pathway	2,12E-13	35,29	6,00	[fen1, lig1, pcna, rfc5, rpa1, rpa2]
R-DRE:73933	Resolution of Abasic Sites (AP sites)	3,91E-12	22,22	6,00	[fen1, lig1, pcna, rfc5, rpa1, rpa2]
R-DRE:73884	Base Excision Repair	3,91E-12	22,22	6,00	[fen1, lig1, pcna, rfc5, rpa1, rpa2]
R-DRE:69239	**Synthesis of DNA**	1,97E-14	16,67	8,00	[fen1, lig1, mcm3, mcm4, pcna, rfc5, rpa1, rpa2]
R-DRE:69242	**S Phase**	1,48E-13	12,12	8,00	[fen1, lig1, mcm3, mcm4, pcna, rfc5, rpa1, rpa2]
GO:0006261	DNA-dependent DNA replication	1,34E-14	11,69	9,00	[lig1, mcm2, mcm3, mcm4, mcm5, pcna, rfc5, rpa1, rpa2]
GO:0006260	**DNA replication**	2,14E-22	10,85	14,00	[chaf1a, fen1, lig1, mcm2, mcm3, mcm4, mcm5, pcna, rbbp4, rfc5, rpa1, rpa2, rrm1, rrm2]
R-DRE:69306	DNA Replication	2,70E-12	8,25	8,00	[fen1, lig1, mcm3, mcm4, pcna, rfc5, rpa1, rpa2]
R-DRE:5696398	Nucleotide Excision Repair	2,23E-09	7,79	6,00	[lig1, pcna, rfc5, rpa1, rpa2, sumo3b]
GO:0071103	DNA conformation change	1,96E-09	5,04	7,00	[chaf1a, mcm2, mcm4, nasp, rbbp4, rpa1, rpa2]
R-DRE:73894	DNA Repair	3,74E-08	3,18	7,00	[fen1, lig1, pcna, rfc5, rpa1, rpa2, sumo3b]
GO:0006259	DNA metabolic process	3,59E-11	2,48	11,00	[chaf1a, dnmt1, fen1, lig1, mcm2, mcm3, mcm4, mcm5, pcna, rpa1, rpa2]
GO:0043010	camera-type eye development	5,07E-07	2,11	7,00	[dnmt1, fen1, mcm2, mcm3, mcm5, rfc5, slbp]
GO:0006281	DNA repair	3,66E-06	2,10	6,00	[chaf1a, fen1, lig1, pcna, rpa1, rpa2]
R-DRE:69278	Cell Cycle, Mitotic	1,00E-07	2,03046	8	[fen1, lig1, mcm3, mcm4, pcna, rfc5, rpa1, rpa2]
R-DRE:1640170	Cell Cycle	1,68E-07	1,88235	8	[fen1, lig1, mcm3, mcm4, pcna, rfc5, rpa1, rpa2]
GO:0051276	chromosome organization	1,68E-08	1,61812	10	[asf1ba, atad2, chaf1a, dnmt1, mcm2, mcm4, nasp, rbbp4, rpa1, rpa2]
GO:0006325	chromatin organization	2,88E-05	1,44578	6	[asf1ba, atad2, chaf1a, dnmt1, nasp, rbbp4]

Table 3.3.5.3 GO term analysis of cells within OPC cluster #2b.

Based on the list of genes shown in **Table 3.3.5.1** (right side). The settings were chosen as described in **section 2.2.6**, the minimum number of associated genes was set to n=6. The *p* value was corrected used Benjamini-Hochberg correction.

Term ID	GO term	*p* value	% of genes	# of genes	Detected genes
GO:0000280	**nuclear division**	6,58E-17	6,45	12,00	[ccna2, ccnb1, ccnb3, ccnf, cdc14b, cdca8, cenpe, kif11, kifc1, mad2l1, nusap1, top2a]
GO:1903047	mitotic cell cycle process	7,73E-24	6,01	17,00	[anln, ccna2, ccnb1, ccnb3, ccnf, cdc14b, cdca8, cdk1, cenpe, kif11, kifc1, mad2l1, mastl, nusap1, tacc3, top2a, tpx2]
GO:0010564	regulation of cell cycle process	1,00E-13	5,68	10,00	[ccna2, ccnb1, ccnb3, ccnf, cdc14b, mad2l1, plk1, prc1a, prc1b, tpx2]
GO:0000278	**mitotic cell cycle**	5,62E-25	4,17	20,00	[anln, aspm, ccna2, ccnb1, ccnb3, ccnf, cdc14b, cdca8, cdk1, cenpe, kif11, kifc1, mad2l1, mastl, nusap1, plk1, tacc3, top2a, tpx2, tuba8l]
R-DRE:69620	Cell Cycle Checkpoints	6,60E-09	4,00	7,00	[cdc20, cdca8, cdk1, cenpe, cenpf, kif2c, ube2c]
GO:0008017	**microtubule binding**	8,02E-09	3,80	7,00	[cenpe, kif11, kif2c, kifc1, nusap1, prc1a, prc1b]
GO:0007346	regulation of mitotic cell cycle	2,94E-10	3,25	9,00	[ccna2, ccnb1, ccnb3, ccnf, cdc14b, cdk1, mad2l1, top2a, tpx2]
R-DRE:68886	**M Phase**	5,35E-09	2,96	8,00	[cdc20, cdca8, cdk1, cenpe, cenpf, kif2c, mastl, ube2c]
GO:0007017	microtubule-based process	8,67E-14	2,82	13,00	[aspm, ccnf, cdc14b, cenpe, kif11, kif2c, kifc1, nusap1, prc1a, prc1b, tacc3, tpx2, tuba8l]
GO:0051726	regulation of cell cycle	1,00E-13	2,75	13,00	[ccna2, ccnb1, ccnb3, ccnf, cdc14b, cdk1, kif11, mad2l1, plk1, prc1a, prc1b, top2a, tpx2]
GO:0007049	cell cycle	1,07E-23	2,56	22,00	[anln, aspm, ccna2, ccnb1, ccnb3, ccnf, cdc14b, cdca8, cdk1, cenpe, kif11, kifc1, mad2l1, mastl, nusap1, plk1, prc1a, prc1b, tacc3, top2a, tpx2, tuba8l]
R-DRE:69278	Cell Cycle, Mitotic	5,22E-09	2,28	9,00	[cdc20, cdca8, cdk1, cenpe, cenpf, kif2c, mastl, tpx2, ube2c]
R-DRE:1640170	Cell Cycle	7,76E-09	2,12	9,00	[cdc20, cdca8, cdk1, cenpe, cenpf, kif2c, mastl, tpx2, ube2c]
GO:0007010	**cytoskeleton organization**	2,10E-09	1,40	12,00	[anln, aspm, ccnf, cdc14b, kif11, kifc1, nusap1, prc1a, prc1b, tacc3, tpx2, tuba8l]

3.3.6 Summary - Molecular Characterization of OL-Lineage Cell Subgroups

In accordance with our live imaging data, single-cell RNA-Sequencing reveals different subclusters of OPCs which most likely correspond to distinct stages along lineage-progression. In the tSNE representations of the data (**Figure 3.3.2A&G**), the tSNE1 dimension corresponds roughly to lineage progression in a reverse manner. The lower the tSNE1 value of a cell, the more progressed it is in the OL-lineage. A cell division is an important and delicate event for a cell and therefore the cell cycle is tightly regulated. Hence the impact of cell cycle-associated genes on the overall expression profile of a cell was high. This is reflected mainly by the tSNE2 dimension of the presented tSNE plots. Low values represent cells which are not in the cell cycle. When the value increases, cells first enter the S phase and later the M phase.

OPC cluster #1 comprises cells that express the classical OPC markers (*nkx2.2a, cspg4* and *olig1*) and have their soma predominantly in the nuclear region. According to their gene expression prolife, the cells are involved in neurotransmitter communication (as indicated by the high expression levels of genes like *gria1a* and *glula*) possibly even via synaptic structures.

OPC subclusters #2a and #2b represent transitional stages between OPC cluster #1 and #2c as they share gene expression with both groups. They are predominantly characterized by the expression of cell cycling genes (e.g. *pcna* and *mki67*) but still have the signature of neuronal activity.

In cells included in **OPC subcluster #2c**, gene expression of neuronal communication markers is shut down and the expression of genes associated with differentiation in oligodendrocytes (e.g. *myrf*) is upregulated. These cells can still undergo cell division, reflected by the expression of proliferation markers. Hence, OPCs in subclusters #2a-c represent kinds of transit-amplifying cells or committed progenitors/precursors according to nomenclatures which can be found in different models of lineage progression (Lui et al., 2011; Marques et al., 2016). OPCs of cluster #2c are found predominantly in the axodendritic region.

Based on their preferred soma localization, it was possible to infer that OPCs of cluster #1 correspond to the OPC type identified during *in vivo* imaging that extend a highly ramified process network from its soma localized in the nuclear region and do not directly differentiate. Conversely, the other, simpler OPC subtype mainly found in the axodendritic region which readily differentiates into myelinating OLs is represented in the single-cell RNA-Sequencing data by OPC subcluster #2c.

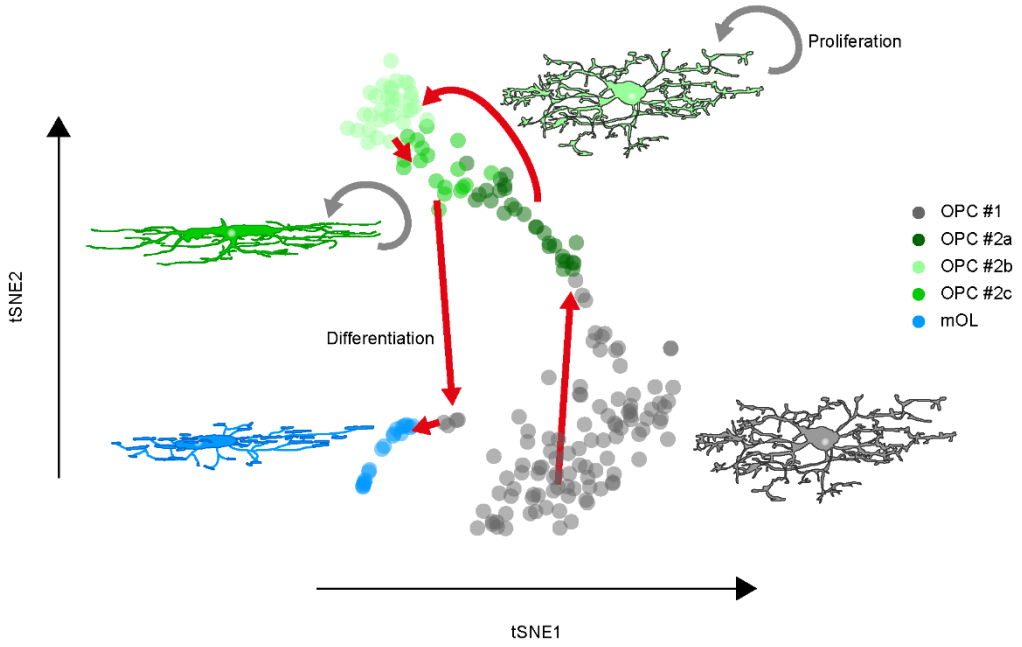

Figure 3.3.6 Schematic drawing how individual clusters likely relate to each other and to subgroups of OPCs identified via *in vivo* live imaging.

4 DISCUSSION

4.1 OPC Heterogeneity: Two Functionally Distinct Types of OPCs

4.1.1 Enabling Methodological Approach

In this thesis, I aimed to investigate heterogeneity within the OPC population. This was the first work in this regard in zebrafish. Based on previously published work in mammalian models, there is evidence that OPCs can differ regarding their proliferation and differentiation potential as well as their responsiveness to different signalling mechanisms (see also **section 1.7**), however, often there are several shortcomings. For example, it is not clear how the single observations fit together and which entities OPCs with different properties, behaviours or potentials actually constitute. Do they represent distinct lineage trajectories or does the diversity rather reflect different stages along lineage progression?

Fate analysis has been carried out in the OL-lineage by lineage tracing (Kang et al., 2010; Vigano et al., 2016; Zhu et al., 2012), but cannot be done on the single-cell level and with sufficient temporal resolution. This can be overcome by live imaging. However, with murine models this was often carried out in slice cultures, which are susceptible for degeneration and cannot be maintained over longer time (Hamilton et al., 2017). Some recent studies even implemented *in vivo* live imaging in mice through cranial windows; but this was mostly limited to the outer layers of the cortical grey matter and is very difficult in regions of extensive myelination like the sub-cortical white matter during development (Hill et al., 2018; Hill et al., 2014; Hughes et al., 2013; Hughes et al., 2018).

I addressed this in a more holistic approach by a variety of methods to analyse OPCs genetically, morphologically and regarding functional differences, i.e. their potential to differentiate in myelinating OLs. Through *in vivo* live imaging in developing zebrafish it was feasible to assess several properties and the fate of individual OPCs at the same time to not only capture a snapshot in time but directly observe the developmental process over long periods. This was supplemented with single-cell RNA-Sequencing, which enabled the identification of molecularly distinct OPC subclusters. This insight would not have been obtained by bulk RNA-Sequencing as easily since appropriate markers for OPC subpopulations are not established.

4.1.2 Synthesis of the Previous Results Referring to the Addressed Research Questions

Indeed, I found different subtypes of OPCs that have distinct properties and different potentials to differentiate in the zebrafish spinal cord. There was a group of OPCs, which only had a limited number of processes which are aligned with the axons in anterior-posterior direction and which were highly motile. A large fraction of these cells differentiated into myelinating OLs within 24 h (**Figure 3.2.3**) and almost all within the time frame of three days during the first weeks of zebrafish development (**Figure 3.2.9**). The majority of these OPCs was not only found with its processes but also with its soma in the axodendritic region (**Figure 3.2.3**). Based on the preferred soma location this OPC subgroup could be linked via RNA *in situ* hybridization to OPC subcluster #2c identified by single-cell RNA-Sequencing. The cells in this cluster were the only ones that had a high expression of cell cycle genes, defining them as progenitors, but also of genes for oligodendrocyte differentiation demonstrating their committed identity.

OPCs of the other subgroup were preferentially found with their somata in the nuclear region in the medial spinal cord. Conversely to the first group, these cells were characterized by a complex, ramified process network covering the whole diameter of the spinal cord. The processes were not elongated along the anterior-posterior body axis but appeared more to be radially organized (**Figure 3.1.4**) and remodel more slowly. These type of OPCs most likely correspond to cells found in OPC cluster #1 in the single-cell RNA-Sequencing data, which are the ones that highly express genes with a function in neuronal communication specifically via neurotransmitters. In line with this, the complex morphology would favour successful axoglial-communication as it would maximize the possible neuronal input.

These complex OPCs were never observed to initiate myelination directly. However, they could divide symmetrically or asymmetrically to generate daughter cells which rapidly transform into the other, differentiation-competent OPC subtype. As cells in OPC cluster #1 did not express cell cycle genes, these intermediate stages are likely represented by OPC subclusters #2a and #2b in the RNA-Sequencing dataset. This transformation process is accompanied by acquiring the simpler morphology, which is at least partly caused by the distribution of processes to both daughter cells during division but might be also an active process (see **section 3.2.6** and **section 4.2.3**). In the majority of cases, the OPCs that switch subtype after cell division also undergo soma transition from the nuclear to the axodendritic region.

However, few exceptions were observed, when OPCs with a simple morphology but the soma in the nuclear region also differentiated. Conversely, OPCs with a complex morphology could have their soma over long time in the axodendritic region, where they proliferated but did not differentiate (**Figure 3.2.4**, **Figure 3.2.5** and **Figure 3.2.6**). Hence, this leads to the conclusion that soma localization is not a definite

predictor for OPC fate. Considering the entirety of their properties and emphasizing their fate, instead it appears more meaningful to refer to the distinct subgroups as **myelination-competent OPCs** and **non-myelinating OPCs**.

Through these two subtypes a functional segregation of the OPC population is implemented. Whereas myelination-competent OPCs have the sole task to contact myelination-competent axons for the initiation of future myelin sheaths, the non-myelinating OPCs act as the post-synapse for neurons, controls the cell number within the OL-lineage and maybe have even more additional functions (see **section 4.1.3** and **4.1.4**).

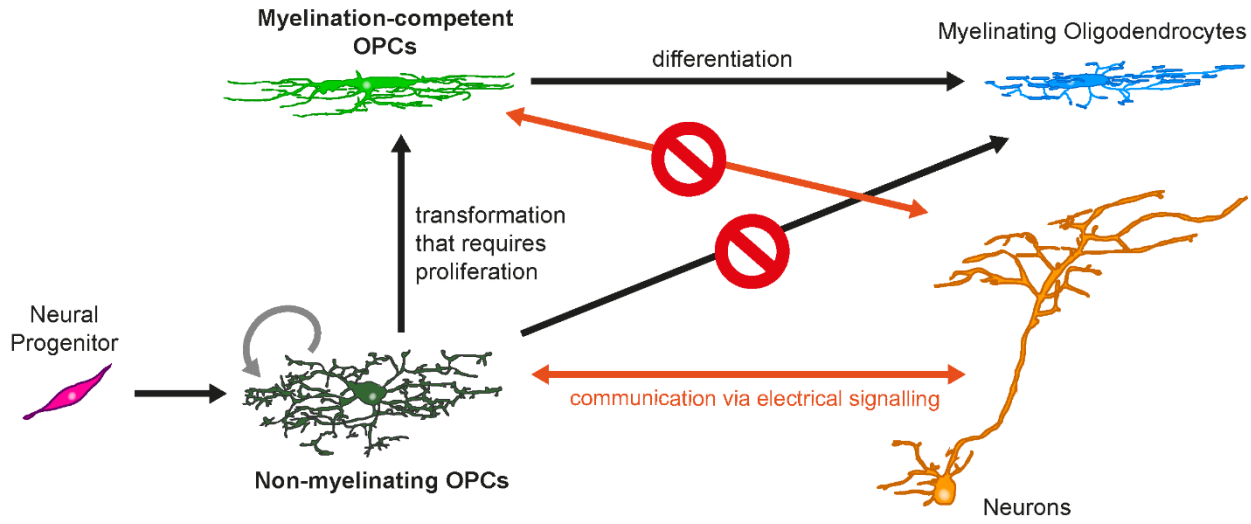

Figure 4.1.1 Schematic overview how different OPC subtypes could be functionally diverse based on the results of this thesis.

4.1.3 Functions of Non-Myelinating OPCs

The single-cell RNA-sequencing data supported the conclusion that OPCs of the non-myelinating type play instead a major role for the communication with neurons and that myelination-competent cells lose this ability. This assumption was also proven by experimental data generated by colleagues in my group using calcium imaging and pharmacological interventions. OPCs with their soma in the nuclear region showed calcium transients which also had a higher amplitude much more frequently than OPCs in the axodendritic region (Marisca et al., 2020).

Despite these OPCs never differentiated directly to OLs in my experiments, they have an indirect influence on myelination since when they divide, they can generate OPCs of the other, myelination-competent subtype. As the latter subtype was observed to differentiate always within few days, the proliferation of non-myelinating OPCs controls the final number of newly generated oligodendrocytes (given the fact that no cell death of immature OLs prior to myelination was observed at all in my data). Again, work by colleagues in our group could show in addition that neuronal activity in non-myelinating cells is linked to proliferation and hence regulates the number of OPCs and myelinating OLs in the zebrafish spinal cord (see also below **section 4.2.2**). Interestingly, the previously reported effect of the drug splitomicin to enhance OL numbers (Early et al., 2018), was found to be mediated also by an increased proliferation of non-myelinating OPCs in the nuclear region and not by increasing the differentiation rate directly (Marisca et al., 2020).

OPCs not only divide but also remodel their morphology extensively prior to differentiation. The myelination-competent OPCs had significantly fewer processes than the non-myelinating ones. This indicates that the complex process network of non-myelinating OPCs functions primarily in axoglial communication and is not to explore sites for future myelin sheaths. Considering the different remodelling rates, branching and morphology of processes in non-myelinating versus myelinating OPCs, this provokes the hypothesis that processes could be quite different in their nature to adapt to their function which is either neuronal communication or myelin sheath formation. For example, they might have – apart from being equipped with neurotransmitter receptors or not – distinct cytoskeletal properties and adhesion molecules (the answer could be partly included in the presented single-cell sequencing data, however the dataset was not analysed to address this aspect).

The complex process network of these cells could help to establish contact to as many axons as possible to enhance or finetune neuronal input accordingly. In this regard, it appears advantageous that these processes are more stable, and remodel more slowly compared to myelination-competent OPCs. This could enable even the establishment of synaptic contacts with neurons as described in mammals (Bergles et al., 2010). Otherwise, even in the non-myelinating OPCs the process tips remodel to a non-neglectable extent and only major branches are stable. It is questionable if these processes are stable enough for synaptic contacts. However, OPCs in the adult mouse brain, cells that have been shown to have synapses, have a comparable process motility *in vivo* as seen in the zebrafish (Hughes et al., 2013).

4.1.4 Possible Additional Functions of Non-Myelinating OPCs

Apart from generating myelination-competent OPCs, non-myelinating OPCs have also been observed frequently to divide symmetrically generating two daughter cells of the same type and hence fulfil the crucial role of maintaining the OPC population throughout development and likely until adulthood. Thus, the inability of non-myelinating OPCs to differentiate could also be a protective mechanism to prevent the depletion of the progenitor pool throughout life. This is of particular importance as after the initial establishment of the OPC population in the spinal cord (at 3&4 dpf) no or only a very limited number of new OPCs seem to be generated from neural progenitors. However, it is possible that this happens still to a low level or in several waves during development (of which only the first wave was captured in my experiments). Although in the mouse brain OPC-like cells have been observed which were constantly generated in the subependymal zone, these cells have a reduced lifespan and lack the ability to differentiate in myelinating OLs (Kazanis et al., 2017).

Together, non-myelinating OPCs seem to be a type of progenitor cell which is maintained long-term outside of a typical stem cell niche. This is fundamentally different as it is described for example for neuronal and intestinal stem cells (Doetsch, 2003; Haegebarth and Clevers, 2009). Even if one would consider the nuclear region close to the central canal in the spinal cord as similar to the subventricular or subendymal zone (SVZ/SEZ), OPCs with similar morphology and behaviour were also found regularly in CNS parenchyma, e.g. in the optical tectum (unpublished observation by others in the group, therefore not shown). Moreover, with their elaborated process network and their ability to integrate electrical signals, non-myelinating OPCs are phenotypically unusually differentiated compared to other known progenitor cells. As previously published and confirmed by our time-lapse observations, these cells can even divide while maintaining their morphology without retracting the process network (Ge et al., 2009; Kukley et al., 2008).

All recent studies investigating the role of OL-lineage cells in learning focused on the importance of OL generation and myelination (Bacmeister et al., 2020; Kato et al., 2020; McKenzie et al., 2014; Pan et al., 2020; Steadman et al., 2019; Xiao et al., 2016). However, as the non-myelinating OPCs are so abundant and cover the whole CNS with their processes even in adulthood when active myelination ceased, there is the hypothesis that they might be directly involved in neuronal circuit regulation apart from their role in myelination. This could be an alternative way how to modulate neuronal plasticity in addition to adaptive myelination. Mechanistically this can be achieved either by proper integration into the neuronal network with a pre-synaptic function, by the secretion of neuromodulatory factors, or by neurotransmitter uptake

and re-cycling. However, the current evidence for this hypothesis is little. Some studies detected action potentials in some OPCs, one study described long-term potentiation (Chittajallu et al., 2004; Ge et al., 2006; Ge et al., 2009; Karadottir et al., 2008), however this was not systematically reproduced within the last ten years. Also, some factors released by OPCs could have neuromodulatory functions. For example, the shedding of the NG2 (Cspg4) ectodomain, which is in turn regulated by electrical activity, influences long term potentiation in pyramidal neurons of the somatosensory cortex as well as AMPAR- and NMDAR-dependent currents (Sakry et al., 2014). Furthermore, OPCs can express Prostaglandin D2 synthase and neuronal pentraxin 2 (Sakry et al., 2015). At least the former is expressed in the some of the non-cycling and non-myelinating OPCs (OPC cluster #1) analysed here. In addition, expression of presynaptic neurexins (*nrxn1-3*), bassoon (*bsnb*) and synapsophysins (*syp*) was detected in these non-myelinating OPCs, which was much higher compared to postsynaptic markers like PSD-95 (*dlg4*) or homer (*homer 1-3*) (**Table 8.1.1.1**).

In this line, in the mammalian CNS astrocytes have been shown to have important neuromodulatory functions (Farmer and Murai, 2017; Ma et al., 2016; Stobart et al., 2018; Xin and Bonci, 2018). Astrocytes also extend processes to nodes of Ranvier, but also OPC processes do so (Serwanski et al., 2017). Astrocytes in the zebrafish are only poorly investigated in the zebrafish so far and most likely less abundant compared to mammals. Under this assumption and given the developmental similarity between astrocytes and OPCs (**Figure 1.1.1**), one could hypothesize that OPCs could have some of the functions that astrocytes have in higher vertebrates. For example, as OPCs express high levels of *slc1a2b* and *glula* it could be possible, that they participate actively in glutamate recycling which is usually done by astrocytes (Hayashi, 2018). This functions for non-myelinating OPCs could be zebrafish-specific and could cause differences between zebrafish OL-lineage cells and their mammalian counterparts.

4.1.5 Myelination-competent OPCs

As outlined above, conversely to the non-myelinating OPCs, the second subtype of OPCs found in the zebrafish CNS readily differentiated into myelinating oligodendrocytes. Their morphology is distinct from their non-myelinating counterparts (oval-shaped soma, fewer processes aligned in anterior-posterior direction etc.). During *in vivo* live imaging, these cells divided regularly, proofing that they are indeed progenitors and not yet pre-oligodendrocytes.

Via RNA *in situ* hybridization, a link between myelination-competent OPCs and OPC subcluster #2c of the single-cell RNA-Sequencing dataset could be established. Remarkably, these OPCs expressed markers of proliferation – another proof of their progenitor identity – but were also the only OPCs that upregulated genes associated with differentiation and OL maturation. For example, *myrf* is one of the most widely used genes to interfere with differentiation in oligodendrocytes (Emery et al., 2009; McKenzie et al., 2014; Steadman et al., 2019; Xiao et al., 2016). *Gpr17* also had a high specificity in this subpopulation and a suggested role in OPC differentiation, however it is mostly considered to be an inhibitory player (Chen et al., 2009; Fumagalli et al., 2011; Ou et al., 2016). It might be that *gpr17* is a maturation stop signal in late OPCs and its downregulation is initiated if new myelinating oligodendrocytes need to be generated to allow previously *gpr17*-positive OPCs to differentiate or to initiate myelination. In accordance with this, by introducing brain injury or ischemia this differentiation blockage seems to be overcome and new OLs are formed by Gpr17-positive OPCs (Bonfanti et al., 2017; Vigano et al., 2016). I can only hypothesize, why in the present data the cells which differentiate are particularly the *gpr17*-positive OPCs. I assume that in our model, either because I investigated a different species from mouse or as I looked only at the stage of early development, the inhibitory pathway regulated by *gpr17* is not active, maybe due to the lack of co-signals or through specific inhibition, as differentiation into OLs is extremely important in this period of development. Hence, *gpr17* might be still expressed but cannot exert its typical function, which also involves to regulate cell survival including the expression of pro-apoptotic genes (Ou et al., 2016). This might be also one reason that pre-mature death of OLs before initiating myelination was not observed in this study. Moreover, *prdm8* is suggested to have a high similarity to mammalian *zfp488* (Sidik and Talbot, 2015), a zinc-finger transcription factor regulated by Olig-transcription factors and which has been shown to be required for OPC differentiation (Soundarapandian et al., 2011; Wang et al., 2006). The functional involvement of *draxin* in OL-lineage cell regulation has not been described yet. However, there is a reported role as antagonist of the Wnt pathway (Hutchins and Bronner, 2018), which could be important for the initiation of differentiation. Conversely, myelination-competent OPCs already downregulated classical OPC markers like *olig1* and *cspg4*, and genes involved in neuronal signalling in accordance with the published literature (De Biase et al., 2010; Etxeberria et al., 2010; Kukley et al., 2010; Zhu et al., 2008), indicating that electrical signalling is not directly required for the actual differentiation into OLs. Afterwards, it is likely that the initiation, maintenance or elongation of myelin sheaths again depends on signalling by axonal vesicle release, which can be regulated by neuronal activity but probably not via neurotransmitter receptors (Hines et al., 2015; Mensch et al., 2015; Wake et al., 2015). However, more work is required to elucidate the underlying pathways, how external signals like neurotransmitters, Wnt

ligands etc. are integrated downstream and regulate the known transcription factors in OPCs and OLs during myelination. Although many players are known, how their interplay generates a certain outcome – may it be proliferation, differentiation, or initiation of myelination – needs further investigation.

4.1.6 Pre-Oligodendrocytes

There is a general uncertainty to distinguish late OPCs from **pre-OLs** which also extends to this study. Several characteristic traits could be used to identify them, for example a highly complex morphology, the disappearance/decline of a fluorescent reporter protein typical for OPCs (De Biase et al., 2010; Hughes et al., 2018), or the immunoreactivity with certain antibodies (Sommer and Schachner, 1982). Accordingly, in my work *olig1*-driven fluorescent protein was less abundant in cells shortly before myelin sheath initiation, which could be the pre-OL state in the zebrafish. However, already OPCs of the myelination-competent subtype downregulate the *olig1* gene and appear dimmer during imaging. Also, OL-lineage cells prior to myelination had a quite complex morphology, which however was comparable with the process network of non-myelinating OPCs at the root of the OL-lineage. Even though there are slight differences between these two groups in morphology, for example when considering the position and morphology of the cell soma, this alone is not sufficient to distinguish between pre-OL and OPCs in the zebrafish spinal cord. More recent studies identified specific markers for transitional stages between OPCs and mature OLs like Enpp6 and BCAS1 (Fard et al., 2017; Xiao et al., 2016). None of these markers had a specific expression pattern within the OL-lineage cells in our single-cell RNA-Sequencing data (**Table 8.1.1.1**). This might be due to species-specific differences in gene expression and regulation (see also **section 4.3**). The identification from specifically expressed genes in pre-OLs in zebrafish from our dataset was not possible. In the results part (see **section 3.3.4**), I describe a small group of 4 OPCs which most likely represent pre-OLs as they upregulated genes specific for the myelinating OPCs (subcluster #2c), but did not express cell cycle genes nor myelin genes or genes involved in neuronal activity communication. This group was most likely too small to build a significant subcluster. Sequencing of more cells could resolve this ambiguity and would allow to identify candidate markers for pre-OLs in zebrafish. Nevertheless, as shown by live imaging the transition of cycling OPCs to myelinating OLs happens quite fast in developing zebrafish (**Figure 3.2.3**). As a consequence, the pre-OL stage is highly transient. For the experiments presented in this thesis it was always sufficient to use the formation of myelin sheaths or the appearance of *mbp*-driven fluorescent reporters as a readout for differentiation. In a zebrafish embryo during the first week of development a myelination-competent OPC in the axodendritic region with a simple morphology transformed into a myelinating cell until the next time of observation which was usually 12 h (sometimes 24 h) later. During

the second and third week of development, however lineage-progression velocity seemed to slow down and the transformation from an OPC to a mOL took approximately 2 days, which makes it more likely that an oligodendrocyte at the pre-myelinating stage was imaged in between. Different lineage-progression speeds in early development and later (adulthood) was already described very early within the OL-lineage (Wolswijk and Noble, 1989).

Moreover, the pre-OL stage is not important as a bottleneck for cell survival in developing zebrafish as it has been reported in mouse CNS (Barres et al., 1992a; Hughes et al., 2018; Sun et al., 2018). Interestingly, in the mouse model, pre-OL survival was described to be PDGF-dependent (Barres et al., 1992b). Maybe the deficiency of *pdgfra* in zebrafish OPCs could explain the different situation in zebrafish. Alternatively, signalling could be time-dependent, e.g. signal molecules need to accumulate over time to induce cell death. This would also make sense, since when pre-OLs do not find a target for myelination over longer time they would undergo cell death. As OPCs in the young zebrafish progresses fast, there might be simply not enough time to accumulate these signals.

4.1.7 Non-OL-Lineage Cells Found by Single-Cell RNA-Sequencing

Regarding the absence of the widely used marker *pdgfra* in zebrafish OPCs, the lack of Pdgfra signalling was also shown in a subset of cortical OPCs in the mouse model proofing that Pdgfra-independence of OPCs is also possible in these models (Zheng et al., 2018).

Conversely, the identity of the *pdgfra*-positive cells in our Sequencing dataset (cluster #4 and #5) is not clear. Based on several common upregulated genes (**Table 8.1.1.1**, e.g. *col1a1, pdgfra, pdgfrb* and *tbx18*) our collaborators suggested that these cells could be equivalent to the previously described vascular and leptomeninges cells (VLMCs) in mice. However, there are also differences to VLMCs, for example cells in clusters #4 and #5 lack the expression of *itih2*, *sod3* and *vtn* (Marques et al., 2018; Marques et al., 2016). It remains to elucidate whether this difference is due to species-specific differences between zebrafish and mice or whether these cells are no actual VLMCs. Marques et al. argue that VLMCs and cells of the pericytes lineage (PLCs) are detected in their dataset not due to a general lineage similarity with oligodendrocytes as these cells do not originate from the same stem/progenitor cells (Yamazaki and Mukouyama, 2018), but mainly due to the expression of *pdgfra* which was used by them as the marker for cell selection prior to RNA-sequencing. Since our selection scheme relied on *olig1* which is highly OL-lineage specific (Lu et al., 2000; Zhou et al., 2000), it was rather unlikely to sort VLMCs. Moreover, all

observed EYFP-positive cells in the Tg(olig1:memEYFP) zebrafish spinal cord displayed the morphology and the behaviour of OL-lineage cells. The same likely applies to the zebrafish brain inferred from incidental observation (no images acquired) and work by colleagues in our laboratory (not published yet). Thus, pdgfra-positive cells of cluster #4 and #5 are probably not another CNS cell type with a common history with OL-lineage cells. Outside the OL-lineage *pdgfra* is frequently expressed, for example in pericytes and fibroblasts (Chen et al., 2011; Horikawa et al., 2015; Marques et al., 2018). Hence more likely, the clusters #4 and #5 represent ectopical expression of EYFP in CNS-unrelated cells. This could happen for example if during the generation of the transgenic line, the olig1:EYFP element integrates in a genomic locus where transcription is controlled by another regulatory element which is specifically used in a group of non-OL-lineage cells. In Tg(olig1:memEYFP) zebrafish EYFP fluorescence can be seen also in pectoral fins outside the CNS where no OL-lineage cell would be expected (no images acquired).

4.2 Interconnection Between the Two OPC Subtypes

4.2.1 OPCs Represent a Continuum of Cells

As described before, non-myelinating OPCs preferentially found in the nuclear region of the spinal cord and myelination-competent OPCs rather found in the axodendritic region distinguish remarkably in a row of properties: morphology, process remodelling rate, soma shape, soma localization, gene expression profile, the ability to migrate, proliferation behaviour and the ability to differentiate into oligodendrocytes directly. However, some of the observed OPCs did not fit clearly to one or the other of these groups. Based on *in vivo* live imaging I concluded that these are cells during transitional states between the two OPC subtypes. Especially the displayed range of morphologically complexity that do not divide in two distinct groups but rather represent a continuum between highly complex and simple morphologies exemplifies this (**Figure 3.1.4**). Furthermore, not all steps in the transition from the non-myelinating to the myelination-competent OPC subtype happen at the same time. For example, after a recent division of a non-myelinating OPCs, daughter cells with a simple morphology could be found which still had their soma in the nuclear region as the soma transition to the axonal region has not occurred already and there might even be a process of active process pruning (see **section 4.2.2**) or a second cell division in between.

Based on the overlapping expression profiles of individual genes but also groups of functionally associated genes, the single-cell RNA-sequencing dataset also indicates clearly that the different clusters represent a distribution of cells along lineage progression with intermediate stages between the two distinct subtypes of non-myelinating OPCs in cluster #1 and myelination-competent cells in cluster #2c (**Table 4.2.1.1** and **Figure 3.3.6**). Given that previous cell division is required to generate OPCs that execute myelination (see **section 3.2.6**), the transitional OPCs are linked likely to cells that are still in the cell cycle but do not yet express markers specific for the myelinating OPCs, which are cells in the OPC subclusters #2a and #2b. Whereas OPC #2a cells had a clear signature of gene expression related to the M phase, OPC #2b cells are presumably in the S phase of the cell cycle. However, not all non-myelinating OPCs divide to produce progeny of the myelination-competent subtype but also can do so to maintain a constant OPC number in the tissue by symmetrically generating two non-myelinating OPCs. These proliferating cells would also be included in the OPC subclusters #2a and #2b. A higher number of analysed cells would be required to reveal whether there are even more subclusters within the proliferating OPCs (i.e. cycling non-myelinating OPCs versus OPCs under transition to the myelination-competent subtype) that are maybe masked by the high expression of cell cycle-associated genes. The cells in subclusters #2a and #2b show also the genetic signature of neuronal signalling that characterized non-myelinating OPCs, only sometimes the expression

levels are slightly decreased in comparison (**Table 8.1.1.1**, e.g. *aplnrb*, *gria1a*, *gria2b*). This might indicate that these genes are already slowly downregulated during the progression to myelination-competent OPCs (#2c), that do not express these genes anymore or only at a very low level. I was not able to establish a working marker for subgroups #2a and #2b using RNA ISH, which would have helped to clarify some of the open questions. Especially, whether these cells are rather found in the nuclear or axodendritic region is not clear.

Table 4.2.1.1 Gene expression signatures along OL-lineage progression.

Genetic signature	OPC #1	OPC #2a	OPC #2b	OPC #2c	(Pre-OL)	OL
Neuronal signalling	YES	YES	YES			
Proliferation		YES	YES	YES		
Differentiation				YES	YES	YES
Maturity (myelin)					?	YES

An interesting idea, which however is hypothetical to a large extent, is to consider the transition from non-myelinating OPCs to myelination-competent OPCs as a kind of de-differentiation. Indeed, non-myelinating OPCs have a number of properties which are usually associated with differentiated cells, e.g. a highly ramified process tree, communication with axons, maybe even synapses and a broad distribution throughout the tissue in absence of a clearly identifiable niche that might keep them undifferentiated. Non-myelinating OPCs are more static in their process remodelling and their soma relocated only over short distances. When they generate progeny of the other OPC type, these cells alter their appearance dramatically, i.e. become migratory and acquire a quite simpler morphology. Furthermore, their progression into myelinating OLs via myelination-competent OPCs can be considered an alternative fate as opposed to residing enduringly in the spinal cord and to be involved in neuronal communication. In addition, myelination-competent OPCs upregulated stemness-associated genes like *mycb* and *notch1a* (**Table 8.1.1.1**). In contradiction with this view that myelination-competent OPCs behave more like progenitors than their non-myelinating counterparts, they have a very limited capacity to proliferate and are committed to progress quickly to myelinating OLs at least at the observed developmental stage.

4.2.2 The Role of Proliferation

A longstanding question is how proliferation and differentiation relate to another. Would proliferation rather facilitate or inhibit subsequent differentiation? And are these processes regulated by the same mechanisms or are different regulatory networks in charge? By *in vivo* live imaging I found that the transformation from an OPC which is not myelination-competent to a cell which is able to execute myelination always involves a recent cell division (within 3-4 days prior to differentiation, **Figure 3.2.9B**) and consequently the generation of new cells, whereby this cell division can symmetrical produce two differentiating cells or asymmetrically only one OPC that is myelination-competent whereas the other remains in the non-myelinating state.

In the single-cell RNA-Sequencing dataset also almost every second sequenced OPC expressed proliferation-associated genes including all the differentiating OPCs in subcluster #2c (**Figure 3.3.2**). Consequently, it was expected to find OPCs positive for such proliferation markers frequently by RNA ISH, which however failed (**Figure 3.3.5**). Possibly, there was a general problem with the used probes, however these were ordered commercially, were synthesized by a specialized laboratory, and underwent quality control. Thus, the following explanations are more likely: First, if proliferating OPCs were indeed present in the zebrafish *in vivo* with the high frequency found in the RNA-Sequencing dataset, then these cells were likely not in the spinal cord but must be in the brain. Alternatively, the single-cell preparation procedure prior to RNA-Sequencing changed the ratio of proliferating to non-proliferating OPCs. This can be explained either by induced proliferation in cells which lose contact to neighbouring cells and ECM, or vice versa if OPCs that lose the contact to neighbours and substratum die – a kind of induced cell death known as anoikis – whereas other OPCs in the cell cycle are less sensitive to this mechanism and survive.

The question whether proliferation and differentiation are connected in the OL-lineage was already discussed 35 years ago, and conflicting evidence was reported to date: In OPC cell culture the authors demonstrated that no recent proliferation is required for progenitors to differentiate into myelinating OLs (Temple and Raff, 1985). However, at that time, the characterization of these progenitors was very vague. Alternatively, it has been shown that inhibition of proliferation of OPC cultures on fixed inactive axons also decreases the number of myelinating OLs tremendously, whereas addition of mitogenic PDGF enhances differentiation, although it is not clear if this is due to a linkage of the two processes or due to effect on the pool of OPCs (Rosenberg et al., 2008). Recent live imaging studies in the adult mouse brain revealed that OPCs differentiate directly into NG2-negative pre-OLs and either generate myelin or die (Hughes et

al., 2013; Hughes et al., 2018). The data from adult mouse were obtained in the upper cortical layers, which are structurally quite uniform tissue, consequently all non-myelinating cells within the OL-lineage had a similar morphology. Hence, a regional or morphological distinction of a myelination-competent OPC, which likely would persist over several days or even weeks in an adult animal and that could differentiate directly, is not feasible using this model. Maybe the OPCs that finally underwent differentiation were already primed for differentiation by a previous cell division but actively prevented from differentiating over longer time to maintain a pool of cells that can quickly achieve adaptive myelination, myelin turnover or response to myelin damage when the inhibition is relieved. This might be as special situation in the adult brain as during postnatal development in mouse OPCs differentiate soon after they have undergone proliferation (Hill et al., 2014). In addition, recent findings prove that new OLs generated in response to demyelination underwent proliferation previously indicated by EdU incorporation and that inhibiting cell cycle progression in OPCs also reduce the number of OLs in this scenario (Foerster et al., 2020). Finally, another study in the adult mouse brain could show that ablating particularly proliferating OPCs leads to significant reduction of new oligodendrocytes (Schneider et al., 2016).

What could be the mechanism how a previous proliferation event influences differentiation? Could it be that the fate of daughter OPCs after cell division is intrinsically pre-determined already during or prior to the actual division? For example, there was the observation that after an asymmetric generation of a morphologically complex and a simple cell, the simple one was much more prone to differentiate (**Figure 3.2.7** and **section 4.2.3**). However, it would also be possible that the distribution of the processes as well as the positioning of the daughter cell nuclei after division just happen randomly and that daughter OPCs which acquired certain differentiation-promoting properties by chance than respond to extrinsic signals in the microenvironment to progress along the OL-lineage. A first hint which of these hypotheses better describes the actual situation could be obtained by time-lapse imaging of a significant number of OPC divisions; additional molecular techniques would be required for more definite conclusions.

4.2.3 Morphology Change during Lineage Progression

All previous reports commenting on the morphology of OL-lineage cells during lineage progression review this as a constant expansion of cellular complexity regarding process length and branching of individual cells (De Biase et al., 2010; Hughes et al., 2018). However, my observations presented in this thesis suggest that the *in vivo* situation can be more intricate. The cells with the most complex morphologies among OL-lineage cells in the developing zebrafish spinal cord were found to be non-myelinating OPCs at the root of

the lineage tree. In line with this, process length and branch point number in OPCs were shown to depend on glutamatergic signalling (Fannon et al., 2015; Kula et al., 2019). It would make sense if the actively communicating OPCs, which would be the ones of the non-myelinating subtype, then also would have the most complex morphology. Additionally, I also presented some evidence that there is an increase in morphological complexity in myelinating OPCs or pre-OLs, respectively, the closer they approach the initiation of myelin sheaths (**Figure 3.2.3**), which might be indeed to explore a higher number of potential target sites for myelination.

Prior to this, during the transition from the non-myelinating to the myelination-competent OPC subtype the process complexity is dramatically reduced (**Figure 3.2.7**), which could be partly due to the linkage to a cell division in which the processes are distributed between the daughter cells. But there might be even an active simplification of the process tree (i.e. process pruning), for example if a complex, non-myelinating OPCs symmetrically generate two simple daughter cells of the myelination-competent subtype. In this case the summed process length of the daughter cells could be much smaller than the process length of the mother cell. If the transitional simple morphology of OPCs that are prone to differentiate is a cause for or a consequence of the behaviour and fate of these cells is still an open question. Measuring the complexity of OPCs repeatedly during or directly after cell division could reveal more clearly whether there is active pruning in the OPCs which is going to differentiate or whether the resulting morphology is already determined during the cell division. A simpler morphology could make it easier for a cell to transit the soma to the axodendritic region (**section 4.2.4**) and to remodel the process network previously adapted for neuronal communication to functioning in myelination.

There is still the possibility that the observed change in OPC morphology during lineage progression is only caused by the anatomy of the spinal cord in developing zebrafish. OPCs localized with their soma between axons, namely within the white matter, often have a bipolar morphology with processes aligned in direction of the axons (Dawson et al., 2003), and are less branched as well as generally simpler (Wang et al., 2018b). These cells resembled the myelination-competent cells in the axodendritic region of the zebrafish spinal cord. In grey matter regions like the cerebral cortex all OPCs display the complex, highly branched morphology (Hughes et al., 2013) and are morphologically similar to the complex OPCs preferentially found in the nuclear region of the zebrafish spinal cord, which were however never observed to differentiate directly.

4.2.4 The Role of Soma Position

Usually OPCs also undergo a transition of the cell body from the nuclear to the axodendritic region between proliferation and differentiation, so that the vast majority of myelinating OLs was found in the axodendritic region (**Figure 3.2.5**). However, OPCs that differentiate with their soma in the nuclear region still account for approximately 10 % of myelinating oligodendrocytes. These cells belong to the same OPC subtype that differentiates in the axodendritic region as they share a similar (simple) morphology and were also generated by a recent cell division of typical non-myelinating OPCs. Hence, an axodendritic soma position is not compulsory for differentiation, which is not surprising, because also the 'nuclear' OPCs extend their processes in the axodendritic region and can contact myelination-competent axons (compare **Figure 3.1.3**). This provokes the question why OPCs of the non-myelinating type actually do not differentiate as they also have their processes projected to the same region. Possible explanations would be that the distance between OPC soma and the process tips contacting the myelination-competent axon is important on a very small scale – the shorter the distance the faster the cell initiates myelination – e.g. for the transport of protein and mRNA from the nucleus to prospective myelination sites. Also, direct signalling from the axodendritic microenvironment to the OPC soma could promote differentiation. However, these explanations do not seem to be sufficient since also OPCs with the morphology and behaviour of non-myelinating OPCs have been observed occasionally with their soma in the axodendritic region, and after asymmetric OPC division the daughter cell going to differentiate can often be identified already due to their simpler morphology despite the soma is still in a nuclear position (see **section 4.2.3**). This indicates that soma position is not the main causal factor determining identity and potential of the OPC subtypes, there is even the possibility that it is rather correlative. As OPCs derive from neural progenitors close to the central canal of the spinal cord, non-myelinating OPCs are simply more likely to reside with their soma in the nuclear region. When OPCs become differentiation-competent (after proliferation) and also migratory, it would make sense that they translocate closer to the substrates for myelination, namely axons, to the axodendritic region. Another explanation why some OPCs do differentiate whereas others do not would be an at least partly intrinsic difference between myelination-competent and non-myelinating OPCs which prevent the latter from differentiation even though they are in proximity to myelination-competent axons (see also **section 4.2.2**).

A hypothesis why some OPCs initiate myelination still with the soma in the nuclear region, which however needs to be confirmed based on more data, could be that these cells contact axons at both sides of the spinal cord (i.e. right and left, or dorsal and ventral), then the soma would be just in the middle between the target regions. In this scenario, adhesion between OPC processes and axons could play a role.

4.2.5 The Potential Role of Biomechanical Constraints

One possible way to signal directly to the cell body to change cellular behaviour could be by biomechanical constraints. During the recent years especially the influence of stiffness of the substrate (*in vitro*) or surrounding tissue (*in vivo*) has been investigated. In the CNS, white matter is approximately only half as stiff as grey matter (Christ et al., 2010). Even as the two distinct regions in the spinal cord are not exactly identical with WM and GM, as discussed above, the nuclear region will develop to the spinal cord grey matter in adult fish whereas the axodendritic region will grow and mature to form the white matter. That white and grey matter have different stiffness has also been shown recently in zebrafish (Mollmert et al., 2020). Hence, it can be assumed that the microenvironment in the axodendritic region is less stiff and probably exerts less strength on the cell within.

On the other hand, most axons in the spinal cord white matter have usually a clear anterior-posterior orientation, which makes it unlikely that mechanical forces are exerted in every direction equally. For example, the oval somata of OPCs in the axodendritic region appear to be more squeezed than the more roundish somata of OPCs in the nuclear region. So, are forces on cell somata in the axodendritic region actually higher compared to the nuclear region, at least in one dimension? To figure this out, ways must be found to measure the impact of mechanical cues on individual cells *in vivo*, e.g. optical force sensors (Guo et al., 2014).

Substrate stiffness adjusted by culturing OPCs on polylysin-coated polyacrylamide gels with different elastic moduli influences survival, proliferation, migration, morphology and differentiation (Jagielska et al., 2012). Interestingly, whereas the influence on survival was rather detrimental if cultured on a stiffer substrate, the proliferation, migration velocity and differentiation into myelinating OLs was enhanced. Recently researchers of the same group published a study reporting that a stiffer microenvironment decreases proliferation and differentiation of OPCs *in vivo* and cultured on hydrogels; a situation which is found in the adult and aged CNS compared to the neonate CNS (Segel et al., 2019). This effect can be reversed by inhibitors of actomyosin contractility and knockdown of the mechanosensitive ion channel PIEZO1. That the second study mainly used aged primary OPCs could perhaps be a reason for these differences between two studies. After injury in the mammalian CNS, which usually results in a poor outcome, tissue softening was observed (in contrast to other non-neural tissues), whereas the tissue after spinal cord transection in zebrafish, who is able to regenerate successfully, stiffens transiently (Eberle et al., 2018; Moeendarbary et al., 2017; Mollmert et al., 2020). These results are still difficult to interpret as it is not clear if the measured change in tissue stiffness in response to injury is a cause or consequence of

successful or failed regeneration, respectively. However, it proves quite clearly that tissue stiffness is a regulator of glia cell behaviour in the CNS.

The suggested pathways how mechanical cues can influence cell behaviour involve the actin cytoskeleton, which can either directly activate signalling cascades leading to transcription factor activation (e.g. YAP/TAZ) or can induce chromatin remodelling through its coupling to the nuclear lamina via the LINC complex (Tsai and Casaccia, 2019).

Another interesting question that is dependent on biomechanical processes, which was not addressed so far, but which would help to understand the shuttling of OPCs from the nuclear to the axodendritic region, is whether the cell body actively moves to or is rather pulled into the axodendritic region by the according processes anchored to axons or ECM in this region.

4.2.6 The Indirect Influence of Neuronal Activity on OPC Differentiation via Proliferation

As already introduced, communication via neurotransmitters between neurons and OPCs has been reported to have an influence on many aspects of OPC behaviour and fate including proliferation and differentiation. This topic is briefly discussed as evidence presented in this thesis and additional work from our group (Marisca et al., 2020) suggested that only non-myelinating OPCs are involved in activity signalling with neurons whereas myelination-competent OPCs do not do so, and that neuronal activity promote the proliferation of non-myelinating OPCs and hence differentiation indirectly.

However, to acquire a comprehensive view on this topic is difficult as experimental interventions have been done on different levels (top-down order): The experimenters can alter sensory input (Etxeberria et al., 2016); they can optogenetically, electrically or pharmacologically stimulate axons directly (Gibson et al., 2014; Wake et al., 2011); they can modulate neurotransmitter vesicle release (Mensch et al., 2015); or change neurotransmitter receptor signalling on OPCs by pharmacology or genetics approaches (De Biase et al., 2011; Gallo et al., 1996; Kougioumtzidou et al., 2017). Whether *in vivo* or *in vitro* models were used also had a huge influence on the outcome, for example axons *in vivo* do not just provide electrical signals but also chemical and biomechanical cues and the substratum for myelination. Furthermore, the efficiency or demand of myelination might be much more variable comparing neonatal OPCs versus adult OPCs versus adult OPCs in remyelination. Finally, several outcomes were used to assess the influence of neuronal activity on myelination. Sometimes the change in the number of OLs is reported, sometimes the change in the amount of myelin produced or in internodal length. However, the underlying mechanisms

might be fundamentally different. Myelinating OL number could be influenced by the proliferation and differentiation of OPCs and the maturation rate or survival of pre-myelinating OLs, whereas internodal length is more likely to depend on the direct interaction between axon and myelinating OL process on a local level. It is not clear how independent or interdependent these sub-processes leading to myelination are, respectively. For example, enhanced proliferation could increase OL number and myelination by generating more OPCs available for differentiation. Conversely, ongoing proliferation could also prevent OPCs from leaving the cell cycle and become committed to differentiate.

Based on pharmacological interventions *in vivo*, it was reported that AMPA but not NMDA receptor mediated glutamate signalling on OPCs inhibits proliferation and in some studies also differentiation via potassium channels and extracellular calcium influx (Gallo et al., 1996; Liu and Almazan, 1995). Other studies conclude that OPC differentiation does not depend on dynamic axonal signalling like electrical activity signalling (Rosenberg et al., 2008). Interestingly, a recent study manipulating AMPA receptors genetically *in vivo* found no effect on proliferation of OPCs but only on the survival and maturation of (pre-)OLs (Kougioumtzidou et al., 2017). Which in turn is in contrast to the reported positive effect on proliferation and negative effect on differentiation caused by a genetically triggered increase of $AMPAR^{Ca2+}$ permeability (Chen et al., 2018). It would be interesting to see in future studies if these genetically altered mice also have abnormal behavioural phenotypes, for example learning or memory impairments.

The results obtained by our group are pointing to another conclusion: Enhancing neuronal activity by the voltage-gated potassium channel blocker 4-Aminopyridine (4-AP) increases also the proliferation of OPCs measured by EdU incorporation (Marisca et al., 2020). Particularly OPCs in the nuclear region are affected. There is also a higher number of OLs, but since the effect is smaller than the increase in OPC number, this is interpreted as a secondary effect caused by increased OPC proliferation. By genetically modifying calcium levels in OPCs it was further shown that the effect of 4-AP is mediated by intracellular calcium. As OPCs also might express certain subunits of voltage-gated calcium channels, it is not completely clear whether the effect of 4-AP is only due to its action on neurons. Furthermore, it was not investigated which neurotransmitter system relay activity by neurons to OPCs in the zebrafish spinal cord. It might be that this is glutamate-independent, in this case even less is known about the possible nature of this interaction.

Conclusively, more standardized research on the effect of neuronal activity on the proliferation and differentiation is required to elucidate its role unambiguously (Kula et al., 2019). There might be no uniform role of neuronal activity signalling in OL-lineage cells but rather context specificity depending likely on developmental stage, investigated tissue and signalling crosstalk. A recent report suggested that even

the strength of electrical signals can generate different outcomes regarding proliferation and differentiation of OL-lineage cells (Nagy et al., 2017). Results of *in vitro* studies might represent an oversimplification and more *in vivo* work is required.

4.2.7 Cell State versus Cell Type

An important theoretical question in this context is to discuss whether the observed subgroups of OPCs in the previous studies in general and in the presented work in particular reflect **transient states of OL-lineage cells** during lineage progression or alternative developmental trajectories generating **functionally distinct subtypes**. The term '**subtypes'** is generally used to describe the differences by the OPCs presented here, because the most intriguing difference was their functionally task sharing. Whereas non-myelinating OPCs integrate neuronal activity to regulate OPC cell number and controls the generation of the second subtype – both are achieved through proliferation, the myelination-competent OPCs differentiate readily to OLs, an ability which lacks the first subtype. On the other hand, due to the missing expression of appropriate receptors the myelination-competent OPC subtype neither can integrate neuronal activity by neurotransmitter signalling nor maintain OPC cell numbers by proliferation. Hence, when myelination-competent OPCs are generated through cell division from non-myelinating OPCs in the nuclear region, within the lineage a new cell with totally different properties is formed. According to their functions both subtypes have different fates, one progresses to a myelinating OLs, whereas the other could stay as an OPC for long-term.

A complication with this definition arises from the fact that one subtype gives rise to the other representing at the same time an earlier stage during lineage progression and a functionally distinct entity. It is possible that some non-myelinating OPCs also enter a state during which they are specialized in specific functions, for example communication with neurons, while losing the ability to generate the second subtype, but at the moment I cannot present any experimental evidence for this idea as non-myelinating OPCs in the young zebrafish appear morphologically and genetically homogenous. Hence, the observed OPC dynamics do not reflect a proper bifurcation within the OL-lineage. In this regard, describing the subgroups of OPCs as either subtypes or states has always some degree of ambiguity and depends on the viewpoint.

4.3 Single-Cell RNA-Sequencing Data in Comparison

Most of the research in this field is still carried out using mouse models or primary cell cultures obtained from mammalian tissue. This includes manifold studies reporting new players that regulate proliferation, differentiation and maturation of OL-lineage cells. Interestingly, often these markers are not or differently expressed in zebrafish based on our single-cell sequencing data presented in this work (**Table 8.1.1.1**). For other candidates, the expression pattern does not meet the expectations, e.g. if a gene is described to be specific to differentiating OPCs but is instead expressed in the entire OL-lineage cell population of the zebrafish. Assuming that all the reported findings are valid, these could either account for species-specific or age-specific regulatory networks. There is also the possibility that important players are not transcriptionally regulated but on the translational or posttranslational level. Another interpretation could be that certain genes/proteins are of minor importance for OL-lineage cell behaviour and its reported significance is only of a correlative nature, this could be especially the case when comparing results from different RNA-sequencing studies. There could also be a certain degree of functional redundancy between one gene and others which makes it eventually dispensable.

For example, *olig1* which is still expressed in committed OL progenitors (COPs) and OLs in the mouse, and which plays a role in differentiation (Kuspert and Wegner, 2016), is particularly downregulated in late OPCs prior to differentiation already in the zebrafish. *Pdgfra* which is an important marker for OPCs in mice and humans is not expressed in zebrafish OPCs at all. The same applies to *axin2* which has been shown to regulate Wnt signalling in OPCs during development and during remyelination (Fancy et al., 2011b). The Wnt signalling induced transcription factor *tcf4* that regulates differentiation of OPCs (Kuspert and Wegner, 2016) was expressed in all OPCs and OLs at the same low level in the zebrafish dataset making it less likely that it has a significant influence in zebrafish OL-lineage cells. Conversely, there is no expression of *draxin* and *prdm8*, which is upregulated in myelinating OPCs in zebrafish in mouse OL-lineage cells (Marques et al., 2018). For *prdm8* there is some homology suggested to *zfp488*, which is not found in zebrafish. The murine COP hallmark markers *bmp4* and *neu4* (Marques et al., 2018) are not expressed in OL-lineage cells in zebrafish, whereas the marker for newly formed OLs *prom1* is found most upregulated in non-myelinating OPCs in the zebrafish. *Hes6*, a gene found to be a marker for the newly described subgroup of primitive OPCs (Weng et al., 2019), is found in the zebrafish in the most progressed OPCs to be expressed at the highest level. Also widely used mature OL markers might not be useful in fish, for example, *apc* (CC1) is evenly expressed at an intermediate level in almost all OL-lineage cells in zebrafish.

It would be helpful to use the huge amount of available data for metanalysis. First, comparing molecular data obtained from zebrafish OL-lineage cells in different studies could confirm the species-specific importance of known and newly identified regulators. In addition to the work presented here, also other single-cell RNA-sequencing studies have been published comprising zebrafish OL-lineage cells (Cosacak et al., 2019; Raj et al., 2018). To compare these datasets also with data obtained in other species would further sharpen our understanding of the most important player in OL-lineage cell regulation.

4.4 Outlook

In the present work I mainly performed *in vivo* live imaging and single-cell RNA-Sequencing analysis to elucidate the behaviour and fate of OPCs in the zebrafish spinal cord. An inherent problem of scRNASeq is that results obtained by this method are purely statistical in the first place and require confirmation, a downside which could be overcome here partly but not completely by linking the sequencing data to the imaging data. *In vivo* Imaging and scRNASeq basically identified the same subgroups of OL-lineage cells. Still, genes which are characteristically regulated within these subgroups are likely but not necessarily meaningful for the properties and biological function of the cells within this cluster. Furthermore, despite the huge amount of transcriptomic data that is generated by scRNASeq, it does not consider the regulation on the other levels. Highly expressed mRNAs could be theoretically silenced by RNA interference and a row of other factors would influence the translation to a functional protein. The proteins itself are subjected to post-translational modifications (PTMs) like phosphorylation, glycosylation or SUMOylation to name just a few. These PTMs can influence the function of proteins tremendously and can even lead to complete functional deactivation or degradation. There are recently invented approaches starting to address these problems of scRNASeq based on bioinformatics, RNA splice status, and the combination comprehensive lineage tracing (La Manno et al., 2018; Lederer and La Manno, 2020; Raj et al., 2018), and it will turn out in the near future whether these technique will become widely used.

To particularly address the data in the present work, almost the entire analysis is based on genes that are upregulated in certain clusters compared to others. However, also the downregulation of genes in distinct subclusters could be a meaningful information and possibly there are a few more interesting aspects of OL-lineage cell gene expression in the zebrafish also considering the downregulated genes in particular.

Regarding the imaging part, some tools which would help to further confirm our results and to get even more insight into lineage progression and differentiation of oligodendrocytes are still not available. In the established zebrafish lines OPCs and myelinating OLs can be labelled, however there is no specific transgenic line addressing intermediate states as the myelination-competent OPC subtype, the transitional states between the OPC subtypes as well as pre-OLs. Good candidate genes as drivers of new transgenic lines to establish in the future would be *gpr17* and *myrf*. This would allow to specifically investigate OL-lineage cells in these reporter fish either by genetic analysis of FACS-sorted cells based on these markers or by *in vivo* live imaging. With the current *olig1*-based approach these cells appeared dimmer as they already downregulated *olig1* expression and are rare compared to groups of non-myelinating OPCs and myelinating OLs. New additional transgenic lines would give the chance to advance our understanding of the processes involved in OPC differentiation and maturation even more.

Despite the conclusion that non-myelinating OPCs receive input of neuronal activity whereas myelination-competent OPCs do not use this signalling mechanism, this work does not answer the question why some OPCs differentiate and others do not. It just renders this question more specific: Why do some non-myelinating OPCs proliferate to give rise to myelinating OPCs, whereas others do not and proliferate if at all only to maintain the number of non-myelinating OPCs within the tissue? Probably differential neuronal input to OPCs together with possible other extrinsic signals play a role.

There is no evidence that non-myelinating OPCs in the zebrafish spinal cord are intrinsically different. However, as soon as the myelination-competent OPC subtype emerges, this one seems to follow an intrinsic program as its fate is committed to differentiate to a myelinating oligodendrocyte. However, this observation was done in developing animals and it would be interesting to now, how this is in adult animals. Maybe myelination-competent OPCs are stopped at a certain stage prior to myelination to generate a pool of cells which can produce myelin quickly if required. A situation like this would explain that in the human disease context the proliferation and differentiation of OPCs do not seem to play a major role during remyelination (Yeung et al., 2019).

Some work has been carried out to investigate the role of OPCs in response to injury (Hughes et al., 2013; Kazanis et al., 2017; Vigano et al., 2016). It would be interesting to see, which of the described OPC subtypes are found in which abundance in the vicinity of the lesion sites and how their behaviour would be modulated in the injury context. Furthermore, *in vivo* live imaging studies at the lesion site are quite rare and developing zebrafish could be used to advance our understanding of the processes accompanied with OPCs response to CNS damage.

The paramount goal of research in this field is to understand the regulation and the behaviour how OPCs differentiate into the adequate number of oligodendrocytes and how they make the necessary myelin especially in situations where homeostasis is disturbed like injury or demyelinating diseases. Remarkably in remyelinated lesions in MS patients little new OLs are found, indicating that OL-lineage cell dynamics might be different as in animal models and that human mature myelinating OLs might be even able to generate new myelin (Jakel et al., 2019; Yeung et al., 2014; Yeung et al., 2019).

In this regard, one also has to consider that it has been reported that remyelination is not necessary for certain types of functional recovery, for example for the recovery of locomotion after incomplete spinal cord injury (Duncan et al., 2018a), which is more likely repaired by rerouting neuronal circuits (Bareyre et al., 2004; Loy et al., 2018; Takeoka et al., 2014; van den Brand et al., 2012). However, failed remyelination can lead to disease progression including accumulating neuronal damage (Reich et al., 2018; Simons et al., 2014).

Within the next years we hopefully will find out when and how exactly OPCs and oligodendrocytes are important to encounter CNS damage and how this is regulated on a cellular and molecular level.

5 REFERENCES

Aboul-Enein, F., Rauschka, H., Kornek, B., Stadelmann, C., Stefferl, A., Bruck, W., Lucchinetti, C., Schmidbauer, M., Jellinger, K., and Lassmann, H. (2003). Preferential loss of myelin-associated glycoprotein reflects hypoxia-like white matter damage in stroke and inflammatory brain diseases. J Neuropathol Exp Neurol *62*, 25-33.

Alizadeh, A., and Karimi-Abdolrezaee, S. (2016). Microenvironmental regulation of oligodendrocyte replacement and remyelination in spinal cord injury. The Journal of physiology *594*, 3539-3552.

Almeida, R.G. (2018). The Rules of Attraction in Central Nervous System Myelination. Front Cell Neurosci *12*, 367.

Almeida, R.G., Czopka, T., Ffrench-Constant, C., and Lyons, D.A. (2011). Individual axons regulate the myelinating potential of single oligodendrocytes in vivo. Development *138*, 4443-4450.

An, W.F., Bowlby, M.R., Betty, M., Cao, J., Ling, H.P., Mendoza, G., Hinson, J.W., Mattsson, K.I., Strassle, B.W., Trimmer, J.S*., et al.* (2000). Modulation of A-type potassium channels by a family of calcium sensors. Nature *403*, 553-556.

Ashrafi, M.R., and Tavasoli, A.R. (2017). Childhood leukodystrophies: A literature review of updates on new definitions, classification, diagnostic approach and management. Brain & development *39*, 369-385.

Assinck, P., Duncan, G.J., Plemel, J.R., Lee, M.J., Stratton, J.A., Manesh, S.B., Liu, J., Ramer, L.M., Kang, S.H., Bergles, D.E*., et al.* (2017). Myelinogenic Plasticity of Oligodendrocyte Precursor Cells following Spinal Cord Contusion Injury. J Neurosci *37*, 8635-8654.

Auer, F., Vagionitis, S., and Czopka, T. (2018). Evidence for Myelin Sheath Remodeling in the CNS Revealed by In Vivo Imaging. Curr Biol *28*, 549-559 e543.

Bacmeister, C.M., Barr, H.J., McClain, C.R., Thornton, M.A., Nettles, D., Welle, C.G., and Hughes, E.G. (2020). Motor learning promotes remyelination via new and surviving oligodendrocytes. Nat Neurosci.

Bareyre, F.M., Kerschensteiner, M., Raineteau, O., Mettenleiter, T.C., Weinmann, O., and Schwab, M.E. (2004). The injured spinal cord spontaneously forms a new intraspinal circuit in adult rats. Nat Neurosci *7*, 269-277.

Barres, B.A., Hart, I.K., Coles, H.S., Burne, J.F., Voyvodic, J.T., Richardson, W.D., and Raff, M.C. (1992a). Cell death and control of cell survival in the oligodendrocyte lineage. Cell *70*, 31-46.

Barres, B.A., Hart, I.K., Coles, H.S., Burne, J.F., Voyvodic, J.T., Richardson, W.D., and Raff, M.C. (1992b). Cell death in the oligodendrocyte lineage. J Neurobiol *23*, 1221-1230.

Barres, B.A., Koroshetz, W.J., Swartz, K.J., Chun, L.L., and Corey, D.P. (1990). Ion channel expression by white matter glia: the O-2A glial progenitor cell. Neuron *4*, 507-524.

Barres, B.A., and Raff, M.C. (1993). Proliferation of oligodendrocyte precursor cells depends on electrical activity in axons. Nature *361*, 258-260.

Bechler, M.E., Byrne, L., and Ffrench-Constant, C. (2015). CNS Myelin Sheath Lengths Are an Intrinsic Property of Oligodendrocytes. Curr Biol *25*, 2411-2416.

Behrendt, G., Baer, K., Buffo, A., Curtis, M.A., Faull, R.L., Rees, M.I., Gotz, M., and Dimou, L. (2013). Dynamic changes in myelin aberrations and oligodendrocyte generation in chronic amyloidosis in mice and men. Glia *61*, 273-286.

Berger, T., Walz, W., Schnitzer, J., and Kettenmann, H. (1992). GABA- and glutamate-activated currents in glial cells of the mouse corpus callosum slice. J Neurosci Res *31*, 21-27.

Bergles, D.E., Jabs, R., and Steinhauser, C. (2010). Neuron-glia synapses in the brain. Brain research reviews *63*, 130-137.

Bergles, D.E., and Richardson, W.D. (2015). Oligodendrocyte Development and Plasticity. Cold Spring Harb Perspect Biol *8*, a020453.

Bergles, D.E., Roberts, J.D., Somogyi, P., and Jahr, C.E. (2000). Glutamatergic synapses on oligodendrocyte precursor cells in the hippocampus. Nature *405*, 187-191.

Bindea, G., Mlecnik, B., Hackl, H., Charoentong, P., Tosolini, M., Kirilovsky, A., Fridman, W.H., Pages, F., Trajanoski, Z., and Galon, J. (2009). ClueGO: a Cytoscape plug-in to decipher functionally grouped gene ontology and pathway annotation networks. Bioinformatics *25*, 1091-1093.

Bonfanti, E., Gelosa, P., Fumagalli, M., Dimou, L., Vigano, F., Tremoli, E., Cimino, M., Sironi, L., and Abbracchio, M.P. (2017). The role of oligodendrocyte precursor cells expressing the GPR17 receptor in brain remodeling after stroke. Cell Death Dis *8*, e2871.

Bunge, R.P. (1968). Glial cells and the central myelin sheath. Physiological reviews *48*, 197-251.

Buschdorf, J.P., Li Chew, L., Zhang, B., Cao, Q., Liang, F.Y., Liou, Y.C., Zhou, Y.T., and Low, B.C. (2006). Brain-specific BNIP-2-homology protein Caytaxin relocalises glutaminase to neurite terminals and reduces glutamate levels. Journal of cell science *119*, 3337-3350.

Butler, A., Hoffman, P., Smibert, P., Papalexi, E., and Satija, R. (2018). Integrating single-cell transcriptomic data across different conditions, technologies, and species. Nat Biotechnol *36*, 411-420.

Butt, A.M., De La Rocha, I.C., and Rivera, A. (2019). Oligodendroglial Cells in Alzheimer's Disease. Adv Exp Med Biol *1175*, 325-333.

Cantone, M., Kuspert, M., Reiprich, S., Lai, X., Eberhardt, M., Gottle, P., Beyer, F., Azim, K., Kury, P., Wegner, M.*, et al.* (2019). A gene regulatory architecture that controls region-independent dynamics of oligodendrocyte differentiation. Glia *67*, 825-843.

Chang, K.J., Redmond, S.A., and Chan, J.R. (2016). Remodeling myelination: implications for mechanisms of neural plasticity. Nat Neurosci *19*, 190-197.

Chen, T.J., Kula, B., Nagy, B., Barzan, R., Gall, A., Ehrlich, I., and Kukley, M. (2018). In Vivo Regulation of Oligodendrocyte Precursor Cell Proliferation and Differentiation by the AMPA-Receptor Subunit GluA2. Cell Rep *25*, 852-861 e857.

Chen, X., Ku, L., Mei, R., Liu, G., Xu, C., Wen, Z., Zhao, X., Wang, F., Xiao, L., and Feng, Y. (2017). Novel schizophrenia risk factor pathways regulate FEZ1 to advance oligodendroglia development. Translational psychiatry *7*, 1293.

Chen, Y., Wu, H., Wang, S., Koito, H., Li, J., Ye, F., Hoang, J., Escobar, S.S., Gow, A., Arnett, H.A.*, et al.* (2009). The oligodendrocyte-specific G protein-coupled receptor GPR17 is a cell-intrinsic timer of myelination. Nat Neurosci *12*, 1398-1406.

Chen, Y.T., Chang, F.C., Wu, C.F., Chou, Y.H., Hsu, H.L., Chiang, W.C., Shen, J., Chen, Y.M., Wu, K.D., Tsai, T.J.*, et al.* (2011). Platelet-derived growth factor receptor signaling activates pericyte-myofibroblast transition in obstructive and post-ischemic kidney fibrosis. Kidney international *80*, 1170-1181.

Chittajallu, R., Aguirre, A., and Gallo, V. (2004). NG2-positive cells in the mouse white and grey matter display distinct physiological properties. The Journal of physiology *561*, 109-122.

Christ, A.F., Franze, K., Gautier, H., Moshayedi, P., Fawcett, J., Franklin, R.J., Karadottir, R.T., and Guck, J. (2010). Mechanical difference between white and gray matter in the rat cerebellum measured by scanning force microscopy. Journal of biomechanics *43*, 2986-2992.

Clarke, L.E., Young, K.M., Hamilton, N.B., Li, H., Richardson, W.D., and Attwell, D. (2012). Properties and fate of oligodendrocyte progenitor cells in the corpus callosum, motor cortex, and piriform cortex of the mouse. J Neurosci *32*, 8173-8185.

Cosacak, M.I., Bhattarai, P., Reinhardt, S., Petzold, A., Dahl, A., Zhang, Y., and Kizil, C. (2019). Single-Cell Transcriptomics Analyses of Neural Stem Cell Heterogeneity and Contextual Plasticity in a Zebrafish Brain Model of Amyloid Toxicity. Cell Rep *27*, 1307-1318 e1303.

Czopka, T. (2015). Insights into mechanisms of central nervous system myelination using zebrafish. Glia.

Czopka, T., Ffrench-Constant, C., and Lyons, D.A. (2013). Individual oligodendrocytes have only a few hours in which to generate new myelin sheaths in vivo. Dev Cell *25*, 599-609.

Czopka, T., and Lyons, D.A. (2011). Dissecting mechanisms of myelinated axon formation using zebrafish. Methods Cell Biol *105*, 25-62.

Dawson, M.R., Levine, J.M., and Reynolds, R. (2000). NG2-expressing cells in the central nervous system: are they oligodendroglial progenitors? J Neurosci Res *61*, 471-479.

Dawson, M.R., Polito, A., Levine, J.M., and Reynolds, R. (2003). NG2-expressing glial progenitor cells: an abundant and widespread population of cycling cells in the adult rat CNS. Molecular and cellular neurosciences *24*, 476-488.

De Biase, L.M., Kang, S.H., Baxi, E.G., Fukaya, M., Pucak, M.L., Mishina, M., Calabresi, P.A., and Bergles, D.E. (2011). NMDA receptor signaling in oligodendrocyte progenitors is not required for oligodendrogenesis and myelination. J Neurosci *31*, 12650-12662.

De Biase, L.M., Nishiyama, A., and Bergles, D.E. (2010). Excitability and synaptic communication within the oligodendrocyte lineage. J Neurosci *30*, 3600-3611.

de Faria, O., Jr., Pama, E.A.C., Evans, K., Luzhynskaya, A., and Karadottir, R.T. (2018). Neuroglial interactions underpinning myelin plasticity. Developmental neurobiology *78*, 93-107.

Demerens, C., Stankoff, B., Logak, M., Anglade, P., Allinquant, B., Couraud, F., Zalc, B., and Lubetzki, C. (1996). Induction of myelination in the central nervous system by electrical activity. Proc Natl Acad Sci U S A *93*, 9887-9892.

Deshmukh, V.A., Tardif, V., Lyssiotis, C.A., Green, C.C., Kerman, B., Kim, H.J., Padmanabhan, K., Swoboda, J.G., Ahmad, I., Kondo, T.*, et al.* (2013). A regenerative approach to the treatment of multiple sclerosis. Nature *502*, 327-332.

Dimou, L., Simon, C., Kirchhoff, F., Takebayashi, H., and Gotz, M. (2008). Progeny of Olig2-expressing progenitors in the gray and white matter of the adult mouse cerebral cortex. J Neurosci *28*, 10434-10442.

Dimou, L., and Simons, M. (2017). Diversity of oligodendrocytes and their progenitors. Current Opinion in Neurobiology *47*, 73-79.

Distel, M., Wullimann, M.F., and Koster, R.W. (2009). Optimized Gal4 genetics for permanent gene expression mapping in zebrafish. Proc Natl Acad Sci U S A *106*, 13365-13370.

Doetsch, F. (2003). A niche for adult neural stem cells. Curr Opin Genet Dev *13*, 543-550.

Duncan, G.J., Manesh, S.B., Hilton, B.J., Assinck, P., Liu, J., Moulson, A., Plemel, J.R., and Tetzlaff, W. (2018a). Locomotor recovery following contusive spinal cord injury does not require oligodendrocyte remyelination. Nat Commun *9*, 3066.

Duncan, I.D., Radcliff, A.B., Heidari, M., Kidd, G., August, B.K., and Wierenga, L.A. (2018b). The adult oligodendrocyte can participate in remyelination. Proc Natl Acad Sci U S A *115*, E11807-E11816.

Early, J.J., Cole, K.L., Williamson, J.M., Swire, M., Kamadurai, H., Muskavitch, M., and Lyons, D.A. (2018). An automated high-resolution in vivo screen in zebrafish to identify chemical regulators of myelination. eLife *7*.

Eberle, D., Fodelianaki, G., Kurth, T., Jagielska, A., Möllmert, S., Ulbricht, E., Wagner, K., Taubenberger, A.V., Träber, N., Escolano, J.-C*., et al.* (2018). Acute but not inherited demyelination in mouse models leads to brain tissue stiffness changes.

Emery, B., Agalliu, D., Cahoy, J.D., Watkins, T.A., Dugas, J.C., Mulinyawe, S.B., Ibrahim, A., Ligon, K.L., Rowitch, D.H., and Barres, B.A. (2009). Myelin gene regulatory factor is a critical transcriptional regulator required for CNS myelination. Cell *138*, 172-185.

Emery, B., and Lu, Q.R. (2015). Transcriptional and Epigenetic Regulation of Oligodendrocyte Development and Myelination in the Central Nervous System. Cold Spring Harb Perspect Biol *7*, a020461.

Etxeberria, A., Hokanson, K.C., Dao, D.Q., Mayoral, S.R., Mei, F., Redmond, S.A., Ullian, E.M., and Chan, J.R. (2016). Dynamic Modulation of Myelination in Response to Visual Stimuli Alters Optic Nerve Conduction Velocity. J Neurosci *36*, 6937-6948.

Etxeberria, A., Mangin, J.M., Aguirre, A., and Gallo, V. (2010). Adult-born SVZ progenitors receive transient synapses during remyelination in corpus callosum. Nat Neurosci *13*, 287-289.

Falcao, A.M., van Bruggen, D., Marques, S., Meijer, M., Jakel, S., Agirre, E., Samudyata, Floriddia, E.M., Vanichkina, D.P., Ffrench-Constant, C*., et al.* (2018). Disease-specific oligodendrocyte lineage cells arise in multiple sclerosis. Nature medicine.

Fancy, S.P., Baranzini, S.E., Zhao, C., Yuk, D.I., Irvine, K.A., Kaing, S., Sanai, N., Franklin, R.J., and Rowitch, D.H. (2009). Dysregulation of the Wnt pathway inhibits timely myelination and remyelination in the mammalian CNS. Genes Dev *23*, 1571-1585.

Fancy, S.P., Chan, J.R., Baranzini, S.E., Franklin, R.J., and Rowitch, D.H. (2011a). Myelin regeneration: a recapitulation of development? Annu Rev Neurosci *34*, 21-43.

Fancy, S.P., Harrington, E.P., Yuen, T.J., Silbereis, J.C., Zhao, C., Baranzini, S.E., Bruce, C.C., Otero, J.J., Huang, E.J., Nusse, R*., et al.* (2011b). Axin2 as regulatory and therapeutic target in newborn brain injury and remyelination. Nat Neurosci *14*, 1009-1016.

Fannon, J., Tarmier, W., and Fulton, D. (2015). Neuronal activity and AMPA-type glutamate receptor activation regulates the morphological development of oligodendrocyte precursor cells. Glia *63*, 1021-1035.

Fard, M.K., van der Meer, F., Sanchez, P., Cantuti-Castelvetri, L., Mandad, S., Jakel, S., Fornasiero, E.F., Schmitt, S., Ehrlich, M., Starost, L*., et al.* (2017). BCAS1 expression defines a population of early myelinating oligodendrocytes in multiple sclerosis lesions. Science translational medicine *9*.

Farmer, W.T., and Murai, K. (2017). Resolving Astrocyte Heterogeneity in the CNS. Front Cell Neurosci *11*, 300.

Fields, R.D. (2015). A new mechanism of nervous system plasticity: activity-dependent myelination. Nat Rev Neurosci *16*, 756-767.

Foerster, S., Hill, M.F.E., and Franklin, R.J.M. (2019). Diversity in the oligodendrocyte lineage: Plasticity or heterogeneity? Glia.

Foerster, S., Neumann, B., McClain, C., Di Canio, L., Chen, C.Z., Reich, D.S., Simons, B.D., and Franklin, R.J.M. (2020). Proliferation is a requirement for differentiation of oligodendrocyte progenitor cells during CNS remyelination. bioRxiv.

Franklin, R.J. (2002). Why does remyelination fail in multiple sclerosis? Nat Rev Neurosci *3*, 705-714.

Franklin, R.J., and Ffrench-Constant, C. (2008). Remyelination in the CNS: from biology to therapy. Nat Rev Neurosci *9*, 839-855.

Fumagalli, M., Daniele, S., Lecca, D., Lee, P.R., Parravicini, C., Fields, R.D., Rosa, P., Antonucci, F., Verderio, C., Trincavelli, M.L.*, et al.* (2011). Phenotypic changes, signaling pathway, and functional correlates of GPR17-expressing neural precursor cells during oligodendrocyte differentiation. J Biol Chem *286*, 10593-10604.

Funfschilling, U., Supplie, L.M., Mahad, D., Boretius, S., Saab, A.S., Edgar, J., Brinkmann, B.G., Kassmann, C.M., Tzvetanova, I.D., Mobius, W.*, et al.* (2012). Glycolytic oligodendrocytes maintain myelin and long-term axonal integrity. Nature *485*, 517-521.

Gallo, V., Zhou, J.M., McBain, C.J., Wright, P., Knutson, P.L., and Armstrong, R.C. (1996). Oligodendrocyte progenitor cell proliferation and lineage progression are regulated by glutamate receptor-mediated K+ channel block. J Neurosci *16*, 2659-2670.

Ge, W.P., Yang, X.J., Zhang, Z., Wang, H.K., Shen, W., Deng, Q.D., and Duan, S. (2006). Long-term potentiation of neuron-glia synapses mediated by Ca2+-permeable AMPA receptors. Science *312*, 1533-1537.

Ge, W.P., Zhou, W., Luo, Q., Jan, L.Y., and Jan, Y.N. (2009). Dividing glial cells maintain differentiated properties including complex morphology and functional synapses. Proc Natl Acad Sci U S A *106*, 328-333.

Geha, S., Pallud, J., Junier, M.P., Devaux, B., Leonard, N., Chassoux, F., Chneiweiss, H., Daumas-Duport, C., and Varlet, P. (2010). NG2+/Olig2+ cells are the major cycle-related cell population of the adult human normal brain. Brain pathology *20*, 399-411.

Gibson, E.M., Purger, D., Mount, C.W., Goldstein, A.K., Lin, G.L., Wood, L.S., Inema, I., Miller, S.E., Bieri, G., Zuchero, J.B.*, et al.* (2014). Neuronal activity promotes oligodendrogenesis and adaptive myelination in the mammalian brain. Science *344*, 1252304.

Goldberg, J.L., Vargas, M.E., Wang, J.T., Mandemakers, W., Oster, S.F., Sretavan, D.W., and Barres, B.A. (2004). An oligodendrocyte lineage-specific semaphorin, Sema5A, inhibits axon growth by retinal ganglion cells. J Neurosci *24*, 4989-4999.

Grinspan, J.B., Reddy, U.R., Stern, J.L., Hardy, M., Williams, M., Baird, L., and Pleasure, D. (1990a). Oligodendroglia express PDGF beta-receptor protein and are stimulated to proliferate by PDGF. Ann N Y Acad Sci *605*, 71-80.

Grinspan, J.B., Stern, J.L., Pustilnik, S.M., and Pleasure, D. (1990b). Cerebral white matter contains PDGF-responsive precursors to O2A cells. J Neurosci *10*, 1866-1873.

Guo, F., Maeda, Y., Ko, E.M., Delgado, M., Horiuchi, M., Soulika, A., Miers, L., Burns, T., Itoh, T., Shen, H.*, et al.* (2012). Disruption of NMDA receptors in oligodendroglial lineage cells does not alter their

susceptibility to experimental autoimmune encephalomyelitis or their normal development. J Neurosci *32*, 639-645.

Guo, F., Maeda, Y., Ma, J., Xu, J., Horiuchi, M., Miers, L., Vaccarino, F., and Pleasure, D. (2010). Pyramidal neurons are generated from oligodendroglial progenitor cells in adult piriform cortex. J Neurosci *30*, 12036-12049.

Guo, J., Sachs, F., and Meng, F. (2014). Fluorescence-based force/tension sensors: a novel tool to visualize mechanical forces in structural proteins in live cells. Antioxid Redox Signal *20*, 986-999.

Haegebarth, A., and Clevers, H. (2009). Wnt signaling, lgr5, and stem cells in the intestine and skin. Am J Pathol *174*, 715-721.

Hamilton, N.B., Clarke, L.E., Arancibia-Carcamo, I.L., Kougioumtzidou, E., Matthey, M., Karadottir, R., Whiteley, L., Bergersen, L.H., Richardson, W.D., and Attwell, D. (2017). Endogenous GABA controls oligodendrocyte lineage cell number, myelination, and CNS internode length. Glia *65*, 309-321.

Hart, I.K., Richardson, W.D., Bolsover, S.R., and Raff, M.C. (1989a). PDGF and intracellular signaling in the timing of oligodendrocyte differentiation. The Journal of cell biology *109*, 3411-3417.

Hart, I.K., Richardson, W.D., Heldin, C.H., Westermark, B., and Raff, M.C. (1989b). PDGF receptors on cells of the oligodendrocyte-type-2 astrocyte (O-2A) cell lineage. Development *105*, 595-603.

Hayashi, M.K. (2018). Structure-Function Relationship of Transporters in the Glutamate-Glutamine Cycle of the Central Nervous System. Int J Mol Sci *19*.

Heinrich, C., Bergami, M., Gascon, S., Lepier, A., Vigano, F., Dimou, L., Sutor, B., Berninger, B., and Gotz, M. (2014). Sox2-mediated conversion of NG2 glia into induced neurons in the injured adult cerebral cortex. Stem cell reports *3*, 1000-1014.

Hildebrand, C., Remahl, S., Persson, H., and Bjartmar, C. (1993). Myelinated nerve fibres in the CNS. Progress in neurobiology *40*, 319-384.

Hill, R.A., Li, A.M., and Grutzendler, J. (2018). Lifelong cortical myelin plasticity and age-related degeneration in the live mammalian brain. Nat Neurosci *21*, 683-695.

Hill, R.A., and Nishiyama, A. (2014). NG2 cells (polydendrocytes): listeners to the neural network with diverse properties. Glia *62*, 1195-1210.

Hill, R.A., Patel, K.D., Goncalves, C.M., Grutzendler, J., and Nishiyama, A. (2014). Modulation of oligodendrocyte generation during a critical temporal window after NG2 cell division. Nat Neurosci *17*, 1518-1527.

Hill, R.A., Patel, K.D., Medved, J., Reiss, A.M., and Nishiyama, A. (2013). NG2 cells in white matter but not gray matter proliferate in response to PDGF. J Neurosci *33*, 14558-14566.

Hines, J.H., Ravanelli, A.M., Schwindt, R., Scott, E.K., and Appel, B. (2015). Neuronal activity biases axon selection for myelination in vivo. Nat Neurosci *18*, 683-689.

Hoche, T., Marisca, R., Agirre, E., Hoodless, L.J., Barkey, W., Auer, F., Castelo-Branco, G., and Czopka, T. (2019). Functionally Distinct Subgroups of Oligodendrocyte Precursor Cells Integrate Neural Activity and Execute Myelin Formation. BioRxiv.

Horikawa, S., Ishii, Y., Hamashima, T., Yamamoto, S., Mori, H., Fujimori, T., Shen, J., Inoue, R., Nishizono, H., Itoh, H*., et al.* (2015). PDGFRalpha plays a crucial role in connective tissue remodeling. Scientific reports *5*, 17948.

Hotta, K., Hosaka, M., Tanabe, A., and Takeuchi, T. (2009). Secretogranin II binds to secretogranin III and forms secretory granules with orexin, neuropeptide Y, and POMC. J Endocrinol *202*, 111-121.

Huang, J.K., Jarjour, A.A., Nait Oumesmar, B., Kerninon, C., Williams, A., Krezel, W., Kagechika, H., Bauer, J., Zhao, C., Baron-Van Evercooren, A.*, et al.* (2011). Retinoid X receptor gamma signaling accelerates CNS remyelination. Nat Neurosci *14*, 45-53.

Hughes, E.G., Kang, S.H., Fukaya, M., and Bergles, D.E. (2013). Oligodendrocyte progenitors balance growth with self-repulsion to achieve homeostasis in the adult brain. Nat Neurosci *16*, 668-676.

Hughes, E.G., Orthmann-Murphy, J.L., Langseth, A.J., and Bergles, D.E. (2018). Myelin remodeling through experience-dependent oligodendrogenesis in the adult somatosensory cortex. Nat Neurosci *21*, 696-706.

Hutchins, E.J., and Bronner, M.E. (2018). Draxin acts as a molecular rheostat of canonical Wnt signaling to control cranial neural crest EMT. The Journal of cell biology *217*, 3683-3697.

Ibrahim, M., Butt, A.M., and Berry, M. (1995). Relationship between myelin sheath diameter and internodal length in axons of the anterior medullary velum of the adult rat. Journal of the neurological sciences *133*, 119-127.

Jabs, R., Pivneva, T., Huttmann, K., Wyczynski, A., Nolte, C., Kettenmann, H., and Steinhauser, C. (2005). Synaptic transmission onto hippocampal glial cells with hGFAP promoter activity. Journal of cell science *118*, 3791-3803.

Jagielska, A., Norman, A.L., Whyte, G., Vliet, K.J., Guck, J., and Franklin, R.J. (2012). Mechanical environment modulates biological properties of oligodendrocyte progenitor cells. Stem Cells Dev *21*, 2905-2914.

Jakel, S., Agirre, E., Falcao, A.M., van Bruggen, D., Lee, K.W., Knuesel, I., Malhotra, D., Ffrench-Constant, C., Williams, A., and Castelo-Branco, G. (2019). Altered human oligodendrocyte heterogeneity in multiple sclerosis. Nature.

Kang, S.H., Fukaya, M., Yang, J.K., Rothstein, J.D., and Bergles, D.E. (2010). NG2+ CNS glial progenitors remain committed to the oligodendrocyte lineage in postnatal life and following neurodegeneration. Neuron *68*, 668-681.

Karadottir, R., Cavelier, P., Bergersen, L.H., and Attwell, D. (2005). NMDA receptors are expressed in oligodendrocytes and activated in ischaemia. Nature *438*, 1162-1166.

Karadottir, R., Hamilton, N.B., Bakiri, Y., and Attwell, D. (2008). Spiking and nonspiking classes of oligodendrocyte precursor glia in CNS white matter. Nat Neurosci *11*, 450-456.

Karttunen, M.J., Czopka, T., Goedhart, M., Early, J.J., and Lyons, D.A. (2017). Regeneration of myelin sheaths of normal length and thickness in the zebrafish CNS correlates with growth of axons in caliber. PLoS One *12*, e0178058.

Kato, D., Wake, H., Lee, P.R., Tachibana, Y., Ono, R., Sugio, S., Tsuji, Y., Tanaka, Y.H., Tanaka, Y.R., Masamizu, Y.*, et al.* (2020). Motor learning requires myelination to reduce asynchrony and spontaneity in neural activity. Glia *68*, 193-210.

Kazanis, I., Evans, K.A., Andreopoulou, E., Dimitriou, C., Koutsakis, C., Karadottir, R.T., and Franklin, R.J. (2017). Subependymal Zone-Derived Oligodendroblasts Respond to Focal Demyelination but Fail to Generate Myelin in Young and Aged Mice. Stem cell reports.

Keirstead, H.S., Levine, J.M., and Blakemore, W.F. (1998). Response of the oligodendrocyte progenitor cell population (defined by NG2 labelling) to demyelination of the adult spinal cord. Glia *22*, 161-170.

Keirstead, H.S., Nistor, G., Bernal, G., Totoiu, M., Cloutier, F., Sharp, K., and Steward, O. (2005). Human embryonic stem cell-derived oligodendrocyte progenitor cell transplants remyelinate and restore locomotion after spinal cord injury. J Neurosci *25*, 4694-4705.

Kessaris, N., Fogarty, M., Iannarelli, P., Grist, M., Wegner, M., and Richardson, W.D. (2006). Competing waves of oligodendrocytes in the forebrain and postnatal elimination of an embryonic lineage. Nat Neurosci *9*, 173-179.

Kevelam, S.H., Steenweg, M.E., Srivastava, S., Helman, G., Naidu, S., Schiffmann, R., Blaser, S., Vanderver, A., Wolf, N.I., and van der Knaap, M.S. (2016). Update on Leukodystrophies: A Historical Perspective and Adapted Definition. Neuropediatrics *47*, 349-354.

Kirby, B.B., Takada, N., Latimer, A.J., Shin, J., Carney, T.J., Kelsh, R.N., and Appel, B. (2006). In vivo time-lapse imaging shows dynamic oligodendrocyte progenitor behavior during zebrafish development. Nat Neurosci *9*, 1506-1511.

Kool, M.J., Proietti Onori, M., Borgesius, N.Z., van de Bree, J.E., Elgersma-Hooisma, M., Nio, E., Bezstarosti, K., Buitendijk, G.H.S., Aghadavoud Jolfaei, M., Demmers, J.A.A.*, et al.* (2019). CAMK2-Dependent Signaling in Neurons Is Essential for Survival. J Neurosci *39*, 5424-5439.

Kougioumtzidou, E., Shimizu, T., Hamilton, N.B., Tohyama, K., Sprengel, R., Monyer, H., Attwell, D., and Richardson, W.D. (2017). Signalling through AMPA receptors on oligodendrocyte precursors promotes myelination by enhancing oligodendrocyte survival. eLife *6*.

Kriegstein, A., and Alvarez-Buylla, A. (2009). The glial nature of embryonic and adult neural stem cells. Annu Rev Neurosci *32*, 149-184.

Kukley, M., Capetillo-Zarate, E., and Dietrich, D. (2007). Vesicular glutamate release from axons in white matter. Nat Neurosci *10*, 311-320.

Kukley, M., Kiladze, M., Tognatta, R., Hans, M., Swandulla, D., Schramm, J., and Dietrich, D. (2008). Glial cells are born with synapses. FASEB J *22*, 2957-2969.

Kukley, M., Nishiyama, A., and Dietrich, D. (2010). The fate of synaptic input to NG2 glial cells: neurons specifically downregulate transmitter release onto differentiating oligodendroglial cells. J Neurosci *30*, 8320-8331.

Kula, B., Chen, T.J., and Kukley, M. (2019). Glutamatergic signaling between neurons and oligodendrocyte lineage cells: Is it synaptic or non-synaptic? Glia.

Kuspert, M., and Wegner, M. (2016). SomethiNG 2 talk about-Transcriptional regulation in embryonic and adult oligodendrocyte precursors. Brain research *1638*, 167-182.

Kwan, K.M., Fujimoto, E., Grabher, C., Mangum, B.D., Hardy, M.E., Campbell, D.S., Parant, J.M., Yost, H.J., Kanki, J.P., and Chien, C.B. (2007). The Tol2kit: a multisite gateway-based construction kit for Tol2 transposon transgenesis constructs. Dev Dyn *236*, 3088-3099.

La Manno, G., Soldatov, R., Zeisel, A., Braun, E., Hochgerner, H., Petukhov, V., Lidschreiber, K., Kastriti, M.E., Lonnerberg, P., Furlan, A.*, et al.* (2018). RNA velocity of single cells. Nature *560*, 494-498.

Lang, J., Maeda, Y., Bannerman, P., Xu, J., Horiuchi, M., Pleasure, D., and Guo, F. (2013). Adenomatous polyposis coli regulates oligodendroglial development. J Neurosci *33*, 3113-3130.

Lederer, A.R., and La Manno, G. (2020). The emergence and promise of single-cell temporal-omics approaches. Current Opinion in Biotechnology *63*, 70-78.

Lee, J., Gravel, M., Zhang, R.L., Thibault, P., and Braun, P.E. (2005). Process outgrowth in oligodendrocytes is mediated by CNP, a novel microtubule assembly myelin protein. Journal of Cell Biology *170*, 661-673.

Lee, Y., Morrison, B.M., Li, Y., Lengacher, S., Farah, M.H., Hoffman, P.N., Liu, Y., Tsingalia, A., Jin, L., Zhang, P.W.*, et al.* (2012). Oligodendroglia metabolically support axons and contribute to neurodegeneration. Nature *487*, 443-448.

Levine, J.M. (1994). Increased expression of the NG2 chondroitin-sulfate proteoglycan after brain injury. J Neurosci *14*, 4716-4730.

Levine, J.M., and Stallcup, W.B. (1987). Plasticity of developing cerebellar cells in vitro studied with antibodies against the NG2 antigen. J Neurosci *7*, 2721-2731.

Li, Q., Brus-Ramer, M., Martin, J.H., and McDonald, J.W. (2010). Electrical stimulation of the medullary pyramid promotes proliferation and differentiation of oligodendrocyte progenitor cells in the corticospinal tract of the adult rat. Neuroscience letters *479*, 128-133.

Lin, S.C., and Bergles, D.E. (2004a). Synaptic signaling between GABAergic interneurons and oligodendrocyte precursor cells in the hippocampus. Nat Neurosci *7*, 24-32.

Lin, S.C., and Bergles, D.E. (2004b). Synaptic signaling between neurons and glia. Glia *47*, 290-298.

Liu, H.N., and Almazan, G. (1995). Glutamate induces c-fos proto-oncogene expression and inhibits proliferation in oligodendrocyte progenitors: receptor characterization. Eur J Neurosci *7*, 2355-2363.

Liu, J., Dietz, K., DeLoyht, J.M., Pedre, X., Kelkar, D., Kaur, J., Vialou, V., Lobo, M.K., Dietz, D.M., Nestler, E.J.*, et al.* (2012). Impaired adult myelination in the prefrontal cortex of socially isolated mice. Nat Neurosci *15*, 1621-1623.

Liu, J., Moyon, S., Hernandez, M., and Casaccia, P. (2016). Epigenetic control of oligodendrocyte development: adding new players to old keepers. Curr Opin Neurobiol *39*, 133-138.

Loy, K., Schmalz, A., Hoche, T., Jacobi, A., Kreutsfeldt, M., Merkler, D., and Bareyre, F. (2018). Enhanced voluntary exercise improves functional recovery following spinal cord injury by impacting the local neuroglial injury response and supporting the rewiring of supraspinal circuits. Journal of neurotrauma.

Lu, Q.R., Yuk, D., Alberta, J.A., Zhu, Z., Pawlitzky, I., Chan, J., McMahon, A.P., Stiles, C.D., and Rowitch, D.H. (2000). Sonic hedgehog--regulated oligodendrocyte lineage genes encoding bHLH proteins in the mammalian central nervous system. Neuron *25*, 317-329.

Lu, Y.C., Weng, W.C., and Lee, H. (2015). Functional roles of calreticulin in cancer biology. BioMed research international *2015*, 526524.

Lui, J.H., Hansen, D.V., and Kriegstein, A.R. (2011). Development and evolution of the human neocortex. Cell *146*, 18-36.

Lundgaard, I., Luzhynskaya, A., Stockley, J.H., Wang, Z., Evans, K.A., Swire, M., Volbracht, K., Gautier, H.O., Franklin, R.J., Charles, F.-C.*, et al.* (2013). Neuregulin and BDNF induce a switch to NMDA receptor-dependent myelination by oligodendrocytes. PLoS Biol *11*, e1001743.

Ma, Z., Stork, T., Bergles, D.E., and Freeman, M.R. (2016). Neuromodulators signal through astrocytes to alter neural circuit activity and behaviour. Nature *539*, 428-432.

Magri, L., Gacias, M., Wu, M., Swiss, V.A., Janssen, W.G., and Casaccia, P. (2014). c-Myc-dependent transcriptional regulation of cell cycle and nucleosomal histones during oligodendrocyte differentiation. Neuroscience *276*, 72-86.

Makinodan, M., Rosen, K.M., Ito, S., and Corfas, G. (2012). A critical period for social experience-dependent oligodendrocyte maturation and myelination. Science *337*, 1357-1360.

Marisca, R., Hoche, T., Agirre, E., Hoodless, L.J., Barkey, W., Auer, F., Castelo-Branco, G., and Czopka, T. (2020). Functionally distinct subgroups of oligodendrocyte precursor cells integrate neural activity and execute myelin formation. Nat Neurosci.

Marques, S., van Bruggen, D., Vanichkina, D.P., Floriddia, E.M., Munguba, H., Varemo, L., Giacomello, S., Falcao, A.M., Meijer, M., Bjorklund, A.K*., et al.* (2018). Transcriptional Convergence of Oligodendrocyte Lineage Progenitors during Development. Dev Cell *46*, 504-517 e507.

Marques, S., Zeisel, A., Codeluppi, S., van Bruggen, D., Mendanha Falcao, A., Xiao, L., Li, H., Haring, M., Hochgerner, H., Romanov, R.A*., et al.* (2016). Oligodendrocyte heterogeneity in the mouse juvenile and adult central nervous system. Science *352*, 1326-1329.

Mattugini, N., Bocchi, R., Scheuss, V., Russo, G.L., Torper, O., Lao, C.L., and Gotz, M. (2019). Inducing Different Neuronal Subtypes from Astrocytes in the Injured Mouse Cerebral Cortex. Neuron *103*, 1086-1095 e1085.

Maturana, A.D., Fujita, T., and Kuroda, S. (2010). Functions of fasciculation and elongation protein zeta-1 (FEZ1) in the brain. ScientificWorldJournal *10*, 1646-1654.

McKenzie, I.A., Ohayon, D., Li, H., de Faria, J.P., Emery, B., Tohyama, K., and Richardson, W.D. (2014). Motor skill learning requires active central myelination. Science *346*, 318-322.

Meijering, E., Jacob, M., Sarria, J.C., Steiner, P., Hirling, H., and Unser, M. (2004). Design and validation of a tool for neurite tracing and analysis in fluorescence microscopy images. Cytometry A *58*, 167-176.

Mensch, S., Baraban, M., Almeida, R., Czopka, T., Ausborn, J., El Manira, A., and Lyons, D.A. (2015). Synaptic vesicle release regulates myelin sheath number of individual oligodendrocytes in vivo. Nat Neurosci *18*, 628-630.

Moeendarbary, E., Weber, I.P., Sheridan, G.K., Koser, D.E., Soleman, S., Haenzi, B., Bradbury, E.J., Fawcett, J., and Franze, K. (2017). The soft mechanical signature of glial scars in the central nervous system. Nat Commun *8*, 14787.

Mollmert, S., Kharlamova, M.A., Hoche, T., Taubenberger, A.V., Abuhattum, S., Kuscha, V., Kurth, T., Brand, M., and Guck, J. (2020). Zebrafish Spinal Cord Repair Is Accompanied by Transient Tissue Stiffening. Biophys J *118*, 448-463.

Monteiro de Castro, G., Deja, N.A., Ma, D., Zhao, C., and Franklin, R.J. (2015). Astrocyte Activation via Stat3 Signaling Determines the Balance of Oligodendrocyte versus Schwann Cell Remyelination. Am J Pathol *185*, 2431-2440.

Nagy, B., Hovhannisyan, A., Barzan, R., Chen, T.J., and Kukley, M. (2017). Different patterns of neuronal activity trigger distinct responses of oligodendrocyte precursor cells in the corpus callosum. PLoS Biol *15*, e2001993.

Nave, K.A. (2010a). Myelination and support of axonal integrity by glia. Nature *468*, 244-252.

Nave, K.A. (2010b). Myelination and the trophic support of long axons. Nat Rev Neurosci *11*, 275-283.

Nishiyama, A., Chang, A., and Trapp, B.D. (1999). NG2+ glial cells: a novel glial cell population in the adult brain. J Neuropathol Exp Neurol *58*, 1113-1124.

Nishiyama, A., Lin, X.H., Giese, N., Heldin, C.H., and Stallcup, W.B. (1996). Co-localization of NG2 proteoglycan and PDGF alpha-receptor on O2A progenitor cells in the developing rat brain. J Neurosci Res *43*, 299-314.

Noble, M., Murray, K., Stroobant, P., Waterfield, M.D., and Riddle, P. (1988). Platelet-derived growth factor promotes division and motility and inhibits premature differentiation of the oligodendrocyte/type-2 astrocyte progenitor cell. Nature *333*, 560-562.

Oberheim, N.A., Goldman, S.A., and Nedergaard, M. (2012). Heterogeneity of astrocytic form and function. Methods Mol Biol *814*, 23-45.

Osorio-Querejeta, I., Saenz-Cuesta, M., Munoz-Culla, M., and Otaegui, D. (2017). Models for Studying Myelination, Demyelination and Remyelination. Neuromolecular medicine.

Ou, Z., Sun, Y., Lin, L., You, N., Liu, X., Li, H., Ma, Y., Cao, L., Han, Y., Liu, M*., et al.* (2016). Olig2-Targeted G-Protein-Coupled Receptor Gpr17 Regulates Oligodendrocyte Survival in Response to Lysolecithin-Induced Demyelination. J Neurosci *36*, 10560-10573.

Ozerdem, U., Grako, K.A., Dahlin-Huppe, K., Monosov, E., and Stallcup, W.B. (2001). NG2 proteoglycan is expressed exclusively by mural cells during vascular morphogenesis. Dev Dyn *222*, 218-227.

Pan, S., Mayoral, S.R., Choi, H.S., Chan, J.R., and Kheirbek, M.A. (2020). Preservation of a remote fear memory requires new myelin formation. Nat Neurosci.

Patel, J.R., and Klein, R.S. (2011). Mediators of oligodendrocyte differentiation during remyelination. FEBS letters *585*, 3730-3737.

Patneau, D.K., Wright, P.W., Winters, C., Mayer, M.L., and Gallo, V. (1994). Glial cells of the oligodendrocyte lineage express both kainate- and AMPA-preferring subtypes of glutamate receptor. Neuron *12*, 357-371.

Picelli, S., Bjorklund, A.K., Faridani, O.R., Sagasser, S., Winberg, G., and Sandberg, R. (2013). Smart-seq2 for sensitive full-length transcriptome profiling in single cells. Nat Methods *10*, 1096-1098.

Raff, M.C. (1989). Glial cell diversification in the rat optic nerve. Science *243*, 1450-1455.

Raff, M.C., Abney, E.R., Cohen, J., Lindsay, R., and Noble, M. (1983a). Two types of astrocytes in cultures of developing rat white matter: differences in morphology, surface gangliosides, and growth characteristics. J Neurosci *3*, 1289-1300.

Raff, M.C., Lillien, L.E., Richardson, W.D., Burne, J.F., and Noble, M.D. (1988). Platelet-derived growth factor from astrocytes drives the clock that times oligodendrocyte development in culture. Nature *333*, 562-565.

Raff, M.C., Miller, R.H., and Noble, M. (1983b). A glial progenitor cell that develops in vitro into an astrocyte or an oligodendrocyte depending on culture medium. Nature *303*, 390-396.

Raj, B., Wagner, D.E., McKenna, A., Pandey, S., Klein, A.M., Shendure, J., Gagnon, J.A., and Schier, A.F. (2018). Simultaneous single-cell profiling of lineages and cell types in the vertebrate brain. Nat Biotechnol *36*, 442-450.

Reich, D.S., Lucchinetti, C.F., and Calabresi, P.A. (2018). Multiple Sclerosis. The New England journal of medicine *378*, 169-180.

Richardson, W.D., Pringle, N., Mosley, M.J., Westermark, B., and Dubois-Dalcq, M. (1988). A role for platelet-derived growth factor in normal gliogenesis in the central nervous system. Cell *53*, 309-319.

Rivers, L.E., Young, K.M., Rizzi, M., Jamen, F., Psachoulia, K., Wade, A., Kessaris, N., and Richardson, W.D. (2008). PDGFRA/NG2 glia generate myelinating oligodendrocytes and piriform projection neurons in adult mice. Nat Neurosci *11*, 1392-1401.

Rosenberg, S.S., Kelland, E.E., Tokar, E., De la Torre, A.R., and Chan, J.R. (2008). The geometric and spatial constraints of the microenvironment induce oligodendrocyte differentiation. Proc Natl Acad Sci U S A *105*, 14662-14667.

Rosenzweig, S., and Carmichael, S.T. (2015). The axon-glia unit in white matter stroke: mechanisms of damage and recovery. Brain research *1623*, 123-134.

Rowitch, D.H. (2004). Glial specification in the vertebrate neural tube. Nat Rev Neurosci *5*, 409-419.

Saab, A.S., Tzvetavona, I.D., Trevisiol, A., Baltan, S., Dibaj, P., Kusch, K., Mobius, W., Goetze, B., Jahn, H.M., Huang, W.*, et al.* (2016). Oligodendroglial NMDA Receptors Regulate Glucose Import and Axonal Energy Metabolism. Neuron *91*, 119-132.

Sakry, D., Neitz, A., Singh, J., Frischknecht, R., Marongiu, D., Biname, F., Perera, S.S., Endres, K., Lutz, B., Radyushkin, K.*, et al.* (2014). Oligodendrocyte precursor cells modulate the neuronal network by activity-dependent ectodomain cleavage of glial NG2. PLoS Biol *12*, e1001993.

Sakry, D., Yigit, H., Dimou, L., and Trotter, J. (2015). Oligodendrocyte precursor cells synthesize neuromodulatory factors. PLoS One *10*, e0127222.

Sampaio-Baptista, C., Khrapitchev, A.A., Foxley, S., Schlagheck, T., Scholz, J., Jbabdi, S., DeLuca, G.C., Miller, K.L., Taylor, A., Thomas, N.*, et al.* (2013). Motor skill learning induces changes in white matter microstructure and myelination. J Neurosci *33*, 19499-19503.

Santos, A.K., Vieira, M.S., Vasconcellos, R., Goulart, V.A.M., Kihara, A.H., and Resende, R.R. (2018). Decoding cell signalling and regulation of oligodendrocyte differentiation. Semin Cell Dev Biol.

Schebesta, M., and Serluca, F.C. (2009). olig1 Expression identifies developing oligodendrocytes in zebrafish and requires hedgehog and notch signaling. Dev Dyn *238*, 887-898.

Schindelin, J., Arganda-Carreras, I., Frise, E., Kaynig, V., Longair, M., Pietzsch, T., Preibisch, S., Rueden, C., Saalfeld, S., Schmid, B.*, et al.* (2012). Fiji: an open-source platform for biological-image analysis. Nat Methods *9*, 676-682.

Schneider, S., Gruart, A., Grade, S., Zhang, Y., Kroger, S., Kirchhoff, F., Eichele, G., Delgado Garcia, J.M., and Dimou, L. (2016). Decrease in newly generated oligodendrocytes leads to motor dysfunctions and changed myelin structures that can be rescued by transplanted cells. Glia *64*, 2201-2218.

Segel, M., Neumann, B., Hill, M.F.E., Weber, I.P., Viscomi, C., Zhao, C., Young, A., Agley, C.C., Thompson, A.J., Gonzalez, G.A.*, et al.* (2019). Niche stiffness underlies the ageing of central nervous system progenitor cells. Nature *573*, 130-134.

Serwanski, D.R., Jukkola, P., and Nishiyama, A. (2017). Heterogeneity of astrocyte and NG2 cell insertion at the node of ranvier. J Comp Neurol *525*, 535-552.

Sherman, D.L., and Brophy, P.J. (2005). Mechanisms of axon ensheathment and myelin growth. Nat Rev Neurosci *6*, 683-690.

Sidik, H., and Talbot, W.S. (2015). A zinc finger protein that regulates oligodendrocyte specification, migration and myelination in zebrafish. Development *142*, 4119-4128.

Sim, F.J., Zhao, C., Penderis, J., and Franklin, R.J. (2002). The age-related decrease in CNS remyelination efficiency is attributable to an impairment of both oligodendrocyte progenitor recruitment and differentiation. J Neurosci *22*, 2451-2459.

Simons, M., Misgeld, T., and Kerschensteiner, M. (2014). A unified cell biological perspective on axon-myelin injury. The Journal of cell biology *206*, 335-345.

Skoff, R.P., Price, D.L., and Stocks, A. (1976). Electron microscopic autoradiographic studies of gliogenesis in rat optic nerve. I. Cell proliferation. J Comp Neurol *169*, 291-312.

Sommer, I., and Schachner, M. (1982). Cell that are O4 antigen-positive and O1 antigen-negative differentiate into O1 antigen-positive oligodendrocytes. Neuroscience letters *29*, 183-188.

Soula, C., Danesin, C., Kan, P., Grob, M., Poncet, C., and Cochard, P. (2001). Distinct sites of origin of oligodendrocytes and somatic motoneurons in the chick spinal cord: oligodendrocytes arise from Nkx2.2-expressing progenitors by a Shh-dependent mechanism. Development *128*, 1369-1379.

Soundarapandian, M.M., Selvaraj, V., Lo, U.G., Golub, M.S., Feldman, D.H., Pleasure, D.E., and Deng, W. (2011). Zfp488 promotes oligodendrocyte differentiation of neural progenitor cells in adult mice after demyelination. Scientific reports *1*, 2.

Spitzer, S.O., Sitnikov, S., Kamen, Y., Evans, K.A., Kronenberg-Versteeg, D., Dietmann, S., de Faria, O., Jr., Agathou, S., and Karadottir, R.T. (2019). Oligodendrocyte Progenitor Cells Become Regionally Diverse and Heterogeneous with Age. Neuron *101*, 459-471 e455.

Steadman, P.E., Xia, F., Ahmed, M., Mocle, A.J., Penning, A.R.A., Geraghty, A.C., Steenland, H.W., Monje, M., Josselyn, S.A., and Frankland, P.W. (2019). Disruption of Oligodendrogenesis Impairs Memory Consolidation in Adult Mice. Neuron.

Stobart, J.L., Ferrari, K.D., Barrett, M.J.P., Gluck, C., Stobart, M.J., Zuend, M., and Weber, B. (2018). Cortical Circuit Activity Evokes Rapid Astrocyte Calcium Signals on a Similar Timescale to Neurons. Neuron *98*, 726-735 e724.

Stuart, T., Butler, A., Hoffman, P., Hafemeister, C., Papalexi, E., Mauck, W.M., 3rd, Hao, Y., Stoeckius, M., Smibert, P., and Satija, R. (2019). Comprehensive Integration of Single-Cell Data. Cell *177*, 1888-1902 e1821.

Sun, L.O., Mulinyawe, S.B., Collins, H.Y., Ibrahim, A., Li, Q., Simon, D.J., Tessier-Lavigne, M., and Barres, B.A. (2018). Spatiotemporal Control of CNS Myelination by Oligodendrocyte Programmed Cell Death through the TFEB-PUMA Axis. Cell.

Svennerholm, L., and Gottfries, C.G. (1994). Membrane lipids, selectively diminished in Alzheimer brains, suggest synapse loss as a primary event in early-onset form (type I) and demyelination in late-onset form (type II). J Neurochem *62*, 1039-1047.

Takeoka, A., Vollenweider, I., Courtine, G., and Arber, S. (2014). Muscle spindle feedback directs locomotor recovery and circuit reorganization after spinal cord injury. Cell *159*, 1626-1639.

Talbott, J.F., Cao, Q., Enzmann, G.U., Benton, R.L., Achim, V., Cheng, X.X., Mills, M.D., Rao, M.S., and Whittemore, S.R. (2006). Schwann cell-like differentiation by adult oligodendrocyte precursor cells following engraftment into the demyelinated spinal cord is BMP-dependent. Glia *54*, 147-159.

Temple, S., and Raff, M.C. (1985). Differentiation of a bipotential glial progenitor cell in a single cell microculture. Nature *313*, 223-225.

Thony, B., Auerbach, G., and Blau, N. (2000). Tetrahydrobiopterin biosynthesis, regeneration and functions. Biochem J *347 Pt 1*, 1-16.

Tognatta, R., Sun, W., Goebbels, S., Nave, K.A., Nishiyama, A., Schoch, S., Dimou, L., and Dietrich, D. (2017). Transient Cnp expression by early progenitors causes Cre-Lox-based reporter lines to map profoundly different fates. Glia *65*, 342-359.

Trapp, B.D., Nishiyama, A., Cheng, D., and Macklin, W. (1997). Differentiation and death of premyelinating oligodendrocytes in developing rodent brain. The Journal of cell biology *137*, 459-468.

Tripathi, R.B., Clarke, L.E., Burzomato, V., Kessaris, N., Anderson, P.N., Attwell, D., and Richardson, W.D. (2011). Dorsally and ventrally derived oligodendrocytes have similar electrical properties but myelinate preferred tracts. J Neurosci *31*, 6809-6819.

Tripathi, R.B., Rivers, L.E., Young, K.M., Jamen, F., and Richardson, W.D. (2010). NG2 glia generate new oligodendrocytes but few astrocytes in a murine experimental autoimmune encephalomyelitis model of demyelinating disease. J Neurosci *30*, 16383-16390.

Trotter, J., and Schachner, M. (1989). Cells positive for the O4 surface antigen isolated by cell sorting are able to differentiate into astrocytes or oligodendrocytes. Brain research Developmental brain research *46*, 115-122.

Tsai, E., and Casaccia, P. (2019). Mechano-modulation of nuclear events regulating oligodendrocyte progenitor gene expression. Glia *67*, 1229-1239.

Ulanska-Poutanen, J., Mieczkowski, J., Zhao, C., Konarzewska, K., Kaza, B., Pohl, H.B., Bugajski, L., Kaminska, B., Franklin, R.J., and Zawadzka, M. (2018). Injury-induced perivascular niche supports alternative differentiation of adult rodent CNS progenitor cells. eLife *7*.

van Bruggen, D., Agirre, E., and Castelo-Branco, G. (2017). Single-cell transcriptomic analysis of oligodendrocyte lineage cells. Curr Opin Neurobiol *47*, 168-175.

van den Brand, R., Heutschi, J., Barraud, Q., DiGiovanna, J., Bartholdi, K., Huerlimann, M., Friedli, L., Vollenweider, I., Moraud, E.M., Duis, S.*, et al.* (2012). Restoring voluntary control of locomotion after paralyzing spinal cord injury. Science *336*, 1182-1185.

van der Knaap, M.S., and Bugiani, M. (2017). Leukodystrophies: a proposed classification system based on pathological changes and pathogenetic mechanisms. Acta Neuropathol *134*, 351-382.

van der Knaap, M.S., Schiffmann, R., Mochel, F., and Wolf, N.I. (2019). Diagnosis, prognosis, and treatment of leukodystrophies. The Lancet Neurology *18*, 962-972.

Vigano, F., and Dimou, L. (2016). The heterogeneous nature of NG2-glia. Brain research *1638*, 129-137.

Vigano, F., Mobius, W., Gotz, M., and Dimou, L. (2013). Transplantation reveals regional differences in oligodendrocyte differentiation in the adult brain. Nat Neurosci *16*, 1370-1372.

Vigano, F., Schneider, S., Cimino, M., Bonfanti, E., Gelosa, P., Sironi, L., Abbracchio, M.P., and Dimou, L. (2016). GPR17 expressing NG2-Glia: Oligodendrocyte progenitors serving as a reserve pool after injury. Glia *64*, 287-299.

Wake, H., Lee, P.R., and Fields, R.D. (2011). Control of local protein synthesis and initial events in myelination by action potentials. Science *333*, 1647-1651.

Wake, H., Ortiz, F.C., Woo, D.H., Lee, P.R., Angulo, M.C., and Fields, R.D. (2015). Nonsynaptic junctions on myelinating glia promote preferential myelination of electrically active axons. Nat Commun *6*, 7844.

Wang, F., Yang, Y.J., Yang, N., Chen, X.J., Huang, N.X., Zhang, J., Wu, Y., Liu, Z., Gao, X., Li, T.*, et al.* (2018a). Enhancing Oligodendrocyte Myelination Rescues Synaptic Loss and Improves Functional Recovery after Chronic Hypoxia. Neuron.

Wang, J., Ho, W.Y., Lim, K., Feng, J., Tucker-Kellogg, G., Nave, K.A., and Ling, S.C. (2018b). Cell-autonomous requirement of TDP-43, an ALS/FTD signature protein, for oligodendrocyte survival and myelination. Proc Natl Acad Sci U S A *115*, E10941-E10950.

Wang, S.Z., Dulin, J., Wu, H., Hurlock, E., Lee, S.E., Jansson, K., and Lu, Q.R. (2006). An oligodendrocyte-specific zinc-finger transcription regulator cooperates with Olig2 to promote oligodendrocyte differentiation. Development *133*, 3389-3398.

Watanabe, M., Toyama, Y., and Nishiyama, A. (2002). Differentiation of proliferated NG2-positive glial progenitor cells in a remyelinating lesion. J Neurosci Res *69*, 826-836.

Weider, M., and Wegner, M. (2017). SoxE factors: Transcriptional regulators of neural differentiation and nervous system development. Semin Cell Dev Biol *63*, 35-42.

Weng, Q., Wang, J., Wang, J., He, D., Cheng, Z., Zhang, F., Verma, R., Xu, L., Dong, X., Liao, Y.*, et al.* (2019). Single-Cell Transcriptomics Uncovers Glial Progenitor Diversity and Cell Fate Determinants during Development and Gliomagenesis. Cell stem cell *24*, 707-723 e708.

Winkler, C., and Yao, S. (2014). The midkine family of growth factors: diverse roles in nervous system formation and maintenance. British journal of pharmacology *171*, 905-912.

Wolswijk, G., and Noble, M. (1989). Identification of an adult-specific glial progenitor cell. Development *105*, 387-400.

Xiao, L., Ohayon, D., McKenzie, I.A., Sinclair-Wilson, A., Wright, J.L., Fudge, A.D., Emery, B., Li, H., and Richardson, W.D. (2016). Rapid production of new oligodendrocytes is required in the earliest stages of motor-skill learning. Nat Neurosci *19*, 1210-1217.

Xin, W., and Bonci, A. (2018). Functional Astrocyte Heterogeneity and Implications for Their Role in Shaping Neurotransmission. Front Cell Neurosci *12*, 141.

Xu, X., Cai, J., Fu, H., Wu, R., Qi, Y., Modderman, G., Liu, R., and Qiu, M. (2000). Selective expression of Nkx-2.2 transcription factor in chicken oligodendrocyte progenitors and implications for the embryonic origin of oligodendrocytes. Molecular and cellular neurosciences *16*, 740-753.

Yamazaki, T., and Mukouyama, Y.S. (2018). Tissue Specific Origin, Development, and Pathological Perspectives of Pericytes. Front Cardiovasc Med *5*, 78.

Yeung, M.S., Zdunek, S., Bergmann, O., Bernard, S., Salehpour, M., Alkass, K., Perl, S., Tisdale, J., Possnert, G., Brundin, L.*, et al.* (2014). Dynamics of oligodendrocyte generation and myelination in the human brain. Cell *159*, 766-774.

Yeung, M.S.Y., Djelloul, M., Steiner, E., Bernard, S., Salehpour, M., Possnert, G., Brundin, L., and Frisen, J. (2019). Dynamics of oligodendrocyte generation in multiple sclerosis. Nature.

Yuan, X., Eisen, A.M., McBain, C.J., and Gallo, V. (1998). A role for glutamate and its receptors in the regulation of oligodendrocyte development in cerebellar tissue slices. Development *125*, 2901-2914.

Zawadzka, M., Rivers, L.E., Fancy, S.P., Zhao, C., Tripathi, R., Jamen, F., Young, K., Goncharevich, A., Pohl, H., Rizzi, M.*, et al.* (2010). CNS-resident glial progenitor/stem cells produce Schwann cells as well as oligodendrocytes during repair of CNS demyelination. Cell stem cell *6*, 578-590.

Zheng, K., Wang, C., Yang, J., Huang, H., Zhao, X., Zhang, Z., and Qiu, M. (2018). Molecular and Genetic Evidence for the PDGFRalpha-Independent Population of Oligodendrocyte Progenitor Cells in the Developing Mouse Brain. J Neurosci *38*, 9505-9513.

Zhou, Q., Wang, S., and Anderson, D.J. (2000). Identification of a novel family of oligodendrocyte lineage-specific basic helix-loop-helix transcription factors. Neuron *25*, 331-343.

Zhu, X., Bergles, D.E., and Nishiyama, A. (2008). NG2 cells generate both oligodendrocytes and gray matter astrocytes. Development *135*, 145-157.

Zhu, X., Hill, R.A., Dietrich, D., Komitova, M., Suzuki, R., and Nishiyama, A. (2011). Age-dependent fate and lineage restriction of single NG2 cells. Development *138*, 745-753.

Zhu, X., Zuo, H., Maher, B.J., Serwanski, D.R., LoTurco, J.J., Lu, Q.R., and Nishiyama, A. (2012). Olig2-dependent developmental fate switch of NG2 cells. Development *139*, 2299-2307.

Ziskin, J.L., Nishiyama, A., Rubio, M., Fukaya, M., and Bergles, D.E. (2007). Vesicular release of glutamate from unmyelinated axons in white matter. Nat Neurosci *10*, 321-330.

Zonouzi, M., Scafidi, J., Li, P., McEllin, B., Edwards, J., Dupree, J.L., Harvey, L., Sun, D., Hubner, C.A., Cull-Candy, S.G.*, et al.* (2015). GABAergic regulation of cerebellar NG2 cell development is altered in perinatal white matter injury. Nat Neurosci *18*, 674-682.

6 PUBLICATIONS RESULTING FROM THIS WORK

Marisca, R., **Hoche, T.**, Agirre, E., Hoodless, L.J., Barkey, W., Auer, F., Castelo-Branco, G., and Czopka, T. (2020). Functionally distinct subgroups of oligodendrocyte precursor cells integrate neural activity and execute myelin formation. Nat Neurosci. [**shared co-first authorship with Roberta Marisca**].

7 TABLE OF FIGURES

8 APPENDIX

8.1.1 Gene expression levels of all mentioned genes based on single-cell RNA-Sequencing

Table 8.1.1.1 Individual expression of genes between clusters expressed as log(TPM).

	VLMC #1	VLMC #2	OPC #1	OPC #2a	OPC #2b	OPC #2c	OL
apc-ENSDARG00000058868	0.2	0.24	1.33	**1.13**	**1.45**	1.46	1.5
aplnra-ENSDARG00000002172	0.45	0.33	3.21	**2.7**	**3.15**	0.24	0.01
aplnrb-ENSDARG00000036670	0.06	0.01	2.87	2.01	2.32	0.13	0.01
aplnrb-ENSDARG00000036670	0.06	0.01	2.87	**2.01**	**2.32**	0.13	0.01
atcaya-ENSDARG00000071678	0.05	0.01	2.22	**1.65**	**1.85**	0.25	0.05
axin2-ENSDARG00000100149	1.16	1	0.14	**0.16**	**0.18**	0.04	0
bmp4-ENSDARG00000019995	0.11	0.85	0.04	**0**	**0.05**	0	0
bsnb-ENSDARG00000079161	0.03	0	0.57	**0.32**	**0.83**	0.29	0.02
calr3a-ENSDARG00000103979	0.68	0.54	1.18	**0.78**	**0.54**	0.13	1.31
calr3b-ENSDARG00000102808	0.41	0.35	0.78	**0.35**	**0.17**	0.25	1.49
calr-ENSDARG00000076290	0.81	0.56	1.34	**0.51**	**0.34**	0.14	1.27
calr-ENSDARG00000076290	0.81	0.56	1.34	**0.51**	**0.34**	0.14	1.27
camk2d2-ENSDARG00000014273	0.02	0	0.87	**0.39**	**0.38**	0.1	0.05
cdk1-ENSDARG00000087554	0.04	0	0.11	**1.28**	**3.26**	3.01	0.01
cnp-ENSDARG00000070822	0.09	0.19	0.33	**0.6**	**0.33**	0.9	0.11
col1a1a-ENSDARG00000012405	6.21	5.78	0.42	0.15	0.29	0.12	0.15
cspg4-ENSDARG00000078227	0.09	0.25	0.97	0.62	0.97	0.17	0
dlg4a-ENSDARG00000041926	0	0	0.07	**0.06**	**0.04**	0	0
dlg4b-ENSDARG00000039385	0.01	0	0.19	**0.27**	**0.06**	0.01	0
draxin-ENSDARG00000058256	0.01	0.01	0.69	**0.81**	**0.9**	2.57	0.65
egfra-ENSDARG00000013847	0.2	0.16	0.14	**0.46**	**0.19**	1.49	0.97
enpp6-ENSDARG00000040469	0.01	0.1	0	0.06	0	0	0
fez1-ENSDARG00000023174	0.05	0.01	1.15	**0.37**	**0.72**	0.34	0.71
glula-ENSDARG00000099776	0.25	0.27	2.9	**1.81**	**2**	0.45	0.89
gpr17-ENSDARG00000062030	0	0	0.15	0.48	0.06	2.17	0.42
gria1a-ENSDARG00000021352	0.08	0.02	2.49	**1.68**	**1.87**	0.84	0.18
gria2b-ENSDARG00000052765	0.04	0	2.17	1.65	1.36	0.09	0
grin1a-ENSDARG00000027828	0.02	0.02	1.47	**1.07**	**1.02**	0.06	0
grin1b-ENSDARG00000025728	0.04	0	1.85	**1.5**	**1.37**	0.12	0
hes6-ENSDARG00000019335	0.03	0.06	0.25	**0.36**	**0.23**	0.99	0.32
homer1b-ENSDARG00000101759	0.01	0	0.1	**0.17**	**0.03**	0	0
homer2-ENSDARG00000059349	0	0	0	**0.02**	**0**	0	0
homer3a-ENSDARG00000102532	0	0	0	**0.02**	**0**	0	0
homer3b-ENSDARG00000010789	0.35	0.26	0.31	**0.22**	**0.43**	0.29	0.01
hsp90b1-ENSDARG00000003570	0.71	0.69	1.24	**0.41**	**0.44**	0.18	2
igsf9ba-ENSDARG00000033845	0.13	0.01	3.47	**3.39**	**3.45**	3.36	0.06
itih2-ENSDARG00000045516	0	0	0	0	0	0	0
kcnip1b-ENSDARG00000034808	0.16	0.06	0.76	**0.33**	**0.21**	0.02	0
kif11-ENSDARG00000010948	0.03	0.01	0.08	0.39	3.09	2.33	0
kpna2-ENSDARG00000038066	0.03	0.02	0.1	0.94	3.66	2.53	0.02

mag-ENSDARG00000104023	0.01	0	0.01	0	0	0	2.47
mbpa-ENSDARG00000036186	0	0	0	0.01	0	0	2.11
mcm2-ENSDARG00000102798	0.01	0.29	0.28	**1.28**	**0**	0.05	0.05
mdkb-ENSDARG00000020708	0.07	0.3	2.23	**1.57**	**1.8**	0.52	0.05
mki67-ENSDARG00000091150	0.03	0.03	0.07	1.49	3.17	2.97	0.07
mpz-ENSDARG00000038609	0	0.02	0	0	0	0	1.95
mycb-ENSDARG00000007241	0.14	0.16	0.15	**0.38**	**0.16**	1.36	0.07
mycb-ENSDARG00000007241	0.14	0.16	0.15	**0.38**	**0.16**	1.36	0.07
myrf-ENSDARG00000078676	0	0.03	0.13	0.62	0.56	2	3.32
ncalda-ENSDARG00000070688	0.71	0.83	3.12	**2.21**	**2.9**	1.76	0.65
neu4-ENSDARG00000057677	0	0.03	0.01	0	0.01	0	0
nkx2.2a-ENSDARG00000053298	0.02	0.01	1.57	1.42	1.32	1.65	0.77
nlgn3a-ENSDARG00000104786	0.07	0.01	2	**1.64**	**1.61**	0.33	0.05
nrxn1a-ENSDARG00000061647	0.08	0.03	2.41	**1.84**	**2.22**	0.84	0.02
nrxn1b-ENSDARG00000063635	0.01	0.02	0.85	**0.95**	**0.82**	0.84	0.01
nrxn2a-ENSDARG00000061454	0.01	0.01	0.88	**0.68**	**0.7**	0.14	0.01
nrxn2b-ENSDARG00000063150	0.05	0.03	1.07	**0.95**	**0.99**	0.95	0
nrxn3b-ENSDARG00000062693	0.02	0.05	0.79	**0.68**	**0.63**	0.27	0.06
nusap1-ENSDARG00000002403	0.02	0.01	0.04	**0.71**	**2.82**	2.47	0
olig1-ENSDARG00000040948	0.12	0.08	2.78	1.97	2.89	0.16	0
olig2-ENSDARG00000040946	0.08	0.01	2.9	2.69	2.78	1.58	1.79
pcna-ENSDARG00000054155	0.12	0.58	0.26	3.56	0.95	1.53	0.07
pdgfra-ENSDARG00000070494	2.09	1.61	0.09	0	0	0	0
pdgfrb-ENSDARG00000100897	1.15	1.03	0.02	0.02	0.02	0.02	0
plp1a-ENSDARG00000103732	0.02	0.01	0.17	0.13	0.21	0.22	2.5
ppp1r14bb-ENSDARG00000030161	0.28	0.25	1.44	1.26	1.79	1.49	0.21
prdm8-ENSDARG00000025017	0.03	0.01	0.74	**1.21**	**0.85**	2.73	0.73
prom1a-ENSDARG00000039966	0.03	0.02	0.67	**0.42**	**0.41**	0.31	0.32
prom1b-ENSDARG00000034007	0.04	0	1.05	**0.91**	**0.66**	0.57	0.4
ptgdsb.1-ENSDARG00000027088	0.43	0.36	0.52	**0.12**	**0.22**	0	0
ptgdsb.2-ENSDARG00000071626	0.29	0.28	0.91	**0.39**	**0.28**	0	0
ptgdsb.2-ENSDARG00000071626	0.29	0.28	0.91	**0.39**	**0.28**	0	0
qdpra-ENSDARG00000040190	4.41	2.95	1.59	**0.81**	**0.91**	0.38	0.4
rpa1-ENSDARG00000003938	0.21	0.34	0.2	**2.3**	**0.43**	0.49	0.16
s1pr1-ENSDARG00000042690	0.09	0.38	0.99	**0.58**	**0.25**	0	0
scg2b-ENSDARG00000038574	0.02	0	1.79	**1.21**	**1.29**	0.06	0
sema5a-ENSDARG00000058821	0.14	0.14	3.43	**3.44**	**3.32**	2.08	0.07
slc1a2b-ENSDARG00000102453	0.08	0.02	3.11	**2.46**	**2.8**	0.65	0.46
slc6a1a-ENSDARG00000045944	0.05	0	1.7	**1.14**	**1.25**	0.15	0.01
slc6a1b-ENSDARG00000039647	0.05	0	1.25	**0.8**	**0.49**	0.3	0.01
snap25a-ENSDARG00000020609	0.02	0.01	0.84	**0.4**	**0.3**	0.07	0
sod3a-ENSDARG00000070168	0.01	0	0	0	0	0	0
sod3b-ENSDARG00000079183	0	0	0	0.01	0	0	0
sox10-ENSDARG00000077467	0.03	0	1.94	2.05	1.98	2.18	1.9
sox9b-ENSDARG00000043923	0.01	0.04	0.6	0.97	0.38	1.89	0.14
sypa-ENSDARG00000110528	0.02	0.03	0.58	**0.32**	**0.45**	0.16	0.08
tbx18-ENSDARG00000036930	0.07	0.47	0.01	0	0	0	0
TCF4-ENSDARG00000107408	0.05	0.17	0.25	0.15	**0.28**	**0.26**	0.16

top2a-ENSDARG00000024488	0.05	0	0.05	**1.49**	**3.28**	2.97	0.02
vav3b-ENSDARG00000075962	0.02	0	0.05	**0.03**	**0.01**	0.98	0.43
vtna-ENSDARG00000055388	0	0	0.01	0	0.01	0	0
yy1b-ENSDARG00000027978	0.51	0.37	0.24	**0.45**	**0.16**	0.57	0.23